Potassium channel-based optogenetic tool development - Establishment and optimization of compartment-specific light-inducible silencing tools

Engel, Anja Jeannine

(2020)

Potassium channel-based optogenetic tool development

Establishment and optimization of compartment-specific light-inducible silencing tools

Vom Fachbereich Biologie der Technischen Universität Darmstadt

zur Erlangung des akademischen Grades

eines *Doctor rerum naturalium*

genehmigte Dissertation von

Anja Jeannine Engel, M.Sc.

aus Darmstadt

1. Referent: Prof. Dr. Gerhard Thiel
2. Referent: Prof. Dr. Adam Bertl

Eingereicht am: 20.05.2020

Mündliche Prüfung am: 10.07.2020

Darmstadt 2020

Engel, Anja Jeannine: Potassium channel-based optogenetic tool development – Establishment and optimization of compartment-specific light-inducible silencing tools

Darmstadt, Technische Universität Darmstadt
Jahr der Veröffentlichung: 2020
URN: urn:nbn:de:tuda-tuprints-117820
Tag der mündlichen Prüfung: 10.07.2020

Most innovations are not obvious to other people at the time.
You have to believe in yourself.
If you've got a good idea, follow it even when others say it's not.
- Frances H. Arnold

Table of contents

Abstract

Optogenetics offers unique possibilities to control cells with a high spatio-temporal precision using light-sensitive proteins. There are two groups of light-inducible proteins: the first comprises retinal-containing proteins, which are light-inducible ion pumps or channels. The second group includes modular photoactuators, in which light induces conformational changes which in turn cause interaction with an effector domain. Optogenetics is most widely used to study excitable cells and has the potential to serve as a treatment for a lot of diseases like neurological disorders or blindness due to degradation of photoreceptors.

In this work, potassium channel-based optogenetic tools were developed, optimized and functionally characterized. The goal was to target the respective GFP-tagged channels to two distinct locations within the cell: (i) the plasma membrane, where potassium channels can serve as optogenetic silencing tools by inducing hyperpolarization, (ii) the inner mitochondrial membrane, where light-inducible depolarization by potassium channel activity offers the chance to study the so far unknown function of potassium channels in mitochondria. To achieve targeting to the plasma membrane, two candidate channels were examined: $Kcv_{PBCV\text{-}1}$ and Kcv_{NTS}. Kesv and $Kmpv_{12T}$ on the other hand served as candidate channels to study the effects of potassium channel expression in the inner mitochondrial membrane.

To allow a most effective sorting of these four candidate channels, two different approaches were pursued to optimize the sorting efficiency of these channels in cultured mammalian cells. One effective way of augmenting sorting of channels to the mitochondria was achieved by codon optimization. For this purpose, rare codons in the channel coding gene were replaced by frequently used codons. This procedure resulted, in particular in Kesv, in an enhanced sorting to the mitochondria. Another effect which markedly increased sorting efficiency to the mitochondria was to shorten the protein linker between the channel protein and its GFP-tag. The combination of these two steps, a codon optimized channel combined with a short protein linker, yielded a very efficient and exclusive sorting of Kesv to the mitochondria. This positive effect of codon optimization on mitochondrial targeting was reproducible in six different cell lines, suggesting that this is a general mechanism in mammalian cells. $Kcv_{PBCV\text{-}1}$, which is by default sorted to the secretary pathway and further to the plasma membrane, was insensitive to codon optimization. In contrast to the mitochondrial potassium channels, the two channels sorted to the plasma membrane favor low expression levels to achieve the most effective sorting.

To design an optogenetic tool for short-term depolarization of the mitochondria, the existing light-gated potassium channel BLINK1 was reengineered for mitochondrial sorting. It occurred that the addition of six canonical mitochondrial targeting sequences to the N-terminus of the protein resulted in an effective sorting of this protein to the mitochondria. Its functionality in the mitochondria remains to be tested.

In a different strategy, optogenetic tools for long-term activation of potassium channels in the plasma membrane or the mitochondria were developed. In this case, two different light-inducible gene expression systems were employed to regulate expression of suitable potassium channels by light. The first approach was based on dimerization of the bacterial light-oxygen-voltage domain from *Erythrobacter litoralis* (EL222). The second system was based on the light-regulated interaction of cryptochrome 2 (CRY2) with its interacting partner CIB1.

In these experiments the expression of a GFP-tagged potassium channel was placed under control of the EL222 system. Based on the intensity of the GFP signal in transfected cells, it became clear that the channel of interest was already significantly expressed in the dark and required a very high light intensity (120 μE for 16 hours) for elevating expression above the dark level. Because of this combination of unspecific leak expression in the dark and high light requirement, the EL222 system was not further pursued.

In an alternative system, potassium channel expression was controlled by the blue light receptor system CRY2/CIB1 from *Arabidopsis thaliana*. This light-sensitive transcription system proved to be effective for the purpose of light-inducible potassium channel expression. It required very low light intensities (6 μE for 1 hour) or short exposure times for a robust expression of the candidate channel. A 5 second pulse of 120 μE was already sufficient for a maximal stimulation of channel expression. Leak expression of the channel in the dark was barely above detection limit. It was also possible to simplify the handling of the system by placing all three necessary components (CRY2, CIB1, potassium channel) in one expression vector without affecting its efficacy. We found that one hour of pulsed light (6 μE) was sufficient to achieve full activation one hour after light-stimulation.

The CRY2 CIB1 system was examined in different functional assays. The properties of channels which were expressed at the plasma membrane in a light-dependent manner, were examined by whole cell patch clamp measurements. The data show that the channels, which were expressed under control of the CRY2 CIB1 system reached the plasma membrane and there exhibited the same functional properties as the constitutively expressed control channels.

The functionality of channels expressed in the inner mitochondrial membrane, were examined in planar lipid bilayer experiments as well as by a set of microscopy assays. By using fluorescent reporters of the mitochondrial membrane voltage and mitochondrial calcium, it occurs that expression of mitochondrially targeted potassium channels under control of the CRY2 CIB1 system caused an effective depolarization of theses organelles. Also, they did significantly lower the mitochondrial calcium levels, but did not induce apoptosis.

Currently, the CRY2 CIB1 constructs undergo functional tests *in vivo* to examine whether they influence the development of zebrafish larvae if expressed in different organ systems.

Zusammenfassung

Optogenetik bietet einzigartige Möglichkeiten, zelluläre Funktionen durch die Verwendung von lichtsensitiven Proteinen mit hoher zeitlicher und räumlicher Präzision zu kontrollieren. Diese lichtsensitiven Proteine können in zwei Gruppen eingeteilt werden: Die erste Gruppe umfasst Proteine welche Retinal enthalten, die als lichtinduzierbare Pumpen oder Kanäle fungieren. Die zweite Gruppe umfasst modulare Photoaktivatoren in welchen durch Licht Konformationsänderungen verursacht werden, welche wiederum die Interaktion mit einer Effektor-Domäne verursachen. Hauptsächlich findet Optogenetik Verwendung in der Untersuchung von erregbaren Zellen und bietet großes Potential für neuartige Behandlungsmöglichkeiten für viele Krankheiten, wie neurologische Störungen oder durch Abbau von Photorezeptoren verursachte Blindheit.

In der vorliegenden Arbeit wurden verschiedene optogenetische Werkzeuge, basierend auf Kaliumkanälen, entwickelt, optimiert und auf ihre Funktionalität untersucht. Das Ziel war die Expression GFP-markierter Kaliumkanäle in der Plasmamembran oder den Mitochondrien von Säugerzellen. In der Plasmamembran können Kaliumkanäle als optogenetische Silencer fungieren, da sie die Zellen hyperpolarisieren und damit das Feuern von Aktionspotentialen verhindern. Um diese Effekte zu untersuchen, wurden zwei Kaliumkanäle verwendet: $Kcv_{PBCV\text{-}1}$ und Kcv_{NTS}. Bei einer lichtinduzierten Expression von Kaliumkanälen in den Mitochondrien ermöglicht die induzierbare Depolarisation die Untersuchung der Wirkung von Kaliumkanälen in den Mitochondrien. Für die Untersuchung dieser Fragestellung wurden die Kaliumkanäle Kesv und $Kmpv_{12T}$ verwendet.

Um die Sortierung der vier verwendeten Kaliumkanäle zu optimieren, wurden zwei verschiedene Wege zur Maximierung der Sortierungseffizienz in Säugerzellen angewendet. Die Optimierung der verwendeten Codone, durch Austausch von Seltenen gegen häufig verwendete Codone, führte zu einer verbesserten Sortierung der Kanäle in die Mitochondrien. Vor allem bei Kesv führte dieses Vorgehen zu einer effektiveren Sortierung in die Mitochondrien. Auch eine Verkürzung des Proteinlinkers zwischen Kanal und GFP führte zu einer vermehrten Sortierung von Kesv in die Mitochondrien. Die Kombination dieser beiden Herangehensweisen – ein codonoptimierter Kanal in Verbindung mit einem verkürzten Linker – führte zu einer hundertprozentigen Sortierung von Kesv in die Mitochondrien. Der positive Effekt dieser beiden Herangehensweisen konnte in sechs verschiedenen Säugerzelllinien nachgewiesen werden und legt damit einen generellen Sortierungsmechanismus in Säugerzellen nahe. Für den an die Plasmamembran sortierten Kanal $Kcv_{PBCV\text{-}1}$ konnte kein Effekt von Codonoptimierung auf die Sortierungseffizienz nachgewiesen werden. Im Unterschied zu den mitochondrialen Kanälen, ist für eine optimale Sortierung der an der Plasmamembran exprimierten Kanäle ein niedriges Expressionslevel von Vorteil.

Für das Design eines optogenetischen Tools zur kurzzeitigen Depolarisation der Mitochondrien wurden verschiedene Änderungen am bestehenden lichtschaltbaren Kaliumkanal BLINK1 vorgenommen. Durch das Hinzufügen von sechs kanonischen mitochondrialen Sortierungssignalen am N-Terminus konnte eine effektive Sortierung des Kanals an die Mitochondrien erreicht werden. Die funktionellen Eingenschaften dieses Konstrukts müssen noch überprüft werden.

In einer alternativen Strategie wurden optogenetische Werkzeuge zur Langzeitaktivierung von Kaliumkanälen in der Plasmamembran oder den Mitochondrien entwickelt. In diesem Fall wurden zwei verschiedene lichtinduzierbare Genexpressionssysteme eingesetzt, um die Expression geeigneter Kaliumkanäle durch Licht zu regulieren. Der erste Ansatz basierte auf der Dimerisierung der bakteriellen *Light-Oxygen-Voltage*-Domäne aus *Erythrobacter litoralis* (EL222). Das zweite System basierte auf der lichtgesteuerten Interaktion von *Cryptochrome* 2 (CRY2) mit seinem Interaktionspartner CIB1.

In diesen Experimenten wurde die Expression eines GFP-markierten Kaliumkanals unter Kontrolle des EL222-Systems untersucht. Anhand der Intensität des GFP-Signals in den transfizierten Zellen wurde deutlich, dass der Kanal bereits im Dunkeln signifikant exprimiert wurde und eine sehr hohe Lichtintensität (120 μE für 16 Stunden) benötigte, um die Expression über das Dunkelniveau zu heben. Aufgrund dieser Kombination aus unspezifischer Leck-Expression im Dunkeln und hohem Lichtbedarf wurde das EL222-System nicht weiter untersucht.

In einem alternativen System wurde die Kaliumkanalexpression durch das Blaulicht-induzierte Rezeptorsystem CRY2/CIB1 aus *Arabidopsis thaliana* kontrolliert. Dieses lichtempfindliche Transkriptionssystem erwies sich als wirksam für die lichtinduzierbare Kaliumkanalexpression. Es benötigte sehr niedrige Lichtintensitäten (6 μE für 1 Stunde) oder kurze Belichtungszeiten mit höherer Lichtintensität für eine robuste Expression des Kandidatenkanals. Ein 5-Sekunden-Impuls von 120 μE war bereits ausreichend für eine maximale Stimulation der Kanalexpression. Die unspezifische Expression des Kanals im Dunkeln lag kaum über dem Detektionsminimum. Es war auch möglich, die Handhabung des Systems zu vereinfachen, indem alle drei notwendigen Komponenten (CRY2, CIB1, Kaliumkanal) in einen Expressionsvektor kloniert wurden, ohne die Wirksamkeit des Systems zu beeinträchtigen. Eine Stunde gepulstes Licht (6 μE) war ausreichend, um eine Stunde nach der Lichtstimulation die volle Aktivierung der Kanalexpression zu erreichen.

Das CRY2 CIB1-System wurde in verschiedenen funktionellen Assays untersucht. Die Eigenschaften von Kanälen, die an der Plasmamembran lichtabhängig exprimiert wurden, wurden durch *whole-cell* Patch-Clamp-Messungen bestätigt. Die Daten zeigen, dass die Kanäle, die unter Kontrolle des CRY2 CIB1-Systems exprimiert wurden, die Plasmamembran erreichten und dort die gleichen funktionellen Eigenschaften wie die konstitutiv exprimierten Kontrollkanäle zeigten.

Die Funktionalität der Kanäle, die in der inneren Mitochondrienmembran exprimiert werden, wurde sowohl in planaren *lipid bilayer* Experimenten, als auch durch eine Reihe von Mikroskopie-Assays

untersucht. Durch die Verwendung von Fluoreszenzreportern zur Untersuchung der mitochondrialen Membranspannung und der mitochondrialen Kalziumkonzentration konnte gezeigt werden, dass die Expression von mitochondrialen Kaliumkanälen unter Kontrolle des CRY2 CIB1-Systems eine effektive Depolarisierung dieser Organellen bewirkt. Auch der mitochondrialen Kalziumspiegel zeigte eine Verringerung, eine Induktion von Apoptose wurde aber nicht beobachtet.

Derzeit werden die CRY2 CIB1-Konstrukte *in vivo* funktionellen Tests unterzogen, um zu untersuchen, ob sie die Entwicklung von Zebrafischlarven beeinflussen, wenn sie in verschiedenen Organsystemen exprimiert werden.

1. General introduction

1.1. Optogenetics

For the detailed study of processes in excitable cells, tissues and animal models, researchers were constantly searching for genetically encoded tools that allowed generation or silencing of action potentials, control of protein levels and other metabolic processes with high spatio-temporal resolution (Deisseroth, 2011; Mühlhäuser et al., 2017). The idea of light being the optimal activator for these tools arose already in 1979 (Crick, 1979, 1999) and hence the search for photoactivatable molecules which could be turned into optogenetic tools to study cellular function began.

The building blocks for these tools are found in plants or photosynthetic bacteria and archaea, where they play important roles in phototaxis. Some of the plant-proteins used in optogenetic tools today were already discovered in the 1970s, like bacteriorhodopsin (BR) (Oesterhelt and Stoeckenius, 1971) and halorhodopsin (HR) (Lanyi and MacDonald, 1976). Light-oxygen-voltage (LOV) proteins (Christie et al., 1999) and cryptochromes (Ahmad and Cashmore, 1993) were discovered in the 1990s. But only the discovery of channelrhodopsin in 2002 by Nagel and coworkers (Nagel et al., 2002) marked the beginning of optogenetic tool development.

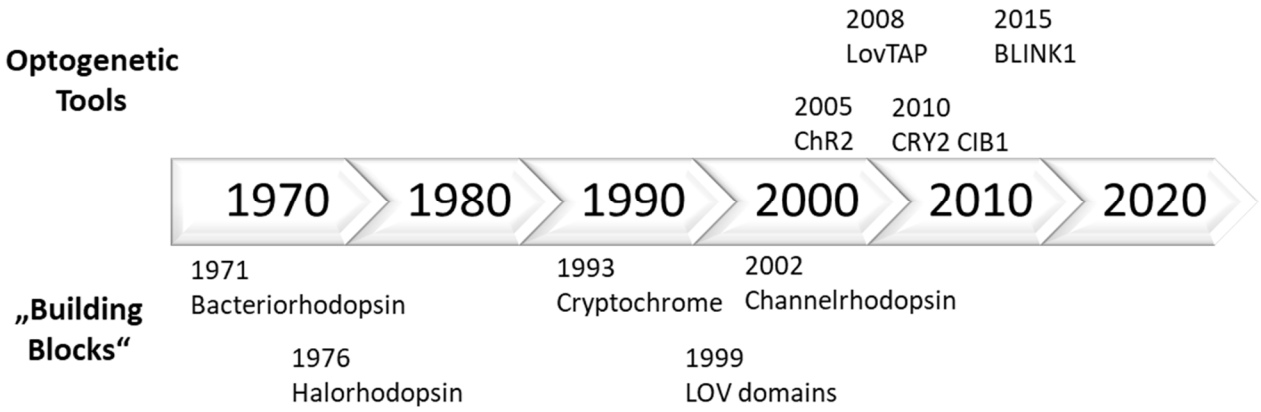

Fig. 1: Timescale of discovery of the building blocks and publication of selected optogenetic tools

In the lower row, the discovery of the most important plant proteins used for optogenetic tool design are depicted. In the upper row, selected optogenetic tools are shown.

From the timeline in Fig. 1, it becomes clear that only three years after the first description of Channelrhodopsin, the first optogenetic tool was designed. Boyden an coworkers showed that ChR2 was able to induce action-potential-spiking when illuminated with blue light pulses (Boyden et al., 2005). The publication of the first LOV-based optogenetic tool occurred in 2008 (Strickland et al., 2008), demonstrating light-induced allosteric coupling and DNA binding. The first optogenetic G-protein coupled receptor (GPCR) was published in 2009. Airan and coworkers demonstrated that optoXRs can control receptor-initiated biochemical signaling pathways in a light-dependent manner (Airan et al., 2009). In 2010 the first set of cryptochrome-based optogenetic tools was designed by Kennedy and coworkers, allowing both the light-inducible dimerization of split proteins as well as their translocation (Kennedy et al., 2010). The first light-gated potassium channel was published in 2015 by Cosentino and coworkers. BLINK1 is based on a rational design approach, rendering a minimal viral potassium channel light gated by its fusion to an asLOV domain (Cosentino et al., 2015).
Until today, there are many more optogenetic tools than the ones shown in Fig. 1, but it becomes clear that optogenetics is a fast emerging field which occurred only fifteen years ago and by now already includes a vast array of tools for many applications in cell biology (Mühlhäuser et al., 2017; Polesskaya et al., 2018), neurology (Boyden, 2011), developmental biology (Fenno et al., 2011; Kushibiki and Ishihara, 2018) and medical research (Agus and Janovjak, 2017; Zhang and Cohen, 2017).
In general, optogenetic actuators can be divided in two groups: the opsin-based tools in which the reaction to illumination occurs within the actuator domain, and the modular photoactuators, where a light-sensitive molecule undergoes a conformational change which is in turn conveyed to the effector domain. These two groups will be discussed in more detail in the next two chapters.

1.1.1. Opsin-based optogenetic tools

Bacteriorhodopsins are retinal containing transmembrane proteins with seven transmembrane helices found in archaeal halophiles (Oesterhelt and Stoeckenius, 1971). In the halophile bacteria they serve as light sensors and are crucial for phototaxis (Bogomolni and Spudich, 1982). Upon activation they work as proton pumps, thereby hyperpolarizing the cells (Fig. 2).
Halorhodopsins also offer a possibility to hyperpolarize cells as they act as chloride pumps upon light-induced activation (Zhang et al., 2007) (Fig. 2). A shortcoming of both Bacterio- and Halorhodopsin as optogenetic tools are their small photocurrents, as they are both pumps and not ion channels. This shortcoming was overcome more recently with the discovery of a cruxhalorhodopsin from *Halobacterium salinarum* (Jaws). Jaws shows three times higher chloride currents upon light-stimulation, compared to other halorhodopsins, and offers the additional advantage of its being activated by red light (635 nm).

This allows non-invasive stimulation of deeper tissue layers. It has already been established successfully as an optogenetic silencing tool in free moving mice (Chuong et al., 2014).

Channelrhodopsins (ChRs) were the last group of microbial opsins to be discovered (Nagel et al., 2002), but they have been studied and used far more excessively than any other photoactuator in optogenetics. Wildtype ChRs were applied successfully to induce action potentials in cultured neurons (Boyden et al., 2005), *C. elegans* (Nagel et al., 2005) and drosophila (Lima and Miesenböck, 2005). Upon illumination with 470 nm blue light, the co-factor retinal, an organic molecule related to vitamin A, isomerizes from its all-trans to the 13-cis conformation (Ullrich et al., 2013). This isomerization of retinal causes a conformational change of the channelrhodopsin and its subsequent opening, leading to an influx of sodium and calcium and an efflux of potassium ions, which causes a depolarization of the plasma membrane (PM) (Bamann et al., 2008) (Fig. 2).

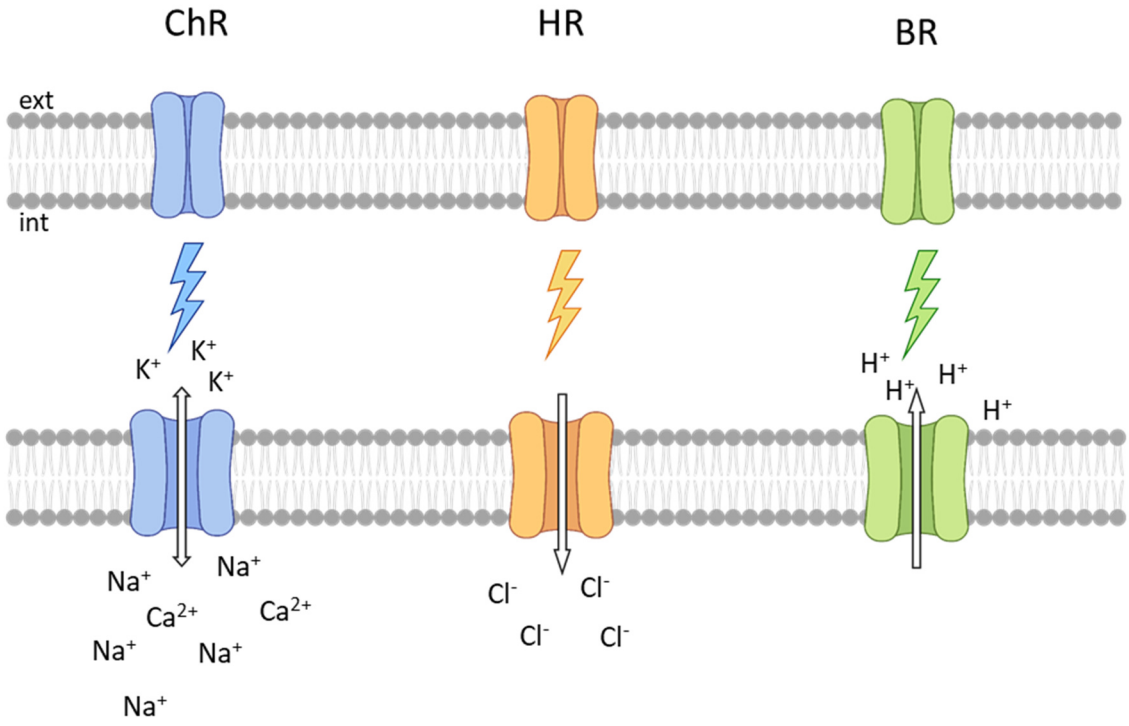

Fig. 2: Opsin-based optogenetic tools

Channelrhodopsins (ChR) conduct cations upon illumination and therefore activate excitable cells by depolarizing the membrane potential. Halorhodopsins conduct chloride ions upon activation, whereas Bacteriorhodopsins (BR) are light-activated proton pumps. These two are capable of silencing neural firing by inducing hyperpolarization. (Figure created with BioRender.com)

However the main drawbacks of wildtype ChRs are their low conductance, cytotoxicity in long-term applications and rapid inactivation kinetics (Feldbauer et al., 2009). To allow for more effective depolarization, multiple mutants with higher single channel currents and abducted voltage dependence have been designed (Berndt et al., 2011), as well as mutants with faster kinetics and enhanced light

sensitivity or a red-shifted activation spectrum (Lin et al., 2013; Klapoetke et al., 2014a). In most cases, these mutants are applied to induce action potentials in hippocampal neurons of free-moving mice (Bitzenhofer et al., 2017) or in human hippocampal slice cultures (Wiegert et al., 2017). In other applications, the possibility to affect intracellular calcium concentrations with ChRs is employed in order to monitor synaptic plasticity (Zhang and Oertner, 2007) or insulin secretion in pancreatic β-cells. To control insulin secretion and blood glucose homeostasis with light, ChR was expressed in pancreatic β-cells of free moving diabetic mice. Upon blue-light illumination, calcium levels increased, triggering insulin secretion and in consequence a decrease in blood glucose levels (Kushibiki et al., 2015).
To allow for optogenetic silencing of excitable cells, the ion selectivity of ChR was reversed to generate a light-inducible chloride channel (ChloC) (Wietek et al., 2014) which has been demonstrated to silence neural firing *in vivo* (Wietek et al., 2015). The discovery of another set of ChRs, found in the algae *Guillardia theta*, opened up another possibility to hyperpolarize cells with ChRs. These naturally occurring anion channelrhodopsins (ACRs) conduct chloride upon activation with blue or green light. In mammalian cell culture, they showed large steady state currents and high light sensitivity (Govorunova et al., 2015).

The chance to regulate neuronal circuits with high spatio-temporal control offers entirely new possibilities in the treatment of neurological disorders like epilepsy, depression or Parkinson's disease (Kaemmerer, 2017). One of the most common neurological disorders is epilepsy, which currently affects more than 60 million people (Ngugi et al., 2011). The underlying factor causing epilepsy is an imbalance between excitation and inhibition which tends towards excitation, causing excessive neural firing. Therefore, there are two basic ways to interfere with epileptiform discharges: downregulation of excitatory neurons or upregulation of inhibitory interneurons. With the availability of both hyper- and depolarizing optogenetic tools, both ways can be taken for the future treatment of epilepsy (Tønnesen et al., 2017). NpHR, a halorhodopsin chloride pump, has been used successfully to control hyperexcitability and prevent epileptiform discharges in both human hippocampal slice cultures (Tonnesen et al., 2009) and free moving mice (Wykes et al., 2012). NpHR was also able to terminate electrographic and behavioral seizures, induced by cortical stroke, in free moving rats if expressed in central neurons of the thalamus (Paz et al., 2013). First proof of principle experiments have also been conducted in free moving sheep with different HRs and ChRs (Kaemmerer, 2017).
The potential to treat depression and addictive behavior by optogenetic stimulation of the dopaminergic neurons in the reward center of the midbrain is the object of ongoing research (Biselli et al., 2019). By specifically inhibiting neurons, using NpHR, projecting from the ventral tegmental area to the nucleus accumbens could induce resilience in mouse models susceptible to depression (Chaudhury et al., 2013). Another approach is to express ChR in the neurons of the medial prefrontal cortex and stimulate these

cells with light in mice exhibiting symptoms of depression. Optogenetically driven firing bursts and an antidepressant effect in behavior of the mice were reported (Covington et al., 2010). There are other approaches to treat depression by optogenetic activation or inhibition in vivo, most studies are conducted in rodent models (Muir et al., 2019).

The most advanced field of optogenetic applications is associated to vision restoration in patients with retinitis pigmentosa. Retinitis pigmentosa includes multiple hereditary diseases, leading to the degeneration of rod and cone opsins in the retina and causing progressive vision impairment in patients, culminating in blindness (Hartong et al., 2006). To overcome the loss of vision caused by the degenerated opsins the deeper layers of the retina are all potential targets for optogenetic tools to reestablish light perception (Busskamp et al., 2012). In healthy retinas, an increase in light intensity is transduced as a depolarization of the photoreceptors, whereas lower light intensities cause hyperpolarization. This activates either ON- or OFF-bipolar cells in the outer plexiform layer. The bipolar cells in turn form excitatory synapses in the inner plexiform layer with ganglion cells (Fig. 3) (Baden et al., 2020).

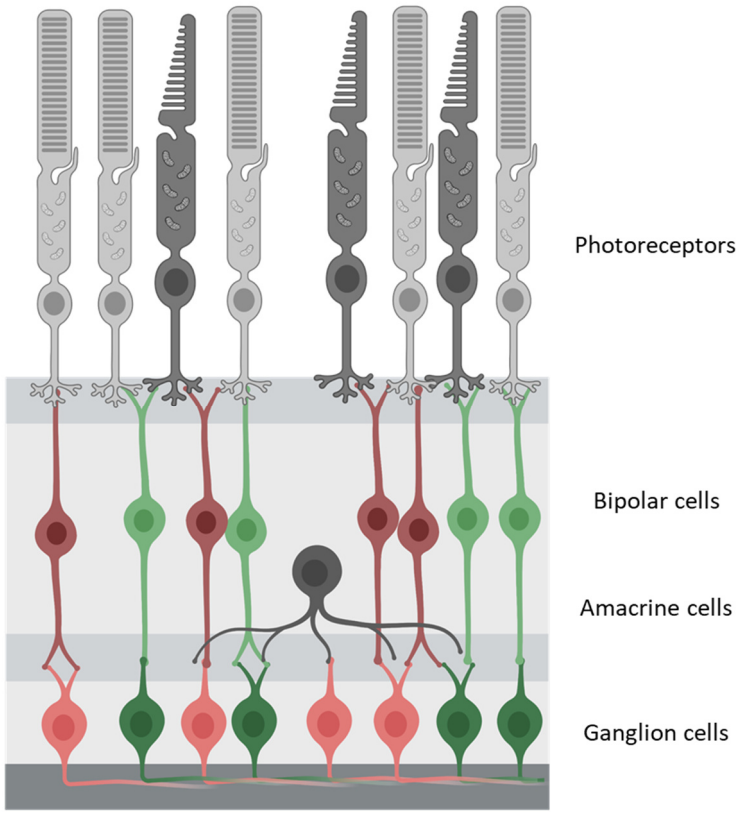

Fig. 3: Simplified schematic representation of the healthy retina

Rods (light grey) and cones (dark grey) project to ON- (green) and OFF- (red) bipolar cells. ON bipolar cells are activated by an increase and OFF-bipolar cells are activated by a decrease in light intensity. In the inner plexiform layer, the axon terminals of the bipolar cells project to the ganglion cells, forming an excitatory synapse. Their interaction is regulated by inhibitory amacrine cells. (Figure created with BioRender.com)

One possible optogenetic approach for vision restoration is the expression of either a depolarizing or hyperpolarizing opsin under control of an ubiquitous promotor in all retinal cell types (Bi et al., 2006). This has been achieved with both ChR2 (Tomita et al., 2010) and HR (Kamar et al., 2020) in rodent model systems, where it induced light-activated spiking and restored patterned vision. To allow for deeper tissue penetration, the red-shifted ChR variant ReaChR has been successfully expressed in mice, macaques and cultured human retinas (Sengupta et al., 2016). From clinical trials in patients who were transplanted with an electronic prosthesis, it is already known that electric stimulation of the retinal cells without discriminating between different cell types enabled the patients to recognize letters and outlines of objects (Stingl et al., 2015; Luo and da Cruz, 2016).

To improve the quality of the restored vision, it is necessary to target individual cell types to retain the processing features of the retina (Klapper et al., 2016). Targeted expression of ChR2 in ON-bipolar cells has the advantage of specific reactivation of the depolarizing ON-pathway, without overriding hyperpolarizing signals from OFF-bipolar cells and allowing for improved vision (Lagali et al., 2008; Macé et al., 2015). Ganglion cells are another important target to treat degenerative retinal diseases, as they undergo the least remodeling during the degeneration of the retina (Marc et al., 2003). The introduction of depolarizing optogenes turns the ON- and OFF-ganglion cells into ON channels, projecting only ON-signals to the cortex. However, the expression of channelrhodopsin in ganglion cells has been shown to restore basic vision in rodent models (Thyagarajan et al., 2010; Pan et al., 2014). To allow for both ON and OFF signals to be propagated to the visual cortex, ChR and HR have been expressed in both ON and OFF-ganglion cells respectively, allowing to restore projection of both ON and OFF responses in free moving mice (Zhang et al., 2009).

Currently, two phase I/II clinical trials for optogenetic restoration of vision are registered, both in their recruiting stages (clinicaltrials.gov, NCT02556736 and NCT03326336). The first study introduces channelrhodopsin into the retina by intravitreous injection. The second study combines the transfection of retinal cells with the optimized channelrhodopsin ChrimsonR (Klapoetke et al., 2014b) under control of an ubiquitous promotor with visual interface stimulating glasses to amplify external visual stimuli.

1.1.2. Modular photoactuators

Apart from the optogenetic applications in neurobiology and other excitable cells, optogenetic tools are also useful to study second-messenger cascades and cell signaling (Beyer et al., 2015), induce gene expression (Muller et al., 2015; Yamada et al., 2020) or control protein activity (Liu and Tucker, 2017). For these applications, a second class of optogenetic molecules are applicable: the modular photoactuators, which interact with an effector domain of choice as a reaction to light-activation

(Shcherbakova et al., 2015). There are a whole array of naturally occurring photoactuators, most of these proteins were found in higher plants and bacteria and some in fungi, their activation wavelength spanning the whole range of visible light, from far-red to blue light activated photoreceptors (Endo and Ozawa, 2017).

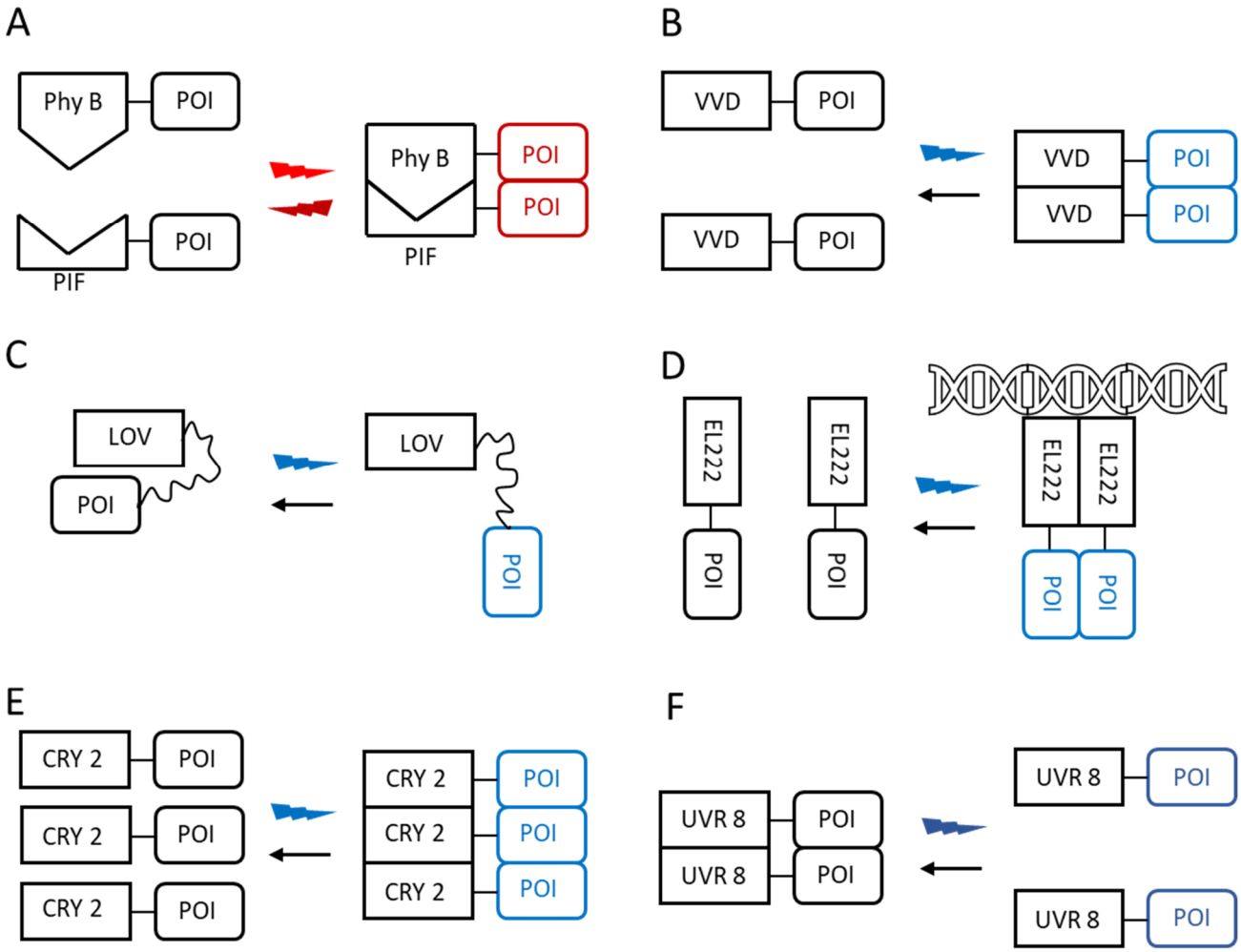

Fig. 4: Light-inducible changes in modular photoactivators

(A) Heterodimerization of two different domains can be found in phytochromes like Phy B / PIF and BphP1 / PpsR2, cryptochromes like CRY2 / CIB1, AsLOV-derived tools like iLID or TULIP and the UV-activated photoreceptor UVR8 / COP1. **(B)** Light-induced homodimerization is the mode of action of the bacterial LOV-domains VVD and YtvA. **(C)** Intramolecular conformational changes occur upon illumination in AsLOV, AtLOV and BcLOV4. **(D)** In EL222, homodimerization and subsequent DNA binding occur upon illumination. **(E)** CRY2 homooligomerizes upon illumination. **(F)** dissociation of homodimers occurs upon illumination with UV-light in UVR8.

Plant phytochromes are converted to their active form by red light and can be converted back to its inactive state with far-red light (Rockwell and Lagarias, 2010). They consist of a light-sensing N-terminal domain containing the bilin chromophore, and the C-terminal dimerization domain, mainly comprising the highly conserved PAS-GAF-PHY domains (Nagatani, 2010; Burgie and Vierstra, 2014). Light-activation of plant phytochromes (Phy) mediates heterodimerization with Phytochrome-interacting factors (PIF) (Pham et al., 2018) (Fig. 4 A), and subsequent translocation to the nucleus where they initiate cGMP-mediated second-messenger cascades regulating expression of different genes important for photomorphogenesis (Li et al., 2011; Legris et al., 2019).

Plant phytochromes have been employed as optogenetic tools in developmental and cell biology. One example is CreLite, a light inducible split-Cre system for tissue-specific expression of fluorescent reporters in zebrafish embryos (Yen et al., 2019). In mammalian cells, phytochromes from *Arabidopsis thaliana* were applied to influence cell morphology, either by mediating light-inducible cell-matrix-interactions (Baaske et al., 2019) or by controlling the actin cytoskeleton with light (Levskaya et al., 2009).

Bacteriophytochromes follow the same molecular mechanisms as plant phytochromes, enabling phototaxis in bacteria (Gourinchas et al., 2019). This regulation of enzymatic cascades has been used in multiple optogenetic tools (Piatkevich et al., 2013). The bacterial phytochrome BphG1 from *Rhodobacter sphaeroides* served as a template to design a light-regulated adenylate cyclase (Ryu et al., 2014; Fomicheva et al., 2019). BphP from *Deinococcus radiodurans*, in combination with the effector module of *Homo sapiens* phosphodiesterase 2A, was engineered into a photoswitchable phosphodiesterase which upregulates hydrolysis of cAMP and cGMP upon red-light illumination and also allows for their downregulation upon illumination with far-red light (Gasser et al., 2014). BphP combined with a guanylate/adenylate cyclase allowed for light-inducible changes in locomotive behavior of *Caenorhabditis elegans* by increasing the cyclase-activity upon light-activation (Etzl et al., 2018).

LOV domains are the light-oxygen-voltage sensing proteins in plants, controlling flowering and circadian clock mechanisms (Demarsy and Fankhauser, 2009). The light-sensing cofactor are flavin-mononucleotides (Kasahara et al., 2002) which induce homodimerization (VVD, YtvA) (Fig. 4 B) intramolecular conformational changes (e.g. AsLOV, AtLOV) (Fig. 4 C), homodimerization and subsequent DNA-binding (e.g. EL222) (Fig. 4 D) or light-induced dissociation of dimers (RsLOV) (Fig. 4 F) (Fraikin et al., 2015; Pudasaini et al., 2015).

The conformational change of AsLOV, caused by the blue-light induced unfolding of the Jα helix, can be applied to uncage effector domains or unmasking binding motifs (Lungu et al., 2012), thereby controlling various cellular processes (Christie et al., 2012a). The GTPase Rac1 has been rendered light-activatable by fusing it to the AsLOV domain in a way that allows the Jα to sterically block the active site

in darkness, but unblocking it upon illumination. This approach allows for light-inducible control of cell motility, as Rac1 is an important factor in the modulation of the action cytoskeleton (Wu et al., 2009). Also utilizing the conformational changes of AsLOV, Strickland and coworkers designed a light-inducible trp repressor, which binds DNA upon illumination, thereby protecting it from nuclease digestion (Strickland et al., 2008). Other tools designed with AsLOV are the improved light-induced dimer (iLID) (Guntas et al., 2015) and tunable light-controlled protein tags (TULIPs) (Strickland et al., 2012) which both allow the light-inducible dimerization of proteins. By anchoring the Jα helix of AsLOV in the plasma membrane and fusing the LOV domain to a minimal potassium channel, the light-gated potassium channel BLINK1 has been generated (Cosentino et al., 2015) (see also chapter 4.1) which has been applied to influence stomatal opening and closing to improve growth and minimize water loss due to transpiration (Papanatsiou et al., 2019).

Another LOV domain, EL222 which has been found in *Erythrobacter litoralis* (Yurkov et al., 1994), homodimerizes upon illumination and subsequently binds DNA (Fig. 4 C) (Zoltowski et al., 2013). Its light-inducible DNA-binding properties make it a useful tool for optogenetic induction of gene expression, which has already been achieved by various research groups. Motta-Mena and coworkers expressed a luciferase reporter system in mammalian cell lines and zebrafish embryos (Motta-Mena et al., 2014) (see also chapter 5.1). Another approach was to engineer a EL222-based light-inducible repressor, which downregulates protein levels upon illumination (Baaske et al., 2018). More recently, EL222 has been applied for optogenetic expression of transcription factor EB, which induces autophagy of tau protein. The aggregation of tau protein in neuronal cells has been shown to play an important role in the pathogenesis of Alzheimer's disease (Spillantini and Goedert, 1998) and this new optogenetic tool offers the chance to reduce the overexpression of tau protein, potentially slowing the progress of Alzheimer's (Binder et al., 2019).

Another blue-light activated plant protein that has been applied for optogenetic tool development is cryptochrome 2 (CRY2) from *Arabidopsis thaliana* (Ahmad and Cashmore, 1993). They comprise the N-terminal photolyase-homologous-region (PHR) which binds the chromophore flavin adenine dinucleotide (FAD) and the CRY C-terminal extension (CCE) (Yu et al., 2010). After photoexcitation, the cryptochromes adopt an open conformation allowing interaction with their interacting partners, e.g. CIB1 (Liu et al., 2008; Liu et al., 2013). However CRY2 also tends to form not only heterodimers with its interacting factors (Fig. 4 A), but also forms homooligomers (Che et al., 2015) (Fig. 4 E).

Heterodimerization of CRY2 and CIB1 has been applied to induce transcription of various target genes with light (Taslimi et al., 2016; Pathak et al., 2017) (see also chapter 6.1), to investigate transcription dynamics (Rademacher et al., 2017) or the spatio-temporal activities of mRNAs (Kim et al., 2020). By tethering CRY2 to the plasma membrane, the system also allows for light-inducible protein recruitment

to the plasma membrane (Benedetti et al., 2018). This approach allowed more recently to control the calcium influx in cultured mammalian cells – by tethering CRY2-ORAI to the plasma membrane. In this way, STIM-CIB1 could be recruited to the plasma membrane upon illumination. This led to the formation of ER-PM junctions and subsequently to the assembly of functional CRAC channels (Prakriya, 2009), thereby inducing calcium flux (Ma et al., 2020). By recruiting proteins of the apoptotic pathway to uveal tumor cells harnessing the light-induced dimerization of CRY2 and CIB1, Zhang and coworkers were able to inhibit tumor growth in cultured uveal cells by targeted induction of apoptosis (Zhang et al., 2019).

Homooligomerization of CRY2 gave rise to tools studying FAK, ß-catenin-signaling and provided a model for amyotrophic lateral sclerosis (ALS). Controlling endo- and exocytosis by activation of the ß-catenin pathway was one of the first applications of CRY2-clustering (Bugaj et al., 2013). More recently, the design of optoFAK was reported. FAK controls cell proliferation, motility and adhesion by reacting to mechanical stress and integrin signaling by activating downstream effector signaling cascades (Schaepfer et al., 1999; Mitra et al., 2005). OptoFAK can be activated independently of physiological stimuli and effectively activates downstream signaling (Hörner et al., 2018). Two tools with enhanced tendency for oligomerization were designed, CRYclust (Park et al., 2017) and CRYolig (Taslimi et al., 2014), allowing for faster and more effective protein clustering. CRYolig was applied as a template to design optoTDP43 (Mann et al., 2019), which offers a model system for amyotrophic lateral sclerosis (ALS). One of the most prominent features of ALS is the accumulation of TDP43 into large clusters which are neurotoxic and cause neuronal degradation (Kiernan et al., 2011). OptoTDP43 allows for light-inducible formation of TDP43-clusters in cultured neurons, generating an effective model for studying the exact effects of the clusters on cellular metabolism (Asakawa et al., 2020).

The UV-B sensor UVR8 found in *Arabidopsis thaliana* is yet another candidate system. It switches from homodimer to monomer upon illumination with 300 nm UV-B light. The UV-light disrupts π-interactions between an arginine and two tryptophan residues which serve as the chromophore leading to the dissociation of the dimer (Di Wu et al., 2012). In *Arabidopsis thaliana*, monomerization of UVR8 leads to its interaction with COP1 (Cloix et al., 2012), which induces a signal cascade inducing flavonoid biosynthesis (Kliebenstein et al., 2002; Tilbrook et al., 2013). Both the dissociation of the homodimer and the interaction with COP1 served as starting points for the design of optogenetic tools.

The dissociation of the UVR8/UVR8 homodimer was applied to study protein secretion in neurons, allowing precise monitoring of proteins trafficking throughout ER and Golgi to the plasma membrane (Chen et al., 2013a). In later experiments, this approach led to optogenetic chemokine secretion in leukocytes, thereby altering the behavior of neighboring cells and allowing exploration of cell-cell communication (Sarris et al., 2016).

The light-induced interaction of UVR8 and COP1 allowed for inducible protein-protein interactions. By fusing the two proteins, whose interaction was to be studied, to either UVR8 and COP1, they interacted upon illumination due to UVR8 / COP1-binding (Crefcoeur et al., 2013).
UVR8 proved to be useful in multi-wavelength approaches to optogenetically influence multiple genes in the same assay. One approach combined the fungal LOV-domain VVD with PhyB/PIF and UVR8/COP1 to induce expression of three angiogenetic genes in cultured mammalian cells (Müller et al., 2013; Müller et al., 2014).

The optogenetic tools described above were chosen as examples to illustrate the wide field of possible applications for both research and medical purposes.

1.2. Mitochondrial potassium channels

Mitochondrial potassium channels play an important role in the regulation of mitochondrial membrane potential, calcium homeostasis, mitochondrial matrix volume and respiration (Szewczyk et al., 2009). The channels found in both the outer mitochondrial membrane (OMM) and inner mitochondrial membrane (IMM) are structurally similar to those of the PM (Bednarczyk, 2009). The expression of potassium channels in the mitochondria strongly differs throughout tissues (Laskowski et al., 2016).

In the outer mitochondrial membrane, the only potassium channel described so far is the inward-rectifying potassium channel (Kir) (Fieni et al., 2010) (Fig. 5). Before the characterization of Kir in the OMM, it was assumed that this membrane is no barrier for potassium and that it enters the intermembrane space by passive diffusion (O'Rourke, 2007).

In the IMM, voltage-gated ($K_V1.3$), calcium-activated (BK_{Ca}, IK_{Ca}, SK_{Ca}), ATP-regulated (K_{ATP}) as well as acid-sensitive potassium channels (TASK-3) have been reported (Fig. 5) (Szabo and Zoratti, 2014). Their presence could be linked to several cellular processes, such as cytoprotection, induction of apoptotic pathways and proliferation (Szewczyk et al., 2009).

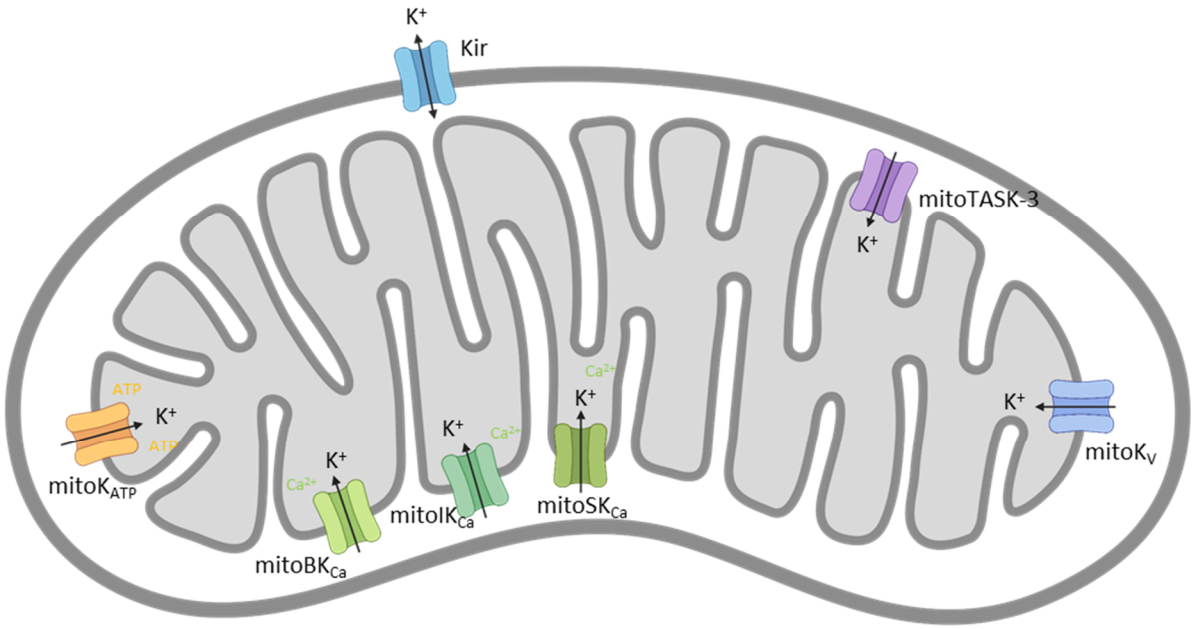

Fig. 5: Mitochondrial potassium channels

In the outer mitochondrial membrane, there are inward rectifying Kir channels. In the inner mitochondrial membrane, the ATP-regulated mitoK$_{ATP}$, the calcium-activated mitoBK$_{Ca}$, mitoIK$_{Ca}$ and mitoSK$_{Ca}$ as well as the acid-sensitive mitoTASK-3 and the voltage-gated mitoK$_V$ are expressed. (Figure created with BioRender.com)

The interaction of the voltage gated mitoK$_V$ channel with Bax, a proapoptotic protein, has been found to be an important step in the induction of apoptosis (Serrano-Albarrás et al., 2018). Knockdown mice which were not expressing Kv1.3 exhibited a resistance to apoptosis-inducing agents, which could be reverted by retransfection with Kv1.3 (Szabò et al., 2008). This important role in the apoptotic pathway makes mitoK$_V$ a viable target in cancer therapy. Selective inhibition of mitoK$_V$ induced apoptosis in melanoma and adenocarcinoma *in vivo* (Leanza et al., 2017; Prosdocimi et al., 2019).

Calcium-activated potassium channels in the IMM (mitoK$_{Ca}$) seem to be important for the regulation of mitochondrial ROS production, maintenance of the mitochondrial membrane potential, regulation of mitochondrial permeability transition pore (mPTP) opening and preservation of mitochondrial calcium homeostasis (Krabbendam et al., 2018). Due to these properties, an activation of mitoK$_{Ca}$ channels induces cytoprotection (Szewczyk et al., 2010). Cellular stress, like that which emerges during ischemia, induces elevated calcium levels, a higher probability of the opening of the mPTP and increased ROS production (Eltzschig and Eckle, 2011). The combination of these events induces mitochondrial dysfunction and triggers apoptosis. Opening of mitoK$_{Ca}$ channels depolarizes the mitochondria. This lowers ROS production and in turn reduces the opening probability of the mPTP (Cheng et al., 2008). These cytoprotective effects could be demonstrated in perfused rat hearts (Wojtovich et al., 2011; Testai et al., 2013) and hippocampal slice cultures (Piwonska et al., 2016).

Many reports also imply cytoprotective effects of the ATP-regulated mitochondrial potassium channel (mitoK$_{ATP}$). The molecular structure of this channel still remains elusive (Davidson et al., 2019). What is known so far is that cellular stress induces opening of mitoK$_{ATP}$ due to ATP-depletion (Checchetto et al., 2018). In this way, mitoK$_{ATP,}$ like mitoK$_{Ca}$, induces cytoprotection (Wang et al., 2011; Vishwakarma et al., 2019) and ischemic pre- and postconditioning in both cardiac and neural cells (Watanabe et al., 2008; Yokoyama et al., 2019).

The function of the acid-sensitive mitochondrial potassium channel mitoTASK-3 is yet unknown. First results suggest that it regulates apoptosis and tumorigenesis as well, but the exact mechanisms are not yet fully understood (Checchetto et al., 2018).

1.2.1. Optogenetic tools targeting mitochondrial function

Mitochondria play an important role in cellular metabolism (Giorgi et al., 2018b; Spinelli and Haigis, 2018) and stress responses (Busija et al., 2008; Tait and Green, 2010). Mitochondrial dysfunction causes a broad range of diseases from cardiac (Bonora et al., 2018) to neurodegenerative diseases (Devine and Kittler, 2018; Wu et al., 2019), stroke (Lo et al., 2003) and diabetes (Szendroedi et al., 2011; Nunnari and Suomalainen, 2012). This asks for a deeper insight into mitochondrial function and dysfunction and

an understanding of the functional implications on metabolism and pathophysiology (Chakrabarty et al., 2018). Optogenetics could provide ideal tools to address such unsolved questions concerning mitochondrial function.

The first optogenetic tool targeting mitochondria was designed in 2015 by van Bergeijk and coworkers. They applied the light inducible dimerization of the cryptochrome CRY2 with its interacting partner CIB1 to control mitochondrial motility and their redistribution within cells by light-dependently recruiting cytoskeletal motor proteins to the mitochondria (van Bergeijk et al., 2015). This approach was used to study the importance of mitochondrial redistribution to induce cytosolic calcium influx following depolarization (Griesche et al., 2019). Upon depolarization of β-cells, cortical mitochondria redistribute to the cell interior. There they form microdomains which induce calcium influx to the cytosol and as a consequence trigger insulin secretion. By light-inducible tethering of mitochondria to their cortical location, calcium influx and insulin secretion were disrupted.

Another approach based on optogenetic dimerizers was employed to addresses the mitochondria – ER contact sites (Shi et al., 2018). Based on iLID, a light-inducible dimerizer derived from AsLOV (Guntas et al., 2015), mitochondria – ER contacts could reversibly be induced with blue-light illumination. Mitochondria – ER contacts offer an important field of research, as they are involved in ROS and calcium signaling (Chakrabarti et al., 2018; Csordás et al., 2018), mitochondrial fusion and fission (Friedman et al., 2011; Lewis et al., 2016), autophagy (Marchi et al., 2014) and apoptosis (Prudent and McBride, 2017). Disruptions of mitochondria – ER contact sites have been implied to play a role in diseases related to both motor and sensory neurons, like Parkinson's disease (Gómez-Suaga et al., 2018) or amyotrophic lateral sclerosis (Bernard-Marissal et al., 2018).

The light-inducible dimerizer iLID has also been applied to study mitophagy. Mitophagy is the aggregation of damaged or aged mitochondria in autophagosomes and their subsequent degradation (Youle and Narendra, 2011). By light-inducible relocation of a pro-autophagy protein to the mitochondria, aggregation of mitochondria and mitophagy could be induced, without causing cell death (D'Acunzo et al., 2019).

So far, only three optogenetic tools were described to influence mitochondrial membrane potential. The light-activated proton pump from *Leptosphaeria maculans* (Mac) was fused to the inner mitochondrial membrane protein (IMMT1) to generate mitochondria-ON (Berry et al., 2020). This tool allows the light-dependent increase of the mitochondrial membrane potential. Hyperpolarization of the mitochondria led to increased ATP production in *Caenorhabditis elegans*. Further, the activation of mitochondria-ON under hypoxic conditions prevented cytoprotection by mitochondrial preconditioning.

Also, two channelrhodopsin-based tools were described to induce optogenetic depolarization of the mitochondria. Tkatch and coworkers fused six repeats of the MTS from cytochrome C oxidase VIII (COX8) to the N-terminus of ChR2 to target the opsin to the IMM (Tkatch et al., 2017). Blue-light

illumination of the construct caused reversible depolarization of the mitochondria and reduced mitochondrial calcium uptake. The second tool is based on channelrhodopsin as well; Ernst and coworkers fused the MTS of the ATP-binding cassette (ABC) transporter to ChR2 (Ernst et al., 2019). Upon illumination the mitochondria were depolarized. Whereas sustained illumination caused apoptosis, mild transient illumination led to cytoprotection by mitochondrial preconditioning.
Compared to the optogenetic tools targeted to the plasma membrane (see overview in chapter 1.1) light-inducible tools for the study of mitochondrial function are still scarce and research is still at an early stage.

1.3. Aim of this work

There are many optogenetic tools to address a wide range of physiological questions, but only a few optogenetic silencing tools based on potassium channels are available. The number of tools to manipulate mitochondrial membrane potential is even lower still. Inspired by the need of such tools, the aim of this work was to design modular potassium channel-based optogenetic tools targeted to either the PM or mitochondria. This should allow for either effective hyperpolarization of the PM or depolarization of the mitochondria.

In chapter 3, suitable potassium channels for expression at both the PM and in the IMM are characterized and their expression optimized. To enhance correct sorting of the channels, there will be placed special focus on codon optimization of the respective channels for expression in mammalian cells and on the length and properties of the peptide linker between the channel protein and its GFP-tag.

Chapter 4 outlines the rational design for targeting the light-gated potassium channel BLINK1 to the IMM. To achieve a shift in sorting from the PM to the IMM, targeting of the single components of BLINK1 has been analyzed. The potassium channel-module was exchanged for a potassium channel that is effectively sorted to the IMM and the initial design of BLINK1 was extended to include mitochondrial targeting signals.

Chapters 5 and 6 outline the design and optimization of a modular light-inducible expression system which allows expression of potassium channels either in the PM or in the IMM in a light-dependent manner. In this context, two optogenetic actuators will be tested and compared for their performance. The first one is based on a LOV-domain, the second on cryptochrome 2 and its interacting partner CIB1. In chapter 7, functional assays are established to test the new optogenetic tools designed in chapter 6. They include standard electrophysiological techniques, such as whole-cell patch clamp or planar lipid

bilayer measurements. The former experiments examine the expression of the channels in the PM. The latter examines the single channel properties of the protein which alters the permeability of the IMM, as well as microscopy assays to gain an insight into their influence on mitochondrial membrane potential, mitochondrial calcium and the induction of apoptosis.

In summary, the goal of this work was to design modular optogenetic tools which are based on potassium channels and allow for modulation of the membrane potential of both PM and mitochondria. A number of proof of concept experiments show that this design approach was successful.

2. Materials and methods

2.1. Chemicals and reagents

The chemicals and reagents used for the experiments in this work were purchased, unless stated otherwise, by the following suppliers: Merck (Darmstadt), Sigma-Aldrich (Taufkirchen), AppliChem (Darmstadt), Carl Roth (Karlsruhe), ThermoFisher (Langenselbold), Bio-Rad (München), Invitrogen (Karlsruhe).

2.2. Mutagenesis

For all the constructs used for microscopy or patch clamp experiments in HEK 293, Cos7, CHO, Hela and HaCaT cells, the standard cloning vector peGFP-N2 (BD Biosciences Clontech, Heidelberg) was used as backbone. For agrobacterium mediated transfection in *Nicotiana benthamiana* pCambia1300mRuby3 was taken as the backbone, for bilayer experiments pET24-dellac, and for *in vivo* experiments in zebrafish, pMnx1 was taken as the plasmid backbone. Representative plasmid maps of key constructs can be found in appendix 10.2. Cloning of all constructs used in this work was either done by standard restriction/ligation cloning (Cohen et al., 1973), overlap-extension PCR (OE PCR) (Horton et al., 1989; Heckman and Pease, 2007) or Gibson Assembly (Gibson et al., 2009). Site-directed mutagenesis (Ho et al., 1989) was used to generate point mutations. PCR for amplification was performed with either Phusion polymerase (Thermo Fisher, Langenselbold) or Q5 polymerase (NEB, Frankfurt am Main), PCR protocols were set up according to manufacturer's protocols. A full list of primers used in this work can be found in the appendix 10.3. Successful amplification was checked by loading the PCR products on agarose gel, performing standard agarose gel electrophoresis. Samples forming bands at the expected size of the fragment were purified by gel extraction with the Zymoclean Gel DNA Recovery Kit (Zymo Research, Freiburg) according to manufacturer's instructions. The purified DNA was used for heat shock transformation (Inoue et al., 1990) in competent DH5α. Colonies were screened for positive clones using colony PCR and the DNA purified with the ZR Plasmid Miniprep Kit Classic (Zymo Research, Freiburg). The plasmid DNA was subsequently sent in for sequencing either by Eurofins Genomics (Ebersberg) or by Microsynth Seqlab (Göttingen).

2.3. Cell lines, cell culture and transfection

Mammalian cell lines used in this work (HEK293, Cos7, CHO, Hela and HaCaT) were kept in standard media and splitted twice a week at 80 % confluency for stable cell culture. For transient transfection, the cells were splitted two to three days in advance to let them grow to 50 % confluency. For transfection, 3 μl of GeneJuice transfection reagent (Merck, Darmstadt) was mixed with 100 μl of transfection medium and 1 μg of plasmid DNA and incubated for 20 minutes before adding it dropwise to the cells. Experiments were performed 16 hours post-transfection to allow for optimal protein expression.
For the experiments in *Nicotiana benthamiana*, agrobacterium mediated transfection as described by Lerich and coworkers was performed (Lerich et al., 2011).

2.4. Blue light illumination setup and protocols

For illumination of cells, a custom-made illumination setup was designed with six 450 nm LEDs (Winger WEPRB3-S1 Power LED Star, 3W) arranged on a plate to fit under a standard 6-Well cell culture plate. To be able to tune illumination times the LEDs were attached to a timer that allowed application of light pulses of defined length on a second to minute timescale. To limit the application of such pulsed light protocols, an additional timer was put in place which allowed application of the light pulses over a defined period. Light intensities applied ranged from 6 to 120 μE.
To establish an optimal combination of light dose and application time for maximal light-induced gene expression whilst minimizing side effects of blue light, several protocols were established. The most frequently used protocols are depicted in Fig. 6.

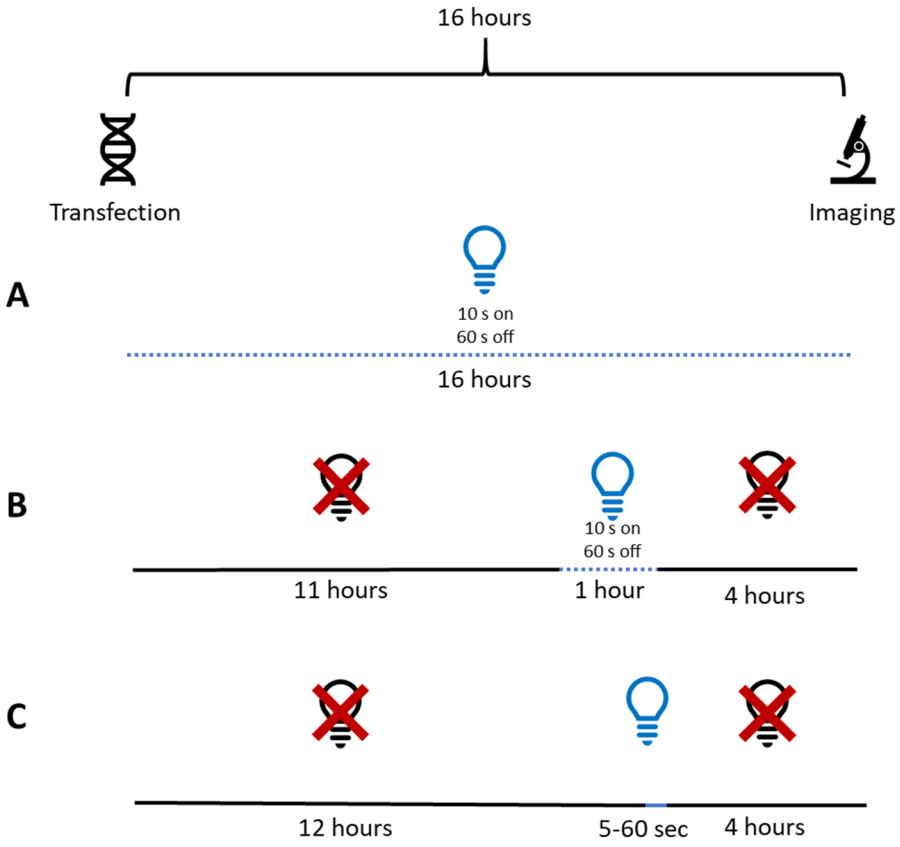

Fig. 6: Overview of the illumination protocols for the EL222 and the CRY2 CIB1 system

Indicated above is the time between transient transfection and execution of the various experiments which was in all cases kept constant at 16 hours. **(A)** Shows a protocol where the pulsed illumination with 10 seconds light and 60 seconds dark was applied for the whole 16 hours. **(B)** Depicts a protocol where the pulsed illumination is applied for only one hour, starting 11 hours post transfection. **(C)** Shows the single pulse protocols, where only one continuous light pulse is applied four hours prior to imaging.

2.5. Confocal microscopy

Confocal microscopy was performed either on Leica TCS SP or the Leica TCS SP5 II (Leica GmbH, Heidelberg, Germany) with PL APO 100,0x1,40 OIL UV or HCX PL APO 63,0x1,20 W CORR UV objectives. The frame average was set between 4 to 8 repeats, and the pinhole was adjusted to 1 airy disc. Depending on the properties of the fluorophores and the fluorescent dyes, argon (488 nm), krypton (568 nm) or helium-neon laser (632 nm) were used for excitation and emission was detected in a range of ±10 nm from the emission maximum of the respective dye or fluorescent protein.

Cells were seeded on glass coverslips and transfected as described in 2.3. Prior to imaging, the coverslips with the adherent cells were inserted in custom-made aluminum rings and covered with 500 μl of PBS.

2.6. Microscopy assays

Determination of the relative fluorescence intensity (RFI)

To determine the RFI of different samples, the microscope was adjusted to defined presets which allowed imaging of the samples with the same energy of the excitation laser. The only variable factor, which was adjusted depending of the brightness of the cell was the gain-factor. The gain was adjusted for each image to the optimal dynamic range of the detector. The optimal settings were checked using a lookup table (LUT) highlighting over- or undersaturated pixels. For the calculation of the RFI, the reciprocal value of the gain was multiplied by 1000, resulting in values from an RFI of 1, representing the detection limit of the confocal setup at a gain of 1000, to an RFI of 2, representing the brightest cells observable at a gain of 500.

Determination of the partial sorting

To determine the sorting efficiency of various constructs, the cells were imaged 16 hours post-transfection. Subsequently their sorting phenotype was determined manually, using either LAS AF Lite Software (Leica Microsystems GmbH, Wetzlar, Germany) or FIJI (Schindelin et al., 2012).

Determination of Pearson Correlation Coefficient (PCC) and Manders Coefficient (MC)

For calculating the correlation of two proteins, the Fiji plugin JACoP (Bolte and Cordelieres, 2006) was used. The two images that were to be compared, were loaded into the plugin and their PCC and thresholded MC values calculated.

To determine the correlation of the fluorescence of a potassium channel protein with that of a marker of a subcellular compartment of interest, either the marker plasmids COX8::mCherry for mitochondria and HDEL::mCherry (both addgene, Teddington, UK) for the ER, or the fluorescent dyes MitoTracker Red for the mitochondria or ERTracker Red (both ThermoFisher Scientific, Langenselbold, Germany) for the ER were used.

Subcellular localization assay

To ascertain the localization of the mitochondrial potassium channels in the inner mitochondrial membrane, a multistep-localization assay was adapted from Tkatch and coworkers (Tkatch et al., 2017). For this assay cells were seeded on poly-D-lysin coated coverslips 2 hours prior to transfection and imaged 16 hours post-transfection. One image was taken every minute during the entire assay. 5 minutes prior to imaging, cells were allowed to equilibrate in extracellular Ca^{2+} free medium (135 mM NaCl, 5 mM KCl, 1 mM $MgCl_2$, 0.4 mM KH_2PO_4, 10 mM Glucose and 20 mM Hepes, adjusted to pH 7.4).

For the first part of the assay, 20 μg/ml proteinase K was added to the extracellular medium and allowed to incubate for 2 minutes, then the medium was removed and replaced by intracellular Ca^{2+} free medium

(10 mM NaCl, 130 mM KCl, 1 mM $MgCl_2$, 1 mM KH_2PO_4, 2 mM succinic acid, and 20 mM Hepes, adjusted to pH 7.4) plus 0.01 % digitonin, which was allowed to incubate for 3 minutes. The medium was then removed and exchanged for intracellular medium plus 20 μg/ml proteinase K which was allowed to incubate for 2 minutes. The medium was removed again and exchanged for intracellular medium containing 0.1 mg/ml trypan blue.

For the second part of the assay, a fresh sample of cells was again allowed to equilibrate in extracellular medium for five minutes. The medium was removed and exchanged for intracellular medium containing 0.01 % digitonin which was allowed to incubate for 2 minutes. The medium was removed again and exchanged for intracellular medium containing 2.5 μg/ml alamethicin and incubated for 3 minutes. The solution was finally exchanged again for intracellular medium containing 0.1 mg/ml trypan blue.

Functional assays to asses mitochondrial membrane potential, mitochondrial calcium levels and apoptosis

To determine the mitochondrial membrane potential in transfected cells compared to untransfected cells, cells were transfected as described in 2.3 and incubated for 16 hours after transfection. Prior to imaging, cells were stained with 50 nM MitoTracker Red CMXRos (Thermo Fisher Scientific, Langenselbold, Germany) in 500 μl of PBS for five minutes. The staining solution was removed again, and the cells were washed with PBS and covered with 500 μl of PBS for subsequent imaging. To avoid artifacts resulting of irregular distribution of dye or differences in staining intensity, overview images were taken which included at least one transfected cell. For evaluation of the RFI value, the respective fluorescence of a transfected cell was compared only to that of its neighboring untransfected cells in the same image.

Mitochondrial calcium levels were determined by Rhod-2 AM (Thermo Fisher Scientific, Langenselbold, Germany). The cells were incubated for 15 minutes in 2 μM Rhod-2 AM diluted in 500 μl of PBS, washed in PBS after staining and covered in 500 μl PBS for subsequent imaging. Here again, only neighboring cells were compared in determining the RFI value of transfected and untransfected cells to avoid artifacts.

To assess induction of apoptosis, transfected cells were washed in PBS, and subsequently incubated for 15 minutes with Annexin V, Alexa Fluor 647 conjugate (Thermo Fisher Scientific, Langenselbold, Germany) in annexin-binding buffer (10 mM Hepes, 140 mM NaCl, and 2.5 mM $CaCl_2$, pH 7.4) in a ration of 1:10. The portion of apoptotic cells was evaluated from the ratio of apoptotic cells in both transfected and untransfected cells. As a positive control, 0.1 mM CCCP was added to untransfected cells and incubated for 15 minutes.

2.7. Total internal reflection (TIRF) microscopy

Single molecule setup

The single molecule detection setup is custom built and consists of a Nikon Eclipse Ti inverse microscope (Nikon Instruments Europe B.V., Amsterdam, Netherlands), with excitation lasers of 488 nm and 640 nm wavelength and an Andor iXon EMCCD camera (Oxford Instruments, Belfast, UK). The images were acquired using Micro-Manager 1.4 software (Edelstein et al., 2010; Edelstein et al., 2014).

Preparation of cells & Nappobac experiments

HEK293 cells were seeded and transfected as described in 2.3 and Nappobac (Guthmann, 2013) experiments were performed 16 hours later.

To ensure robust adhesion of the cells to the surface, which is necessary to allow subsequent osmotic shock and removal of the cell body, for examination of separated membrane patches the surface needs to be coated with poly-D-lysine (Kalish et al., 1978). Before coating, coverslips were cleaned by incubating them for 5 minutes in technical grade acetone. After drying, the coverslips were hydrophilized in a Diener zepto plasma cleaner (Diener electronic, Ebhausen, Germany) for 2 minutes (0.6 mbar, 40 kHz, 100 W) with water saturated air as process gas. After activation of the coverslips, they were coated in a spin coater (SPS Europe Spin coating, Putten, Netherlands) with 50 μl of poly-D-lysine (Sigma Aldrich, Schnelldorf, Germany) for 30 s at 500 rpm and 30 s at 3000 rpm.

The transfected cells were washed with PBS and disengaged from the culture dish with accutase. The cell-suspension was centrifuged for 4 minutes at 500 xg, resuspended in 1 ml PBS and placed on a poly-D-lysine coated coverslip. After allowing the cells to adhere for 10 minutes a hypotonic shock was performed by incubating the cells in ice-cold ddH_2O for 5 minutes. To remove all membrane parts not attached to the coverslip, 5 washing steps with fresh ice-cold ddH_2O were performed.

TIRF experiments & cluster analysis

To allow for easier localization of the membrane patches, they were dyed with Cell Mask Deep Red (ThermoFisher Scientific, Langenselbold, Germany) for 2 minutes prior to imaging. Samples were illuminated using total internal reflection fluorescence (TIRF) microscopy (Fish, 2009; Shashkova and Leake, 2017). The images were analyzed using the Fiji plugin ThunderSTORM (Ovesný et al., 2014) and an adapted custom written script by S. Paech (Paech, 2019).

2.8. Whole-cell patch clamp

For whole cell patch clamp measurements, HEK293 cells were cultured and transfected as described in chapter 2.3. Experiments were performed 16 hours after transfection to allow comparison between the optogenetic and electrophysiologic experiments, illumination protocols for light-induced expression of the channel proteins were performed as described in chapter 2.4.

Borosilicate patch pipettes (Tube Capillary, Melting point, 1.5-1.8 ×100 mm, Kimble Chase, Vineland, USA) were pulled using a PP 830 puller (Narishige, Japan) with pipette resistance between 3-7 MΩ. All measurements were conducted with standard bath solution (50 mM KCl, 120 mM mannitol, 1 mM $MgCl_2$, 1.8 mM $CaCl_2$ and 5 mM Hepes, adjusted to pH 7.4 with KOH and 330 mosmol/kg with mannitol) and pipette solution (130 mM D-gluconic acid, 10 mM NaCl, 5 mM Hepes, 5 mM EGTA, 0.1 mM GTP, 0.1 μM $CaCl_2$, 2 mM $MgCl_2$, 5 mM phosphocreatine adjusted to pH 7.4 with KOH and 330 mosmol/kg with mannitol, 2 mM ATP were added directly before use). Whole cell currents were recorded with an EPC-9 patch clamp amplifier (HEKA, Ludwigshafen, Germany) with a recording rate of 4 kHz using PatchMaster software (HEKA, Ludwigshafen, Germany). For analysis, FitMaster (HEKA, Ludwigshafen, Germany) was used and the data were exported to IgorPro 6 (Wave Metrics, Portland, OR, USA).

Using standard pulse protocols, the cells were clamped to an initial holding potential of 0 mV for 200 ms and subsequently to test-pulses of -80 mV to +120 mV for 1000 ms respectively. After each test pulse, the cells were clamped to a holding potential of -80 mV for 200 ms.

2.9. Planar lipid bilayer measurements

Protein expression and purification

The channel proteins for planar lipid bilayer experiments were cloned in the pET24-dellac plasmid, as described in chapter 2.2. Subsequent *in vitro* expression of the proteins was performed with the MembraneMax HN Protein Expression Kit (Invitrogen, Karlsbad, CA, USA) following manufacturer's instructions. Expression takes place in the presence of nanodiscs, ring-shaped scaffolding proteins surrounding DMPC (1,2-Dimyristoyl-sn-glycero-3-phosphcholine) membranes (Bayburt et al., 1998; Ritchie et al., 2009), in which the channel proteins insert to enable proper protein folding (Winterstein et al., 2018a). Nanodiscs contained multiple His-tags to allow for chromatographic purification with HisPur Ni-NTA spin columns (Thermo Scientific, Rockford, IL, USA) following manufacturer's instructions. The channel protein-containing nanodiscs were eluted in 250 mM imidazole in aqueous solution (Winterstein et al., 2018a).

Vertical lipid bilayer setup

All bilayer experiments were performed in a vertical lipid bilayer setup (IonoVation, Osnabrück, Germany), with recording chambers set up as described by Winterstein and coworkers (Winterstein et al., 2018a), in pure 1,2-diphytanoyl-sn-glycero-3-phosphocholine (DPhPC) membranes (Avanti Polar Lipids, Alabaster, AL, USA). For generation of the lipid bilayer, either the monolayer folding technique (Montal and Mueller, 1972) or the pseudo painting technique (Braun et al., 2014) were used. Measurements were performed in 100 mM KCl solution (pH 7, buffered with 10 mM Hepes) or 100 mM $CaCl_2$ solution. Single channel measurements were conducted with the equipment and settings described by Rauh and coworkers (Rauh et al., 2017). Recording of single-channel current traces was performed using PatchMaster (HEKA, Ludwigshafen, Germany) and for subsequent analysis the custom-made program KielPatch (http://www.zbm.uni-kiel.de/aghansen/software.html) was used.

3. Choice and optimization of suitable candidate channels for mitochondria- and PM-targeted expression

3.1. Codon usage bias and its influence on proteins

To determine the most promising potassium channel candidates which show the most effective sorting in mammalian cells, and which are therefore most suitable for the design of optogenetic tools, four viral potassium channels were examined on their sorting pattern in different cell types. To optimize sorting and expression of the candidate channels, they were codon optimized for expression in mammalian cells and their sorting effectiveness evaluated.

The genetic code is redundant, meaning that more than one amino acid is encoded by more than one codon. It became known already in 1987 that there is a codon usage bias in different organisms between rare and frequently used codons, which differs between species (Sharp and Li, 1987). Studies showing the functional effects of codon usage on proteins, and in effect on cellular metabolism, regulation and function appear only much more recently. So far, codon usage has been shown to play important roles in cotranslational folding, covalent modifications, secretion and regulation of protein expression levels (Chaney and Clark, 2015; Hanson and Coller, 2018).

Optimal codons enhance mRNA stability, leading to a prolonged half-life and thereby enhancing expression levels of the protein (Presnyak et al., 2015). This enhancement of protein expression is frequently used in heterologous expression, as the effects of the protein of interest are heightened by its higher abundance in the expression system (Fath et al., 2011). However, the optimized protein might differ in its properties from the wildtype one, as codon optimization can disrupt the functionality of proteins by inducing a different conformation. This has been demonstrated for the circadian clock protein FRQ (Zhou et al., 2013). It has been shown that rare codons often occur in clusters (Clarke and Clark, 2008) which regulate protein folding by locally slowing down translation (Chaney et al., 2017). A translational stalling induced by clusters of non-optimal codons often occurs between different subdomains of the protein, enhancing correct cotranslational folding (Yu et al., 2015; Jacobson and Clark, 2016). But not only protein folding, but also cotranslational protein sorting can be strongly affected by non-optimal codons downstream of the SRP binding-site (Pechmann et al., 2014).

So called “silent” mutations, which alter the sequence of the codon but do not affect the amino acid sequence, are implicated to be involved in many diseases (Fåhraeus et al., 2016). They can lead to aberrant splicing and act as driver mutations in various forms of cancer (Lamolle et al., 2006; Supek et al., 2014). An increase in protein level due to silent mutations has been described to induce melanoma (Gartner et al., 2013). Misfolding of proteins by altered elongation rates is also a suggested player in genesis of cystic fibrosis (Lazrak et al., 2013; Pizzo et al., 2015). In a different context, reduced mRNA stability, leading to lower protein levels is implied in various cognitive disorders (Duan et al., 2003).

Not only do changes in codon usage alter protein sorting and function and are involved in the genesis of various diseases, it has also been demonstrated that viruses adapt the codon usage bias of their host (Bahir et al., 2009), to enhance their virulence (Mueller et al., 2006) and even circumvent immune responses (Tindle, 2002).

3.1.1. Characterization of candidate channels for expression in the inner mitochondrial membrane

One of the main objectives of this work is the targeting of optogenetic tools to the inner mitochondrial membrane. The library of viral potassium channels contains two candidate channel proteins, which seem to be sorted to the mitochondria.

The first of these two channels is Kesv, a potassium channel which has been identified in the genome of *Ectocarpus siliculosus* virus 1 (Esv1) (Chen et al., 2005). Its mitochondrial sorting has been the object of several previous works (Balss et al., 2008; Engel, 2014; Charpuis et al., 2015).

In HEK293 cells, Kesv is sorted to the mitochondria in 61 % of cells expressing this protein with a GFP-tag. In 37.4 % the GFP fluorescence does not show a distinct localization of the channel in a compartment, but can be detected uniformly throughout the cell, in some cases also including the nucleus. A small portion of the channels is sorted to the ER (1.6 %) (Fig. 7 G). A representative image of a Kesv-expressing cell can be seen in Fig. 7 A-C. In this case the fluorescence appears throughout the entire cell. On this background, the distinct punctate structures of accumulated GFP fluorescence in the mitochondria are visible. This type of GFP fluorescence with clear accumulation of the signal in the mitochondria, but also high levels of background fluorescence in the cytosol is the predominant phenotype of Kesv sorting in mammalian cells.

A pronounced improvement in sorting efficiency could be achieved by codon-optimization of Kesv for expression in mammalian cells (Engel, 2016; Kithil, 2018). This new channel variant, $Kesv_{Opt}$, shows greatly enhanced sorting properties in mammalian cells. Fig. 7 G illustrates that $Kesv_{Opt}$ is sorted to the mitochondria in 100 % of the cells. Fig. 7 D-F shows a representative image of a HEK293 cell expressing $Kesv_{Opt}$. In this image, it is quite obvious that there is almost no undefined background fluorescence and that the codon optimized channel is sorted to the mitochondria much more effective than the wildtype.

The codon usage in the wildtype channel gene is not optimal for the expression in humans, its estimated mean codon optimality, determined with the codon calculator (Clarke and Clark, 2008), being 9.3±19 %. Hence it can be expected that translation may be relatively slow. The optimized channel has a much higher estimated codon optimality value of 93.4±9 %, indicating a faster translation of the nascent protein (Fig. 7 H). According to current publications, this increase in translational speed may

hinder binding of cotranslational sorting proteins, like the SRP to the nascent protein. This may in turn favor posttranslational sorting pathways (Pechmann et al., 2014), like the chaperone-mediated canonical pathway to the mitochondria (Chacinska et al., 2009).

Kesv carries two mitochondrial import signals. One of these was able to target GFP to the mitochondria, if expressed independently of the channel and fused to the fluorophore. Since the channel without this mitochondrial sorting signal surprisingly was still targeted to the mitochondria, the channel must contain a second non-canonical sorting signal (Balss, 2007). These two sorting signals together with the newly introduced codon optimization seem to be the optimal combination to target $Kesv_{Opt}$ to the mitochondria in a very robust and effective manner.

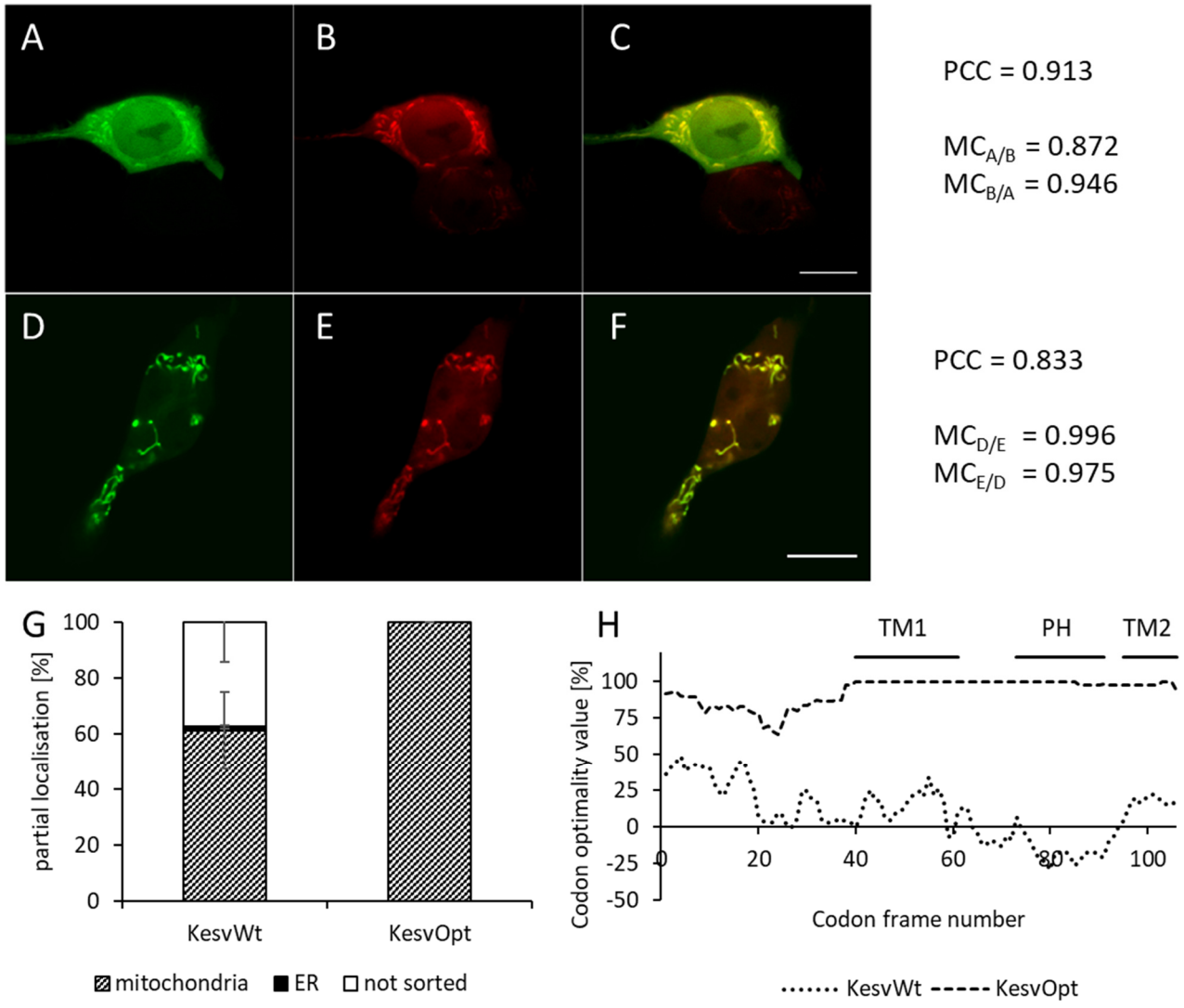

Fig. 7 : Comparison of $Kesv_{Wt}$ and $Kesv_{Opt}$

(A – F): Confocal images of $Kesv_{Wt}$ (A – C) and $Kesv_{Opt}$ (D – F), panel A shows $Kesv_{Wt}$::eGFP, panel D: $Kesv_{Opt}$::eGFP, panels B & E: COX8::mCherry as mitochondrial marker, panels C & F show the merged images. On the right the PCC and the MC are indicated for each construct. Scale bar represents 10 µm. **(G)** Sorting of $Kesv_{Wt}$ (N=5, n=259) and $Kesv_{Opt}$ (N=4, n=245) in HEK293 cells. **(H)** Codon optimality plot for $Kesv_{Wt}$ and $Kesv_{Opt}$.

The second candidate channel for expression in the mitochondria, is $Kmpv_{12T}$. This channel has been characterized by F. Siotto (Siotto, 2017). The channel exhibits an ohmic conductance and a voltage-dependent open probability in planar lipid bilayer measurements. However, while active in bilayer measurements, the channel did not generate a specific conductance in the plasma membrane of HEK293 cells. Confocal microscopy studies of the GFP-tagged channel in HEK293 cells showed that it is not sorted to the PM, but to the mitochondria. Mitochondrial sorting is to be observed in 92 % of the cells expressing the channel. Only 3 % of the cells showed localization of the channel in the ER and in 5 % of the cells the fluorescence was uniformly distributed throughout the cells (Fig. 8 G). Fig. 8 A-F show representative images of $Kmpv_{12T}$ expressed in HEK293 cells. The channel shows robust colocalization with the mitochondrial marker plasmid, as is indicated by the high PCC and MC (Fig. 8 A-C), whereas no significant colocalization can be observed with the ER marker plasmid (Fig. 8 D-F).

As in case of Kesv, codon optimization led to a significantly enhanced sorting to the mitochondria, the same approach was taken for $Kmpv_{12T}$. Calculation of codon optimality with the codon calculator (Clarke and Clark, 2008) revealed a mean value of 3±10 % for the wildtype channel (Fig. 8 H). This value is even lower than the one calculated for Kesv. Therefore, it was reasonable to assume that codon optimization for expression in mammalian cells would lead to the same positive effects as observed for Kesv. After applying the codon optimization algorithm on $Kmpv_{12T}$, the mean codon optimality increased to 88±6 % (Fig. 8 H).

However, codon optimization did not have the desired effect on $Kmpv_{12T}$. The codon optimized channel, $Kmpv_{12TOpt}$, is sorted to the mitochondria in 69%. In the remaining 31 % of the cells, the fluorescence signal did not show visible sorting to any compartment, but a uniform distribution of GFP-fluorescence, (Fig. 8 G).

Because of this variable effect of codon optimization on sorting of the two channel proteins, the exact structure of both plasmids expressing $Kmpv_{12T}$ or $Kmpv_{12TOpt}$ was examined. The backbone vector is in both cases peGFP-N2. Due to a slight difference in cloning strategy, the amino acid linker between $Kmpv_{12TOpt}$ and its GFP-tag is three amino acids longer than that linking $Kmpv_{12T}$ and GFP. This small difference is interesting in the context of reports showing that linker length can play an important role in proper protein targeting and folding (Chen et al., 2013b). Possible influences on channel sorting efficiency will be discussed in chapter 3.2.

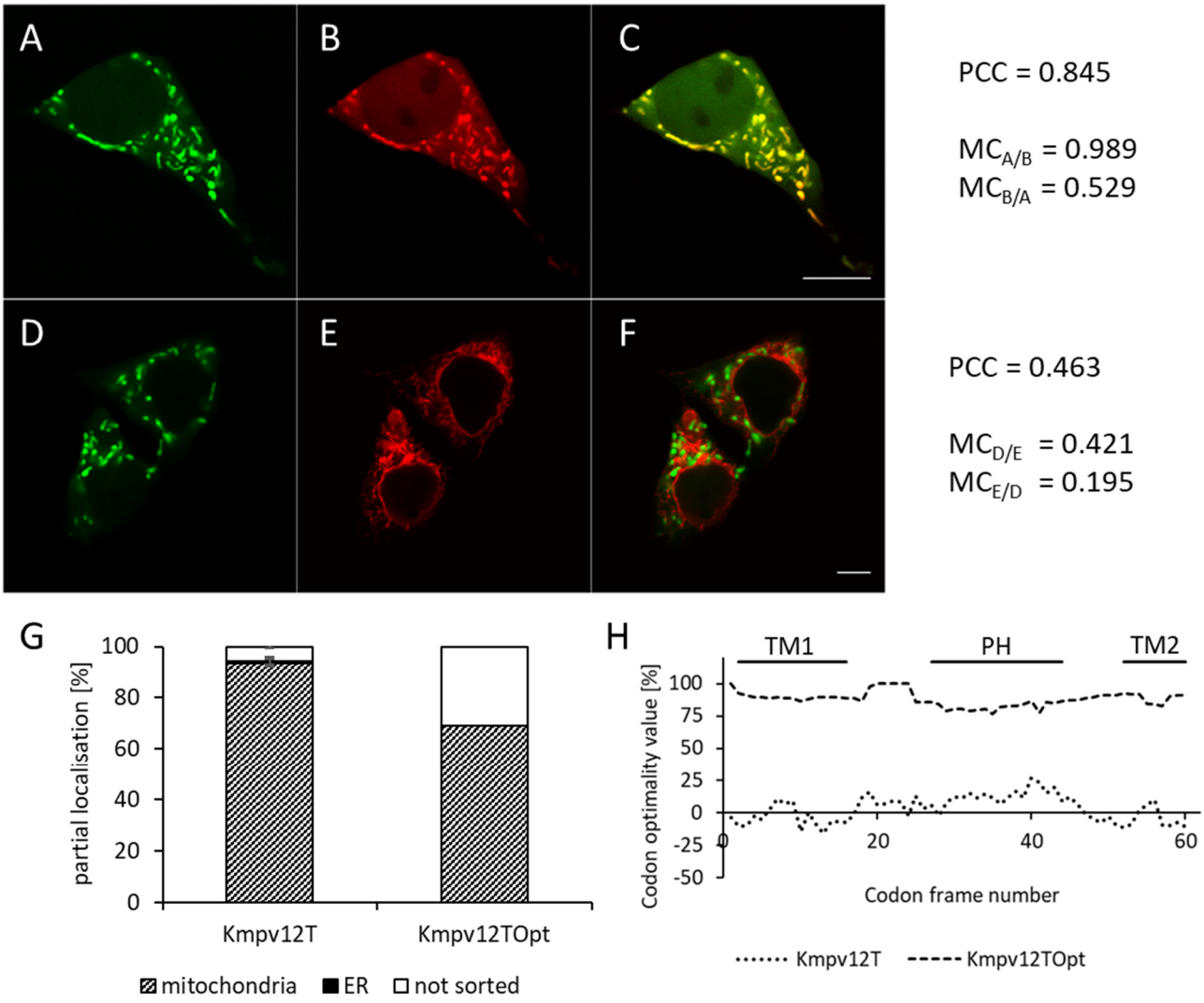

Fig. 8: Properties of Kmpv$_{12T}$ and Kmpv$_{12TOpt}$

(A – F): Confocal images of Kmpv$_{12T}$ (A – C) and Kmpv$_{12TOpt}$ (D – F), panel A shows Kmpv$_{12T}$::eGFP, panel D: Kmpv$_{12TOpt}$::eGFP, panel B: COX8::mCherry as mitochondrial marker panel E: HDEL::mCherry as ER marker, panels C & F show the merged images. On the right PCC and MC are indicated for each construct. Scale bar represents 10 µm. **(G)** Sorting of Kmpv$_{12T}$ (N=3, n=147) and Kmpv$_{12TOpt}$ (N=2, n=100) in HEK293 cells. **(H)** Codon optimality plot for Kmpv$_{12T}$ and Kmpv$_{12TOpt}$.

3.1.2. Characterization of viral potassium channels which are sorted to the plasma membrane

For a modular applicability of the optogenetic tools constructed in this work, not only mitochondrial sorted potassium channels will be examined, but also channels which are targeted to the plasma membrane (PM). Two channels will be tested in the following work: Kcv$_{PBCV-1}$ and Kcv$_{NTS}$. The electrophysiological properties of both have been extensively studied by patch clamp recordings in oocytes and HEK293 cells (Hertel, 2005; Greiner, 2011) as well as by reconstitution in planar lipid bilayers (Braun, 2014; Rauh, 2018). This extensive knowledge about these functionally different

channels is useful as it allows to target a channel with a high (Kcv_{NTS}) or low (Kcv_{PBCV-1}) open probability to the PM.

Kcv_{PBCV-1} is a potassium channel encoded in the genome of the *Paramecium bursaria chlorella* virus 1 (Plugge et al., 2000). It exhibits a near ohmic conductance with inactivation at higher negative voltages upon heterologous expression in HEK293 cells (Hertel, 2005). In microscopic studies, the channel showed an effective sorting to the plasma membrane in 41 % of the cells, whereas in 59 % the fluorescence signal of the GFP-tag shows a uniform distribution throughout the cell (Fig. 9 G). Fig. 9 A-F shows representative confocal images of Kcv_{PBCV-1} expressed in HEK293 cells. The upper panels illustrate effective sorting to the ER, with a distinct perinuclear ring and the typical ER-network surrounding the nucleus. The fluorescent signal of the GFP-tagged channel protein colocalizes with the ER marker plasmid. This is also illustrated by the very high PCC and MC values of over 90 %, further proving evidence for the effective sorting to the ER. In the lower panels (Fig. 9 D-F) a cell with a uniformly distributed eGFP signal is shown, indicating a mis-sorting of the channel. Notable are the darker puncta in the cytosol, which negatively correlate with the mitochondrial marker plasmid. This suggests that the channel is excluded from the mitochondria. This is reflected especially in the low MC values which illustrate that the channel does not correlate with the mitochondrial marker plasmid.
With a sorting efficiency of only 41 %, there is still potential to improve protein expression and sorting of Kcv_{PBCV-1}. To test if codon optimization has an impact on protein sorting, a codon optimized gene variant of Kcv_{PBCV-1} ($Kcv_{PBCV-1Opt}$) was synthesized (compare Fig. 9 H). This optimized version showed an enhanced sorting to the ER, with 61 % of the cells expressing the channel protein in the ER. In 39 % of the cells, GFP fluorescence was still uniformly distributed throughout the whole cell (Fig. 9 G).

Another channel from the family of chlorella virus-derived potassium channels is Kcv_{NTS}. It is characterized by a high open probability and a high single-channel conductance (Rauh, 2018). The channel is sorted to the ER in 44 % of the cells upon heterologous expression in HEK293 cells. 56 % of the cells exhibit a uniform fluorescence throughout the whole cell (Fig. 9 G).
Closer examination of cells expressing Kcv_{NTS} showed that sorting efficiency correlated with the expression level. Only cells with weak expression show a distinct sorting to the ER. On the other hand, cells which exhibited a strong fluorescence signal, showed no sorting of the channel. It was even possible to determine a clear threshold of relative fluorescence intensity (RFI): In cells with an RFI value below 1.38 AU (for definition of RFI value, see chapter 2.6) the channel was sorted exclusively to the ER in 100 % of the cells imaged. In the cases in which the RFI value exceeded 1.38 AU the channel showed no longer any distinct sorting.

For Kcv_{NTS}, a moderate expression level seems to be crucial for an efficient channel sorting. If the expression reaches higher levels, the sorting machinery seems to be unable to handle the amount of protein produced and becomes highly ineffective.

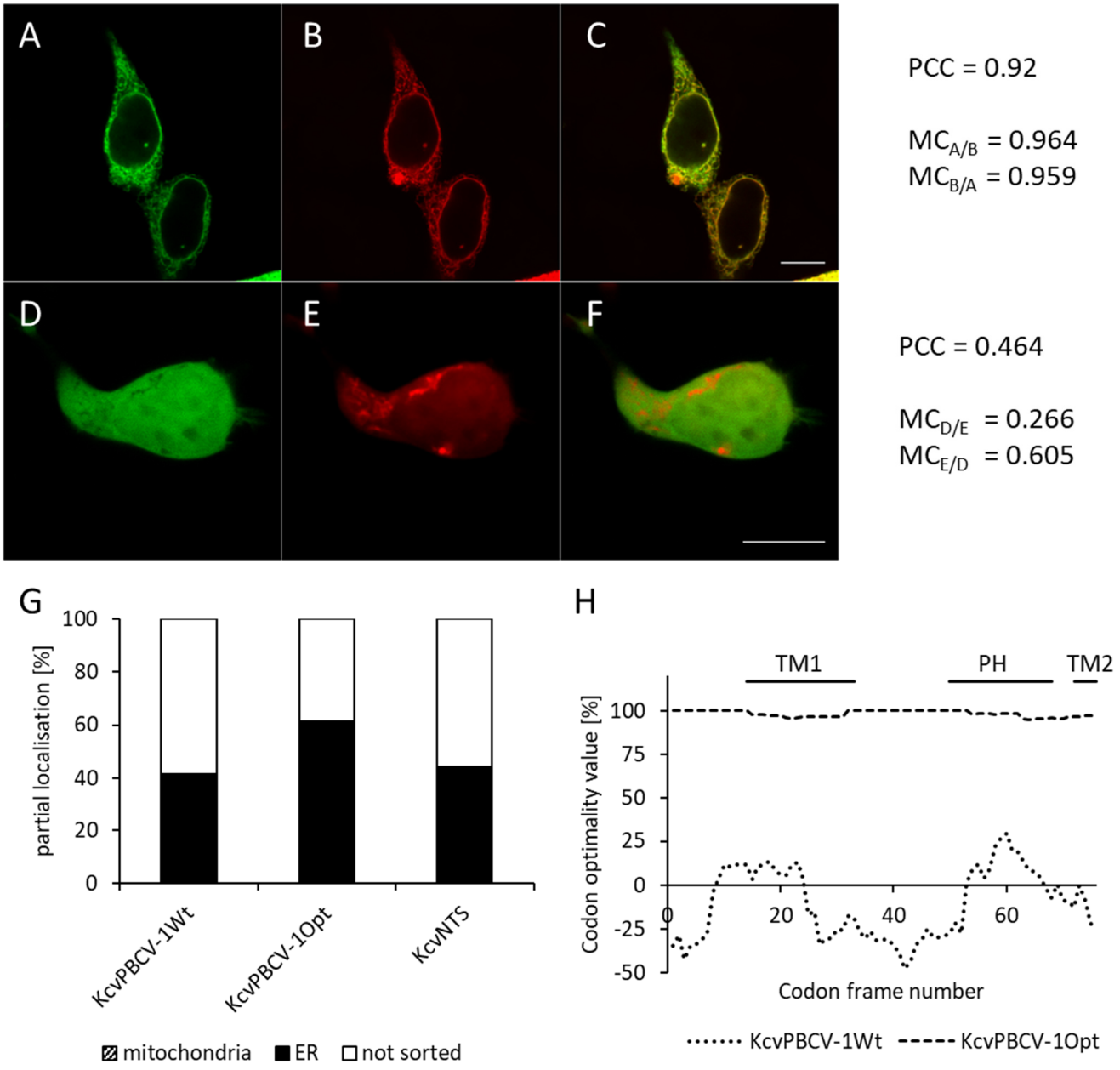

Fig. 9: Properties of Kcv_{PBCV-1}, $Kcv_{PBCV-1Opt}$ and Kcv_{NTS}

(A – F): Representative confocal images of $Kcv_{PBCV-1Opt}$ sorted to the ER or showing a uniform distribution throughout the cell. Panels A & D show $Kcv_{PBCV-1Opt}$::eGFP, panel B: HDEL::mCherry as ER marker, panel E: COX8::mCherry as mitochondrial marker, panels C & F show the merged images. On the right PCC and MC are indicated for each construct. Scale bar represents 10 µm. **(G)** Sorting of Kcv_{PBCV-1} (N=5, n=261), $Kcv_{PBCV-1Opt}$ (N=5, n=223) and Kcv_{NTS} (N=2, n=184) in HEK293 cells. **(H)** Codon optimality plot for Kcv_{PBCV-1} and $Kcv_{PBCV-1Opt}$.

3.2. Variation in linker length can influence protein sorting efficiency

Previous studies reported that linker length can influence protein sorting (Shewmake et al., 2008) and folding (Cutler et al., 2009). In the light of these findings, a closer look was taken on the impact of linkers in different constructs described in this work. Most abundantly, three different linkers were used, 1) a long linker which is 18 amino acids (AA) long, 2) a medium linker (15 AA) and 3) a short linker (8 AA). Since sorting seemed more prone to subtle influences for the mitochondrial potassium channels, these were used for the following studies. Kesv and $Kesv_{Opt}$ were therefore cloned into peGFP-N2 with the long (LL) and the short linker (SL) and $Kmpv_{12TOpt}$ with the medium (ML) and the long linker (LL).

Fig. 10 A-H shows representative images of $Kmpv_{12T}$ with the medium (A-D) or the long linker (E-H). They clearly illustrate that the sorting efficiency is strongly reduced in the construct with the long linker. $Kmpv_{12T\ ML}$ shows a very distinct sorting to the mitochondria, which is also underscored by the high MC value of 0.774 for the correlation of the GFP-signal of the channel with the MitoTracker DeepRed signal. $Kmpv_{12T\ LL}$ on the other hand shows a mostly uniform distribution of the GFP fluorescence throughout the cell. There are some dot-shaped structures recognizable, which colocalize with the MitoTracker DeepRed. Notably, most mitochondria stained by the MitoTracker DeepRed are however not distinguishable in the GFP-signal. This observation is also confirmed by the low correlation of the GFP-fluorescence with the MitoTracker, as is indicated by the MC of 0.369.

The statistical evaluation confirmed the observations from the images. $Kmpv_{12T\ LL}$ is sorted to the mitochondria in 21±13 % of the cells, sorting to the ER was observed in 4±3.5 % of the cells. The majority (75±16 %) however did not show sorting to the channel to any distinct compartment, but a uniform distribution of the GFP-signal (Fig. 10 I). $Kmpv_{12T\ ML}$ on the other hand, shows a very robust sorting to the mitochondria, with 93.5±1.6 % of the cells showing a clear-cut sorting to the mitochondria. The portion of cells which show sorting to the ER decreases to 1±1.6 % and the fraction of cells which do not show any sorting decreases to 5.5±0.6 % (Fig. 10 J).

For Kesv the effect of a change in linker length was less pronounced. $Kesv_{LL}$ shows a sorting efficiency of 61±14 % to the mitochondria, 1.6±0.5 % exhibit sorting to the ER and 37.4±14 % show a uniform distribution of the GFP-signal throughout the cells (Fig. 10 I). For $Kesv_{SL}$ 54±2.6 % of the cells showed sorting to the mitochondria, and 46±2.6 % showed a uniform distribution of the GFP-fluorescence. Sorting of the channel to the ER could not be observed (Fig. 10 J).

$Kesv_{Opt}$ proved to be more sensitive to the shortening of the linker, compare to the wildtype channel. $Kesv_{Opt\ LL}$ was sorted to the mitochondria in 79.6±9.8 % of the cells, the remaining 20.4±9.8 % did not show sorting of the channel (Fig. 10 I). With the short linker, 100 % of the examined cells did show pronounced sorting to the mitochondria (Fig. 10 J).

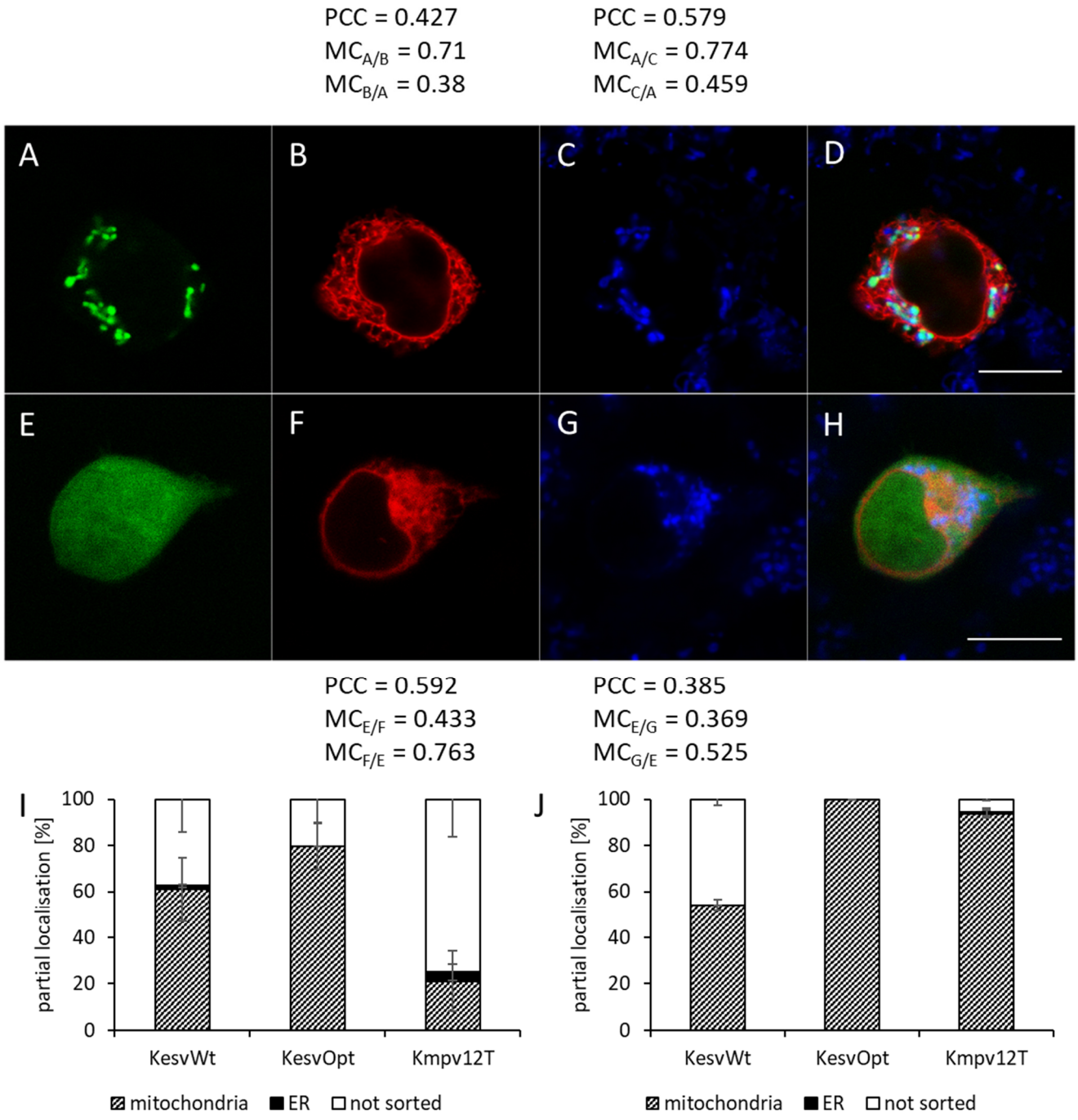

Fig. 10: Influence of the linker length on the sorting of Kesv, Kesv$_{Opt}$ and Kmpv$_{12T}$

(A – H): Representative confocal images of Kmpv$_{12T}$ in HEK293 cells with a medium (A-D) or long linker (E-H). Panel A shows Kmpv$_{12T}$::eGFP with a medium linker, panel E shows Kmpv12T::eGFP with a long linker, panels B & F: HDEL::mCherry as ER marker, panels C & G: MitoTracker DeepRed as mitochondrial marker, panels D & H show the merged images. Above and below PCC and MC are indicated for each construct. Scale bar represents 10 µm. **(I)** Sorting of Kesv (N=5, n=259), Kesv$_{Opt}$ (N=4, n=245) and Kmpv$_{12T}$ (N=3, n=175) with a long linker in HEK293 cells. **(J)** Sorting of Kesv (N=3, n=198), Kesv$_{Opt}$ (N=4, n=150) with a short linker and Kmpv$_{12T}$ (N=5, n=271) with a medium linker in HEK293 cells.

Taken together, the results show that a short linker strongly favors effective sorting to the mitochondria. Sorting to the ER was strongly reduced or even abolished entirely and the part of the cells showing a uniform fluorescence of the GFP-signal throughout the whole cell, indicating mis-sorting of the channel, degradation or cleaving of the GFP, was pronouncedly lower for all three channels examined as well.

The most surprising result was obtained from experiments with $Kmpv_{12T}$ constructs, as linker lengths differed in only three AA. Therefore, a further look into the properties of the three different linkers was taken. The AA sequence of the three linkers is shown in Fig. 11 A. It becomes is evident, that the linkers are structurally identical and only differ in the AAs which are responsible for the elongation. Differences in their behavior in combination with the channels therefore have to be attributed to the parts forming the long or the medium linker, as the last eight AAs forming the short linker are identical in all three linkers observed.

Possible explanations for the pronounced effects the three linkers have on the sorting of the channel proteins might lie in the introduction of charged AAs, changes in hydrophobicity or protonation state or the introduction of enzymatic cleavage sites.

With the elongation of the peptide linker from eight to 15 AAs two additional positive charges are introduced by the two arginine-residues at positions six and eight, in between these two lies another amino acid with a bulky side chain, the aromatic ring of tyrosine. From the short linker to the medium linker, both hydrophobicity and net charge increase, whereas the isoelectric point (pI) remains at a high basic pH (Fig. 11 B). With the further addition of another three AAs, forming the long linker, the only negatively charged AA is introduced: glutamic acid at position one, as well as another aromatic ring system with phenylalanine at position two. The pI shifts to less basic values and hydrophobicity further increases (Fig. 11 B). The linkers therefore do not only get longer but also more reactive, which might increase the possibility of unwanted interactions with the channel protein where it might influence correct folding. Another possible explanation for the decreased sorting efficiency might be the steric blocking of potential sorting sequences by the eGFP-tag, which can move more freely with increasing linker length.

Another option might be that the GFP-tag is enzymatically cleaved off the channel protein. To address this question, potential enzymatic cut sides in the peptide linker were calculated using the peptide cutter tool provided at expasy.org. The results of these calculations are shown in Fig. 11 C. The short linker has an overall 12 possibilities for enzymatic cleavage, the elongation to the medium linker adds another 12 cutting sites, leaving the medium linker with overall 24 enzymatic cleavage sites. The addition of another three amino acids to generate the long linker adds another nine cleavage sites, including several endopeptidases (full list of cleaving enzymes shown in appendix 10.5). It is therefore reasonable to

assume that the increased cytosolic fluorescence signals are a result of free cleaved-off GFP and do not necessarily have to indicate a disruption of channel sorting by the elongation of the peptide linker.

A

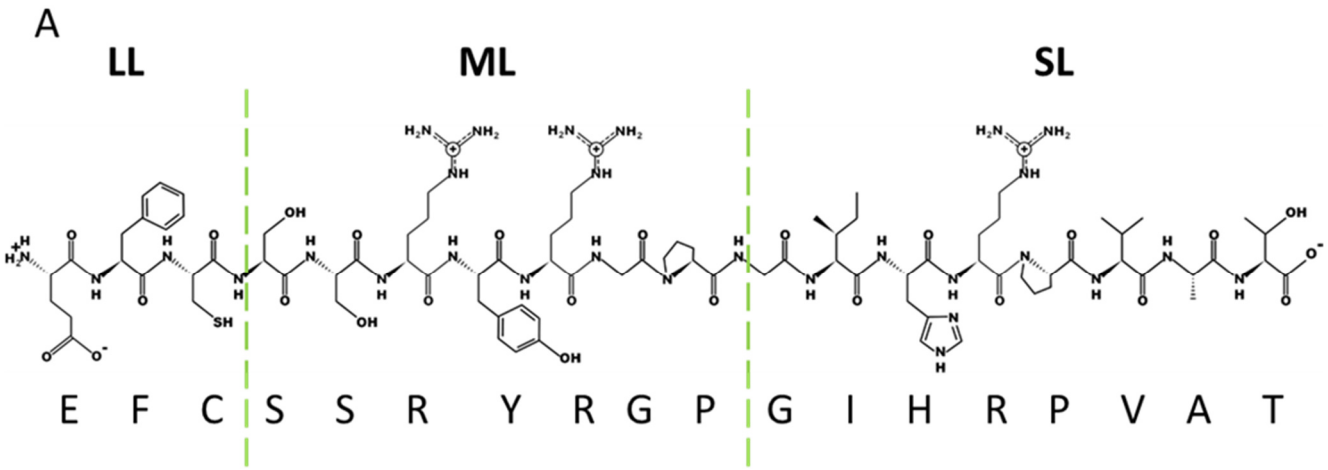

B

	LL	ML	SL
Length [AA]	18	15	8
pI	9.8	12.19	11.13
Net charge	+2	+3	+1
Hydrophobicity [Kcal/mol]	+19.52	+17.62	+12.5

C

	E	F	C	S	S	R	Y	R	G	P	G	I	H	R	P	V	A	T
No. of cleavage sites	4	5			3	3	3	3			1	1	1	2	2	2	1	2

Fig. 11: Overview of the three different linker lengths

(A) Amino acid sequence of the short (SL), medium (ML) and long linker (LL). **(B)** Linker length, isoelectric point (pI), net charge and hydrophobicity calculated for the three different linker lengths calculated with pepdraw. **(C)** Number of cleavage sites for each amino acid in the three different linker lengths calculated with the peptide cutter, as provided by expasy.org. The cut occurs always to the right of the marked AA.

3.3. Both the influence of codon usage and of linker length on channel sorting are cell type specific

To determine whether the influence of codon optimization and linker length are specific for HEK293 cells or a general effect, two additional human cell lines (Hela and HaCaT) as well as two non-human mammalian cell lines (Cos7 and CHO) were transfected with Kesv or $Kesv_{Opt}$ with either the short or the long linker.

From the data in Fig. 12 it becomes clear, that both codon usage and linker length strongly influence the sorting efficiency of the channel protein. A cell-type specific influence is visible only for the wildtype channel. The long linker in combination with the wildtype channel shows by far the least effective sorting of all four combinations (Fig. 12 A). The cell lines showing the least effectiveness of mitochondrial sorting were Cos7 (6 %) and HaCaT cells (12 %). The other three cell lines showed sorting efficiencies of 60 % (CHO), 61 % (HEK293) and 71 % (Hela). It is to be noted as well, that the only occurrence of channel sorting to the ER occurred for the wildtype channel in combination with the long linker. The most pronounced sorting to the ER was observed in CHO cells with 12.5 %. Also, a small fraction of HEK293 cells (2 %) exhibited this sorting phenotype (see also chapter 3.1.1).

A pronounced increase in sorting efficiency was to be observed for the wildtype channel in combination with the short linker (Fig. 12 C). Here the sorting to the mitochondria increased to 100 % for Hela cells, to 98 % for CHO cells and to 95 % for Cos7 cells. Only in case of HEK cells, the sorting efficiency of the construct with the short linker decreased compared to that of the long linker to 54 %. Sorting of Kesv to the ER could not be observed in any cell line transfected with $Kesv_{SL}$.

For $Kesv_{Opt}$, the overall sorting efficiency was greatly enhanced in all cell types and most effective in combination with the short linker. For the codon optimized Kesv channel, all the cell lines showed 100 % effective sorting to the mitochondria (Fig. 12 D). With the long linker, the sorting efficiency was 100 % for Hela, CHO and HaCaT cells. 93 % of the Cos7 cells showed mitochondrial sorting of the protein, and in HEK293 cells 80 % of the cells showed fluorescence in the mitochondria (Fig. 12 B).

Taken together, these results demonstrate that cell-type specific sorting of Kesv occurs only for the wildtype channel and is most pronounced with a longer peptide linker between the channel protein and the GFP-tag. The most important finding is that codon optimization of Kesv seems to override any cell-type specific differences in sorting efficiency of the protein. Furthermore, for $Kesv_{Opt}$ the mitochondrial sorting is most effective if combined with a short linker.

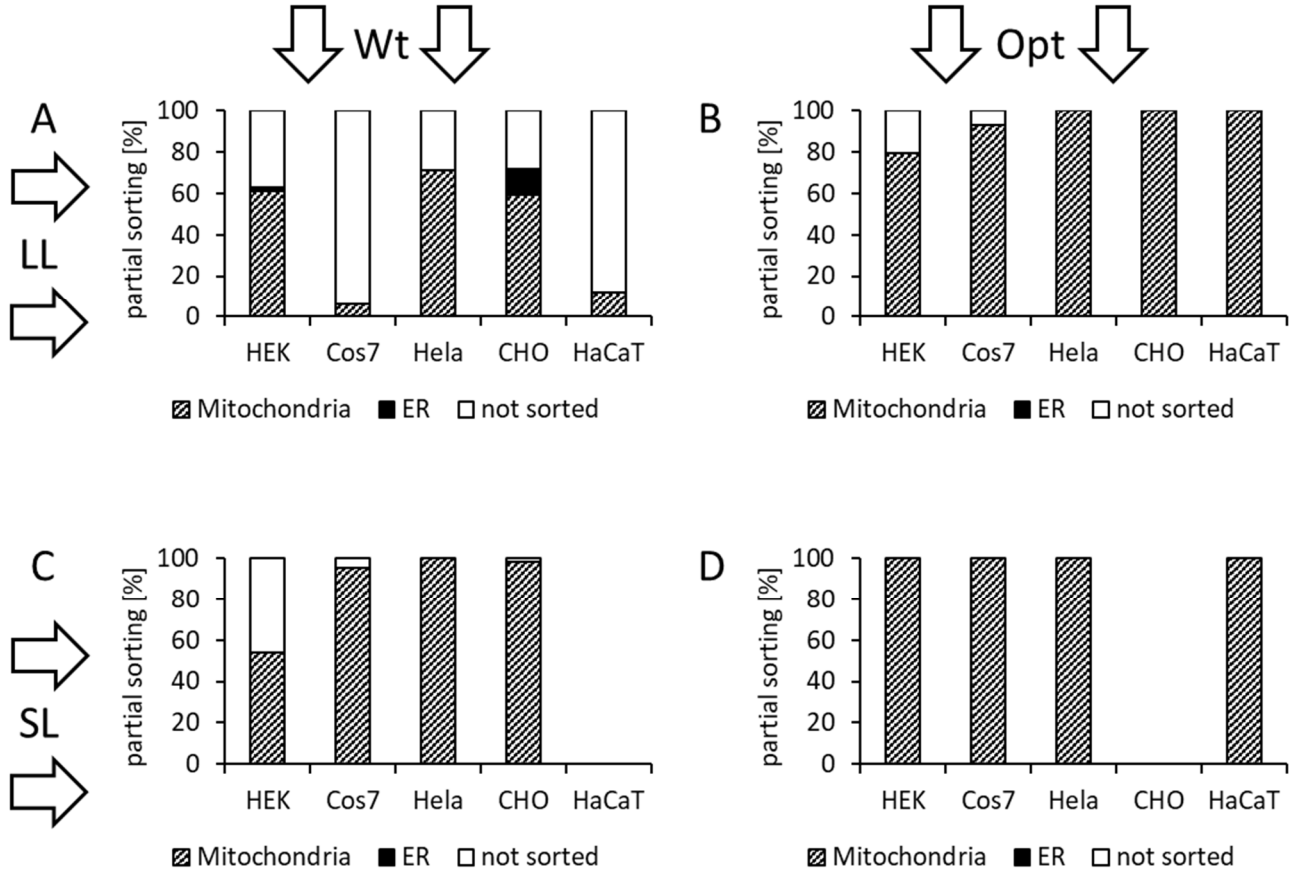

Fig. 12: Influence of codon usage and linker length on the sorting of Kesv and Kesv$_{Opt}$ in HEK293, Cos7, Hela, CHO and HaCaT cells

(A) Sorting of Kesv with a long linker in HEK293 (n=259), Cos7 (n=67), Hela (n=110), CHO (n=32) and HaCaT (n=58) cells. **(B)** Sorting of Kesv$_{Opt}$ with a long linker in HEK293 (n=245), Cos7 (n=56), Hela (n=101), CHO (n=62) and HaCaT (n=15) cells. **(C)** Sorting of Kesv with a short linker in HEK293 (n=100), Cos7 (n=104), Hela (n=105) and CHO (n=61) cells. **(D)** Sorting of Kesv$_{Opt}$ with a long linker in HEK293 (n=245), Cos7 (n=91), Hela (n=169), and HaCaT (n=94) cells.

To obtain more information on the influence of the linker and the choice of cell type on the efficiency of mitochondrial sorting, Kmpv$_{12T}$ with either the long or the medium linker was expressed in HEK293 and Cos7 cells.

In HEK293 cells, the respective channel construct was sorted to the mitochondria in 93.5 % of the cells if the medium peptide linker is present. The mitochondrial sorting efficiency dropped to only 21±13 % if the long linker was present between the channel and the GFP-tag. Sorting of Kmpv$_{12T}$ to the ER occurred slightly more frequently in presence of the long linker in HEK293 cells. The value increased from 1 % with the ML to 4±3 % with the LL. In Cos7 cells, the differences between the two linker lengths were even more pronounced. The sorting efficiency to the mitochondria dropped from 70 % to only 4±3 % if the linker was elongated. The sorting of the channel to the ER increased from 3.6 % to 17±8 % with the long linker.

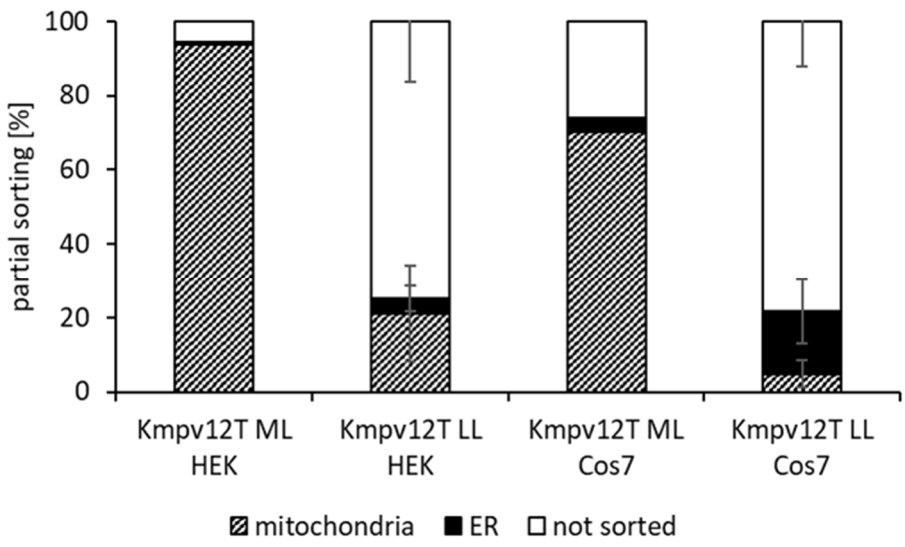

Fig. 13: Influence of codon usage and linker length on the sorting of $Kmpv_{12T}$ in HEK293 and Cos7 cells

Sorting of $Kmpv_{12T}$ with a short (SL) (N=2, n=124) and medium (ML) linker (N=3, n=175) in HEK293 cells and sorting of $Kmpv_{12T}$ with a short (N=2, n=32) and medium linker (N=3, n=188) in Cos7 cells. Error bars indicate standard deviation.

By comparing the results of sorting efficiency for Kesv and $Kmpv_{12T}$, it becomes clear that Cos7 cells are more sensitive to changes in linker length than HEK293 cells. In both cases the wildtype channels turned out very sensitive to changes in linker length with shorter linkers favoring a more effective sorting to the mitochondria. Longer linkers increased the fraction of cells in which the channel was sorted to the ER. On the background of these data, it will be interesting to find the kind of linker that is most suitable to optimize sorting of channel proteins which are by default sorted to the ER.

The data underscore that codon optimization overrides both cell type specificity and the strong influence of linker length on sorting, as could be observed in $Kesv_{Opt}$. At this point, it is important to mention that $Kmpv_{12TOpt}$ was expressed in all aforementioned experiments with the long linker. This offers a probable explanation for the failure of improving its sorting compared to the wildtype channel with the medium linker (compare Fig. 8). If its mitochondrial sorting efficiency of 69 % is compared to the wildtype channel with the long linker, where only 21 % of the cells exhibit targeting of the channel to the mitochondria, it becomes clear that codon optimization did profoundly enhance sorting efficiency of $Kmpv_{12TOpt}$ as well. Further experiments of $Kmpv_{12T}$, in both the wildtype and the codon optimized version, with the short linker would probably result in an even better mitochondrial sorting efficiency of the channel.

A full list of all peptide linkers used in this work and the mainly occurring sorting pattern of the constructs can be found in the appendix 10.4.

To address the question on whether the effects of codon optimization on sorting of potassium channels is a general phenomenon in eukaryotes or specific to mammalian cells, further experiments were performed in *Nicotiana benthamiana*. For this purpose, another variant of an optimized Kesv channel was generated: $Kesv_{NbOpt}$, which was codon optimized for *N. benthamiana* (Murray et al., 1989; Perlak et al., 1991). The channel was cloned in the pCambia_mRuby3 vector and expressed in agrobacteria. The leaves of *N. benthamiana* were injected with the channel-expressing agrobacteria and incubated for two days before imaging. To determine the location of both the wildtype and the optimized channel, the plants were co-transfected with different marker proteins to indicate mitochondria, ER, golgi, PM, cytosol and ER exit sites (ERES).

Fig. 14 A-H illustrates the localization of Kesv (A-D) and $Kesv_{NbOpt}$ (E-H) in *N. benthamiana* leaf cells. The sorting pattern differs strongly from the one observed in mammalian cells. The wildtype channel showed robust colocalization with the ER marker protein HDEL, as can be seen from the high MC value of 0.958 of the mCherry signal with the YFP signal of the marker protein. The optimized channel showed no such strong colocalization with the ER, but seemed to be present in the surrounding cytosol instead. The MC value for correlation of the mCherry signal with the ER marker is low (0.311) in accordance with the image. In line with a cytosolic localization, the very distinct pattern that occurred for the ER marker and the wildtype channel was not present in case of the codon optimized channel.

In other images, bright clusters occurred in the mCherry fluorescence of the wildtype channel, which did only partially colocalize with the mitochondria (Fig. 14 I-K), the hypothesis was formed that these clusters may originate from accumulations of the channel protein at ERES, indicating further transport to the plasma membrane. A colocalization of the wildtype channel with the 6 kDa ERES marker (MC=0.785) could prove this hypothesis (Fig. 14 A-D). While these clusters at ERES were routinely seen for the wildtype channel, they were not visible in the optimized channel. The latter did not colocalize with the ERES marker protein (Fig. 14 E-G).

Upon imaging both the wildtype and the optimized channel with a set of different markers for Golgi, PM and cytosol, it became clear that the two channels exhibit a different pattern of colocalization in *N. benthamiana*. The wildtype channel was identified to be present in the ER, mitochondria, PM and the nuclear envelope. The codon optimized channel on the other hand was mostly present in the cytosol and accumulated in the nucleus (Fig. 14 L). Collectively the data show that codon optimization is also affecting the sorting of the protein in a plant cell. This implies that the codon structure of a gene is a general secondary code for protein sorting in eukaryotes. The impact of codon optimization in plant cells however is different from that in mammalian cells. While codon optimization favors targeting to the mitochondria in mammalian cells, it seems to promote a mis-targeting in plant cells.

PCC = 0.8
$MC_{A/B}$ = 0.958
$MC_{B/A}$ = 0.824

PCC = 0.436
$MC_{A/C}$ = 0.785
$MC_{C/A}$ = 0.39

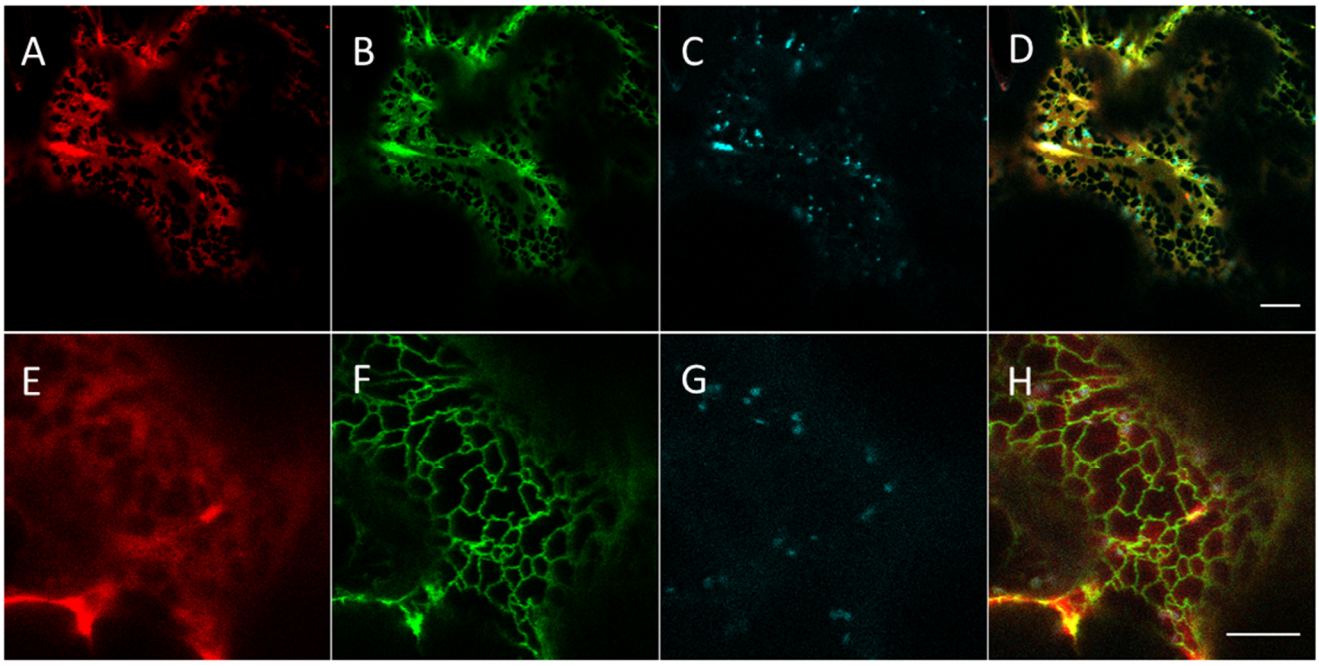

PCC = 0.547
$MC_{E/F}$ = 0.311
$MC_{F/E}$ = 0.781

PCC = 0.216
$MC_{E/G}$ = 0.322
$MC_{G/E}$ = 0.446

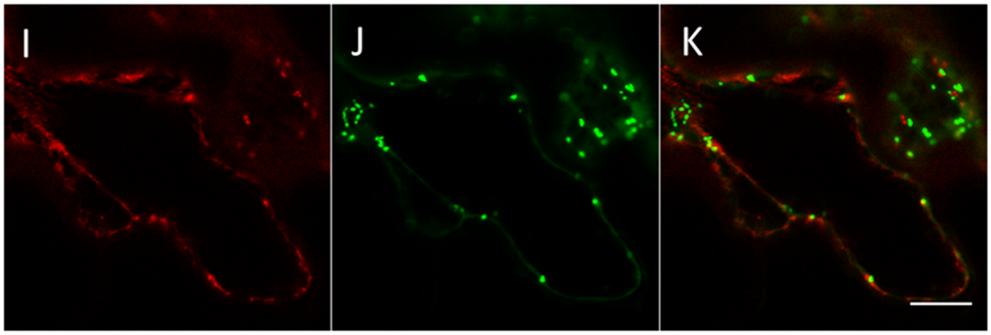

PCC = 0.556
$MC_{I/J}$ = 0.106
$MC_{J/I}$ = 0.81

L

	Kesv	KesvNbOpt
ER (HDEL)	✓	✗
Golgi (Man1)	✗	✗
Mitochondria (ScCOX4)	✓	✗
PM (PIP2A)	✓	✗
Cytosol (Sec24)	✗	✓
ERES (6kDA)	✓	✗
Nucleus	✗	✓
Nuclear envelope	✓	✗

Previous page:

Fig. 14: Codon optimization influences sorting of Kesv in *Nicotiana benthamiana*

(A–H): Representative confocal images of Kesv (A-D) and $Kesv_{NbOpt}$ (E-H) in *N. benthamiana*. Panel A shows Kesv::mRuby, panel E shows $Kesv_{NbOpt}$::mRuby, panels B & F: HDEL::eYFP as ER marker, panels C & G: 6kDa::BFP as ER exit site (ERES) marker, panels D & H show the merged images. Above and below PCC and MC are indicated for each construct. Scale bar represents 10 µm. **(I-K)** Representative confocal images of Kesv in *N. benthamiana* cotransfected with a mitochondrial marker plasmid. Panel I shows Kesv::mRuby, panel J: ScCOX4::eYFP as mitochondrial marker, panel K shows the merged image. On the right-hand side PCC and MC are indicated for. Scale bar represents 10 µm. (**L)** Sorting of Kesv and $Kesv_{NbOpt}$ in *N. benthamiana*. Indicated in the left row are the possible colocalizations with the marker protein used indicated in brackets.

4. Targeting a light gated potassium channel to the mitochondria

4.1. Light gated potassium channels

The development of light-switchable potassium channels for hyperpolarizing cells with a high spatio-temporal control, is a widely sought for application for the silencing of excitable cells. The advantage of potassium channels over other optogenetic silencing tools is related to the fact that a potassium conductance is the physiological hyperpolarizing mechanism in mammalian cells (Hille, 1978; MacKinnon, 2003). By using light gated potassium channels for hyperpolarizing cells, unphysiological responses, which are associated with other optogenetic tools (Häusser, 2014), are avoided and the negative effects on cells are minimized.

There is already a range of light-gated potassium channels available, each with their own potential applications, advantages and drawbacks (Banghart et al., 2006; Paoletti et al., 2019) .
One approach to introduce light dependent gating in potassium channels is based on tethering photoswitches to the channel protein, which block the channel in the dark or upon red / far red illumination, and release this block upon illumination with UV light. Examples of this mode of action are the SPARK (synthetic photo-isomerizable azobenzene-regulated K^+ channel) (Banghart et al., 2004) and TREKLight (Sandoz et al., 2012) channels. In both cases, a photoisomerizable azobenzene was used, which switches from its longer *trans*-state to its shorter *cis*-state upon illumination with short wavelength light. The former configuration allows the pore blocker – a quaternary ammonium – to occlude the pore, while the latter withdraws the blocker and allows ion flux through the channel.
Quaternary ammonium ions have also been employed as a diffusible photoswitch: this has been shown for voltage gated K^+ channels (Fortin et al., 2008; Banghart et al., 2009) and GIRK channels (Barber et al., 2016) so far. The blockers are in their active *trans*-state in the dark, and revert to the less active *cis*-isoform upon illumination with UV light. The drawback of these quaternary ammonium-based approaches is that the chromophore needs to be constantly supplied.

Another strategy for the introduction of light gating in K^+ channels is the application of photoactive unnatural amino acids (UAA). This approach has been taken to generate PIRK (photoinducible inward rectifying K^+ channel), a photoswitchable Kir2.1 channel (Kang et al., 2013). The channel is in this case blocked by the genetically encoded UAA 4,5-dimethoxy-2-nitrobenzyl-cysteine (Cmn), which occludes the pore in the dark. Upon illumination Cmn is released, which leads to an outward potassium current. This strategy has found little application because it requires heterologous expression or genomic integration of both the gene of interest (GOI) and the unnatural amino acid. Additionally, the expression level of the target protein might be affected, the rate limiting step being the supply of the UAA.

A fully genetically encoded approach without the need of supplying external factors is offered by the application of light oxygen voltage (LOV) domains as photoswitches in combination with a potassium channel. So far there are two rather different approaches to render a potassium channel light-gated which both rely on the LOV domain from *Avena sativa* (asLOV) – one is Lumitoxin (Schmidt et al., 2014), whose functionality has been shown on voltage dependent K^+ channels of the Kv channel family, the other one is BLINK, which renders a minimal viral potassium channel light sensitive (Cosentino et al., 2015; Alberio et al., 2018).

To generate Lumitoxin, the LOV domain was targeted to the secretory pathway with the aid of cleavable targeting sequences and anchored to the extracellular side of the plasma membrane (PM) by a single transmembrane helix. A selective channel blocker, which can occlude the extracellular pore mouth of Kv channels in the dark was attached to the LOV domain. Upon illumination, the LOV domain unfolds, and this in turn lowers the concentration of the blocker near the cell surface, which thereby unblocks the channels (Schmidt et al., 2014).

BLINK also relies on the structural changes of *as*LOV by blue light illumination, but by a rather different approach. To generate a light-switchable potassium channel the photosensory module of *as*LOV was directly fused to a minimal viral potassium channel. Upon illumination the conformational change of the photosensory module directly applies a mechanical strain on the channel, thereby stabilizing the open state (Fig. 15).

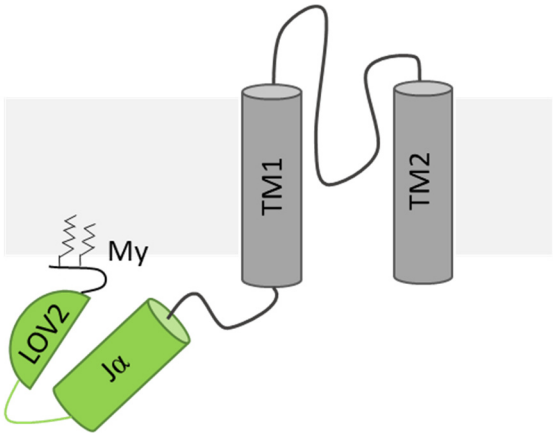

Fig. 15: Schematic image of BLINK1

A monomer of Kcv_{PBCV-1} is shown in grey (TM1 and TM2 linked by the pore-helix), the LOV photosensory module consisting of LOV2 and Jα in light green and the myristoilation site (My) inserted in the PM.

BLINK1 is rapidly activated in response to illumination with blue light, followed by slow but full inactivation in the dark. The system is more sensitive to illumination than the canonical channelrhodopsins (Cosentino et al., 2015; Alberio et al., 2018), which makes it possible to work with rather low light intensities, abolishing potential harmful effects of blue light on cells or tissue. Membrane expression is low, but the high unitary conductance of the channel is sufficient to hyperpolarize cells to

the K^+ equilibrium voltage. The light-dependence of BLINK1 was not only shown in cells but also *in vivo*, where an expression of BLINK rendered the escape reflex of zebrafish embryos blue light sensitive (Cosentino et al., 2015). Improvement of membrane expression in BLINK2 was achieved by the addition of c-terminal trafficking sequences. BLINK2 also shows slower activation and inactivation kinetics, rendering it the ideal tool for long term silencing of excitable cells. This mode of action was already confirmed in proof of principle experiments *in vivo* in zebrafish and in a mouse model (Alberio et al., 2018).

BLINK offered the optimal starting point for the development of a potassium channel-based optogenetic tool targeted to the mitochondria. Due to its modular design, it allows for an easy exchange of components to change its subcellular localization to the mitochondria.

4.2. Rational design approach for a light gated potassium channel

Inspired by the positive impact of codon optimization on potassium channel sorting to the mitochondria, as has been shown by the experiments in chapter 3, a rational design approach was chosen to create a light-gated channel with an effective sorting to the IMM. As a template BLINK1 was used, because its properties are already well studied and the modular design makes it easy to swap functional parts in this synthetic channel to generate a new construct with the desired new features.

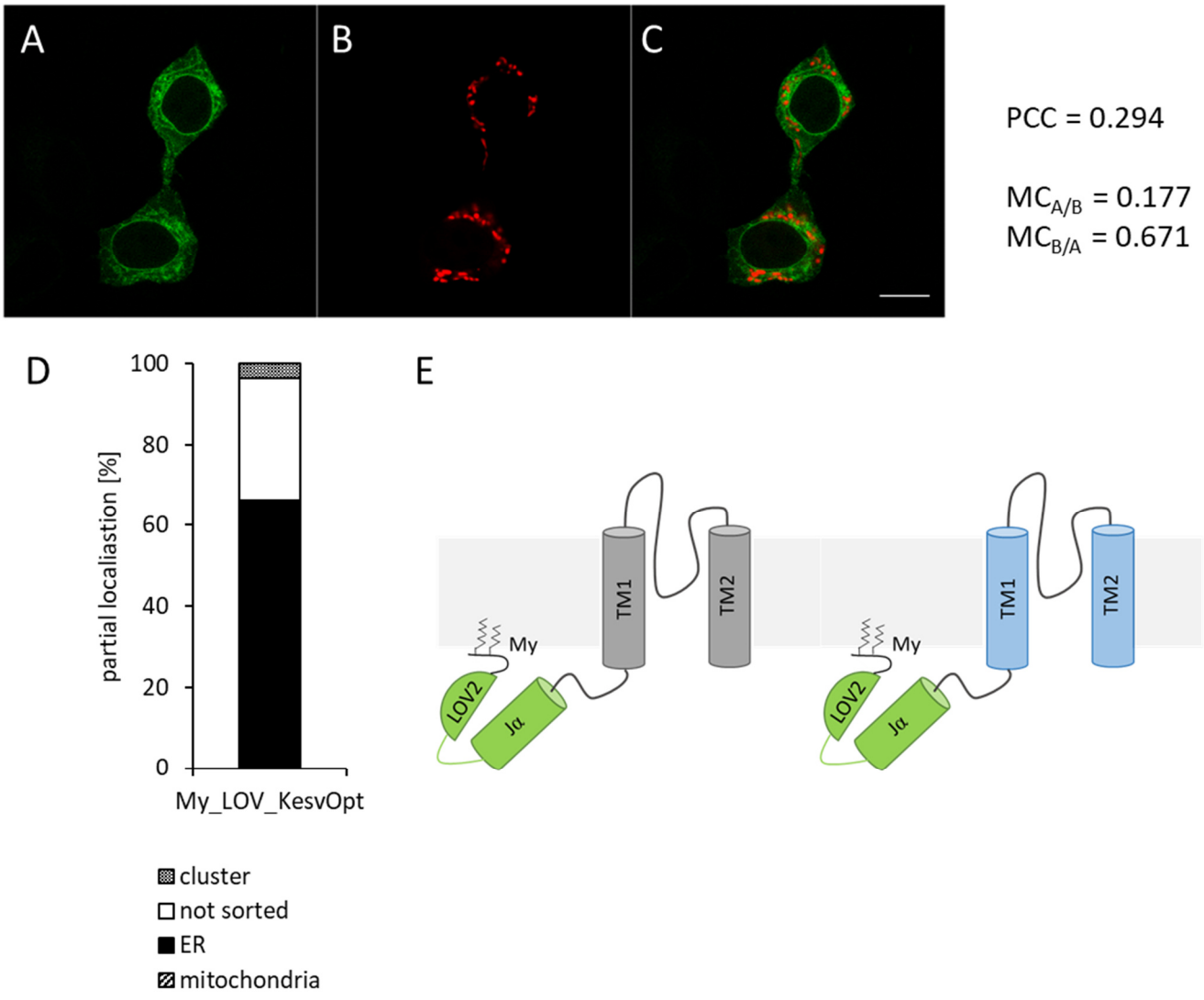

Fig. 16: Design and sorting of My_LOV_Kesv$_{Opt}$

(A-C): Confocal image of My_LOV_Kesv$_{Opt}$::eGFP, Panel A: My_LOV_Kesv$_{Opt}$::eGFP, Panel B: COX8::mCherry, Panel C: Merged Image of A and B. Scale bar represents 10 µm. On the right PCC and MC are indicated. **(D)** Shows the sorting pattern of My_LOV_Kesv$_{Opt}$ (N=4, n=83). **(E)** Depicts the rational design approach taken to generate the construct. On the left, a schematical depiction of BLINK1 is shown, with Kcv$_{PBCV-1}$ in grey, the LOV-domain in light green and the myristoilation site (My) inserted in the PM. On the right side, we can see the identical design, but with Kesv$_{Opt-SL}$ (light blue) instead of Kcv$_{PBCV-1}$.

In the first design step Kcv_{PBCV-1}, the potassium channel used in BLINK1, was switched for $Kesv_{Opt-SL}$ as the latter showed the most stable and effective sorting propensity to the mitochondria (compare chapter 3). The schematic design of both BLINK1 and the new channel can be seen in Fig. 16 E. Not shown in the sketch is the C-terminal GFP-tag on both Kcv_{PBCV-1} and $Kesv_{Opt-SL}$.

This first approach did not show the expected outcome. The construct did not show the desired sorting to the mitochondria, but was still sorted to the ER in 66% of the cells, while 30% did not show any visible sorting to a compartment, but were in this case uniformly distributed in the cytosol and in 4% cytosolic clustering was observed (Fig. 16 D). Fig. 16 A-C shows a representative image of My_LOV_$Kesv_{Opt-SL}$. The construct (A), clearly does not colocalize with the mitochondrial marker plasmid COX8::mCherry (B). This is also verified by the low PCC of 0.294, which is well below the threshold for a robust correlation of the two channels. The same holds true for the MC, which shows for a colocalization of (A) with (B) a value of 0.177 and therefore also excludes a sorting of My_LOV_$Kesv_{Opt-SL}$ to the mitochondria. The ostensible colocalization of (B) with (A) might be explained by the coiled structure of the ER, in which the mitochondria are embedded. So even with confocal resolution, they seem to lie within the ER structures. This results in the high $M_{B/A}$ of 0.671.

The unchanged sorting of My_LOV_$Kesv_{Opt-SL}$, in comparison to BLINK1, could mean that one of the other components apart from the potassium channel has a strong propensity to be sorted to the ER and that this sorting message overrules the targeting of the channel to the mitochondria.

To address the unwanted clustering an attempt was made to image the construct without GFP. GFP has the tendency to form clusters (Wang et al., 2019), which might have a negative impact on the sorting. In addition to this, GFP molecules are rather bulky and might hinder the tetramerization of a functional potassium channel surrounded by the necessary membrane anchored LOV-domains.

Therefore the *as*LOV-domain was swapped for phiLOV2.1 (Christie et al., 2012b; Buckley et al., 2015), a fluorescence reporter designed from *at*LOV (Chapman et al., 2008a). By designing two sets of constructs – one with the functional *at*LOV and one with the fluorescent phiLOV2.1, a potential negative impact of GFP on the sorting may be bypassed and the sorting of the constructs studied with the aid of phiLOV2.1 instead.

Unexpectedly there was no fluorescence detectable after exchanging the necessary amino acids in *at*LOV to generate phiLOV2.1 (Chapman et al., 2008b; Christie et al., 2012b), which are required to turning this protein into a stable fluorescence reporter. In the following studies it was therefore necessary to rely on GFP as a fluorescence reporter.

4.3. Localization studies of the necessary components to achieve the desired sorting pattern

As it was not possible to detect any cells that showed the desired sorting of My_LOV_Kesv$_{Opt\text{-}SL}$ to the mitochondria, but instead a robust sorting to the ER was retained, the next step was to determine whether one of the building parts used has the propensity to be sorted to the ER. Therefore, four new constructs were generated, in each of which an additional element was added. This should pinpoint which component might enhance the unwanted ER sorting pattern.

When just the LOV-domain is expressed, none of the cells show sorting of the construct to a compartment, instead the tendency of GFP to form clusters leads to 69% of the cells showing cytosolic clusters which colocalize neither with the ER nor with mitochondria. Further scrutiny of the images shows that this effect depends on the expression level: the brighter a cell appears, the more probable it is that clusters appear. The remaining 31% of the cells show a uniform distribution of GFP throughout the cell (see Fig. 17J).
The addition of a myristoilation sequence at the N-terminus of the LOV-domain led to a decrease in cells with clusters: only 34% of the imaged cells showed aggregates. In the rest of the cells (66%) no sorting could be detected. The addition of a membrane anchor like the myristoilation sequence was hence not sufficient to pull the construct to the plasma membrane.

For both LOV and My_LOV in about half the “not sorted” constructs, an interesting detail was to be observed, namely the appearance of distinct gaps in the GFP-fluorescence where the ER and mitochondria are located. Examples are shown in Fig. 17 A-F. In the first row the negative colocalization with the mitochondrial marker is illustrated, in the second row the decrease of GFP-fluorescence at the perinuclear ring. This shows clearly that both constructs are really excluded from the ER and the mitochondria. This type of cytosolic distribution, where the organelles appear as dark spots in an otherwise uniformly green cell is not the usual phenotype that can be seen when a protein is not sorted to any compartment. Much more usual would be a distribution throughout the whole cell, without distinct gaps in it (compare Fig. 10 panel E). This phenomenon could not be attributed to be related to the expression level of the constructs within the cell, both examples shown here emit a bright fluorescence but there were also weak fluorescing cells that showed these gaps in the fluorescence.

Since the first two constructs clearly showed that the LOV-domain remains strictly cytosolic, an attempt was made to target it to the mitochondria with the addition of a COX8 mitochondrial targeting sequence (MTS). The images in Fig. 17 J report that MTS_LOV was indeed sorted to the mitochondria in 9% of the cells, 56% the construct was not sorted and in 35% of the cells, clusters occurred

Encouraged by the small fraction of cells showing the desired mitochondrial sorting, a fifth construct was generated in which $Kesv_{Opt\text{-}SL}$ was included again. The hope that this channel, which is by itself very effectively sorted to the mitochondria, would increase the positive impact of the MTS was only partly confirmed. The MTS_LOV_$Kesv_{Opt}$ construct was sorted to the mitochondria in 10% of the cells, 33% did not show any sorting to a compartment and 8% had visible clusters. Unexpectedly, 49% of the cells showed again a pronounced sorting to the ER (Fig. 17 J).

In Fig. 17 G-I, a representative image of MTS_LOV_$Kesv_{Opt\text{-}SL}$ with mitochondrial sorting is shown. Notable here is the high background fluorescence in the cytosol, which indicates ineffective protein sorting or cleavage of GFP. This construct is therefore a good starting point for further optimization, as both the portion of correctly sorted cells and the sorting efficiency within one cell need to be improved to generate a useful optogenetic tool.

Following page:

Fig. 17: Screening for ways to improve LOV-domain sorting to the mitochondria

(A-F): Confocal images of My_LOV::eGFP, Panel A&D: My_LOV::eGFP, Panel B: COX8::mCherry, Panel E: HDEL::mCherry, Panel C: Merged Image of A and B, Panel F: Merged image of D and E. Scale bar represents 10 µm. On the right PCC and MC are indicated as well as a schematic image of My_LOV. **(G-I)** Confocal image of MTS_LOV-$Kesv_{Opt}$::eGFP, Panel G: MTS_LOV-$Kesv_{Opt}$::eGFP, Panel H: COX8::mCherry, Panel I: Merged Image of G and H. Scale bar represents 10 µm. On the right PCC and MC are indicated as well as a schematic representation of the construct. **(J)** Shows the sorting pattern of LOV (N=2, n=35), My_LOV (N=2, n=47), MTS_LOV (N=2, n=96), My_LOV_$Kesv_{Opt}$ (N=4, n=83) and MTS_LOV_$Kesv_{Opt}$ (N=2, n=39).

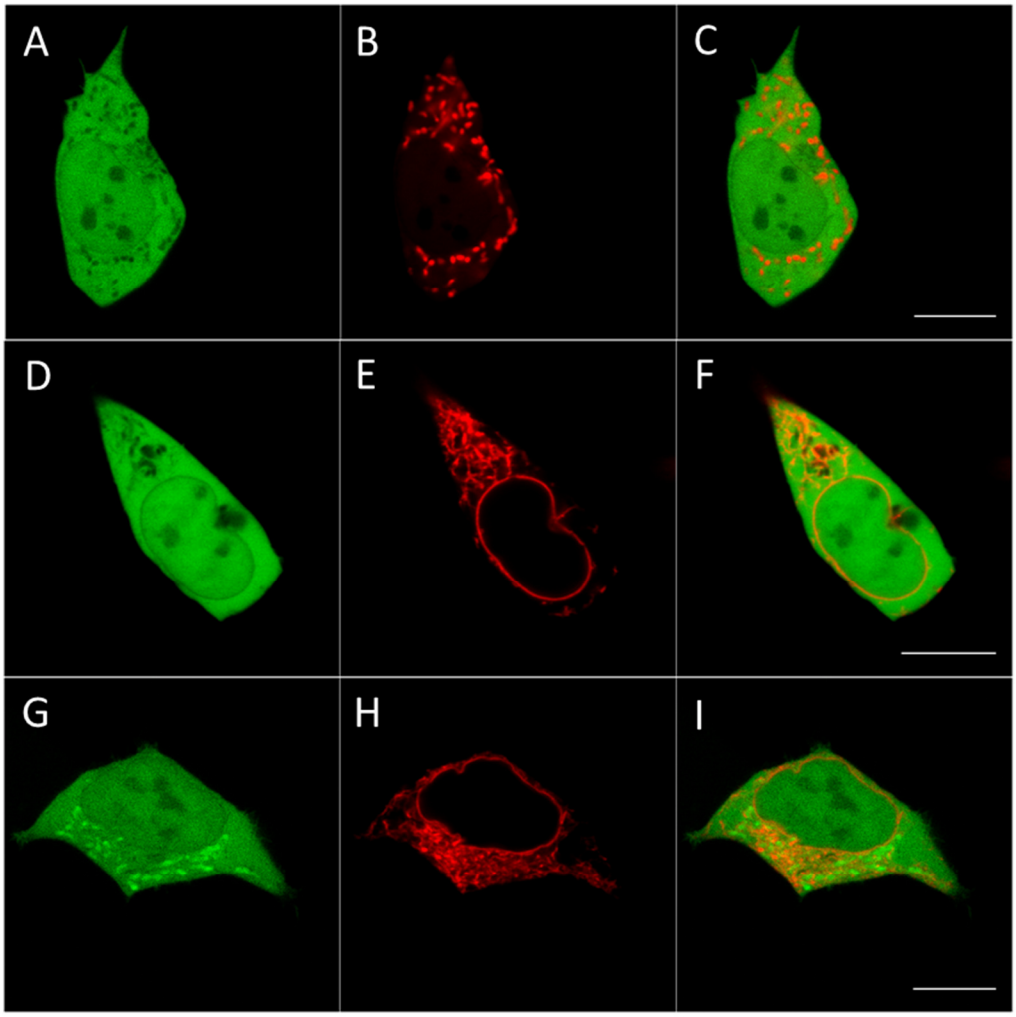

PCC = 0.216

$MC_{A/B}$ = 0.13
$MC_{B/A}$ = 0.624

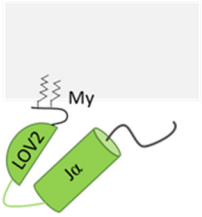

PCC = 0.26

$MC_{D/E}$ = 0.083
$MC_{E/D}$ = 0.34

PCC = 0.334

$MC_{G/H}$ = 0.223
$MC_{H/G}$ = 0.481

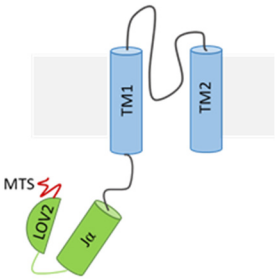

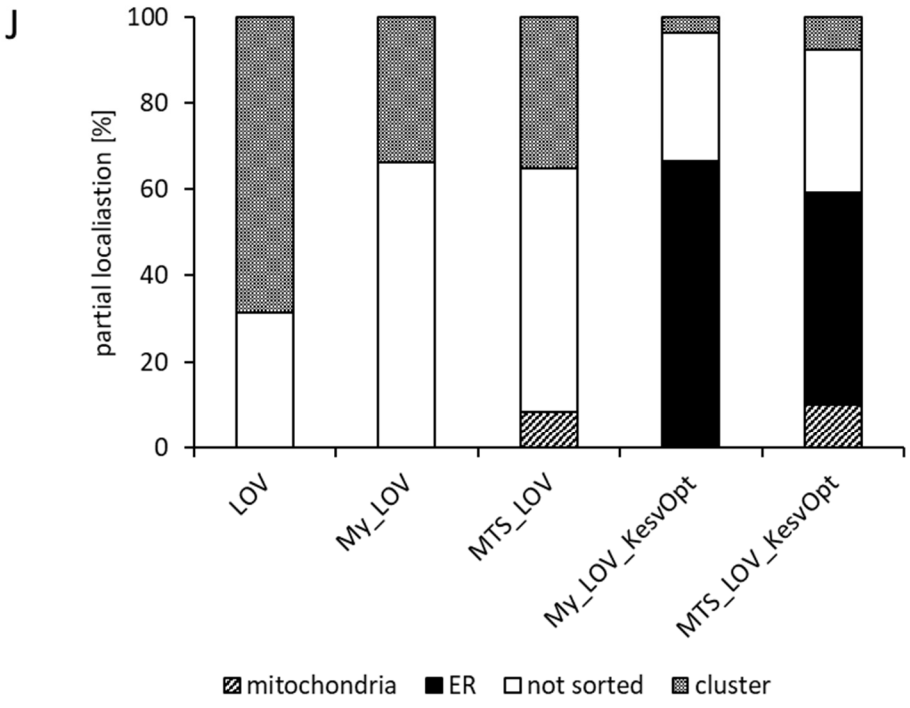

4.4. Multiplying the MTS leads to an effectively sorted channel

It has previously been shown that multiplication of the mitochondrial targeting signal can improve sorting efficiency to the desired organelle (Tkatch et al., 2017). Based on these finding, the next approach was to clone not one but six MTS in front of the LOV_ $Kesv_{Opt}$ construct. This led to a mitochondrial sorting efficiency of 100% (Fig. 18 G). In addition to this, there could be almost no unspecific cytosolic background fluorescence observed in any of the cells. The results of this experiment underscore that multiple MTS generate an efficient sorting of the construct to the mitochondrial membrane (Fig. 18 A and D). In direct competition with COX8::mCherry, the six COX8 mitochondrial presequences in the new construct had a so much higher affinity that the sorting of the mitochondrial marker was hindered (Fig. 18 E) or even entirely abolished (Fig. 18 B). This is also illustrated by the relatively low PCC value of 0,55 and 0,3 respectively and the MC which shows that almost 100% of the construct overlap with the mitochondrial marker, but the marker overlaps with the GFP signal only to 20% respectively 10%.

By adding the six repeats of the MTS to the putative light gated channel, a high efficiency and a very stable sorting to the mitochondria is obtained.

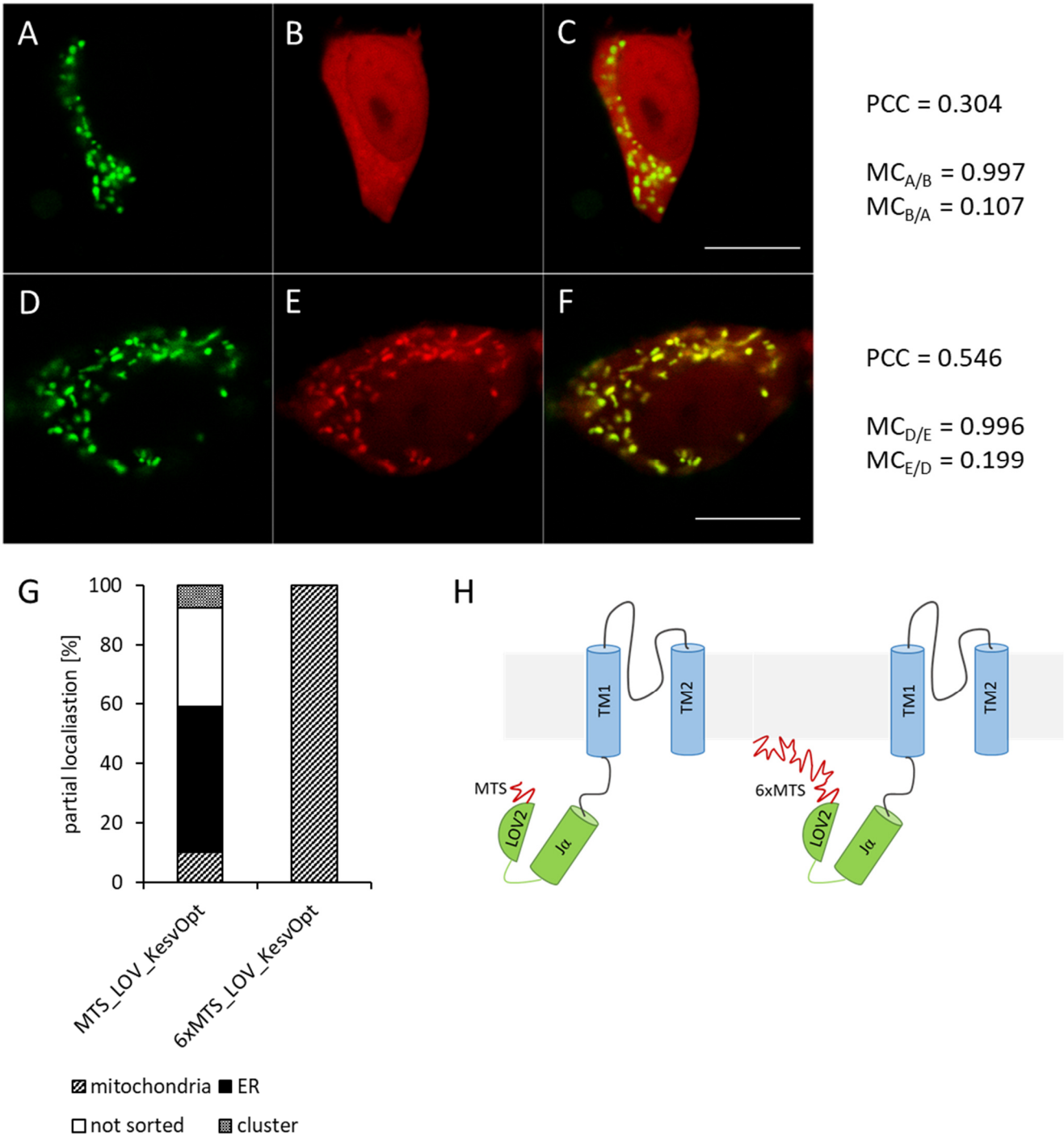

Fig. 18: Multiplication of the MTS leads to an effective sorting to the mitochondria

(A-F): Confocal images of 6xMTS_LOV_Kesv$_{Opt}$::eGFP, Panel A&D: 6xMTS_LOV_Kesv$_{Opt}$::eGFP, Panel B&E: COX8::mCherry, Panel C: Merged Image of A and B, Panel F: Merged images of panel D and E. Scale bar represents 10 µm. On the right PCC and MC are indicated. **(G)** shows the sorting pattern of MTS_LOV_Kesv$_{Opt}$. (N=2, n=39) and 6xMTS_LOV_Kesv$_{Opt}$ (N=2, n=159). **(H)** Schematic depiction of MTS_LOV_Kesv$_{Opt}$ and 6xMTS_LOV_Kesv$_{Opt}$.

4.5. MitoBLINK1

During the work at the constructs shown in this chapter, questions of the functionality of Kesv arose. It failed to depolarize mitochondrial membranes in FACS measurements (Kithil, 2018) and cannot be measured in patch clamp experiments, due to its sorting to the IMM. An attempt to reconstitute the channel in planar lipid bilayers also failed (data not shown).

To ensure a working light gated potassium channel, the original BLINK1 channel was used again, and the 6xMTS were added to the N-terminus of the myristoilation sequence (Fig. 19 E).

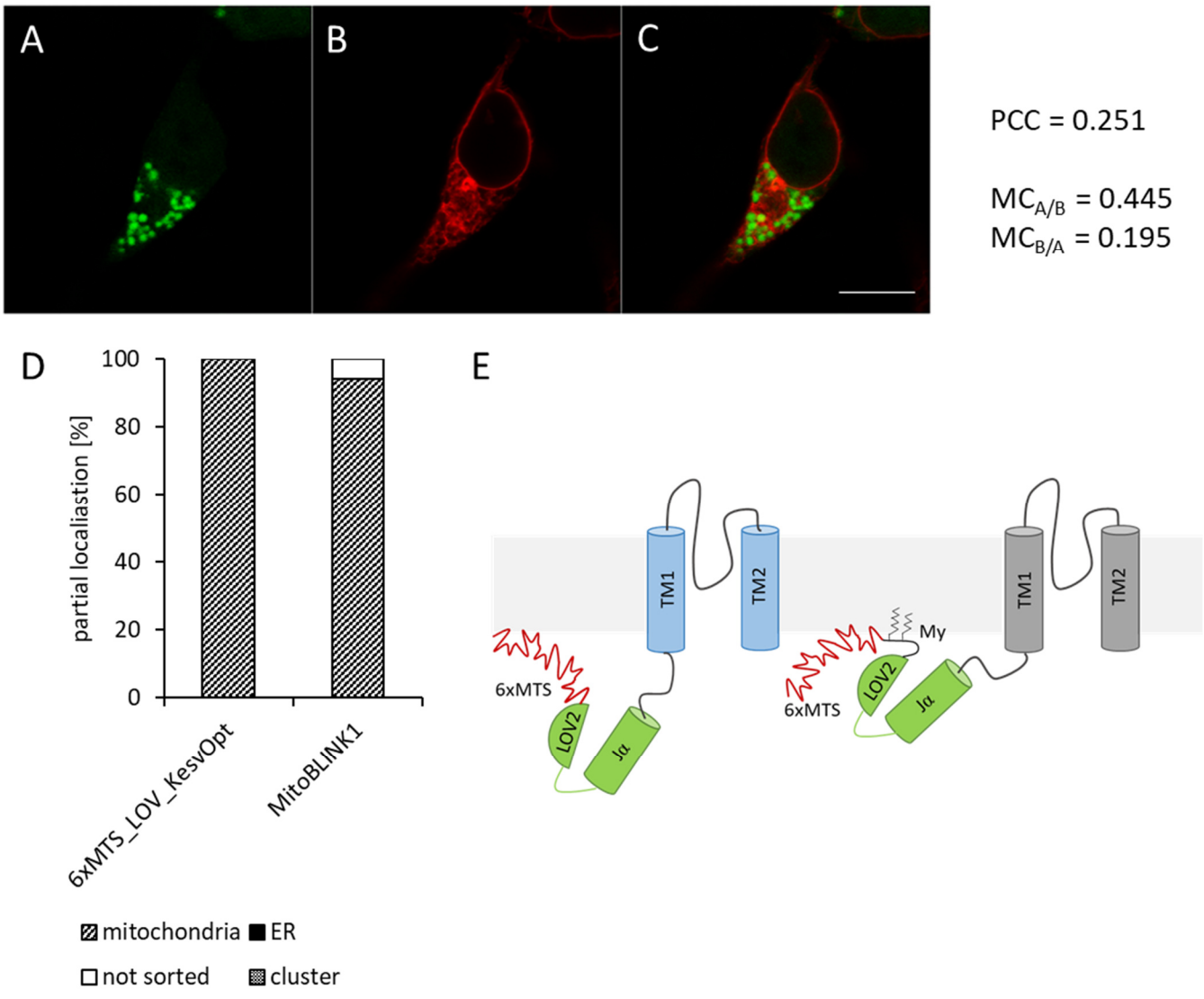

Fig. 19: MitoBLINK1 retains the stable mitochondrial sorting achieved through the six MTS

(A-C): Confocal image of MitoBLINK1::eGFP, Panel A: MitoBLINK1::eGFP, Panel B: HDEL::mCherry, Panel C: Merged Image of A and B. Scale bar represents 10 µm. On the right PCC and MC are indicated. **(D)** shows the sorting pattern of 6xMTS_LOV_Kesv$_{Opt}$ (N=2, n=159) and MitoBLINK1 (N=4, n=241). **(E)** shows the exchange of Kesv$_{Opt}$ back to Kcv$_{PBCV-1}$ and the insertion of a myristoilation sequence between the 6xMTS and the LOV-domain, the construct is now designed like the initial BLINK1, with the addition of 6xMTS at the N-terminus.

This new construct exhibited a stable mitochondrial sorting with low background fluorescence in the cytosol (Fig. 19 A-C), and did not colocalize with the ER marker. This is also verified by the low PCC and MC values. The portion of correctly sorted channels to the mitochondria amounts to 94% of the cells, only 6% did not show sorting to a specific compartment. But even in the not sorted cells, there are no gaps in the uniform GFP fluorescence where the organelles are located, as was observed for My_LOV (compare Fig. 17 A-F). So, it cannot be ruled out that in these cells a small portion of the MitoBLINK1 still reaches the mitochondria, but with a too high background fluorescence to distinguish the organelles from the cytosol.

4.6. MitoBLINK1 is a putative light-gated potassium channel that is effectively sorted to the mitochondria

In this chapter the sorting of the individual components of the light gated potassium channel BLINK1 are determined. The data show that the LOV-domain with and without the myristoilation sequence contributes no sorting signal. These building modules remain in the cytosol when expressed independently of a potassium channel, the myristoilation sequence is not sufficient to target the LOV-domain to the plasma membrane by itself. Unexpectedly, the addition of $Kesv_{Opt}$, which is by itself sorted to the mitochondria with a high effectivity, does not alter the sorting destination of the construct to the mitochondria, but enhances targeting to the ER instead. This can be in part be counteracted by the introduction of a COX8 mitochondrial presequence at the N-terminus. The data further show that to enable a really effective and stable sorting to the mitochondria, the introduction of a six-fold repetition of the COX8 sequences was necessary. The resulting sorting signal however is even strong enough to pull the initial BLINK1 construct to the mitochondria – resulting in MitoBLINK1.

There is still evidence lacking that MitoBLINK1 exhibits the same functional properties in the mitochondria as BLINK1 does at the PM. It is not sure, if the myristoilation sequence will insert as readily into the IMM as it does in the PM, concerning the fact the IMM has a very different lipid composition (Houtkooper and Vaz, 2008; Horvath and Daum, 2013), protein content (Sjöstrand, 1963; Frey and Mannella, 2000) and thereby different membrane thickness (Toshiyuki Yamamoto, 1963). Apart from this problem, functionality should not be compromised compared to BLINK1. If the myristoilation sequence anchors itself into the IMM, then the mechanical strain, which is generated by conformational changes of the LOV-domain under blue light illumination, should gate the channel in the same way as it is the case in the PM.

There is also a possibility that different membrane properties of the IMM compared to the PM can also influence the functional properties of Kcv_{PBCV-1}. It is known that the small viral potassium channels are sensitive to different lipids in their environment which alter the unitary conductance and the open probability of these channels (Winterstein, 2019). If this is the case with MitoBLINK1, there is a library of point mutations described for Kcv_{PBCV-1} which specifically address the issue of unitary conductance or open probability (Rauh, 2018), that might compensate any negative impact of the membrane environment on channel function, thereby modeling the channel according to the desired properties.

5. Light dependent protein expression: LOV-based system

5.1. The EL222 system

In the previous chapter, different methods have been described for the engineering of a light-gated potassium channel. In order to control hyperpolarization of cells with light on an even longer timescale, stable levels of hyperpolarization for several hours to days are necessary. This is for example necessary in long-term silencing experiments during the development of neural networks or other organ systems that harbor excitable cells. To satisfy such a desire, a light-induced gene expression system might be better suited than light-gated channels.

One example for such an optogenetic expression system is the EL222 system. EL222 was first described in 2013 as a blue-light induced DNA-binding protein (Zoltowski et al., 2013). EL222 is the LOV-domain from *Erythrobacter litoralis*, an obligately anaerobic, bacteriochlorophyll-containing marine proteobacterium (Yurkov et al., 1994). Upon blue light illumination the sensory LOV domain reorientates and thereby drives the reorientation of helix-turn-helix (HTH) effector domains. These structural changes lead to the transition from the inactive monomeric state of EL222 to its active dimeric DNA-binding form (Zoltowski et al., 2013).

The functionality of the EL222 based optogenetic system has been reported for *E. coli* (Jayaraman et al., 2016), HEK293 cells and in zebrafish larvae (Motta-Mena et al., 2014).

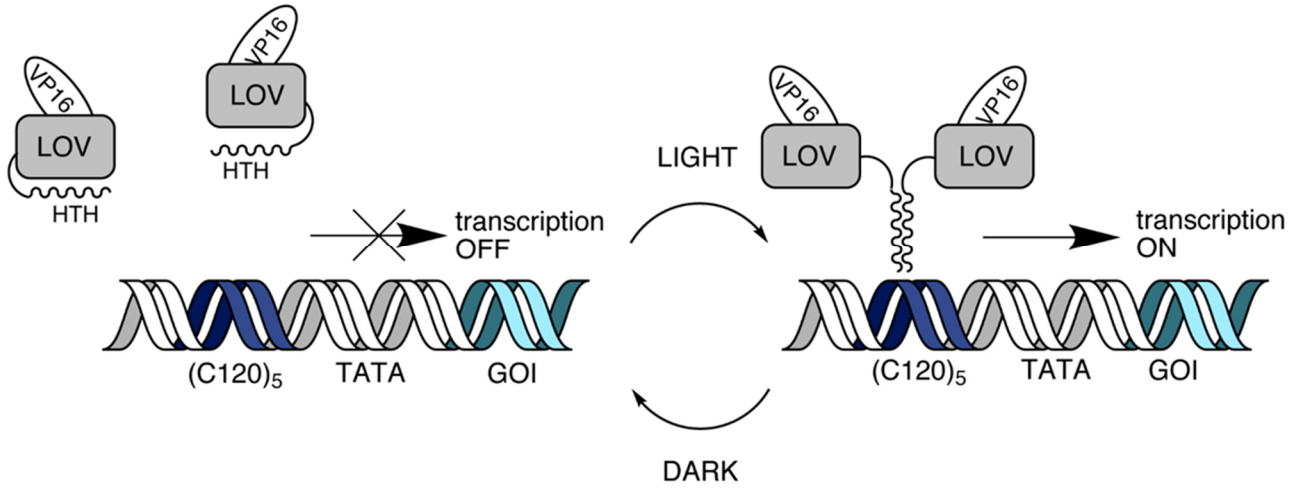

Fig. 20: Schematic representation of the EL222 system

One vector carries a VP16 activator domain, fused to the core domain of EL222 (LOV-HTH). A second vector encodes five copies of the EL222 binding clone C120, upstream of a TATA-Box promotor and the Gene of Interest (GOI). In the dark, EL222 is depicted in the inactive monomeric state. Upon illumination two HTH-motives dimerize and bind to C120, bringing the VP16 activator domain in close proximity to the promotor, thereby initiating transcription of the GOI.

For the application in mammalian cells, an inducible promotor system has been developed by Motta-Mena and coworkers. (Motta-Mena et al., 2014) In the dark, the HTH DNA-binding motive remains tightly bound to the LOV domain, keeping the system in its monomeric inactive state. Upon illumination with 450 nm blue light the photochemical reaction of the flavin-chromophore in the LOV domain triggers a conformational change which leads to the activation of the HTH motive and subsequent dimerization. A second promotor encodes five copies of an EL222 binding clone (C120) are encoded, followed by a TATA-box promotor. Downstream the gene of interest (GOI) is inserted. The active HTH motive binds the C120, bringing the VP16 activator domain in close proximity to the promotor and thereby initiates transcription of the GOI (comp. Fig. 20). In a proof of concept study, the authors demonstrated the light dependent expression of luciferase in different mammalian cell lines, as well as *in vivo* in zebrafish larvae (Motta-Mena et al., 2014).

More recently, the tuning of gene expression in *Saccharomyces cerevisiae* has been reported. With the modulation of the applied light pulses and the use of a promotor library with different strengths, the tuned expression of multiple genes was demonstrated (Benzinger and Khammash, 2018).

One major advantage of this LOV based approach is that it is fully genetically encoded. The LOV-HTH motive is relatively small (33 kDa), and there are no cofactors or precursors which need to be added separately, as the flavin chromophore is endogenously present in eukaryotic cells.

5.2. The EL222 system leads to a light-dependent expression of different viral potassium channels

Inspired by the work of Motta-Mena and coworkers, who described an EL222 expression system which is already optimized for expression in mammalian cells, the logical approach, was to replace the luciferase with $Kesv_{Opt}$. This should result in light-dependent expression of a potassium channel targeted to the IMM. With the same rationale, the luciferase was also replaced by $Kcv_{PBCV\text{-}1Opt}$ to induce light-inducible expression at the plasma membrane. This would be the first attempt so far to use the EL222 system not only for the expression of a reporter but of a functional potassium channel in a specific compartment in mammalian cells.

In a first step the light-dependence of the system was established. To verify an increased gene expression upon illumination over that observable in the dark state controls, cells transfected with the EL222 $Kesv_{Opt}$ system were exposed to pulsed light for either 5 or 16 hours (Fig. 21 A). As protocols, different pulse lengths with light-on-times ranging from 20 to 120 seconds were checked. Off-times between the pulses were kept at 60 seconds. If the system was exposed to 16 hours of pulsed light an increase in fluorescence intensity was observed. A notable increase above dark state levels starting with 60 s illumination pulses. The highest relative fluorescence intensity (RFI) was observed with 75 s on-time, here the RFI is 1.29±0,07 AU. For pulse lengths from 75 s to longer illumination times, the fluorescence decreased again to low levels of 1.10±0.03 AU at continuous illumination. This decrease is probably due to increasing cytotoxic effects caused by the prolonged effect of the blue light. Important to notice is the RFI of the dark state control, which is 1.15±0.05 AU (Fig. 21 A, black diamonds). The system therefore shows leak expression, even if the cells are kept in total darkness. The maximum increase in fluorescence obtained by 16 hours of pulsed light is 0.15 AU at 75 s on-time.

In a second set of experiments the pulses were limited to 5 hours, overall incubation time remaining constant at 16 hours post transfection, the dark state control is unchanged (1.15±0.06 AU) compared to the value for 16 hours of pulses (Fig. 21 A) as was to be expected. The level of leak expression is therefore reproducibly on the same level. For the 5-hour pulses, the maximum change of RFI occurs if the cells are treated with continuous light, with 1.24±0.14 AU (Fig. 21A, white diamonds). It can be concluded from this, that 5 hours of pulsed light is not sufficient to reach the full expression of EL222::$Kesv_{Opt}$. If the illumination is limited to 5 hours, the maximum increase is even smaller than at 16 hours, the peak value being 0.08 AU at 5 hours of continuous illumination.

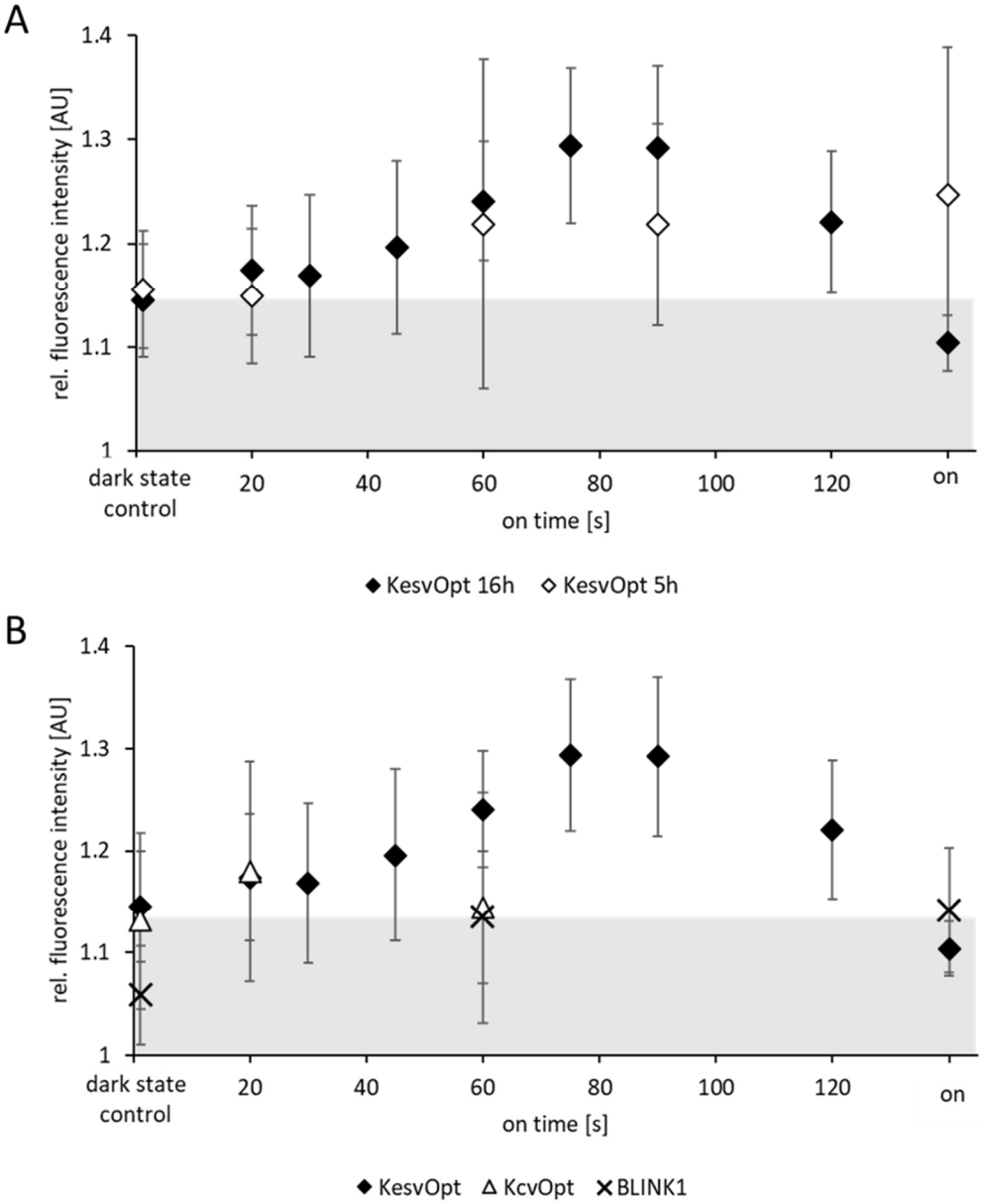

Fig. 21: Illumination dependent change in fluorescence intensity using the EL222 system

(A) Rel. fluorescence intensity [AU] plotted against the on-time [s] of $Kesv_{Opt}$ illuminated with pulsed light for 16 hours (black diamond) or 5 hours (white diamond). Off time between pulses is always 60 s, on times as indicated on the x-achsis, light intensity 120 µE. For each timepoint, 30 cells were imaged and the fluorescence intensity measured. The gray shaded part represents the mean level of fluorescence without illumination as indicated by the values for the dark state control. Error bars represent standard deviation. **(B)** Rel. fluorescence intensity [AU] plotted against the on-time [s] of $Kesv_{Opt}$ (black diamond), $Kcv_{PBCV\text{-}1Opt}$ (white triangle) and BLINK1 (black X) illuminated with pulsed light for 16 hours. Off-time between pulses is always 60 s, on-times as indicated on the x-achsis. For each timepoint, 30 cells were imaged and the fluorescence intensity measured. The gray shaded part represents the mean level of fluorescence without illumination as indicated by the values for the dark state control. Error bars represent standard deviation.

To obtain light-dependent expression of a potassium channel in the plasma membrane, the EL222 construct was also generated using $Kcv_{PBCV\text{-}1Opt}$. Here again the 16 hours pulse protocols were used. For comparison the values of $Kesv_{Opt}$ are shown in the graph again (Fig. 21 B).

Again, the construct shows leak expression in the dark. The value of 1.13±0.09 AU being in the same range as before. A difference however occurs for the two constructs in their increase in fluorescence upon illumination. The increase in RFI for $Kcv_{PBCV\text{-}1}$ is much lower compared to the values obtained for $Kesv_{Opt}$. The highest value was 1.18±0.11 AU for 20 s on-time. This translates to a maximal increase in RFI of only 0.05 AU.

In an attempt to generate a double light-dependence, BLINK1 was also cloned into the EL222 expression system. In this case the dark state control exhibits a relative fluorescence value of 1.06±0.05 AU, showing a lower leakiness compared to the other constructs. But this positive effect is abolished by an equally low RFI upon illumination. The maximum fluorescence reached after continuous illumination was not higher than 1.14±0.06 AU. This translates to a maximum increase in RFI of 0.12 AU.

To give a better overview of the maximum increase in RFI, all values are plotted in Fig. 22. It becomes evident, that the most pronounced increases were obtained from protocols with 16-hours illumination of $Kesv_{Opt}$ and BLINK1. Notable among these results are the generally low values for BLINK1 expression, which stay below the threshold for the dark state controls. In all the other constructs, which were examined here this leak expression in the dark was much higher. (compare Fig. 21 B).

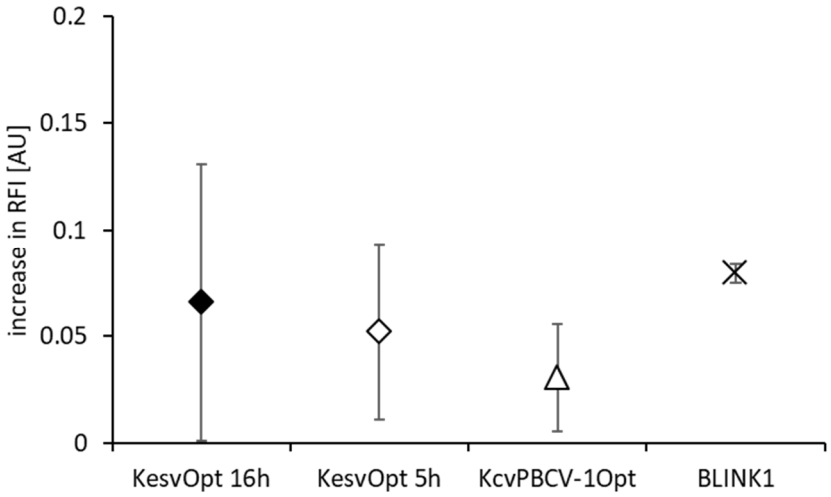

Fig. 22: Increase in rel. fluorescence intensity upon illumination (RFI) for all EL222 constructs

Shown are the ratios of the RFI of the dark state controls divided by the mean RFI upon illumination for $Kesv_{Opt}$ illuminated for 16 hours (N=9, n=270), $Kesv_{Opt}$ illuminated for 5 hours (N=5, n=150), $Kcv_{PBCV\text{-}1Opt}$ (N=3, n=90) and BLINK1 (N=3, n=90) expressed under control of the EL222 system. Error bars indicate standard deviation.

5.3. Expression in the EL222 system corrupts the sorting of Kcv_{PBCV-1} but not of $Kesv_{Opt}$

In the aforementioned experiments only the global increase in fluorescence from GFP-tagged channels was monitored, which were expressed under control of the EL222 system. Here the question is addressed, whether the EL222 system has any impact on the sorting of the channel proteins. Therefore, the images were reevaluated and the sorting patterns of the constructs determined.

Fig. 23 A-C shows, a representative image of a HEK293 cell expressing $Kesv_{Opt}$ under control of the EL222 system. The image clearly that the effective sorting of $Kesv_{Opt}$ to the mitochondria with low cytosolic background fluorescence is not compromised. This is also confirmed by the PCC value of 0.548 and the high MC of 75% for colocalization of the channel (Fig. 23 A) with the mitochondrial marker (Fig. 23 B). As in this case the mitochondria-staining fluorescent dye MitoTracker Red was used to stain the mitochondria, the marker colocalizes with the channel only to 37%. This is caused by the signals of the surrounding cells, which are also stained with the marker, but do not express the EL222 $Kesv_{Opt}$ construct, leading to non-colocalizing signals and thereby lowering the coefficient of MitoTracker (Fig. 23 B) with the channel protein expressing cell.

This robust sorting of $Kesv_{Opt}$ when expressed in the EL222 system is also underscored by the statistical analysis: 98 % of the EL222 $Kesv_{Opt}$ expressing cells show mitochondrial sorting of the channel protein, and only in 2 % a uniform GFP fluorescence throughout the cell was observed, indicating a cytosolic distribution of the construct (Fig. 23 G). Compared with the constitutively expressed $Kesv_{Opt}$, which is sorted with 100% efficiency to the mitochondria, the sorting of the channel is hence well conserved when expressed in a light-dependent manner in the EL222 system.

For EL222 $Kcv_{PBCV-1Opt}$ a rather different picture emerged. This construct showed an unexpected shift of sorting from the ER to the mitochondria. In Fig. 23 D-F representative images of the observed localizations are shown. The channel could be observed in three different destinations: in the ER, the mitochondria and uniformly distributed throughout the entire cell.

Even more surprising was the observation that the sorting of the construct to the mitochondria is with 54% the most pronounced one. Only 2% of the cells expressing the EL222 $Kcv_{PBCV-1Opt}$ construct showed a sorting of the protein to the ER and 44% of the cells showed uniform fluorescence throughout the cell (Fig. 23 G). Collectively, the results of these experiments show that the expression of $Kcv_{PBCV-1Opt}$ under control of the EL222 system causes a major shift in sorting. Compared to the non-light dependent $Kcv_{PBCV-1Opt}$, which is sorted to the ER in 61% and shows a cytosolic distribution in 39%, the sorting is strongly affected if the channel is expressed in a light dependent manner in the EL222 system.

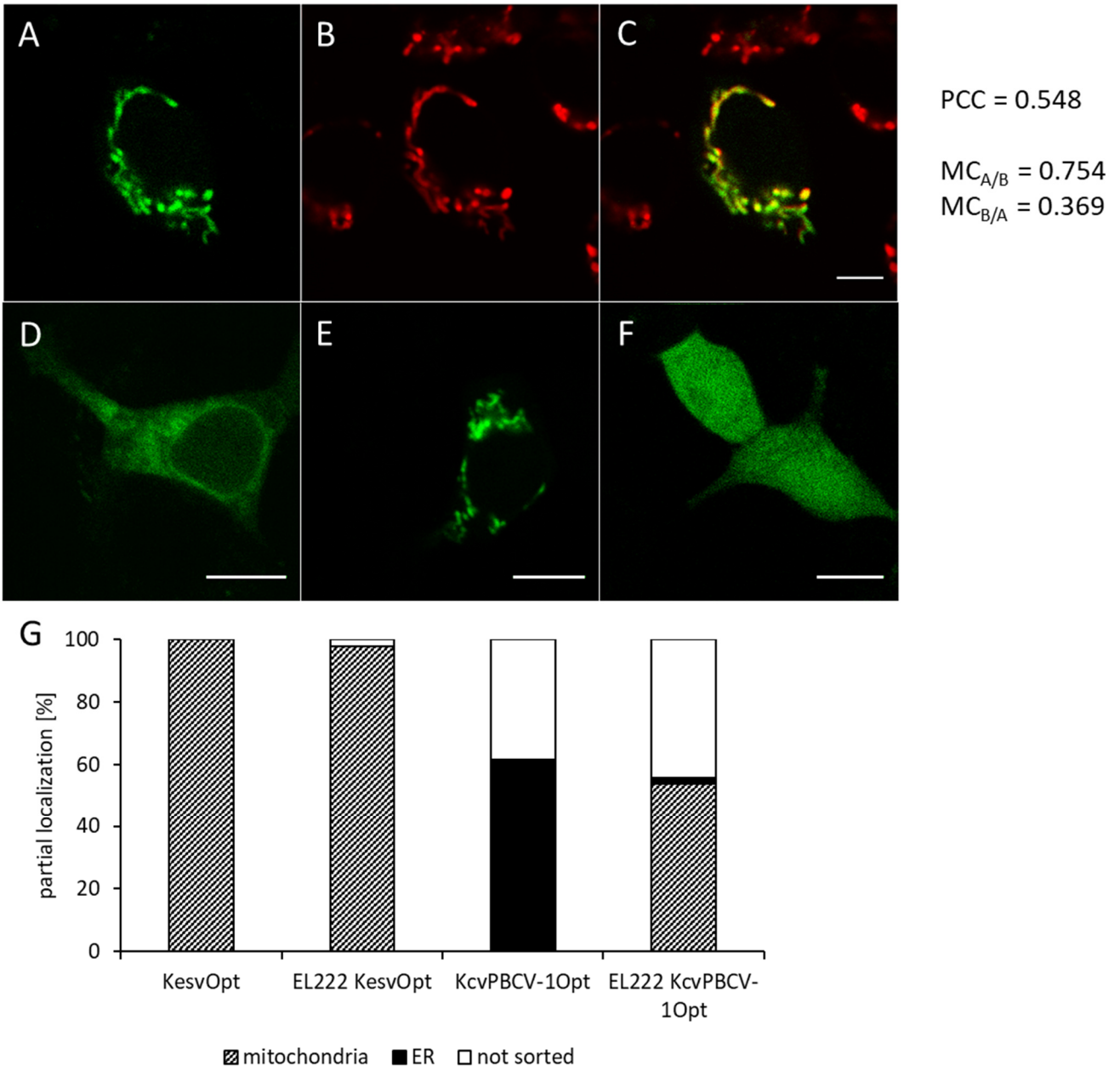

Fig. 23: Sorting of EL222 Kesv$_{Opt}$ and EL222 Kcv$_{PBCV\text{-}1Opt}$

(A-F): Confocal images of EL222 Kesv$_{Opt}$::eGFP, Panel A: EL222 Kesv$_{Opt}$::eGFP, Panel B: MitoTracker Red, Panel C: Merged Image of A and B, on the right PCC and MC are indicated. Panel D-F: Representative images of EL222 Kcv$_{PBCV\text{-}1Opt}$::eGFP. Scale bar represents 10 µm. **(G)** shows the sorting pattern of Kesv$_{Opt}$ (N=4, n=150), EL222 Kesv$_{Opt}$ (N=10, n=323), Kcv$_{PBCV\text{-}1Opt}$ (N=5, n=223) and EL222 Kcv$_{PBCV\text{-}1Opt}$ (N=4, n=104).

5.4. Leakiness and corruption of sorting render EL222 is a suboptimal choice for a modular K^+ channel-based optogenetic tool

The combination of the EL222 system with small viral potassium channel proteins demonstrates several key problems which render the current construct not suitable as a long term optogenetic silencing system.

The first issue which needs to be addressed to render the construct effectively light-dependent, is the leakiness of the construct in the dark. The mean RFI value of the dark state controls was 1.14 AU, which means that the LOV domain must dimerize and promote gene expression independent of illumination. To abolish the activation of the LOV domain in the dark, mutational screening for a tighter binding of the HTH-motive under dark state conditions would be necessary (Song et al., 2011).

The second issue which needs to be addressed is the low dynamic range of the illumination effect. The maximum increase in light-induced channel expression to be observed was 0.15 AU for $Kesv_{Opt}$ after 16 hours of pulsed illumination. This represents only a doubling of expression, compared to the leakiness in the dark. Here again mutational screenings would be necessary for enhancing dimerization of the LOV domain upon illumination as has been shown for *as*LOV (Strickland et al., 2010; Zimmerman et al., 2016). Another approach would be to search for a stronger binding motive (Salomon et al., 2000) or to put the GOI under a stronger promotor (Javahery et al., 1994). The difficulty here being, that optimizing gene expression with increased affinity of the LOV domain for its binding partner or the use of a stronger promotor would probably lead to a rise in leakiness again.
Another drawback of the EL222 system is the necessity of a rather high light intensity for illumination. The short wavelength of 450 nm blue light necessary for the activation of the LOV domain conveys a lot of energy to the cells. Altogether this bears the risk of potentially harmful effects in the target cells from light triggered induction of ROS production and mitochondrial stress (Godley et al., 2005; Kuse et al., 2014). In the experiments described above, attempts were made to limit the light dose on cells by shortening the light pulses or the overall illumination time. However, all these approaches resulted in a decrease in gene expression (compare Fig. 21). Here again optimization of the dimerization would be necessary, to enable a good activation of gene expression under low lighting conditions (Strickland et al., 2010; Zimmerman et al., 2016). One approach to overcome this shortcoming could be spectral tuning of the LOV domain, shifting its sensitivity to longer wavelengths, as has been demonstrated for channelrhodopsins (Lin et al., 2013). A spectral shift of the LOV domain to longer wavelength would not only decrease harmful side effects of the system, but also promote a deeper penetration of the stimulating light, making it more suitable for the use in thicker samples e.g. tissue cultures or 3D cell culture (Muller et al., 2013; Kaberniuk et al., 2016).

The final issue to be addressed to improve the EL222 system is to understand its impact on the sorting of the $Kcv_{PBCV\text{-}1Opt}$ channel. As this construct was intended to hyperpolarize the whole cell by inserting into the PM, the change in sorting from the ER to the mitochondria is highly undesirable. So far, no rational explanation can be offered for this change in channel localization. After translation, the channel with its GFP-tag should undergo the same sorting pathway, independent of whether it is constitutively or light-dependently expressed. Since there are no additional tags, proteins or sorting sequences attached to the channel when expressed in the EL222 system, the sorting destiny should not differ in any way from that of the constitutive construct. Also, an influence of linker-length on sorting as is described in chapter 3.2 can be ruled out in this case as well. The channel was cloned into the vector with the same linker which was also used in the constitutive construct.

Taken together, the experimental results rule out the EL222 system in combination with a small viral potassium channel as a suitable optogenetic silencing tool. The overall behavior of the system is not sufficiently promising to justify further experiments or approaches for optimization.

6. Light dependent protein expression: cryptochrome-based expression system

6.1. The CRY2-CIB1 system

The photolyase homology region (PHR) of *Arabidopsis thaliana* cryptochrome 2 (CRY2) was first described in 1998 by Somers and coworkers (Somers et al., 1998) as the synchronizing element in the circadian clock mechanism of *A. thaliana*. Later on, it was found that CRY2 also plays an important role in floral initiation, where it interacts upon blue-light illumination with the cryptochrome-interacting basic-helix-loop-helix protein 1 (CIB1) (Liu et al., 2008). CIB1 acts as a transcription factor, initiating gene expression in a variety of plant metabolism pathways, such as seedling growth, root development, photoperiodic control of flowering time, stomatal opening, magnetoreception and programmed cell death in *A. thaliana* (Yu et al., 2010).

For photoexcitation of CRY2, a flavin-adenine dinucleotide (FAD) has to be non-covalently bound in the chromophore-binding domain of the PHR. In the dark, FAD is oxidized, while blue-light illumination causes a reduction of FAD. In this way, dark-light transitions lead to reversible conformational changes in CRY2, causing in turn an interaction with CIB1, and as a consequence an initiation of gene expression (Liu et al., 2010; Liu et al., 2011).

The first approach in harnessing this photoinduced activation of gene expression as an optogenetic tool to induce protein translocation and light-induced transcription was described in 2010 (Kennedy et al., 2010). Since then, the CRY2-CIB1 interaction has been used to study synaptic composition and function (Sinnen et al., 2017), insulin secretion (Xu et al., 2016), optogenetic protein interaction and clustering (Taslimi et al., 2016; Xu et al., 2016; Benedetti et al., 2018), the role of β-arrestin in G-protein coupled receptor trafficking (O'Neill and Gautam, 2014; Takenouchi et al., 2018) and phosphoinositide metabolism (Idevall-Hagren et al., 2012). There are also multiple systems to apply the CRY2 CIB1 system as a tool for epigenetic manipulations, such as the reversible modulation of endogenous gene expression and chromatin modifications in mouse neurons (Konermann et al., 2013), the loci-specific alteration of methylation state in the genome of neural stem cells (Lo et al., 2017), the light dependent induction of gene expression in a cell line stably expressing CRY2 and CIB1, using the CRISPR/Cas9 system (Polstein and Gersbach, 2015).

Upon illumination, CRY2 does not only interact with CIB1, but also forms CRY2-CRY2 dimers (Che et al., 2015). This dimerization of CRY2 has been used to induce optogenetic protein clustering for the study of protein interactions in plant and mammalian cells (Taslimi et al., 2014).

Since the CRY2-CIB1 system is only activated by blue light, it is also possible to combine it with other optogenetic tools. This has been done by Yüz and coworkers for studying the control of cell adhesion on different substrates. For this purpose, the CRY2-CIB1 system was combined with the far-red light activated PhyB/PIF system to attach different substrates to CIB1 and PIF respectively. In this way the

growth of cells on two different substrates is regulated, depending on the wavelength of the light (Yüz et al., 2018).

For the present study, the CRY2-CIB1 gene expression system described by Pathak et al. was taken as the starting point (Pathak et al., 2017). In this system, CRY2 is fused to a galactose binding domain (Gal4BD), and CIB1 to a VP64 activator domain (VP64AD). The GOI is located upstream of a galactose upstream activator sequence (GAL4UAS) (Fig. 24). In the dark, CRY2 and CIB1 remain as monomers in the cytosol, and upon illumination with 450 nm blue light the two components dimerize, the Gal4BD interacts with the Gal4UAS. This brings the VP64AD in close proximity to the GOI forming an initiation point for transcription.
In the following chapters, this CRY2-CIB1-based optogenetic gene expression system, was used to induce the expression of minimal viral potassium channels in both the PM and the IMM to generate a modular optogenetic toolbox for the long-term hyperpolarization of cells.

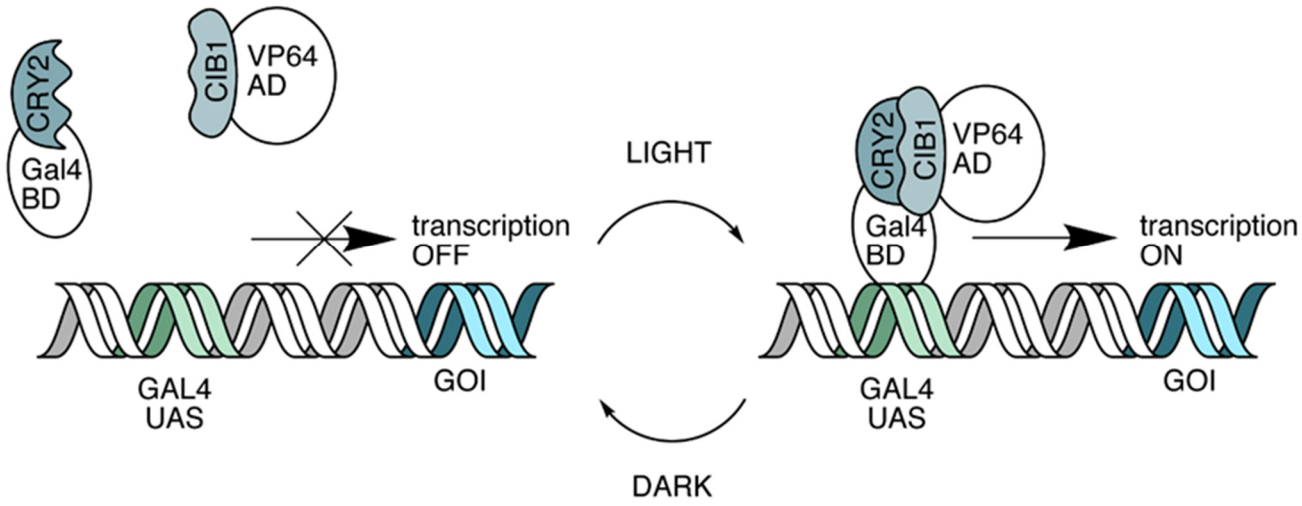

Fig. 24: Schematic representation of the CRY2 CIB1 expression system

In the dark, CRY2::Gal4BD and CIB1::VP64AD remain free in the cytosol, the GOI under the control of the Gal4UAS is not transcribed. Upon illumination CRY2 and CIB1 dimerize, bringing the VP64AD in close proximity to the GOI and transcription starts.

6.2. Establishing light-dependence and optimal illumination protocols for the CRY2 CIB1 system

Based on the experimental results obtained from the EL222 system (compare chapter 5), the first step was to ensure the functionality of the CRY2 CIB1 system as a light-induced gene expression system. This included the establishment of illumination protocols, which ensure an effective activation of the system whilst keeping any potentially damaging effects of the blue-light illumination minimal.

Initially the pulse protocols described for the EL222 system were tested, illuminating the cells for 16 hours with 120 μE of 450 nm blue-light. This approach led to a robust increase in fluorescence compared to the dark state control. It becomes clear from Fig. 25 A that already the illumination with the shortest light pulse (10 s on, 60 s off) led to a full activation of the system. Longer on-times than the 90 s shown here were even lethal for the cells, indicating an expression level too high to be tolerated by the cells. This led to the stepwise reduction of the light intensity, as shown in Fig. 25 B. The initially used 120 μE used in the previous experiments were taken as the base value of 100%. From there on, the intensity was reduced stepwise to 5% (6 μE). It becomes clear that the reduction of light-intensity did not lead to a decrease in expression level, which can be seen from the stable fluorescence intensity around 1.6 AU. To further minimize harmful effects of the illumination, the duration of the light-application was reduced from 16 hours to half an hour (Fig. 25 C). The reduction from 6 hours to half an hour led only to a slight decrease in fluorescence intensity of 0.2 AU.

From this first set of experiments it became quite clear, that the CRY2 CIB1 system is far more light-sensitive than the EL222 system. Reduction of light intensity and illumination time did not have adverse effects on the expression level of $Kesv_{Opt}$. Important to note is that not only the maximum expression level of the new system is higher, but also the background activity in the dark is lower, making it a promising candidate for light-inducible expression potassium channels.

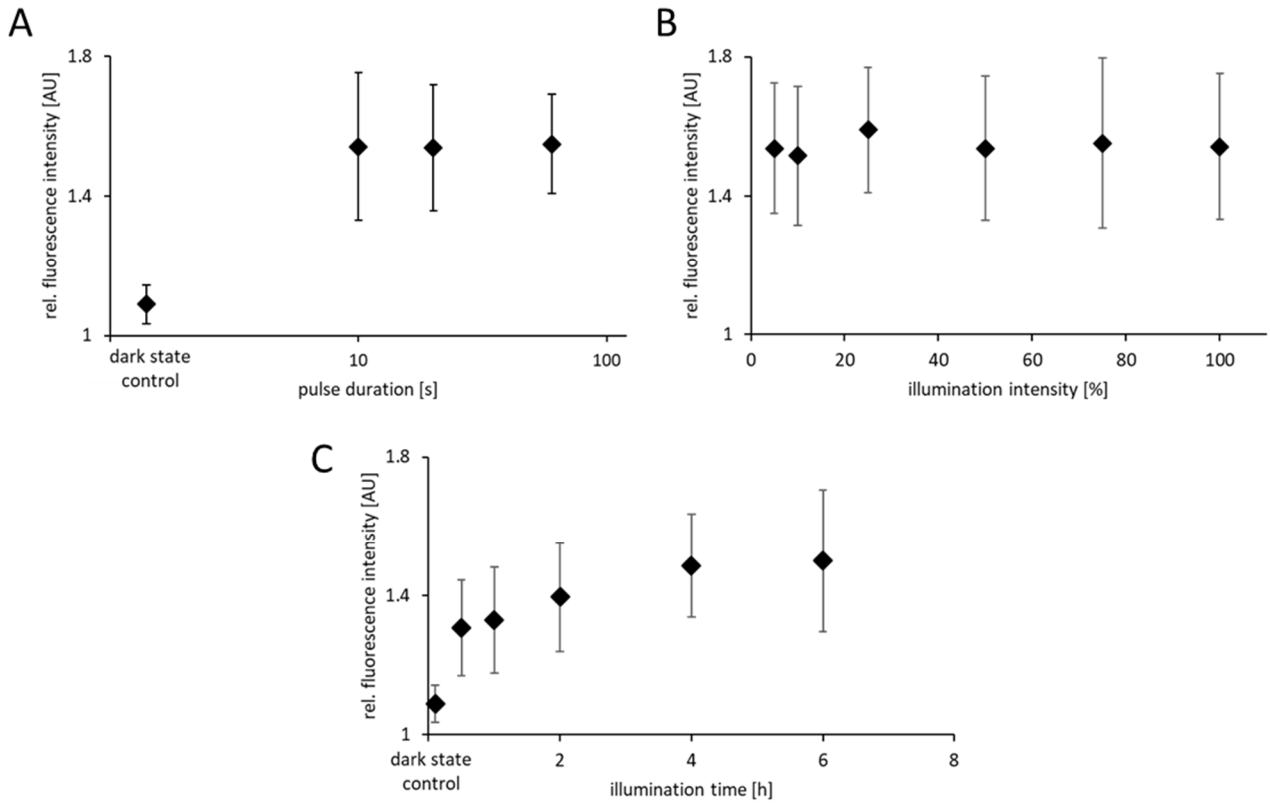

Fig. 25: Determination of the optimal illumination protocols for expression of $Kesv_{Opt}$ in the CRY2 CIB1 system

(A) shows the RFI of CRY2 CIB1 $Kesv_{Opt}$ illuminated for 16 hours with light pulses from 10 to 90 s, off-time between pulses is always 60 s. Light intensity: 120 µE. Dark state control is indicated on the left. For each timepoint, 20 cells were imaged, overall incubation time after transfection: 16 h. Error bars represent standard deviation. **(B)** shows the stepwise reduction in light intensity from 120 µE (100%) to 6 µE (5%). For all timepoints, cells were illuminated for 16 hours with pulsed light (10 s on, 60 s off). Overall incubation time: 16 h. Error bars represent standard deviation. **(C)** shows the influence of different illumination durations from 0.5 to 6 hours. The dark state control is indicated on the left. Again, the cells were illuminated with pulses (10 s on, 60 s off), light intensity 6 µE, overall incubation time: 16 h. Illumination was always ended 4 hours prior to imaging. Error bars represent standard deviation.

6.3. Activation of the CRY2 CIB1 system is comparatively fast, and the expression level remains stable for a prolonged time

After having obtained encouraging results in the first set of experiments with the CRY2 CIB1 system, the next question to address was the response time and duration of light induced gene expression. To monitor the kinetics, an experiment was designed in which HEK293 cells were incubated for 16 hours after transfection and illuminated for one hour with pulsed light at varying timepoints. In Fig. 26 the fluorescence intensity of GFP is plotted as a function of the off time after illumination. It becomes clear that the fluorescent signal already rises immediately after illumination above control level (1.08±0.05 AU) to 1.14 AU. Maximum expression with an RFI of 1.31 is reached half an hour after

illumination. This elevated expression level remains stable until 9 hours post transfection, before the expression drops again to dark state levels.

This experiment clearly demonstrates that the CRY2 CIB1 system allows the robust light-induced expression of a model potassium channel in mammalian cells. The system exhibits a fast response with full activation already within the first hour after illumination. The data furthermore show that the system is reversible. After light-induced stimulation the channel stably expressed for 9 hours, during which it enables long-term optogenetic silencing with stable protein levels. After 9 hours in the dark the protein is degraded again.

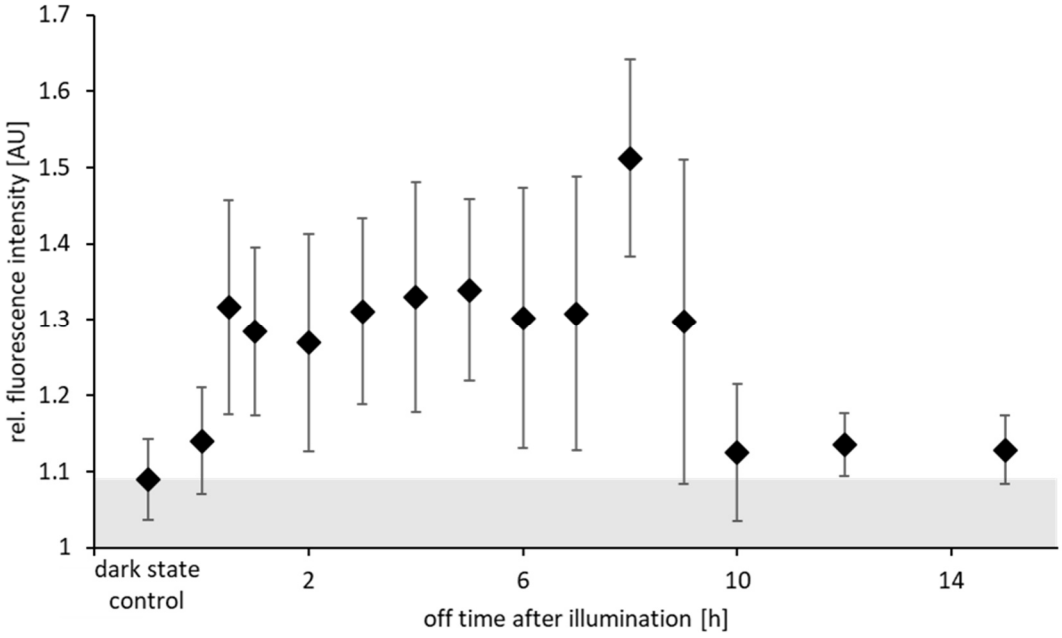

Fig. 26: On- and off kinetics of CRY2 CIB1 Kesv$_{Opt}$

Depicted is the mean RFI of cells transfected with CRY2 CIB1 Kesv$_{Opt}$ and illuminated for one hour with pulsed light (10 s on, 60 s off, 6 µE). Again, the overall incubation time was kept constant at 16 hours post-transfection, but the time point for the one-hour illumination was varied, resulting in different off-times after illumination. Mean RFI of the dark state control is indicated by the gray shading. For each timepoint, 20 cells were imaged. Error bars represent standard deviation.

6.4. Simplification of the handling protocols by designing an all-in-one vector does not impair the functionality of the system

One drawback observed during the experiments with the CRY2 CIB1 system described in the previous chapters, was its relatively low transfection efficiency. This is probably due to the original design of the CRY2 CIB1 system making it necessary to transfect the cells with three vectors (as shown in Fig. 27 A, upper row). This triple transfection bears the hazard of a low transfection efficiency, because not every

cell takes up all three necessary vectors, therefore not showing expression of the GOI. To bypass this problem, an all-in-one vector was designed, coding for all necessary building parts on one plasmid. This was achieved by putting CIB1-VP64 and CRY2-Gal4BD under the control of a CMV promotor. Both proteins are first transcribed together, before they are split into two independent proteins by the introduction of a P2A self-cleaving site between the two proteins. The third component, the GOI with the n-terminal 6xGalBS and the c-terminal GFP-tag was cloned in downstream of the CRY2-CIB1 coding region (see Fig. 27 A, second row).

To test whether this all-in-one vector design has any adverse effects on the light-induced channel expression system, the experiment described in chapter 6.3 was repeated with the new vector.

Fig. 27 B clearly shows that the new vector is still functional: it does neither affect on- and off-kinetics, nor does it corrupt maximum expression levels or the low activation levels in the dark.

The dark state control of the all-in-one construct was 1.07±0.03 AU, a value which is unchanged compared to that of 1.08±0.05 AU measured for the triple transfection (compare Fig. 26). The light-induced rise in expression level was slightly slower for the new vector, reaching steady state levels of protein expression at 1.32 AU one hour after illumination stops. Just like the triple transfection approach, protein levels return back to dark state levels after about nine hours in the dark.

The results of these experiments confirm that the simplification of the vector design from three individual vectors to one vector did not affect the performance of the system. The all-in-one vector neither had adverse effects on steady state expression levels, nor did it lead to an increase in leakiness, as the dark state values clearly document. Due to all functional components necessary for expression are now encoded on the same vector, an increase in transfection efficiency of about 25% compared to the triple transfection was to be observed. These advantages led to the decision to continue further experiments only with the all-in-one CRY2 CIB1 vector.

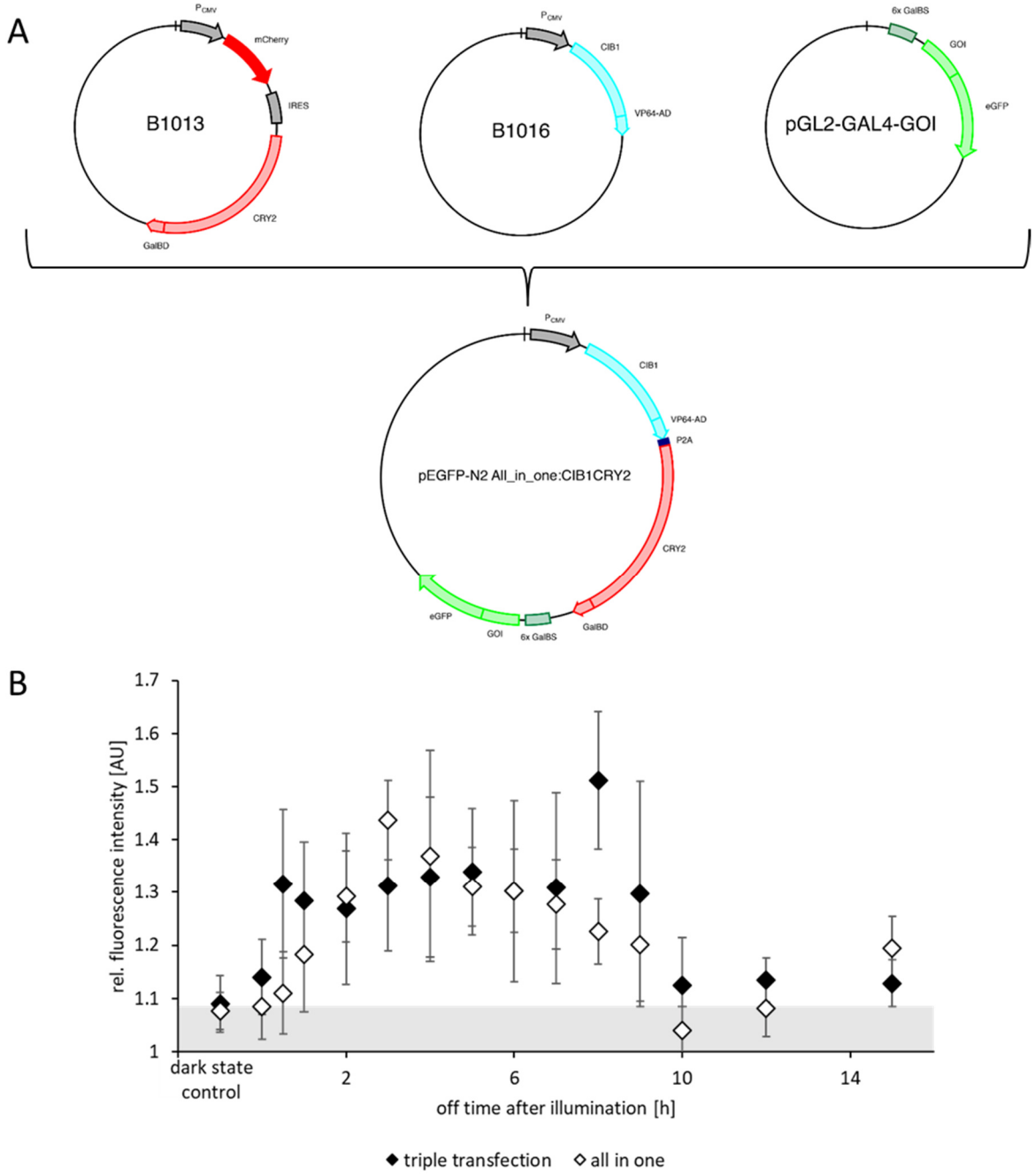

Fig. 27: Schematic depiction of the all-in-one vector design approach and comparison of on- and off kinetics of the all-in-one construct compared to the initial three-vector design

(A) The initial CRY2 CIB1 expression system consists of three vectors. B1013 on which CRY2 and the GalBD encoded, B1016 which codes for CIB1 with the VP64 activation domain and pGL2-Gal4-GOI which codes for the GOI which is fused to a 6xGalBS and has an c-terminal eGFP-tag. The functional parts of these three vectors were cloned together into one vector, putting CIB1 and CRY2 under control of a CMV promotor, separating them by a self-cleaving P2A sequence. Downstream are the 6xGalBS with the GOI and the eGFP-tag. **(B)** Depicted is the mean RFI of cells illuminated for one hour with pulsed light (10 s on, 60 s off, 6 µE), the triple transfection is plotted again as obtained from the previous experiments to allow comparison with the all-in-one construct. Again, the overall incubation time was kept constant at 16 hours post-transfection, but the time point for the one-hour illumination was varied, resulting in different off-times after illumination. Mean RFI of the dark state control is indicated by the gray shading. For each timepoint, 20 cells were imaged. Error bars represent standard deviation.

6.5. Single short illumination pulses are sufficient to induce full activation of the CRY2 CIB1 system

With the simplified handling of the CRY2 CIB1 construct, it was possible to test not just $Kesv_{Opt}$, but also two other mitochondrial potassium channels, namely $Kmpv_{12T}$ and $Kmpv_{12TOpt}$. In addition to this, also two potassium channels ($Kcv_{PBCV\text{-}1Opt}$ and Kcv_{NTS}), which are targeted to the PM via the ER, were cloned into the system.

To further minimize the illumination time, a single pulse protocol was established. This included illuminating the cells four hours prior to imaging with just a single light pulse which ranged in length from 20 minutes to only 5 seconds.

The light sensitivity of the CRY2 CIB1 system even was beyond expectations. Already the 5 second light pulse was sufficient to induce full expression of the tested channels. The fluorescence values ranged from 1.27±0.08 AU for $Kmpv_{12T}$, to 1.3±0.05 AU for $Kmpv_{12TOpt}$, to 1.34±0.14 AU for $Kesv_{Opt}$. All of those values are well within the range obtained with the longer illumination protocols. The fluorescence levels of non-illuminated control cells remained low, also with the two new channels. The background fluorescence being 1.04±0.03 AU for $Kmpv_{12T}$ and only 1.02±0.02 AU for $Kmpv_{12TOpt}$. These values are even slightly lower than those recorded for $Kesv_{Opt}$, which shows a dark state fluorescence of 1.07±0.03 AU.

For $Kmpv_{12TOpt}$, also the specificity of the system for blue light was tested. Cells were therefore illuminated with 1 minute of 660 nm far red light (120 μE). There was no increase in fluorescence, and thereby no activation of the CRY2 CIB1 system, detectable. The fluorescence level remained at the level of the dark state value (comp. Fig. 28 A). The results of these experiments confirm that the CRY2 CIB1 system is specifically activated by blue light.

For the two PM-sorted channels, equally good light-induced expression values were observed. For $Kcv_{PBCV\text{-}1Opt}$ and Kcv_{NTS} the dark state fluorescence was 1.05±0.02 AU, and 1.01±0.01 AU respectively. Both channels were activated by a single light pulse to maximum values of 1.22±0.04 AU for $Kcv_{PBCV\text{-}1Opt}$ and 1.29±0.05 AU for Kcv_{NTS} (Fig. 28 B).

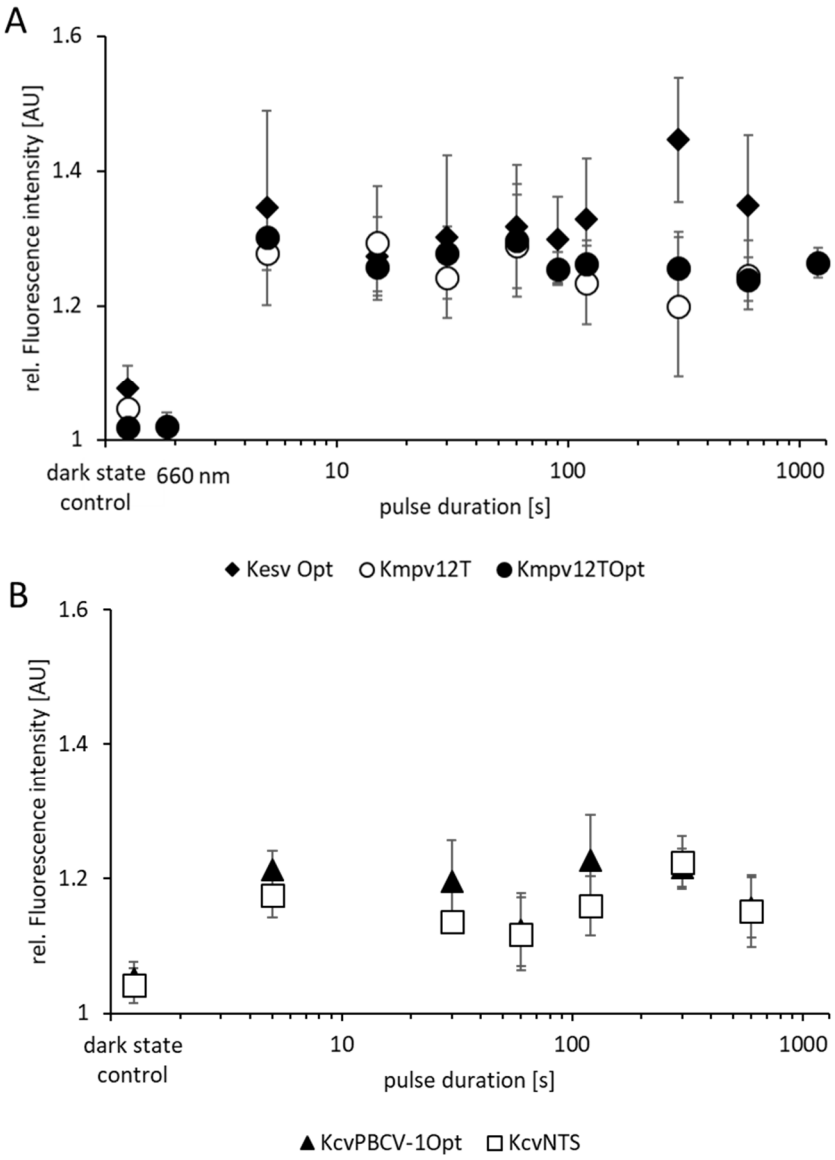

Fig. 28: Fluorescence intensity of cells transfected with the all-in-one CRY2 CIB1 system and illuminated with a single light pulse

(A) shows the RFI of $Kesv_{Opt}$, $Kmpv_{12T}$ and $Kmpv_{12TOpt}$ illuminated with a single light pulse from 5 to 1200 seconds (120 µE, over all incubation time: 16 hours post transfection, light pulse applied 4 hours prior to imaging). **(B)** shows the RFI of $Kcv_{PBCV\text{-}1Opt}$ and Kcv_{NTS} illuminated with a single light pulse from 5 to 1200 seconds (120 µE, over all incubation time: 16 hours post transfection, light pulse applied 4 hours prior to imaging). Dark state control is in both cases depicted on the left hand side. For each data point 20 cells were imaged. Error bars represent standard deviation.

The results of these experiments underscore the high light sensitivity of the CRY2 CIB1 system. With this apparent high light sensitivity, the question arose, whether the system tolerates handling under daylight conditions even for short time periods without causing transcriptional activation. To test the impact of daylight, cells were kept in ambient daylight in the laboratory for 10 minutes. Imaging of the cells four hours later showed that this exposure to daylight was sufficient for a full activation of the system. The

fluorescence values were ranging from 1.24±0.03 AU for Kcv_{NTS} and $Kcv_{PBCV\text{-}1Opt}$ to 1.33±0.06 AU for $Kesv_{Opt}$ (Fig. 29).

The data show that the portion of blue light occurring in ambient daylight is enough, to induce activation of the CRY2 CIB1 system. This underscores the importance of keeping the samples in total darkness to avoid unwanted activation.

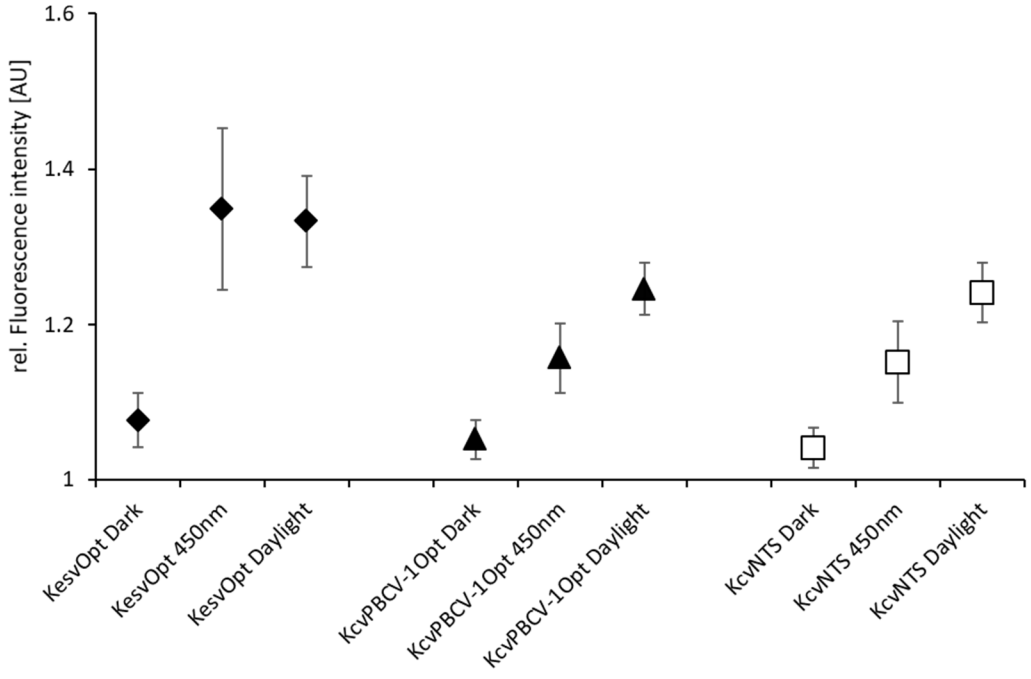

Fig. 29: CRY2 CIB1 is highly sensitive to daylight exposure

Plotted are the rel. fluorescence intensity values [AU] for $Kesv_{Opt}$, $Kcv_{PBCV\text{-}1Opt}$ and Kcv_{NTS}. They were either kept in the dark, illuminated for 10 minutes with 450 nm blue light (6 µE) or kept in daylight for 10 minutes. Overall incubation time was 16 hours for all conditions, illumination took place 4 hours prior to imaging. For each condition, 20 cells were imaged. Error bars represent standard deviation.

6.6. Sorting of the different potassium channels expressed in the CRY2 CIB1 system is unchanged compared to the constitutive constructs

In the next series of experiments, it was tested whether an expression of the model potassium channels under control of the CRY2 CIB1 system has any impact on channel protein sorting. Therefore, the localization of the light-dependent constructs was determined and compared to that of the constitutively expressed ones.

$Kesv_{Opt}$ showed in both cases a localization to the mitochondria in 100% of the cells. $Kmpv_{12TOpt}$ also showed the same distribution independently of the expression condition. The constitutive construct was sorted to the mitochondria in 69% of the cells, and in the CRY2 CIB1 system in 65.4 % (representative image shown in Fig. 30 A-C). The remaining cells did not show any distinct sorting of the channel to any compartment. The fluorescence appeared uniformly distributed throughout the cytosol (Fig. 30 D).

The only potassium channel in which the expression in the CRY2 CIB1 system had an influence on sorting, was $Kmpv_{12T}$. The channel showed robust sorting to the mitochondria in 91.8 % of the cells, 2.7 % show sorting to the ER and in 5.4 % the fluorescence is distributed evenly throughout the cells. If it is expressed in the CRY2 CIB1 system, the sorting efficiency to the mitochondria was dramatically reduced. Mitochondrial sorting was no longer observed, instead the GFP-signal was distributed throughout the cytosol in 100 % of the cells (Fig. 30 D).

Unlike in some other experiments on channel sorting shown in this work, where the perinuclear ring and the mitochondria were free of GFP fluorescence (compare Fig. 17) the signal was found in $Kmpv_{12T}$ expressing cells throughout the entire cell body. Hence, it cannot be ruled out that a small fraction of the channel is properly sorted to a defined membrane while the majority of the protein is mis-sorted and degraded. It is also possible, that GFP is enzymatically cleaved off of the channel and therefore under this condition the confocal images don't show the actual location of the channel. If some fraction of $Kmpv_{12T}$ expressed in the CRY2 CIB1 system still reaches the IMM, as it is the case for the constitutively expressed channel, an effect on mitochondrial membrane potential is to be expected. In functional assays, shown later in this work (compare chapters 7.1 and 7.2), it could indeed be demonstrated that $Kmpv_{12T}$ retains its functionality in the IMM when expressed under control of the CRY2 CIB1 system.

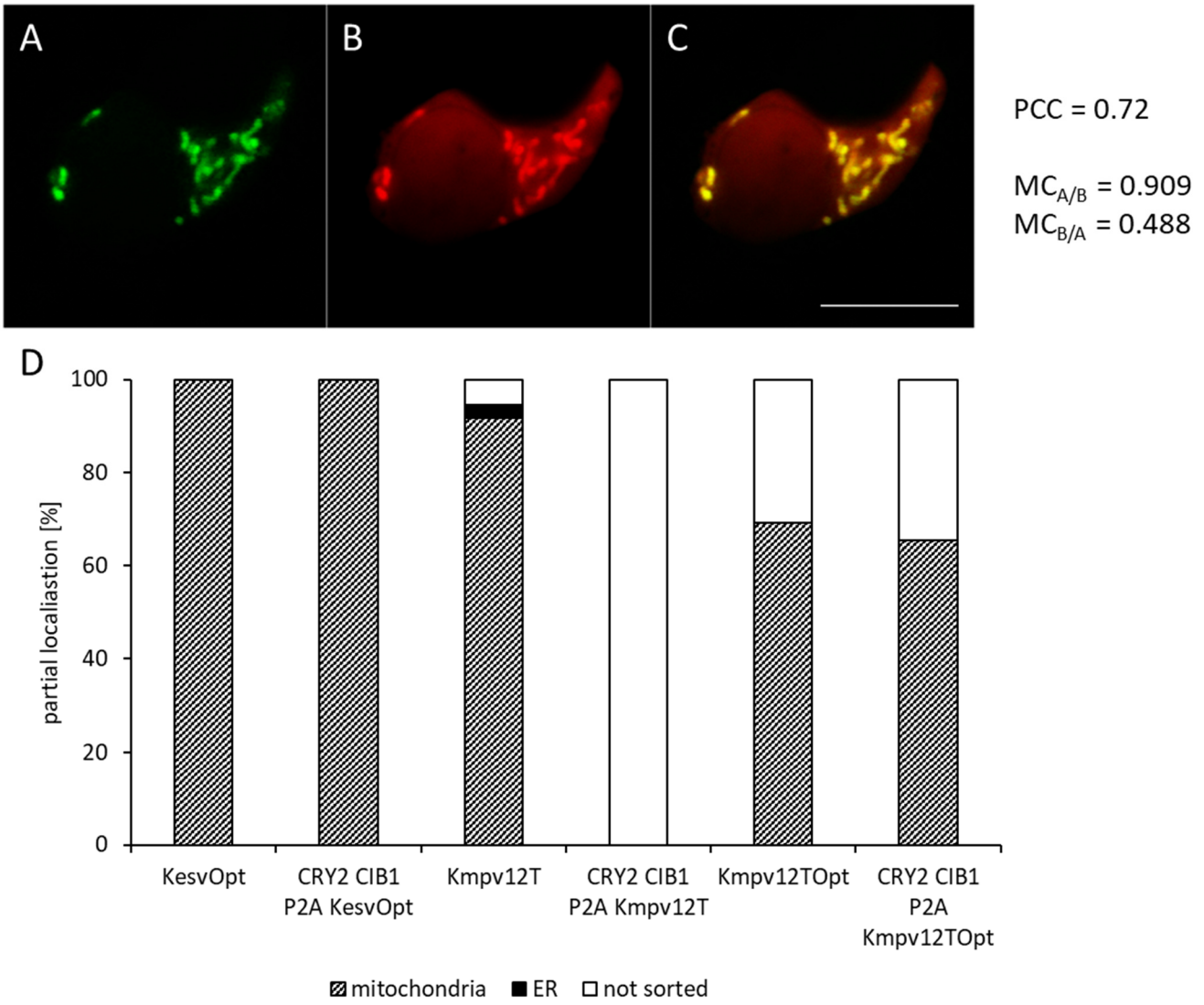

Fig. 30: Sorting of mitochondrial channels expressed in the CRY2 CIB1 system compared to the constitutive constructs

(A-C): Confocal image of Kmpv$_{12TOpt}$ expressed in the all-in-one CRY2 CIB1 system, Panel A: Kmpv$_{12TOpt}$::eGFP, Panel B: COX8::mCherry, Panel C: Merged Image of A and B. Scale bar represents 10 µm. On the right PCC and MC are indicated. **(D)** shows the sorting pattern of Kesv$_{Opt}$, Kmpv$_{12T}$ and Kmpv$_{12TOpt}$ expressed either constitutively or light-dependent in the CRY2 CIB1 system (Kesv$_{Opt}$: N=4, n=150, CRY2 CIB1 Kesv$_{Opt}$: N=22, n=440, Kmpv$_{12T}$: N=3, n=147, CRY2CIB1 Kmpv$_{12T}$: N=8, n=204, Kmpv$_{12TOpt}$: N=2, n=100, CRY2 CIB1 Kmpv$_{12TOpt}$: N=11, n=228).

In further experiments the sorting of the two potassium channels, which were used as candidates for PM expression, was determined as well.

The experiments show that Kcv$_{PBCV\text{-}1Opt}$ is sorted to the ER in 61.4 % of the cells, while 38.6 % of the cells show no distinct sorting. When the same channel it is expressed in the CRY2 CIB1 system, the sorting efficiency drops. Only 1.9 % of the cells show effective sorting to the ER, whereas a uniform GFP fluorescence is detectable in 98.1 % (Fig. 31 D).

Kcv_{NTS} on the other hand shows a more distinct sorting to the ER when it is expressed under control of the CRY2 CIB1 system. In case of the constitutive construct, 44 % of the cells show sorting to the ER, whereas a distinct sorting to the ER is discernible in 70 % of the cells in which Kcv_{NTS} is expressed in the CRY2 CIB1 system (Fig. 31 D).

One reason for this shift in sorting could be the difference in the expression levels. While the level of protein expression is high for a constitutive expression, it is lower under control of the light sensitive system. In the studies with the constitutive Kcv_{NTS} (compare chapter 3.1.2), it already became clear that a lower fluorescence intensity favors sorting of the channel to the ER. In these experiments, it was possible to draw a clear threshold for the critical fluorescence intensity: Cells with an RFI ≥ 1.38 AU were not sorted properly any more, whereas cells with an RFI ≤ 1.38 AU were sorted to the ER in 100 % of the cells. As the mean RFI for CRY2 CIB1 Kcv_{NTS} is about 1.25 AU (compare Fig. 28 B), it becomes clear that more cells are below the threshold established from the previous experiments. This explains the enhanced sorting to the ER.

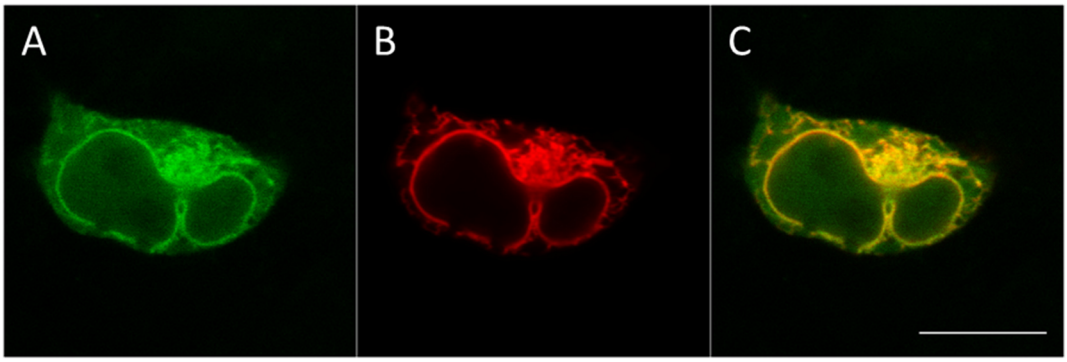

PCC = 0.878

$MC_{A/B}$ = 0.77
$MC_{B/A}$ = 0.803

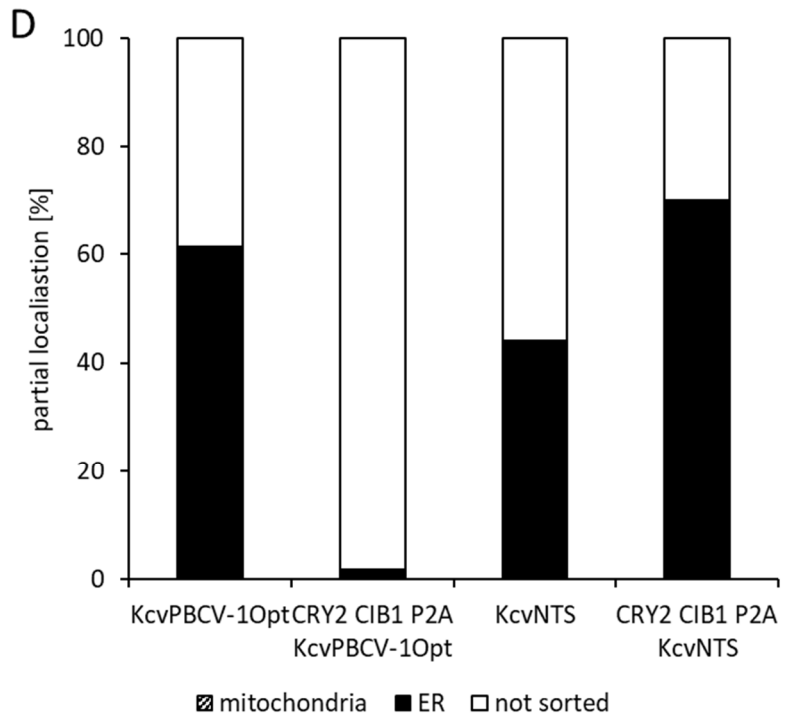

Previous page:

Fig. 31: Sorting of plasma membrane channels expressed in the CRY2 CIB1 system compared to the constitutive constructs

(A-C): Representative confocal image for Kcv_{NTS} expressed in the all-in-one CRY2 CIB1 system, Panel A: Kcv_{NTS}::eGFP, Panel B: HDEL::mCherry, Panel C: Merged Image of A and B. Scale bar represents 10 µm. On the right PCC and MC are indicated. **(D)** shows the sorting pattern of $Kcv_{PBCV\text{-}1Opt}$ and Kcv_{NTS} expressed either constitutively or light-dependent in the CRY2 CIB1 system ($Kcv_{PBCV\text{-}1Opt}$: N=5, n=223, CRY2 CIB1 $Kcv_{PBCV\text{-}1Opt}$: N=9, n=270, Kcv_{NTS}: N=2, n=184, CRY2 CIB1 Kcv_{NTS}: N=8, n=207).

6.6.1. Both the constitutive and the light-dependent expressed $Kesv_{Opt}$ are indeed localized in the IMM

Confocal resolution allows the clear distinction of the sorting of various proteins to different compartments, however it is not sufficient to determine, whether a protein is localized in the OMM or the IMM. In order to influence the mitochondrial membrane potential, it would be necessary for the potassium channels to be inserted in the IMM. To address the question, whether $Kesv_{Opt}$ is indeed sorted to the IMM, as we postulated earlier, a two-step subcellular localization assay was performed. The procedure was adapted from Tkatch and coworkers (Tkatch et al., 2017).

In the first part of the assay, a drop in fluorescence would indicate that the protein of interest is localized on the extracellular side of the PM or facing the cytosolic sides of all organelles. The cells, were incubated in extracellular medium and imaged every minute before adding proteinase K to the buffer. This enzyme indiscriminately cleaves all proteins it can reach. In the present assay this would be the GFP-tag on the channel protein. With the cells still intact, a decrease in RFI would indicate here, that the protein of interest is exposed to the extracellular side of the PM. To permeabilize the PM in the next step, digitonin was added. In this step, cytosolic proteins can diffuse out of the cell, leading to a drop in RFI. In the following step, proteinase K was again added, the kinase can now reach membrane proteins which are exposed to the cytosol, like those on the cytosolic side of the OMM, the inner side of the PM, or the cytosolic side of the ER. To eliminate the contribution of cut-off GFP still diffusing freely in the cytosol to the fluorescence signal, trypan blue was added in the final step. This quenches the fluorescence of any GFP molecules that might not yet have diffused out of the permeabilized cells (for visual summary of the experimental setup, see Fig. 32, upper panel).

The graph in Fig. 32 shows the normalized RFI of cells expressing $Kesv_{Opt}$ either constitutively or under control of the CRY2 CIB1 system as a function of time, with the addition of each reagent being indicated by arrows. It occurs, that both constructs do not show a decrease in fluorescence during the first part of the assay. This means that the GFP-tag on the channel is neither in the plasma membrane, nor exposed to the cytosol from the outer membrane of the mitochondria.

The data show rather large standard deviations. This is due to the fact that the cells became increasingly necrotic during the assay and thereby also changed their morphology. An example of two cells which change their morphology, but maintain their fluorescence intensity during the experiment is shown above the graph in Fig. 32.

To ensure that both the constitutively and the light-dependently expressed $Kesv_{Opt}$ is indeed inserted into the IMM, the second part of the assay was performed. For this procedure, a fresh batch of cells was again incubated in extracellular medium. Digitonin was added directly to permeabilize the cells. Afterwards, alamethicin was added. This reagent permeabilizes both the OMM and the IMM. An alamethicin-induced decrease in RFI would indicate a localization of the channel in the intermembrane space of the mitochondria or in the mitochondrial matrix. The final step was the addition of trypan blue, which quenches the fluorescence of the now exposed GFP, thereby indicating an IMM protein.
For both expression systems, the fluorescence only begins to decrease after the addition of trypan blue, reaching values close to zero within nine minutes (graph in Fig. 33). The fact that the fluorescence did not decrease until this last step, confirms that the GFP-tagged channel protein is located in the IMM. This development can also be tracked in the two exemplary cells shown above the graph in Fig. 33.

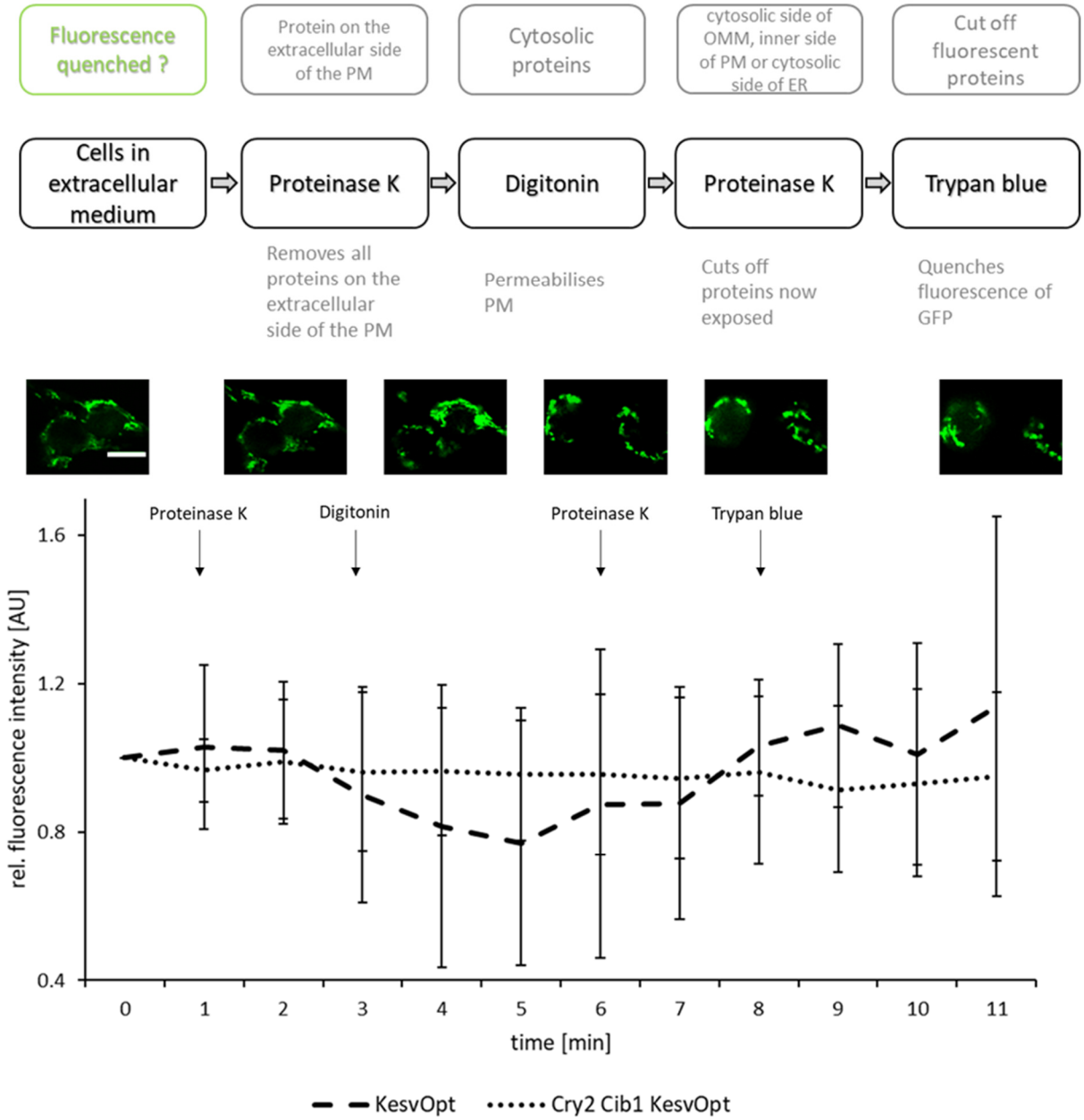

Fig. 32: First part of the subcellular localization assay

Indicated in the upper panels is the successive exchange of reagents to detect the localization of the protein of interest. In the graph is depicted the normalized rel. fluorescence intensity [AU] of the constitutive (N=4, n=21) and the light dependent $Kesv_{Opt}$ (N=11, n=52) over time. Indicated by the arrows is the exchange of reagents. Error bars represent standard deviation.

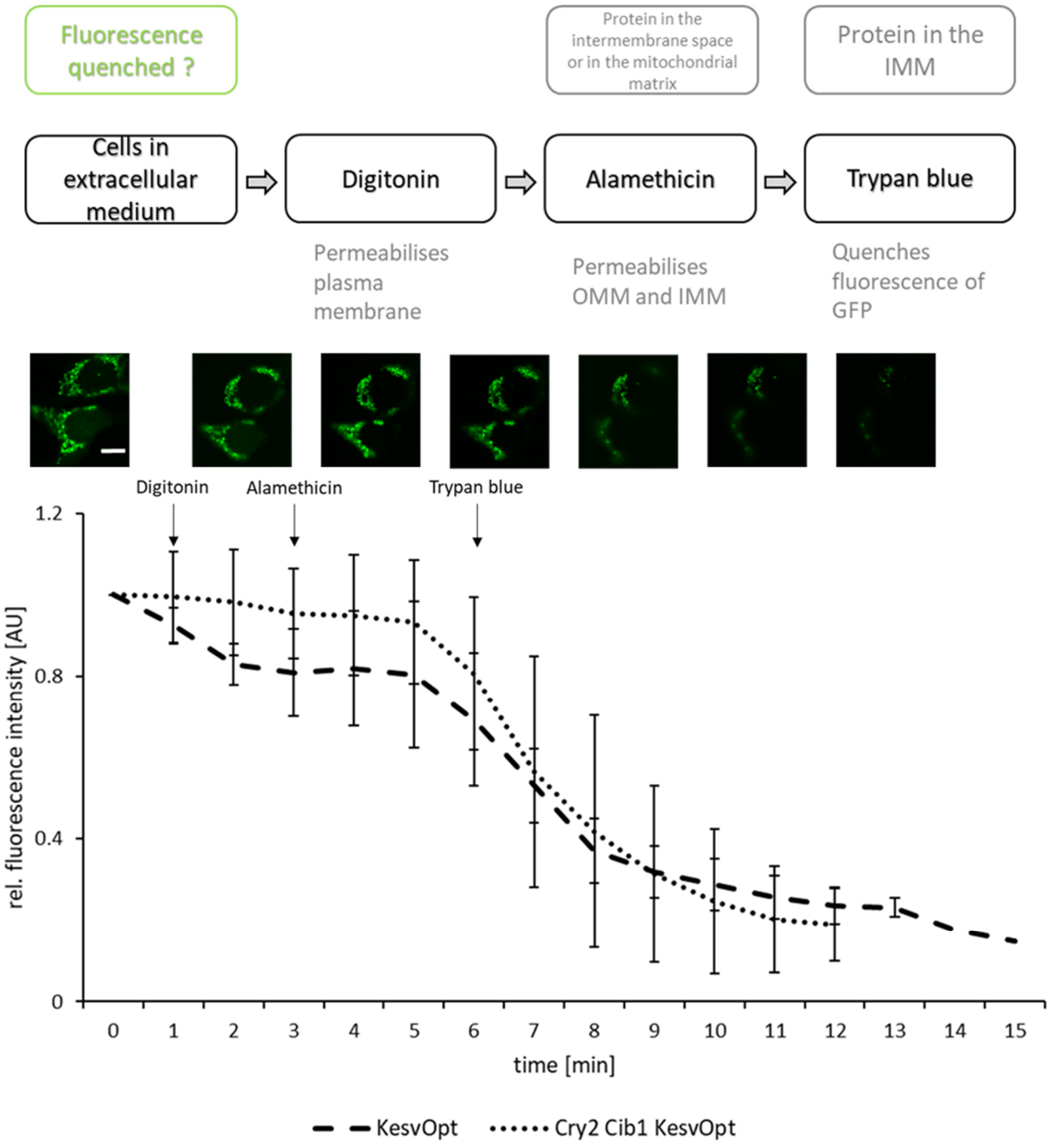

Fig. 33: Second part of the subcellular localization assay

Indicated in the upper panels is the successive exchange of reagents to detect the localization of the protein of interest. In the graph is depicted the normalized rel. fluorescence intensity [AU] of the constitutive (N=4, n=32) and the light dependent $Kesv_{Opt}$ (N=11, n=50) over time. Indicated by the arrows is the exchange of reagents. Error bars represent standard deviation.

6.7. Comparison of the plasma membrane availability of Kcv_{NTS} and $Kcv_{PBCV\text{-}1Opt}$ during constitutive and light-dependent expression

To further look into the properties of light-induced and constitutive expression of channel proteins, the question arose, whether a lower overall expression level of the channel protein under control of the CRY2 CIB1 system, has an influence on the number of channels reaching the PM. An indirect indication that the CRY2 CIB1 system lowers the amount of synthesized protein compared to a constitutive expression was inferred by lower fluorescence intensities in confocal microscopy experiments (compare chapter 6.9).

As confocal microscopy does not offer sufficiently high resolution to distinguish channel proteins or channel protein clusters in the plasma membrane from the very high background of protein in the ER, cell decapitation (Nappobac) in combination with TIRF (total internal reflection fluorescence) microscopy (Fish, 2009; Shashkova and Leake, 2017) offers a better option to address this question. This procedure increases microscopic resolution and allows detection of individual channels and clusters in the plasma membrane.

From work on other membrane proteins, it is reasonable to assume that the channel proteins tend to form clusters in the membrane, as they assemble in membrane domains which provide the thermodynamically most suitable membrane composition and bilayer thickness (Reynwar et al., 2007). Based on this rationale, a cluster analysis software was used to analyze the images which has been established and validated previously by S. Paech (Paech, 2019) and A. Krömmelbein (Krömmelbein, 2020) for the analysis of membrane proteins in mammalian cells.

The script creates in a first step a density heat map of the raw data (Fig. 34 A & B) and from this calculates a binary mask to eliminate background signals (Fig. 34 E). The data are then analyzed for clustering of signals using a Density Based Clustering Algorithm with Noise (DBscan). The latter defines clusters by two fixed parameters: The minimum of signals that forms a cluster (min points) and the maximum distance (ε) of two points which still belong to the same cluster (Fig. 34 D & H) (Hahsler et al., 2019). Another analysis was performed with a hierarchical DBscan (HDBscan) which only needs one fixed parameter: the minimal number of signals. ε is calculated in this case independently for each cluster in the analysis (Campello, Ricardo J. G. B. et al., 2013). Evaluated in further analysis was only the masked HDBscan, as HDBscan proved to be more accurate in defining several clusters in close proximity (Fig. 34 G, dotted circle), compared to DBscan (Fig. 34 H, dotted circle).

Parameters that were addressed during image analysis were the number of clusters, the cluster area and the number of signals in each cluster. If the amount of channel proteins reaching the plasma membrane is influenced by the different channel proteins ($Kcv_{PBCV\text{-}1}$ or Kcv_{NTS}), codon optimization ($Kcv_{PBCV\text{-}1}$ or

$Kcv_{PBCV\text{-}1Opt}$) or the choice of expression system (constitutive with a strong promotor or light dependent under control of the CRY2 CIB1 system), a change in one of these parameters should be expected.

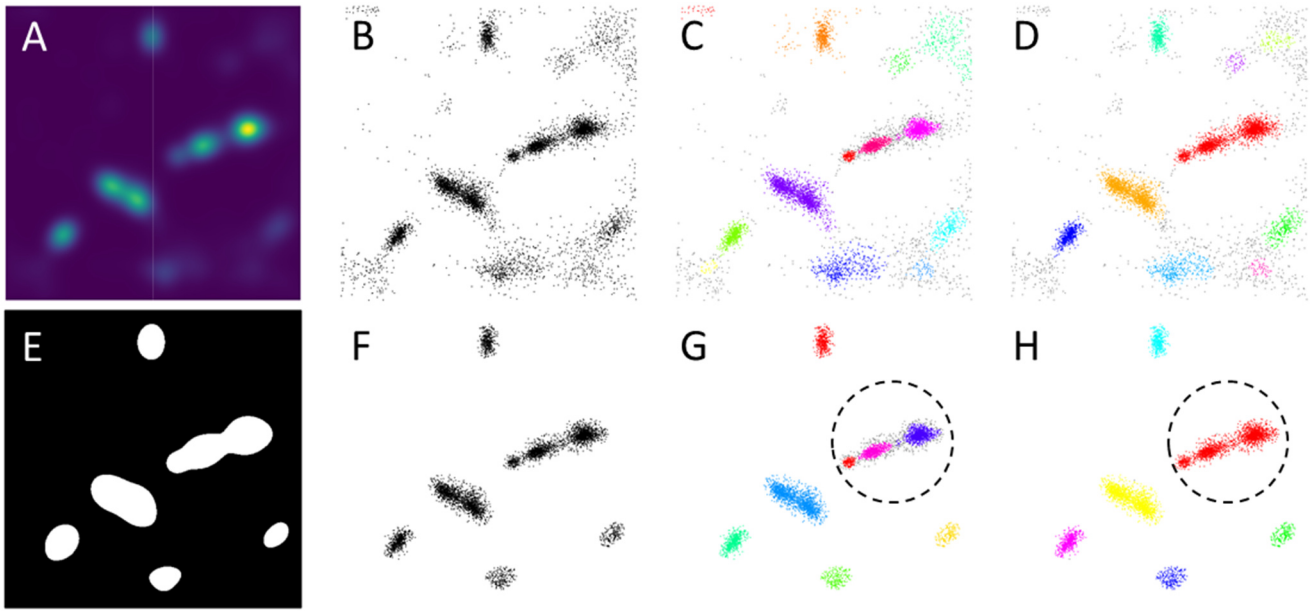

Fig. 34: Steps of cluster analysis

(A) shows the raw data of 2000 frames/ image generated by ThunderSTORM depicted as a density heat map (bins=500, bandwidth=400) and **(B)** as a point diagram. To exclude background signals which do not represent clusters, a binary mask **(E)** was generated from the heatmap to exclude signals below threshold. **(F)** shows the point diagram of the masked raw data. To determine the most suitable method for cluster detection both a Density Based Clustering Algorithm with Noise (DBscan) and a hierarchical DBscan (HDBscan) were performed with both the masked and unmasked data. **(D)** shows the DBscan with unmasked data (ε=83, min points=20), **(H)** with masked data (ε=83, min points=20). **(C)** the HDBscan with unmasked (cluster count=13, min points=20) and **(G)** with masked data (cluster count=8, min points=20). The dotted circle shows that the HDB scan is more efficient in separating close populations of clusters. Image size 4x4 µm.

The number of clusters was analyzed for each 4x4 μm region of interest (ROI) and is depicted in Fig. 35. All $Kcv_{PBCV\text{-}1}$ constructs showed very similar cluster numbers, with only a very slight decrease in case of the optimized $Kcv_{PBCV\text{-}1}$ under control of the CRY2 CIB1 system. $Kcv_{PBCV\text{-}1}$ showed 11.3±4.8 clusters per ROI, the codon optimized $Kcv_{PBCV\text{-}1}$ 11±3.6 clusters per ROI and the light-dependent $Kcv_{PBCV\text{-}1Opt}$ 9.3±2.8 clusters per ROI. Kcv_{NTS} showed a slightly higher number of clusters per ROI (13.3±4.5), compared to the $Kcv_{PBCV\text{-}1}$ constructs. The number of clusters for Kcv_{NTS} under control of the CRY2 CIB1 system was with 7.2±3 clusters per ROI the lowest value.

The results of these experiments show that the number of clusters do not greatly differ from each other and all values lie within the range of standard deviations. These results therefore indicate, that the number of clusters is not influenced by different protein expression levels. It is possible that the density

of channels in the PM is already saturated with the low number of proteins which are expressed under control of the CRY2 CIB1 system.

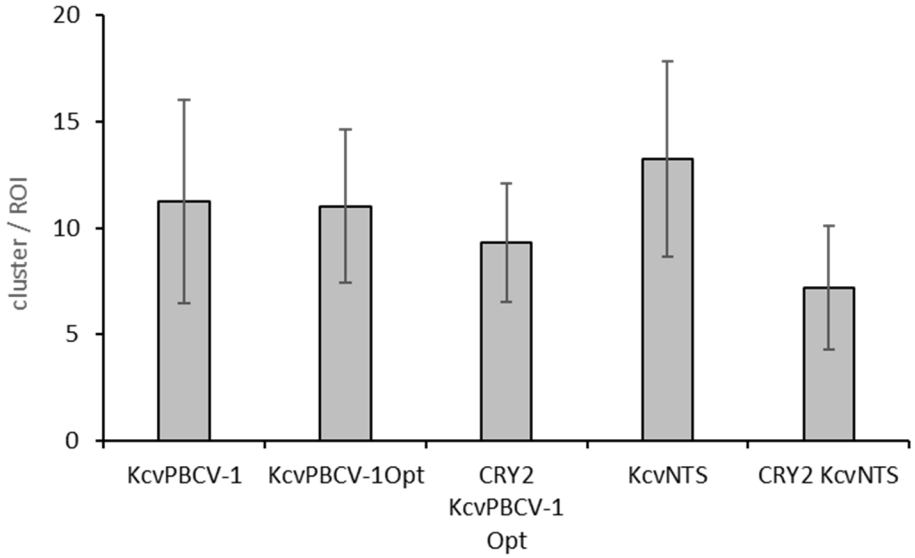

Fig. 35: The number of clusters does not depend on the expression level

Plotted is the mean number of clusters per 4x4 µm ROI for Kcv_{PBCV-1} (N=3, n=52), $Kcv_{PBCV-1Opt}$ (N=3, n=49), CRY2 $Kcv_{PBCV-1Opt}$ (N=3, n=57), Kcv_{NTS} (N=3, n=94) and CRY2 Kcv_{NTS} (N=3, n=49). Error bars represent standard deviation.

Cluster areas were calculated from the HDBscans of the 4x4 μm ROIs as well. The histograms illustrating the distribution of cluster size are depicted in Fig. 36. All channel constructs exhibited a peak for relatively small clusters with areas smaller than 200.000 nm^2. Worth mentioning is the wider deviation of cluster sizes for both constructs expressed under control of the CRY2 CIB1 system (Fig. 36 C & E). For these two constructs, bigger clusters occurred with sizes up to 500.000 nm^2. These larger clusters did not occur in all the constitutively expressed constructs, independently of the type of channel protein or on codon bias (Fig. 36 A,B & D). The occurrence of these large clusters are also reflected in the median values of the cluster area (Fig. 36 F). The median values for both Kcv_{NTS} and $Kcv_{PBCV-1Opt}$ expressed under control of the CRY2 CIB1 system are roughly twice the size of those formed by the constitutive constructs. The constitutive constructs showed a median area of 58898.91 nm^2 for Kcv_{NTS}, 46553.7 nm^2 for Kcv_{PBCV-1} and 67072.81 nm^2 for $Kcv_{PBCV-1Opt}$. Kcv_{NTS} under control of the CRY2 CIB1 system had a median area of 118391.1 nm^2 and $Kcv_{PBCV-1Opt}$ under control of the CRY2 CIB1 system of 101873.5 nm^2.

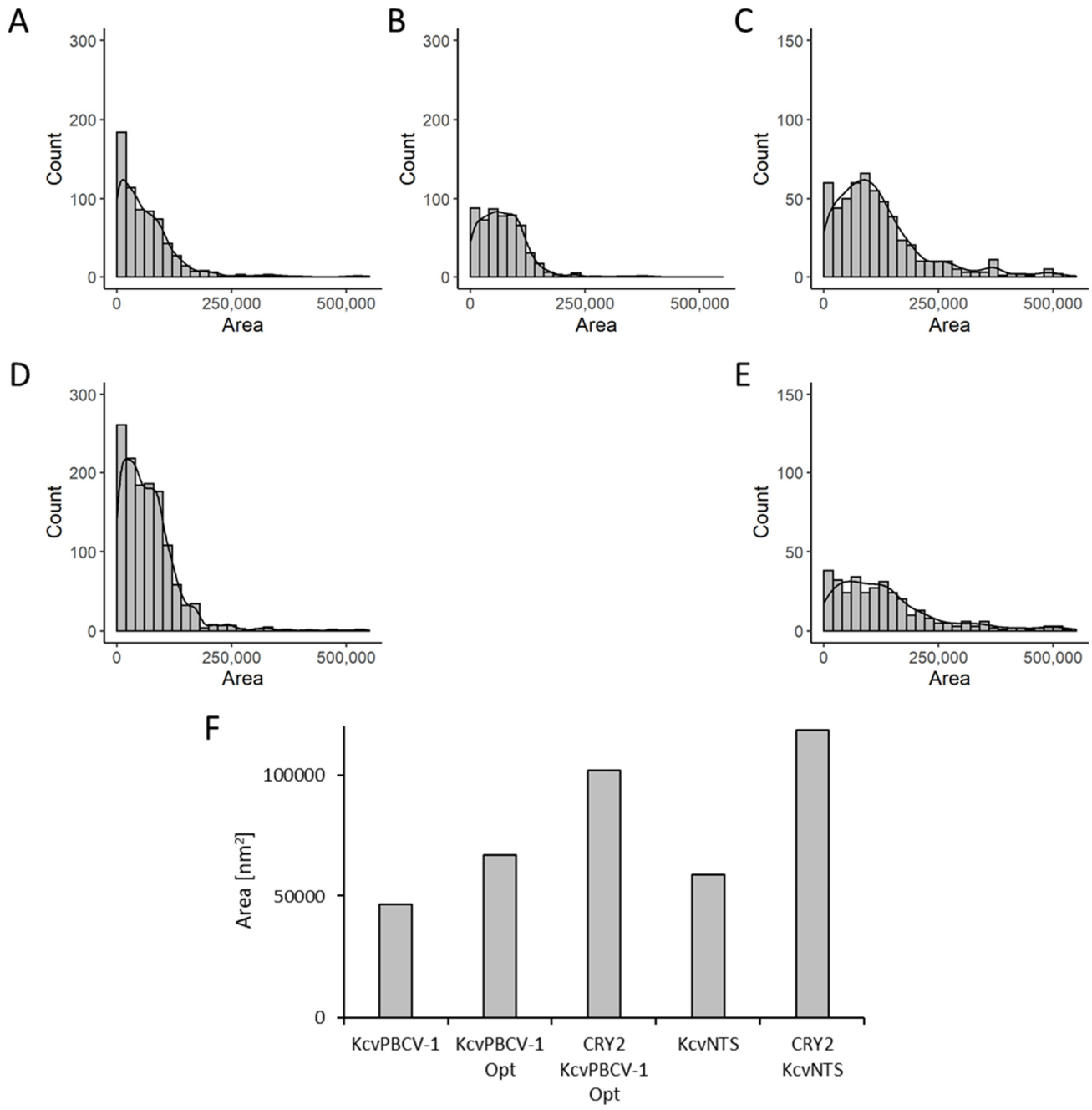

Fig. 36: Cluster area of various Kcv channels expressed constitutively or under control of the CRY2 CIB1 system

Histograms representing the cluster area in nm² of **(A)** Kcv_{PBCV-1} (N=3, n=57), **(B)** $Kcv_{PBCV-1Opt}$ (N=3, n=57), **(C)** CRY2 $Kcv_{PBCV-1Opt}$ (N=3, n=57), **(D)** Kcv_{NTS} (N=3, n=63) and **(E)** CRY2 Kcv_{NTS} (N=3, n=51). Binning width: 20.000 nm² **(F)** Median values of the cluster area of Kcv_{PBCV-1}, $Kcv_{PBCV-1Opt}$, CRY2 $Kcv_{PBCV-1Opt}$, Kcv_{NTS} and CRY2 Kcv_{NTS}.

To gain further insight in the number of GFP molecules in each cluster, the signals per cluster were evaluated (Fig. 37). In this analysis it became clear again, that the characteristics of the constitutively expressed constructs differ from the ones expressed under control of the CRY2 CIB1 system. Each of the histograms of the constitutive constructs exhibited two populations (Fig. 37 A, B & D). The first

population contained clusters with less than 1000 signals per cluster, peaking around 400 molecules per cluster. The second population contained clusters with more than 1000 signals per cluster, peaking steeply at 2000 dots per cluster and declining rapidly afterwards. In both light dependent constructs, the first population showed the same features as for the constitutive constructs. The second population however, was barely detectable in the light-dependent constructs and present only as an elongation of the decline of the first population.

The steep peak at 2000 dots per cluster, which was observed for all three constitutive constructs, correlates with the number of images taken per stack. This peak might therefore be an artifact, caused by a dense accumulation of GFP-molecules, which did not bleach during image acquisition and were slightly out of the focal plane. This would lead to the detection of a seemingly “new” molecule in every image of the stack and cause the peak at 2000 signals per cluster (Shivanandan et al., 2016). The higher expression level of the constitutive constructs therefore seems to lead to aggregations of proteins near the PM. This was not observed in the two light-induced constructs, indicating a more effective sorting of the channel proteins.

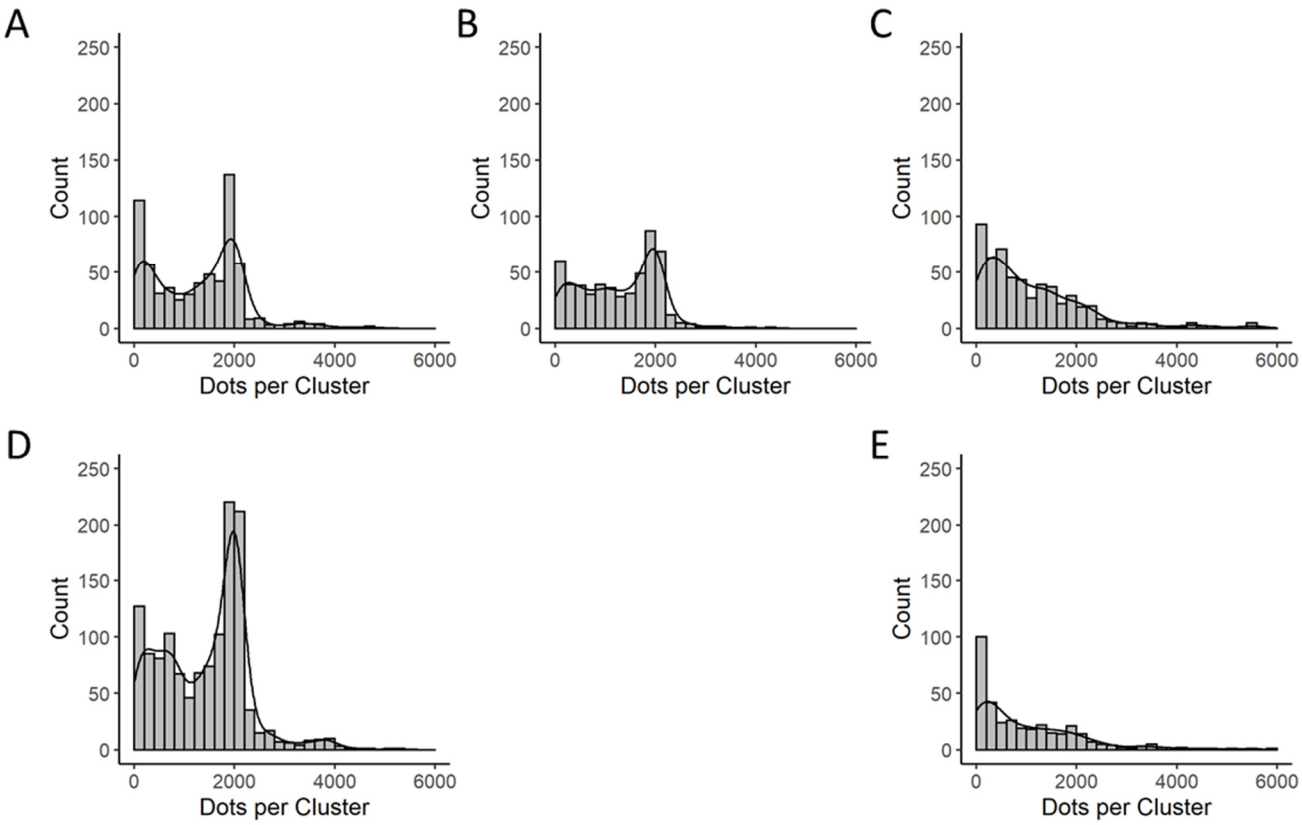

Fig. 37: Signals per cluster of various Kcv channels expressed constitutively or under control of the CRY2 CIB1 system

Histograms representing the dots per cluster of **(A)** $Kcv_{PBCV\text{-}1}$, **(B)** $Kcv_{PBCV\text{-}1Opt}$, **(C)** CRY2 $Kcv_{PBCV\text{-}1Opt}$, **(D)** Kcv_{NTS} and **(E)** CRY2 Kcv_{NTS}. Binning width: 200.

Taken together, the high-resolution imaging experiments with the five different potassium channel constructs show that the amount of protein present in the plasma membrane is neither affected by codon optimization, nor by the expression system. The overall number of clusters detected in the membrane patches was on equal levels for all the constructs observed. This is in good agreement with patch clamp experiments, which also showed a similar current density of whole cell currents for Kcv_{NTS} expressed both constitutively or in a light-dependent manner (see chapter 7.5).
However, both cluster size and number of signals per cluster differ between the constitutive and the light-dependent constructs. The high expression levels of the constitutive constructs might cause unspecific aggregation of GFP molecules and therefore impair sorting of the channel proteins. This has already been shown in other experiments examining the sorting efficiency of potassium channel proteins. The effect was most distinctly observed for Kcv_{NTS} (see chapter 6.6). This pattern seems to be repeated in the cluster analysis data, as Kcv_{NTS} shows by far the highest percentage of artifacts at a value of 2000 signals per cluster (Fig. 37, D) compared to $Kcv_{PBCV\text{-}1}$. A decrease of expression level seems to have beneficial effects on the sorting of Kcv_{NTS}. This can be deduced from the fact that a lower expression level under control of the CRY2 CIB1 system augments the sorting efficiency compared to that of the constitutive construct (see Fig. 31). This effect seems to be mirrored in the high-resolution imaging data. Notably, the peak at 2000 dots per cluster, which is presumably reflecting the amount of aggregated proteins, is not detectable for Kcv_{NTS} expressed under control of the CRY2 CIB1 system. Hence, a lower protein expression level seems to positively influence an effective sorting to the PM, whereas high protein levels hinder it.

The present data are a first indication for the effects of protein levels on the mechanism of sorting efficiency of potassium channels to the PM. A critical evaluation of the available dataset shows that it is not of a sufficient size to fully prove the aforementioned hypotheses. The experiments will need further repetitions with different fluorophores better suited to TIRF microscopy. Also, microscopy techniques such as stochastic optical reconstruction microcopy (STORM), which provide even higher resolution may be required. These technical refinements might eliminate the artifacts observed during determination of the cluster area.

6.8. Different approaches to further optimize the CRY2 CIB1 system

So far, the CRY2 CIB1 system has shown very promising features concerning both the light-induced increase in gene expression and the lack of an effect on sorting of the viral potassium channels of interest. Several approaches to further improve the system have been made, the first one being the exchange of eGFP for the brighter and more photostable fluorophore mClover (Bajar et al., 2016). Unexpectedly, the exchange of the fluorophore did not result in an enhanced fluorescent signal (Fig. 38 A). Dark state control values were 1.01±0.01 AU for Kcv_{NTS}::eGFP and 1.04±0.02 AU for Kcv_{NTS}::mClover. Mean fluorescence for Kcv_{NTS}::eGFP was 1.28 AU and 1.29 AU for Kcv_{NTS}::mClover. The data clearly shows that the exchange of eGFP for mClover did not result in the expected brighter fluorescence signal. However, when the sorting of the two constructs was compared, the construct with the mClover-tag showed enhanced sorting to the ER, compared to the initial eGFP construct (Fig. 38 C). Kcv_{NTS}::eGFP is sorted to the ER in 70 % of the cells, whereas for Kcv_{NTS}::mClover 87 % of the cells showed a pronounced sorting to the ER. This enhanced sorting to the ER may be explained in two ways: Either the tendency of eGFP to form clusters (Wang et al., 2019) hinders a more effective sorting of the channel, whereas the non-clustering mClover (Thorn, 2017) promotes are more effective binding of the nascent protein to the SRP for sterical reasons. An alternative explanation could be that the mClover construct is expressed less efficiently, compared to the eGFP construct. It has already been shown that a lower expression level of Kcv_{NTS}, independent of the expression system, favors a more effective sorting of the channel to the ER (chapter 3.1.2 and 6.7). A lower expression level would also explain why the brighter mClover-tag does not increase the overall fluorescence intensity level compared to eGFP. Taken together, the CRY2 CIB1 Kcv_{NTS}::mClover construct can still be considered as an improved tool. Even though it failed in showing a brighter fluorescence, it augments the sorting efficiency of the channel to the ER. With this feature, it might come in handy as an optogenetic tool to investigate light-inducible changes in membrane potential.

So far, the CRY2 CIB1 system, lacks the possibility to identify transfected cells in the dark. The data however show that the system has some dark state activity, which is detectable in very few cells. The fluorescence intensity is just barely above detection limit of 1 AU. It is therefore reasonable to assume, that there are more transfected cells in the dark state controls, which are not expressing eGFP in a detectable amount. As low expression levels in the dark are in itself desirable, insofar as they indicate very weak leak expression of the channels, the downside is that there is no way to investigate the behavior of these cells, e.g. in electrophysiological experiments. To overcome this obstacle, a construct was designed, which carries an additional mCherry-tag. mCherry was cloned into the all-in-one CRY2 CIB1 Kcv_{NTS} vector with an additional P2A sequence, which induces its constitutive expression under control of the CMV promotor. In the dark, it was therefore expected to observe red-fluorescent cells with

a cytosolic mCherry signal, but no GFP signal. The new construct was studied in cells kept in the dark, as well as with cells exposed to a short single light pulse. mCherry fluorescence was very weak, and the transfection efficiency reduced dramatically, when compared to samples transfected with the regular all-in-one construct. Additionally, the increase of the GFP-signal in illuminated cells was very low, indicating a loss of light-induced potassium channel expression (Fig. 38 B). Mean fluorescence intensity of Kcv_{NTS} mCherry after light stimulation was 1.04 AU, the corresponding dark state control was 1.02±0.03 AU. Hence, illumination caused an increase of only 0.02 AU, which is 10-fold lower compared to the increase of 0.26 AU for Kcv_{NTS} without the additional mCherry-tag. Sorting efficiency was also reduced: only 23 % of the cells showed localization of the channel in the ER. Collectively, the data show that an additional tag, which allows identification of transfected cells, was unfavorable for the system. All following experiments showing the functionality of Kcv_{NTS} (chapter 7.5), under control of the CRY2 CIB1 system, were therefore performed with illuminated cells.

In a third optimization approach, CRY2 was truncated and negatively charged amino acids were added to the C-terminus. This was motivated by data from Duan and coworkers (Duan et al., 2017), which indicated that C-terminal charges at positions 489 and 490 induce CRY2-CRY2 homo-oligomerization, by truncating CRY2 this propensity to form homo-oligomers is strongly reduced. To further diminish the unwanted homo-oligomerization, negative charges were added to the C-terminus which further prevented CRY2-CRY2 interactions (Duan et al., 2017). A reduction in the propensity of unspecific CRY2-CRY2 interactions should increase the likelihood of CRY2-CIB1 interactions, as there is more free CRY2 to interact with CIB1, binding the latter to induce gene expression. Based on these observations, CRY2 was truncated and two glutamates and two aspartates were added to the C-terminus in the all-in-one CRY2 CIB1 $Kesv_{Opt}$ construct, generating CRY2 1-488 EEDD $Kesv_{Opt}$. The relative fluorescence intensity of the new construct was compared to the all-in-one construct with the full length CRY2. Dark state control values were on the same low levels as observed for all other constructs tested. CRY2 1-488 EEDD $Kesv_{Opt}$ had a mean RFI value of 1.03±0.02 AU, compared to the full-length construct expressing $Kesv_{Opt}$ which showed an RFI of 1.07±0.04 AU. The mean fluorescence intensity for the construct with the truncated CRY2 was 1.35 AU, which is only marginally higher than the respective value of 1.33 AU for the full-length construct. Transfection efficiency and sorting efficiency did not change in any way, compared to the full-length construct (Fig. 38 D). Taken together, there was no appreciable improvement obtained from the truncation of CRY2.

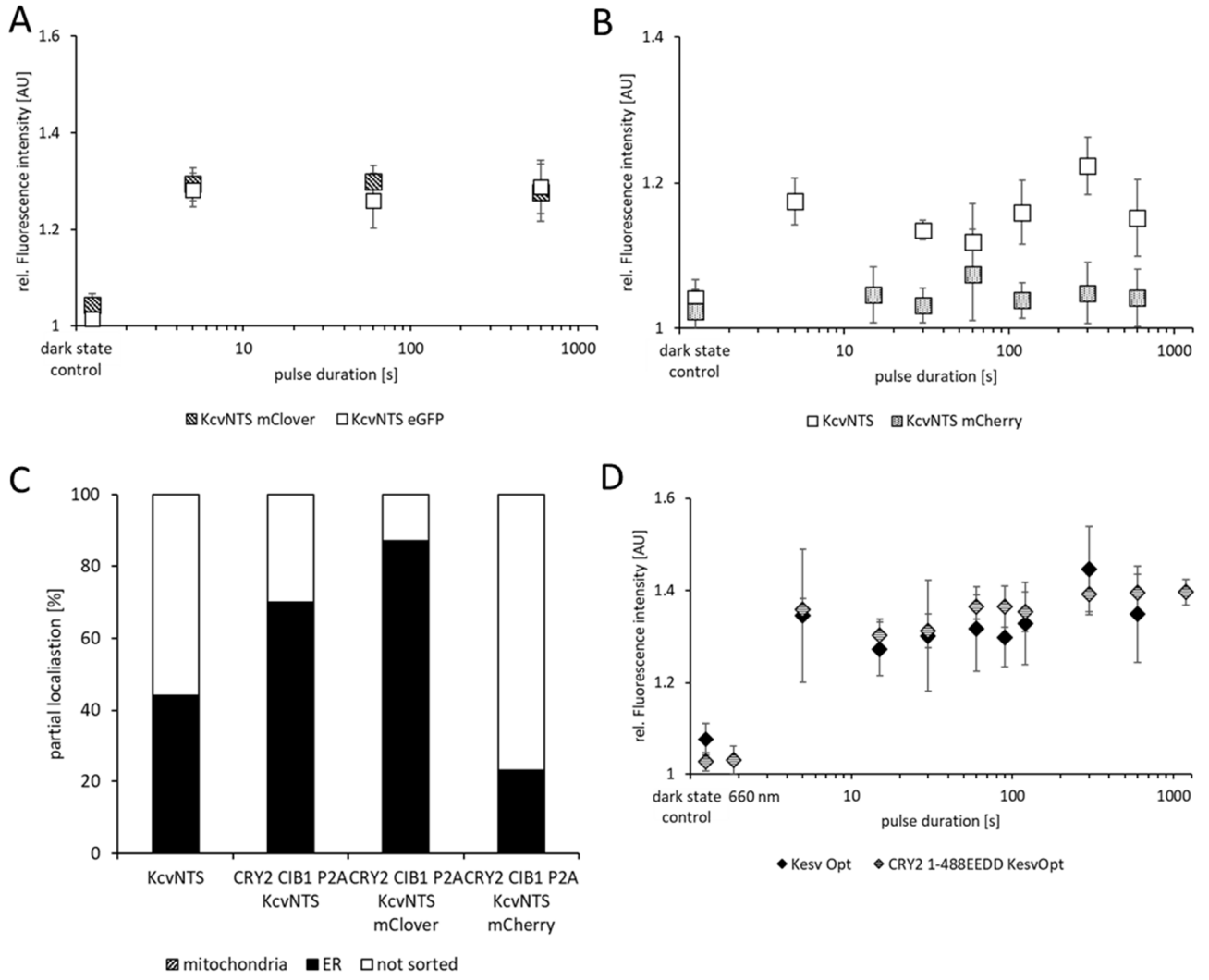

Fig. 38: Modifications and optimizations of the all-in-one CRY2 CIB1 system

(A) shows the rel. fluorescence intensity of CRY2 CIB1 Kcv_{NTS} mClover compared to the initial eGFP construct. Used were single light pulses of different lengths, applied 4 hours prior to imaging, overall incubation time: 16 hours. For each timepoint, 20 cells were imaged. Error bars indicate standard deviation. **(B)** shows the comparison of CRY2 CIB1 Kcv_{NTS} with CRY2 CIB1 Kcv_{NTS} with an additional mCherry constitutively expressed on the same vector. Used were again the short single light pulses, light intensity 120 µE, error bars indicate standard deviation. **(C)** shows the sorting pattern of Kcv_{NTS} (N=2, n=184) and CRY2 CIB1 Kcv_{NTS} (N=8, n=207) compared to CRY2 CIB1 Kcv_{NTS}::mClover (N=3, n=62) and CRY2 CIB1 Kcv_{NTS} mCherry (N=8, n=178). **(D)** shows the rel. fluorescence intensity of CRY2 1-488 EEDD $Kesv_{Opt}$ compared to the initial full length CRY2 construct. Used were single light pulses of different lengths, applied 4 hours prior to imaging, overall incubation time: 16 hours. For each timepoint, 20 cells were imaged. Error bars indicate standard deviation.

6.9. The CRY2 CIB1 system offers an easily applicable and highly light-sensitive approach to induce potassium channel expression in the IMM and the PM

To sum up the results of the experiments with the CRY2 CIB1 system as an optogenetic tool to induce expression of viral potassium channels in different cellular compartments, we can say that these constructs shown in the previous chapters have very good potential to serve as modular optogenetic tools with easy handling and high light-sensitivity.
A robust expression of the various mitochondrial and PM-sorted channels was observable either with pulsed light of very low intensity (6 μE) (compare Fig. 25) or with a single five second light pulse of higher intensity (120 μE) (compare Fig. 28). This allows full activation of the construct while avoiding negative effects of energy-rich blue light application by keeping the light dose very low.
One hour after illumination, gene expression is already observable and remains on a stable level for nine hours afterwards (compare Fig. 27). This enables long term experiments while applying a light pulse only every eight hours and maintaining a stable protein level for prolonged times throughout the experiment.

If we compare the increase in RFI of all channels tested in the chapters above in the CRY2 CIB1 system, it becomes clear that the four channels sorted to the IMM show higher values, compared to those trafficking to the PM via the ER (Fig. 39). $Kesv_{Opt}$ shows an increase of 0.26±0.05 AU, in combination with the truncated CRY2 1-488 EEDD the value increases even further to 0.33±0.03 AU. $Kmpv_{12T}$ and $Kmpv_{12TOpt}$ show a slightly lower increase of 0.21±0.03 AU for $Kmpv_{12T}$ and 0.25±0.02 AU for $Kmpv_{12TOpt}$. Taken together, these results for the mitochondrial channels indicate a good activation of gene expression, leading to a robust increase in fluorescence intensity. The best activation is shown by $Kesv_{Opt}$ with the shorter CRY2, albeit this effect results from a lower dark state activity and not from a higher absolute value in RFI (compare Fig. 38 D). The other three mitochondrial constructs show activation in the same range, which is higher than the level for the two PM-targeted channels. $Kcv_{PBCV\text{-}1Opt}$ shows an increase of 0.14±0.04 AU and Kcv_{NTS} an increase of 0.12±0.04 AU, the activation of Kcv_{NTS} with eGFP exchanged for mClover shows activation on the level of the mitochondrial constructs, the value being 0.25±0.01 AU, this seemingly better activation also resulting from a lower dark state activity. It becomes quite clear, that the light dependency is lost if an additional mCherry is constitutively expressed, resulting in almost no increase of fluorescence for the Kcv_{NTS} mCherry construct (0.02±0.01 AU) (Fig. 39).

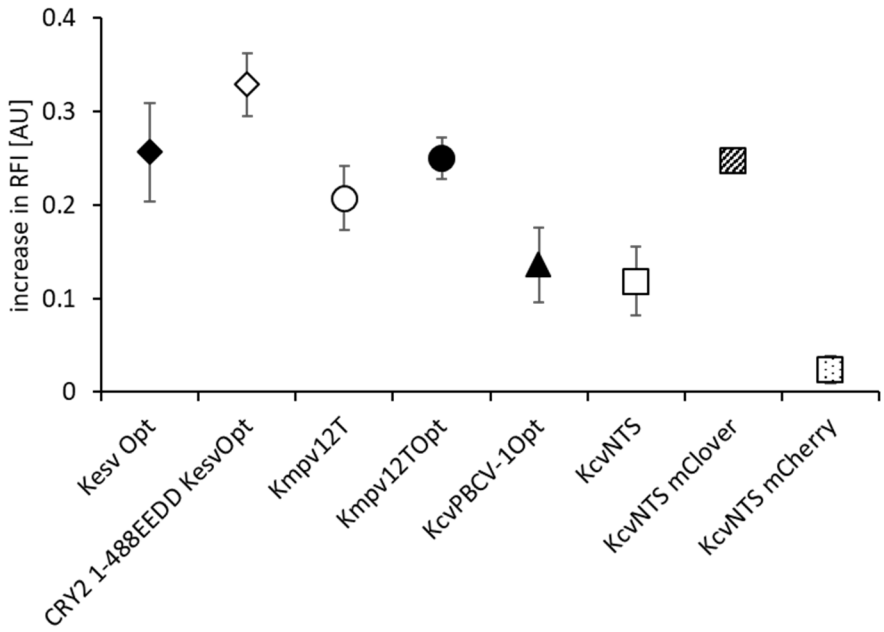

Fig. 39: Increase in rel. fluorescence intensity (RFI) upon illumination for all CRY2 CIB1 constructs

Shown are the ratios of the RFI of the dark state controls divided by the mean RFI upon illumination for each construct expressed in the all-in-one CRY2 CIB1 system. Error bars indicate standard deviation.

The higher ratios for the mitochondrial channels do not necessarily have to be the results of a more effective light activation: they could also result from the different structures of mitochondria and the ER in the cell. Mitochondria are very distinct puncta in the cells, the maximum fluorescence is therefore higher than in cells with fluorescent ER structures as the ER is more widely spread and diffuse, due to its netlike structures. This was observed as well for the constitutive constructs – the mean fluorescence intensity for $Kesv_{Opt}$ (2.11±0.26 AU) is much higher, compared to $Kcv_{PBCV\text{-}1Opt}$ (1.55±0.14 AU) and Kcv_{NTS} (1.40±0.19 AU).

The goal to design a modular tool for the optogenetic expression of potassium channels suitable for long term experiments yielded promising results in HEK293 cells. In the next steps, the functionality of the new constructs will be addressed (compare chapter 7), as well as preliminary results in *in vivo* studies in zebrafish larvae (compare chapter 8.4).

7. Establishing the functionality of the optogenetic constructs

In the previous chapters, the sorting and the light sensitivity of the CRY2 CIB1 constructs have been established. To generate useful optogenetic tools that may be suitable for the depolarization of either the PM or the IMM, proof of their functionality is essential. In this chapter, the functionality of the channels, which are expressed in a light-dependent manner in either the mitochondria or the PM will be examined.

So far, four endogenous mitochondrial potassium channels have been described: mitoK_{ATP}, mitoBK_{Ca}, mitoKv1.3 and TASK-3 (Laskowski et al., 2016). Their function is in most cases not completely understood and remains the subject of controversial discussion (Laskowski et al., 2016). Most studies agree on the facts that mitochondrial potassium channels decrease the MMP (Serrano-Albarrás et al., 2018), increase ROS production (Zhang et al., 2001) and influence mitochondrial calcium levels (Hoth et al., 1997; Bednarczyk et al., 2013). The effects of these alterations in the mitochondrial metabolism are very diverse and range from the induction of cytoprotection by preconditioning due to increased ROS production (Malinska et al., 2010; Wang et al., 2011), to the induction of necrosis or apoptosis (Brookes et al., 2004).

A point to be addressed in the following experiments is whether expression of $Kesv_{Opt}$, $Kmpv_{12T}$ and $Kmpv_{12TOpt}$ affects the MMP. A decrease in MMP has been shown to induce mitochondrial swelling and reduced mitochondrial motility (Safiulina et al., 2006) and can lead to the induction of apoptosis (Gottlieb et al., 2003). But fluctuations of the MMP do not necessarily have to be a sign of pathological conditions, they also occur during mitochondrial fusion and fission: during fission the mitochondria are depolarized while they hyperpolarize again during fusion (Suzuki et al., 2018).

Another point to be addressed is whether an expression of potassium channels has an impact on the mitochondrial calcium homeostasis. This is an interesting issue, since an increase in calcium level induces ROS production which in turn triggers the induction of apoptosis (Brookes et al., 2004), cell cycle arrest (Giorgi et al., 2018a) or can lead to cytoprotection if the increase in calcium is moderate (Guidarelli et al., 2019).

To obtain a first overview of potential effects on mitochondrial metabolism an investigation of changes in mitochondrial morphology is a good indicator. It is well established that alterations in mitochondrial shape can be linked to calcium signaling, changes in mitochondrial membrane potential and cell death (Campello and Scorrano, 2010). Changes in mitochondrial morphology are the results of altered fusion and fission activity. Responsible for these processes are the dynamin-related GTPases Mitofusin 1 and 2 (MFN1, MFN2), optic atrophy1 (OPA1) as well as dynamin-related peptide 1 (DRP1). MFN1 and 2 play an important role in metabolism, establishment of mitochondria / ER contacts and cell proliferation

(Santel and Fuller, 2000). Mutations in MFN2 are linked to Charcoth-Marie-Tooth disease (Züchner et al., 2004). OPA1 is anchored in the IMM, enhances mitochondrial fusion and plays a role in apoptosis and cytochrome c release (Karbowski and Youle, 2003). DRP1 is a cytosolic protein which needs to be activated and recruited to the mitochondria to induce fission (Yoon et al., 2003). Changes in mitochondrial morphology have been studied in many metabolic conditions and diseases, such as calcium signaling (Szabadkai et al., 2004), ROS generation (Yu et al., 2006), neuronal plasticity (Li et al., 2004), neurodegeneration (Palmer et al., 2011), diabetes (Trudeau et al., 2010), Alzheimer's and Parkinson (Trimmer et al., 2000), and ischemia (Brady et al., 2006; Ong and Hausenloy, 2010). Changes in mitochondrial morphology and motility imply changes in cellular metabolism, as mitochondria accumulate in the cell where large amounts of ATP are needed, thereby leading to a spatial compartmentalization (Verstreken et al., 2005). If the mitochondrial network is disrupted by a predomination of fission, apoptosis (Wasilewski and Scorrano, 2009) or mitophagy occur. Mitophagy being a known survival mode during mitochondrial stress recovery which leads to fragmented mitochondria and uptake by autophagosomes (D'Acunzo et al., 2019).
Motivated by this rich source of information on mitochondrial morphology in a first set of experiments, potential changes in mitochondrial morphology in relation to an expression of potassium channels in these organelles will be examined (compare chapter 7.1). In the next steps, three microscopic assays were used to address the question whether these channels affect MMP, mitochondrial calcium levels or induce apoptosis (compare chapter 7.2).

To test the functionality of the two channels which are expressed at the PM, a more straightforward approach can be taken. Kcv_{NTS} was expressed in HEK293 cells either as constitutively expressed construct under control of the CMV promotor, or in the all-in-one CRY2 CIB1 vector. The functional expression of the channels was then tested by whole cell patch clamp measurements. This enabled comparison of the channel properties as a function of the expression system (compare chapter 7.5).

7.1. The expression of functional potassium channels in the IMM leads to changes in mitochondrial morphology

To examine the impact of potassium channels on the morphology of mitochondria Cos7 cells were used, which are far mor suitable compared to HEK293 cells, because of their greater size and flatter spread on the surface, thereby allowing for images with higher resolution and therefore easier study of mitochondria within the cells.

In a first set of experiments, Cos7 cells were transfected with either $Kesv_{Opt}$, $Kmpv_{12T}$ or $Kmpv_{12TOpt}$ and their mitochondrial morphology was assessed in a descriptive approach. In Fig. 40 all three GFP-tagged channels can be seen in Cos7 cells, revealing their representative mitochondrial sorting pattern (compare chapter 3.1.1). Here it becomes clear again, that $Kesv_{Opt}$ shows the most distinct sorting to the mitochondria. This is apparent from the very low background fluorescence in the cytosol compared to $Kmpv_{12T}$ and $Kmpv_{12TOpt}$. Taken together, all three channels show robust sorting to the mitochondria, as is also underscored by the high PCC and MC for correlation with the mitochondrial marker plasmid (Fig. 40, 1st, 3rd and 5th row). The higher background fluorescence of $Kmpv_{12T}$ and $Kmpv_{12TOpt}$ is best represented in the values for the PCC with the ER marker plasmid: $Kesv_{Opt}$ shows the lowest correlation with the ER marker (2nd row, PCC 0.233), compared to $Kmpv_{12T}$ (4th row, PCC 0.423) and $Kmpv_{12TOpt}$ (6th row, PCC 0.75). These higher values result from the cytosolic background fluorescence, which is most pronounced in for $Kmpv_{12TOpt}$ (Fig. 40, panel P).

To look further into mitochondrial morphology, the regions indicated by the white squares in Fig. 40 were further enlarged, allowing a closer look at the shape of the mitochondria (Fig. 41). Here the differences in mitochondrial morphology are quite pronounced. The mitochondria are long, linear and branching in the cells expressing $Kesv_{Opt}$ (1st and 2nd row, Fig. 41) and short and spherical in cells expressing either $Kmpv_{12T}$ (3rd and 4th row, Fig. 41) or $Kmpv_{12TOpt}$ (5th and 6th row, Fig. 41). The dramatic differences are in good agreement with the fact that $Kesv_{Opt}$ is a non-active channel (Kithil, 2018), whereas both $Kmpv_{12T}$ and $Kmpv_{12TOpt}$ are active channels (compare chapters 7.2 and 7.3). This activity presumably affects mitochondrial metabolism and alters the morphology of the organelles.

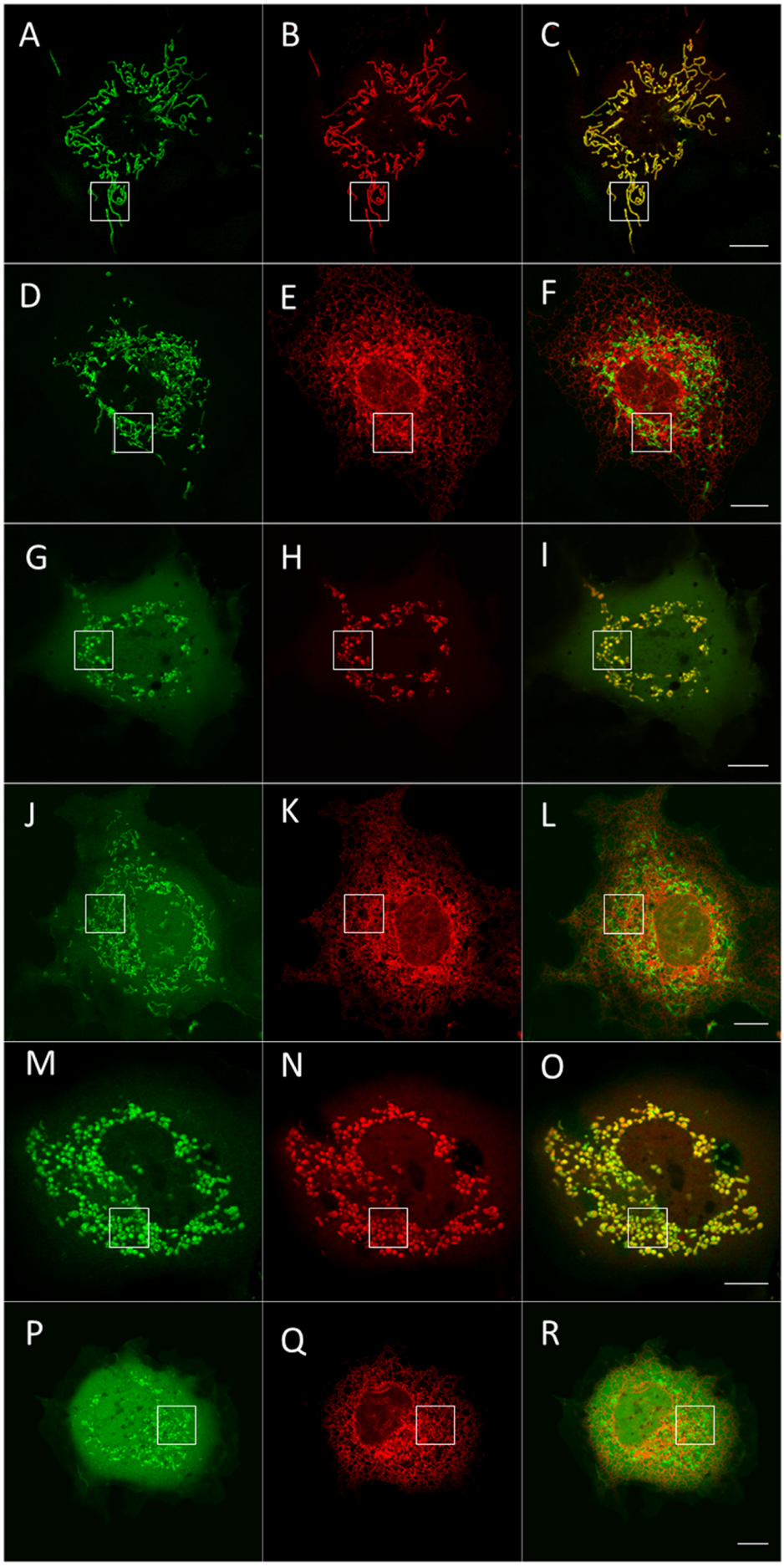

PCC = 0,805

$MC_{A/B}$ = 0,899
$MC_{B/A}$ = 0,588

PCC = 0,233

$MC_{D/E}$ = 0,671
$MC_{E/D}$ = 0,158

PCC = 0,643

$MC_{G/H}$ = 0,196
$MC_{H/G}$ = 0,999

PCC = 0,423

$MC_{J/K}$ = 0,609
$MC_{K/J}$ = 0,646

PCC = 0,854

$MC_{M/N}$ = 0,94
$MC_{N/M}$ = 0,806

PCC = 0,75

$MC_{P/Q}$ = 0,417
$MC_{Q/P}$ = 0,984

Previous Page

Fig. 40: $Kesv_{Opt}$, $Kmpv_{12T}$ and $Kmpv_{12TOpt}$ expressed in Cos7 cells

(A-F) Confocal images of $Kesv_{Opt}$::eGFP, Panel A&D: $Kesv_{Opt}$::eGFP, Panel B: COX8::mCherry, Panel E: HDEL::mCherry, Panel C: Merged Image of A and B, Panel F: Merged image of D and E. Scale bar represents 10 µm. On the right PCC and MC are indicated. **(G-L)** Confocal images of $Kmpv_{12T}$::eGFP, Panel G&J: $Kmpv_{12T}$::eGFP, Panel H: COX8::mCherry, Panel K: HDEL::mCherry, Panel I: Merged Image of G and H, Panel L: Merged image of J and K. Scale bar represents 10 µm. On the right PCC and MC are indicated **(M-R)** Confocal images of $Kmpv_{12TOpt}$::eGFP, Panels M&P: $Kmpv_{12TOpt}$::eGFP, Panel N: COX8::mCherry, Panel Q: HDEL::mCherry, Panel O: Merged Image of M and N, Panel R: Merged image of P and Q. Scale bar represents 10 µm. On the right PCC and MC are indicated.

Following Page

Fig. 41: Mitochondrial morphology of Cos7 cells expressing $Kesv_{Opt}$, $Kmpv_{12T}$ and $Kmpv_{12TOpt}$

Magnifications of the images shown in Fig. 40, the white squares in Fig. 40 indicate the location of the magnifications. **(A-F)** Confocal images of $Kesv_{Opt}$::eGFP, Panel A&D: $Kesv_{Opt}$::eGFP, Panel B: COX8::mCherry, Panel E: HDEL::mCherry, Panel C: Merged Image of A and B, Panel F: Merged image of D and E. Scale bar represents 5 µm. **(G-L)** Confocal images of $Kmpv_{12T}$::eGFP, Panel G&J: $Kmpv_{12T}$::eGFP, Panel H: COX8::mCherry, Panel K: HDEL::mCherry, Panel I: Merged Image of G and H, Panel L: Merged image of J and K. Scale bar represents 5 µm. **(M-R)** Confocal images of $Kmpv_{12TOpt}$::eGFP, Panels M&P: $Kmpv_{12TOpt}$::eGFP, Panel N: COX8::mCherry, Panel Q: HDEL::mCherry, Panel O: Merged Image of M and N, Panel R: Merged image of P and Q. Scale bar represents 5 µm.

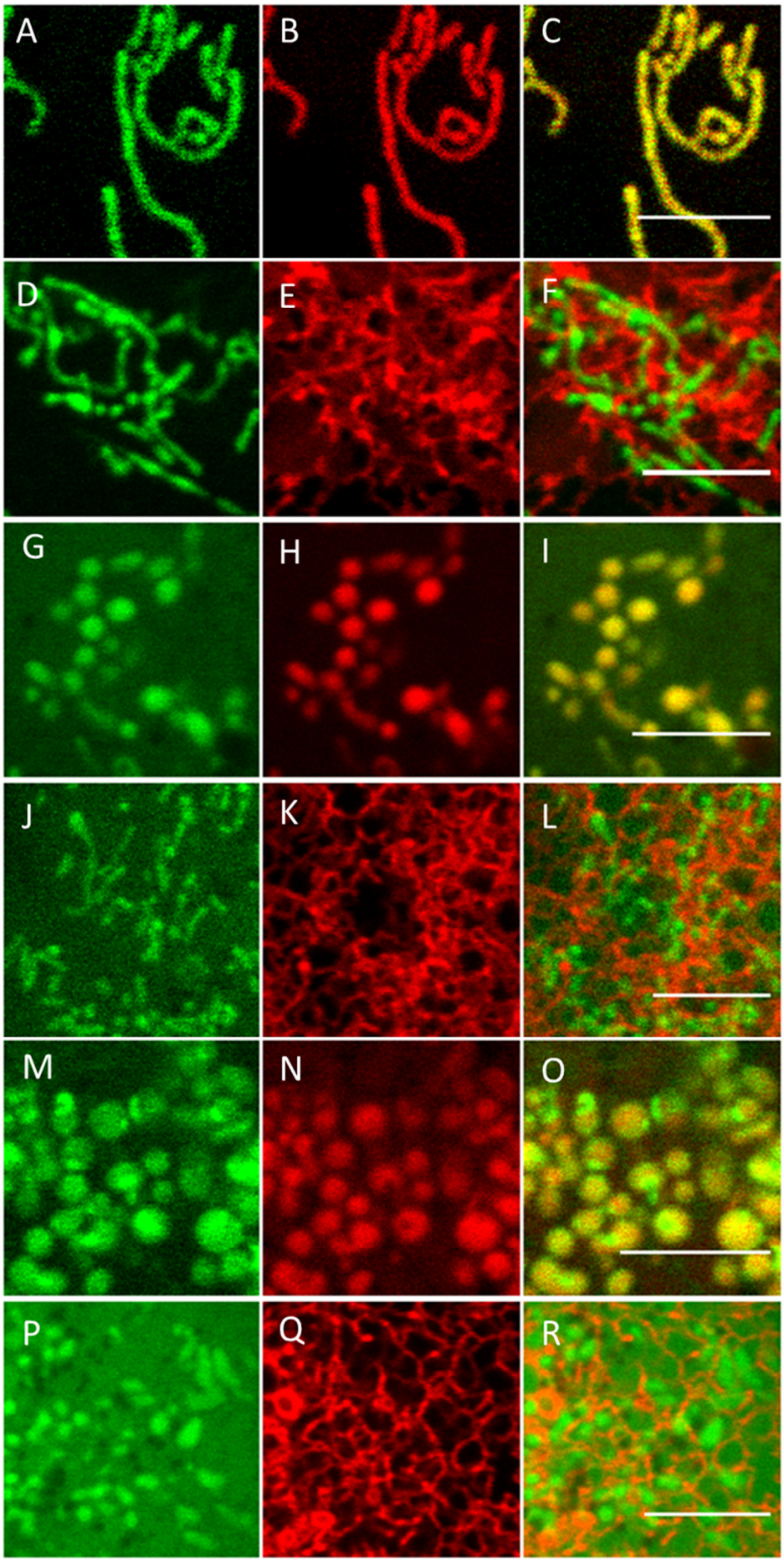
A
B
C
D
E
F
G
H
I
J
K
L
M
N
O
P
Q
R

The long and branching mitochondria, as seen in $Kesv_{Opt}$ expressing cells (Fig. 41, 1st and 2nd row) are usually observed in healthy cells, which are not under metabolic stress, and where mitochondrial fusion and fission occurs in a balanced manner (Santel and Fuller, 2000). The fragmented mitochondrial phenotype, where mitochondrial networks are broken and fission predominates, as can be seen here for both $Kmpv_{12T}$ (Fig. 41, 3rd and 4th row) and $Kmpv_{12TOpt}$ (Fig. 41, 5th and 6th row) is associated with mitochondrial depolarization or uncoupling (Miyazono et al., 2018). This morphology is often reported as part of the apoptotic pathway (Wasilewski and Scorrano, 2009) prior to cytochrome c release (Frank et al., 2001). Other studies also state that an imbalance in mitochondrial fission does not necessarily have to induce apoptosis, but can also be part of other metabolic states which are only poorly understood so far (Autret and Martin, 2009). Mitochondrial fission also occurs during mitophagy, prior to the uptake of the mitochondria in the autophagosomes (Glick et al., 2010). Mitophagy is induced during the recovery period after cellular stress (D'Acunzo et al., 2019).

The present findings on mitochondrial fusion and fission imply that $Kmpv_{12T}$ and $Kmpv_{12TOpt}$ induce some kind of cellular stress, which still needs to be further defined. The data are a good starting point for further experiments to take a more defined look into the changes induced by the expression of functional potassium channels in the IMM. The data also confirm that the non-functional $Kesv_{Opt}$ serves as a perfect negative control for a channel which is sorted to the IMM but shows no activity. In the next chapter, the question will be addressed whether $Kmpv_{12T}$ and $Kmpv_{12TOpt}$ induce changes in MMP and mitochondrial calcium concentration. Also, the question whether the active channels induce apoptosis will be addressed and discussed in the context of the altered mitochondrial morphology.

7.2. The expression of functional potassium channels in the IMM leads to a decrease of IMM-potential and mitochondrial calcium concentration but does not induce apoptosis

To study the effects of a functional potassium channel in the IMM of human cells, mitochondrial membrane potential, mitochondrial calcium concentration and induction of apoptosis were addressed. All assays described here were conducted for both the regular constitutive constructs and the optogenetic constructs expressed in the all-in-one CRY2 CIB1 system (chapter 6) to establish possible differences in effectivity of the induced changes.

In the first assay, cells were transfected with $Kesv_{Opt}$, $Kmpv_{12T}$ or $Kmpv_{12TOpt}$, incubated for 16 hours and in case of the CRY2 CIB1 constructs illuminated with a single 1-minute light pulse 4 hours prior to imaging. The cells were stained with MitoTracker CMXRos, a fluorescent dye that accumulates in the mitochondria in a membrane potential dependent way (Wolter et al., 1997; McDonald et al., 2002). The higher the MMP, the stronger the fluorescence of MitoTracker CMXRos. To assess changes induced by

the mitochondrial potassium channels, the fluorescence intensity of transfected cells was compared to the fluorescence intensity of the surrounding untransfected control cells.

The two rows of confocal images in Fig. 42 show representative cells transfected with $Kesv_{Opt}$ (upper row) or $Kmpv_{12TOpt}$ (lower row). It is apparent from the images that $Kmpv_{12TOpt}$, but not $Kesv_{Opt}$ shows a weaker accumulation of MitoTracker CMXRos in the mitochondria and thereby a weaker fluorescence compared to the surrounding untransfected cells. These visual impressions are confirmed by the statistical analysis of the mean RFI values, shown in Fig. 42 G. Neither $Kesv_{Opt}$ nor CRY $Kesv_{Opt}$ show a reduction in mean fluorescence intensity. The ratios of CMXRos fluorescence between transfected and untransfected cells are 1.04±0.2 AU and 1.01±0.04 AU for $Kesv_{Opt}$ and CRY $Kesv_{Opt}$ respectively. In contrast, $Kmpv_{12T}$ shows a pronounced reduction in fluorescence, with both the constitutive (0.59±0.04 AU) and the light dependent (0.58±0.14 AU) construct being 40% less bright than the untransfected cells. The same result can also be observed for $Kmpv_{12TOpt}$, here the ratio for the constitutive construct is 0.57±0.18 AU and for the CRY2 CIB1 construct 0.54±0.08 AU.

As a positive control, cells were treated with the uncoupler CCCP. It is well established that this treatment causes a depolarization of the mitochondria (Trumpower and Katki, 1975) The data show that addition of the uncoupler to the bath medium generates a strong reduction in the CMXRos fluorescence, with a ratio of 0.65±0.07 AU. This value is higher than the ratios of the mean RFI obtained for the functional potassium channels. At this point it is worth mentioning that the results for CCCP treatment are not directly comparable to the ones obtained for the channels. The staining and imaging procedure had to be adapted to allow for comparison of the same cells with and without CCCP treatment. The cells were stained, imaged, incubated with CCCP and imaged again. MitoTracker CMXRos, which as expected accumulated well in the untransfected cells, dissociated from the mitochondria after CCCP treatment but did not diffuse out of the cells again. This resulted in a higher cytosolic background fluorescence and thereby in an elevated ratio of treated / untreated cells.

This is represented by the ratio of the maximum RFI, which ranges around 0.8 AU in case of the channels, but drops to 0.3 AU for CCCP (compare appendix, Fig. 51). These data show that CCCP reduces the mitochondrial membrane potential much stronger than the channels, as would be expected for uncoupled mitochondria.

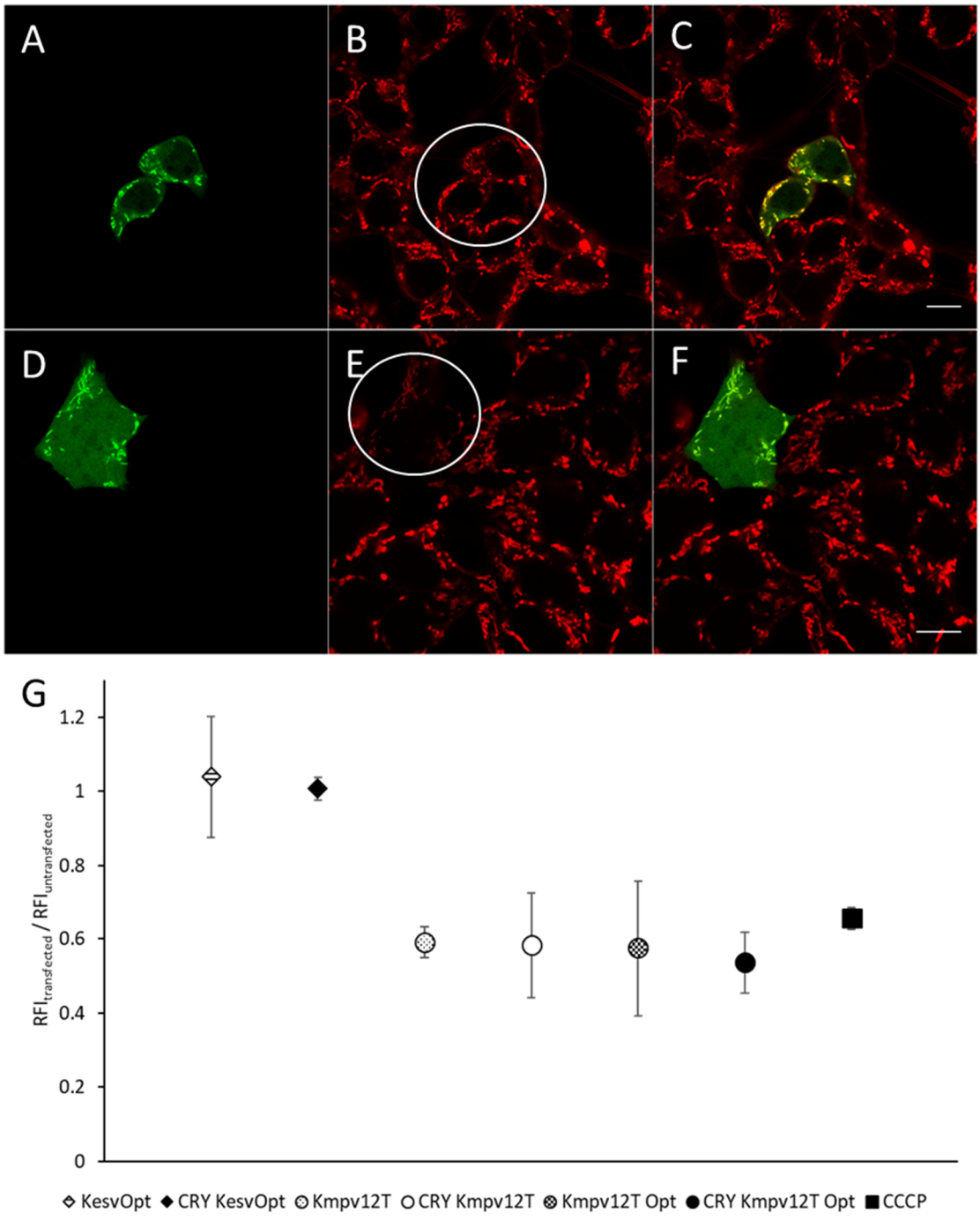

Fig. 42: Changes in mitochondrial membrane potential induced by $Kmpv_{12T}$ and $Kmpv_{12TOpt}$ expressed both constitutively and light-dependently

(A-F): Confocal images of $Kesv_{Opt}$::eGFP and $Kmpv_{12TOpt}$::eGFP, Panel A: $Kesv_{Opt}$::eGFP, Panel D: $Kmpv_{12TOpt}$::eGFP, Panel B&E: MitoTracker CMXRos, transfected cell is indicated by a white circle, Panel C: Merged Image of A and B, Panel F: Merged image of D and E. Scale bars represent 10 µm. **(G)** Ratio of mean RFI of MitoTracker CMXRos transfected / untransfected cells for $Kesv_{Opt}$ (N=3, n_{transf}=90, $n_{untransf}$=273), CRY $Kesv_{Opt}$ (N=3, n_{transf}=56, $n_{untransf}$=162), $Kmpv_{12T}$ (N=3, n_{transf}=54, $n_{untransf}$=200), CRY $Kmpv_{12T}$ (N=3, n_{transf}=41, $n_{untransf}$=165), $Kmpv_{12TOpt}$ (N=3, n_{transf}=59, $n_{untransf}$=205), CRY $Kmpv_{12TOpt}$ (N=3, n_{transf}=34, $n_{untransf}$=178) and untransfected cells treated with CCCP (N=4, n=1088).

In a second assay, changes in mitochondrial calcium level induced by the expression of a potassium channel were examined. For this assay, cells were transfected with $Kesv_{Opt}$, $Kmpv_{12T}$ or $Kmpv_{12TOpt}$, incubated for 16 hours and in case of the all-in-one CRY2 CIB1 constructs illuminated 4 hours prior to imaging with a 1-minute blue light pulse. The cells were stained with Rhod-2 AM, a cell permeant dye that accumulates in the mitochondria in a calcium-level dependent manner (Nguyen et al., 1998; Paredes et al., 2008).

The confocal images shown in Fig. 43 illustrate that $Kmpv_{12TOpt}$ (lower row) but not $Kesv_{Opt}$ (upper row) does induce a decrease in mitochondrial calcium concentration. Only cells transfected with either one of the active channels, $Kmpv_{12T}$ or $Kmpv_{12TOpt}$, show a decrease in Rhod-2 AM fluorescence. This can also be seen in the statistical results for both the constitutive and the light-dependent constructs (Fig. 43 G). Both $Kesv_{Opt}$ (1.04±0.03 AU) and CRY $Kesv_{Opt}$ (1.00±0.04 AU) generate a ratio of the fluorescence intensity which shows their intensity not being different from the surrounding untransfected cells, indicating no effects on the mitochondrial calcium level. This shows that active potassium channels in the IMM favor a decrease in the concentration of calcium in the mitochondria while the expression of a silent channel has no impact on this parameter. $Kmpv_{12T}$ (0.58±0.09 AU) and CRY $Kmpv_{12T}$ (0.57±0.02 AU) as well as $Kmpv_{12TOpt}$ (0.60±0.06 AU) and CRY $Kmpv_{12TOpt}$ (0.60±0.03 AU) exhibit basically the same difference in fluorescence ratio between channel expressing and non-expressing control cells indicating that all four constructs have the same potency in lowering the mitochondrial calcium concentration.

The situation is different in cells treated with CCCP. In this case the ratio increases to 1.52±0.14 AU. This increase in fluorescence after CCCP treatment implies an increase in cytosolic calcium caused by the efflux of calcium from the mitochondria (Hehl et al., 1996), so the increase in mean fluorescence is not due to a rise in mitochondrial calcium level but to the rise in cytosolic calcium (Werth and Thayer, 1994) caused by the loss of calcium buffer capacity of the mitochondria, due to the CCCP-induced uncoupling (Zoeteweij et al., 1993).

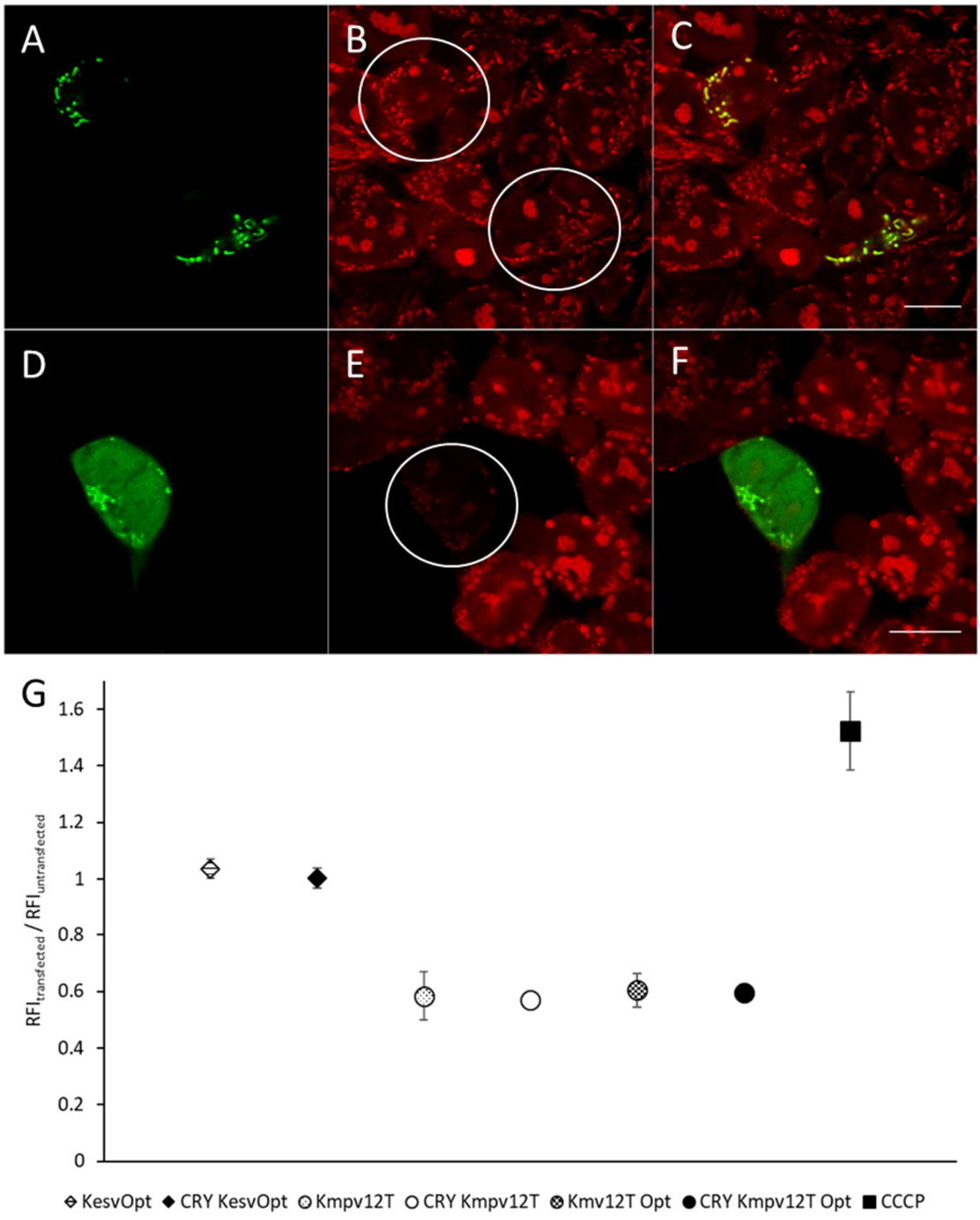

Fig. 43: Changes in mitochondrial calcium level induced by $Kmpv_{12T}$ and $Kmpv_{12TOpt}$ expressed both constitutively and light-dependently

(A-F): Confocal images of $Kesv_{Opt}$::eGFP and $Kmpv_{12TOpt}$::eGFP, Panel A: $Kesv_{Opt}$::eGFP, Panel D: $Kmpv_{12TOpt}$::eGFP, Panel B&E: Rhod-2 AM, transfected cell is indicated by a white circle, Panel C: Merged Image of A and B, Panel F: Merged image of D and E. Scale bars represent 10 µm. **(G)** Ratio of RFI of Rhod-2 AM transfected / untransfected cells for $Kesv_{Opt}$ (N=3, n_{transf}=71, $n_{untransf}$=267), CRY $Kesv_{Opt}$ (N=3, n_{transf}=38, $n_{untransf}$=202), $Kmpv_{12T}$ (N=3, n_{transf}=54, $n_{untransf}$=253), CRY $Kmpv_{12T}$ (N=3, n_{transf}=41, $n_{untransf}$=249), $Kmpv_{12TOpt}$ (N=3, n_{transf}=48, $n_{untransf}$=262), CRY $Kmpv_{12TOpt}$ (N=3, n_{transf}=46, $n_{untransf}$=259) and untransfected cells treated with CCCP (N=4, n=1293).

It has been previously reported, that both the decrease of mitochondrial membrane potential and the decrease of mitochondrial calcium levels can trigger the induction of apoptosis (Kruman and Mattson, 1999; Barroso et al., 2006; Hajnóczky et al., 2006), the next question to be examined was if apoptosis is induced by the expression of $Kesv_{Opt}$, $Kmpv_{12T}$ or $Kmpv_{12TOpt}$ either constitutively or under control of the CRY2 CIB1 system.

During imaging of cells expressing these channels during the experiments described in the previous chapters, there was no obvious increase in apoptotic cells to be observed. Apoptotic cells are quite easily recognized during microscopy, due to their change in cell shape (Su et al., 2019) and the appearance of apoptotic vesicles during late apoptosis (Galluzzi et al., 2007; Henry et al., 2013). Since no increase of cells in late apoptosis could be observed so far, for this reason a marker of early apoptosis was chosen to detect apoptotic events in relation to the expression of potassium channels in the mitochondria.

A classical marker for the early stages of apoptosis is the switch of phosphatidylserine (PS) to the extracellular side of the PM (Rimon et al., 1997). To detect this translocation of PS, Annexin V is a suitable marker as it binds PS, but is cell impermeant and therefore only binds if PS is present on the outside of the cell, thereby indicating early stages of apoptosis (Vermes et al., 1995; Crowley et al., 2016; Kupcho et al., 2019).

For this assay, cells were transfected with the three mitochondrial potassium channels, in the constitutive and light-dependent version, incubated for 16 hours, stained with Annexin V Alexa 647 and imaged after fifteen minutes of incubation.

Of the untransfected cells, 0.88±0.5 % showed apoptosis and from Fig. 44 A, it becomes clear that none of the potassium channels, expressed either constitutively or under control of the CRY2 CIB1 system, showed elevated apoptosis levels compared to the untransfected cells. The constitutive constructs all showed lower levels of apoptosis compared to the untransfected cells. Of the cells transfected with $Kesv_{Opt}$ 0.34±0.1 % showed apoptosis, 0.17±0.1 % of the cells transfected with $Kmpv_{12T}$ and 0.15±0.1 % of the cells transfected with $Kmpv_{12TOpt}$. The levels of apoptosis for the channels if expressed under control of the CRY2 CIB1 system was slightly higher but still well within the range of the untransfected cells. Cells transfected with $Kesv_{Opt}$ under control of the CRY2 CIB1 system showed apoptosis in 1.72±1.5 %, 0.59±0.5 % of the cells transfected with $Kmpv_{12T}$ and 0.80±0.3 % of the cells transfected with $Kmpv_{12TOpt}$. The positive control of untransfected cells treated for one hour with 0.1 mM CCCP showed an apoptosis-level of 5.1±1.4 %.

These results clearly demonstrate that the expression of functional potassium channels in the IMM does not lead to the induction of the apoptotic pathway in HEK293 cells. The portion of apoptotic cells was generally very low and did not increase above the level of untransfected control cells. Also, the levels of apoptotic cells observed after the expression of the two functional potassium channel constructs, $Kmpv_{12T}$ and $Kmpv_{12TOpt}$, do not differ from the ones obtained for $Kesv_{Opt}$, which has been shown to be non-

functional and therefore serves as a negative control in this case. These results are in accordance with studies performed by P. Ernst and coworkers (Ernst et al., 2019). In their work channelrhodopsin 2 was targeted to the mitochondria and used to influence the mitochondrial membrane potential in a light-dependent manner. They also showed that there is no induction of the apoptotic pathway, but a cytoprotective effect instead, if the expression level of the channelrhodopsin is induced at a moderate level. In earlier studies also targeting channelrhodopsin 2 to the mitochondria, no induction of apoptosis was reported as well (Tkatch et al., 2017).

With the data gained from the apoptosis-assay, it was also possible to study the transfection efficiency of both the constitutive and light-dependent potassium channel constructs, as the high number of images necessary to provide solid data concerning the induction of apoptosis, made it possible to also evaluate transfection levels for all six constructs. As can be seen in Fig. 44 B, transfection levels are generally higher for the constitutive constructs, compared to the light-induced ones. 22.9±5.6 % of the cells showed expression for $Kesv_{Opt}$, 18.4±2.2 % for $Kmpv_{12T}$ and 19.6±1.5 % for $Kmpv_{12TOpt}$ in the constitutive constructs. Under control of the CRY2 CIB1 system, 5.2±1.2 % of the cells transfected with $Kesv_{Opt}$ showed expression of the channel, 7.9±0.3 % showed expression in case of $Kmpv_{12T}$ and 9.1±2.9 % in case of transfection with $Kmpv_{12TOpt}$.

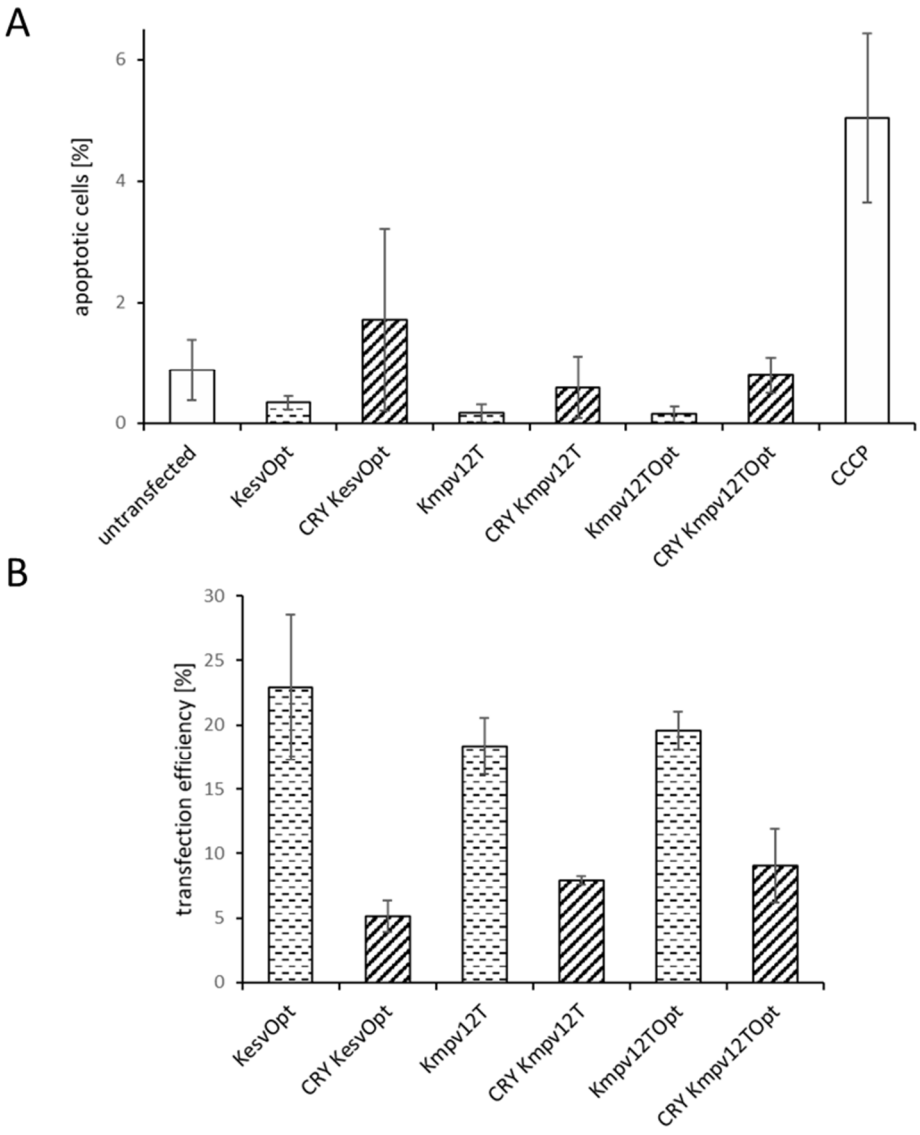

Fig. 44: Portion of apoptotic cells and transfection efficiency of constitutive and light dependent constructs

(A) shows the percentage of apoptotic cells in untransfected cells (N=3, n=24230), cells transfected with $Kesv_{Opt}$ (N=3, n=795), $Kmpv_{12T}$ (N=3, n=740), $Kmpv_{12TOpt}$ (N=3, n=822) and untransfected cells treated with 0.1 mM CCCP for 1 hour (N=3, n=4651), as well as cells transfected with $Kesv_{Opt}$ (N=3, n=184), $Kmpv_{12T}$ (N=3, n=355) and $Kmpv_{12TOpt}$ (N=3, n=425) under control of the CRY2 CIB1 system. Error bars represent standard deviation. **(B)** shows the transfection efficiency in % of $Kesv_{Opt}$ (N=3, n=3915), $Kmpv_{12T}$ (N=3, n=4561) and $Kmpv_{12TOpt}$ (N=3, n=5186) expressed constitutively or $Kesv_{Opt}$ (N=3, n=4046), $Kmpv_{12T}$ (N=3, n=4848) and $Kmpv_{12TOpt}$ (N=3, n=5004) under control of the CRY2 CIB1 system. Error bars represent standard deviation.

7.3. Codon optimization does not influence the functionality of Kmpv$_{12T}$

Changes in codon optimization can lead to altered or abolished functionality of proteins (Zhou et al., 2013; Bali and Bebok, 2015). Therefore, it was important to test the functional properties of the codon-optimized Kmpv$_{12T}$ channel version Kmpv$_{12TOpt}$, as it is the most promising candidate channel for the establishment of channel expression under control of the CRY2 CIB1 system in the mitochondria. In the previous chapters, it has been demonstrated that both Kmpv$_{12T}$ and Kmpv$_{12TOpt}$ are functional in the IMM and cause a depolarization of the mitochondria (compare chapters 7.1 and 7.2). To further characterize the functional properties of Kmpv$_{12TOpt}$, the protein was synthesized in vitro and functionally reconstituted in planar lipid bilayers as described for other viral channels (Winterstein et al., 2018b).
Fig. 45 shows the single channel properties of Kmpv$_{12TOpt}$ in comparison to those of Kmpv$_{12T}$. As has been described for Kmpv$_{12T}$ in previous studies (Siotto, 2017; Winterstein, 2019), its gating behavior is voltage dependent. This is due to a shortening of the open channel times at positive voltages (Fig. 45 A). The same behavior was also observed for Kmpv$_{12TOpt}$ (Fig. 45 B). The i/V curve of both channel variants shows the same approximately ohmic conductance between -100 and +100 mV. At more negative and more positive voltages the current amplitudes tend to saturate (Fig. 45 C). Fig. 45 D illustrates the increase of the open probability at higher negative voltages from 1.8±1.5 % at 200 mV to 15±7.7 % at -200 mV for Kmpv$_{12T}$ and 5.3±3.8 % at 200 mV to 17±4.8 % at -200 mV for Kmpv$_{12TOpt}$.

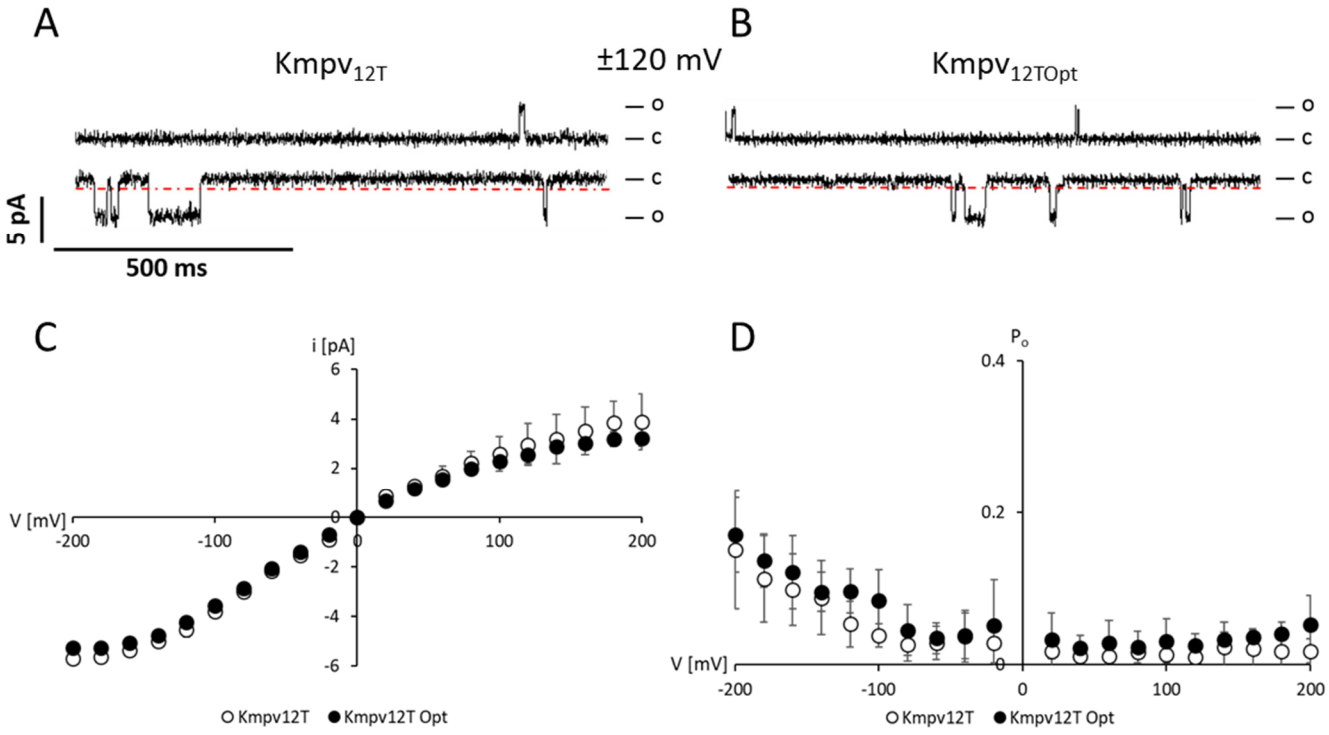

Previous page:

Fig. 45: Comparison of the single channel properties of Kmpv$_{12T}$ and Kmpv$_{12TOpt}$ in planar lipid bilayers

Representative single channel current traces of Kmpv$_{12T}$ **(A)** and Kmpv$_{12TOpt}$ **(B)** at ±120 mV in DPhPC membranes. Closed (c) and open (o) levels are indicated next to the current traces. Amplitude of sublevel gating events are indicated by the dotted red line. **(C)** Mean i/V curves for Kmpv$_{12T}$ (n=4) and Kmpv$_{12TOpt}$ (n=7). Error bars indicate standard deviation. **(D)** Mean open probability for Kmpv$_{12T}$ (n=4) and Kmpv$_{12TOpt}$ (n=7). Error bars indicate standard deviation.

Closer examination of the current traces shows sublevel gating events which have been first described by L. Winterstein (Winterstein, 2019). These sublevel gating events were also observed in the codon optimized version of Kmpv$_{12T}$, the properties of the sublevel events are shown in Fig. 46. Due to its low amplitude and linear increase at higher voltages, the sublevel can be detected only at voltages higher than ±80 mV. It also shows voltage dependent behavior, with its open probability decreasing from 11.5±3.9 % at -200 mV to 2.1±0.2 % at 200 mV for Kmpv$_{12T}$ and 6.8±6.3% at -200 mV to 1.5% at 200 mV for Kmpv$_{12TOpt}$.

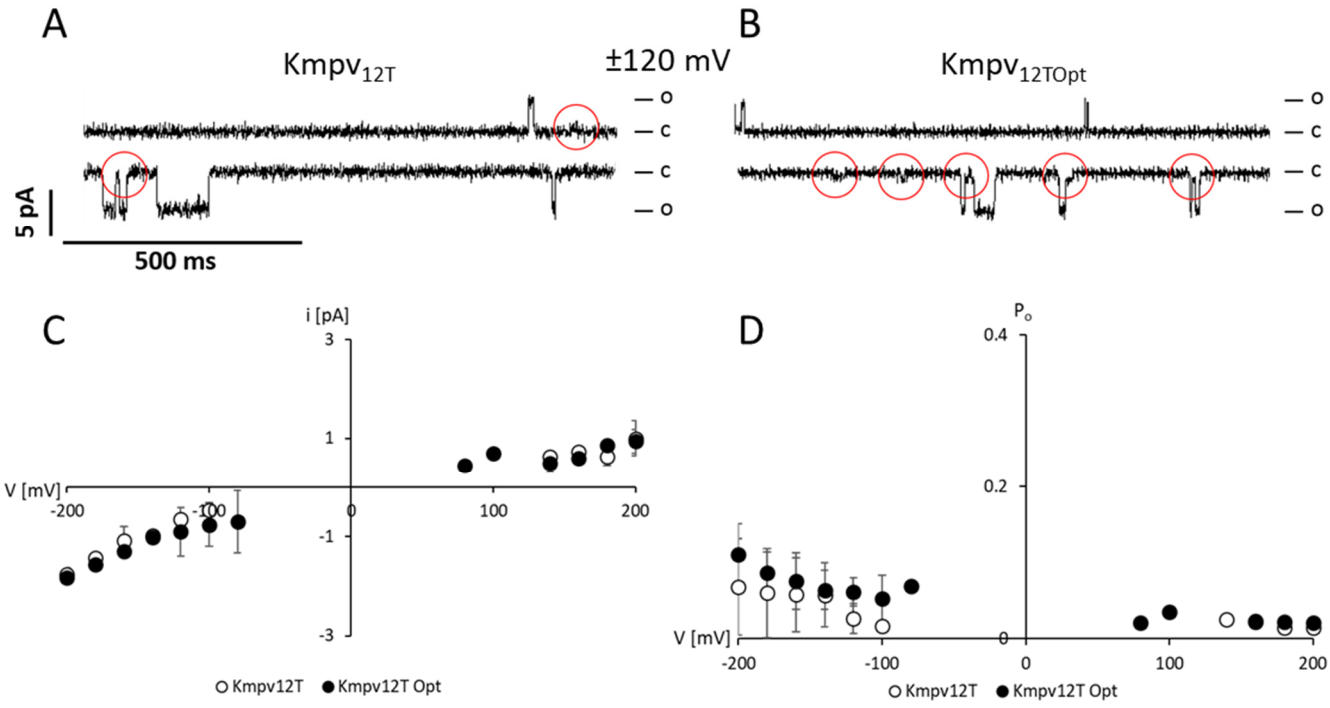

Fig. 46: Comparison of the sublevel properties of Kmpv$_{12T}$ and Kmpv$_{12TOpt}$ in planar lipid bilayers

Representative single channel current traces exhibiting sublevels (indicated by red circles) of **(A)** Kmpv$_{12T}$ and **(B)** Kmpv$_{12TOpt}$ at ±120 mV in DPhPC membranes. Closed (c) and open (o) levels are indicated next to the current traces. **(C)** Mean i/V curves for the sublevels of Kmpv$_{12T}$ (n=4) and Kmpv$_{12TOpt}$ (n=7). Error bars indicate standard deviation. **(D)** Mean open probability for the sublevels of Kmpv$_{12T}$ (n=4) and Kmpv$_{12TOpt}$ (n=7). Error bars indicate standard deviation.

7.4. Kmpv$_{12TOpt}$ does not conduct calcium ions

During the studies characterizing the effects of heterologous potassium channel expression in the mitochondria, it was found that the channels do not only affect mitochondrial membrane potential, as had been expected, but also cause a pronounced decrease of mitochondrial calcium concentration (chapter 7.2). To establish the selectivity of the potassium channels and to rule out a calcium conductance as the cause for the decrease of the calcium levels, planar lipid bilayer measurements were performed in which potassium was exchanged for calcium on the intracellular or the extracellular side.

Fig. 47 clearly illustrates that Kmpv$_{12TOpt}$ is indeed selective for potassium ions and does not conduct calcium ions. In the presence of 100 mM KCl, the channel exhibits its characteristic gating behavior, as has been already described in chapter 7.3. Upon exchange of potassium for calcium ions, no gating events of the channel can be recorded (Fig. 47 A). If potassium is replaced by calcium only on either the extracellular or the intracellular side, the channel exhibits gating events only if a potassium flux occurs. If the calcium is present at the extracellular side, gating events were only recorded at positive voltages indicating a potassium efflux. If calcium is present on the intracellular side, gating events occur only at negative voltages indicating an influx of potassium (Fig. 47 B).
The i/V curves and the open probabilities underscore these findings. If calcium is present only on the intracellular side, both the current and the open probability match the curves of the control measurement with potassium at positive voltages and then drop to zero, matching the symmetrical calcium measurements. If calcium is present only at the extracellular side, the image is reversed. The i/V curve and the open probability match the values for potassium at negative voltages and the values for calcium at positive voltages (Fig. 47 C & D).
These results prove that Kmpv$_{12TOpt}$ does not exhibit a calcium-conductance and is strictly selective for potassium ions. If only calcium is present in the measuring solutions, no gating events are recorded, ruling out a calcium-conductance of the channel. The decrease of mitochondrial calcium levels, as described in chapter 7.2, is therefore not caused by a calcium-conductivity of Kmpv$_{12TOpt}$.

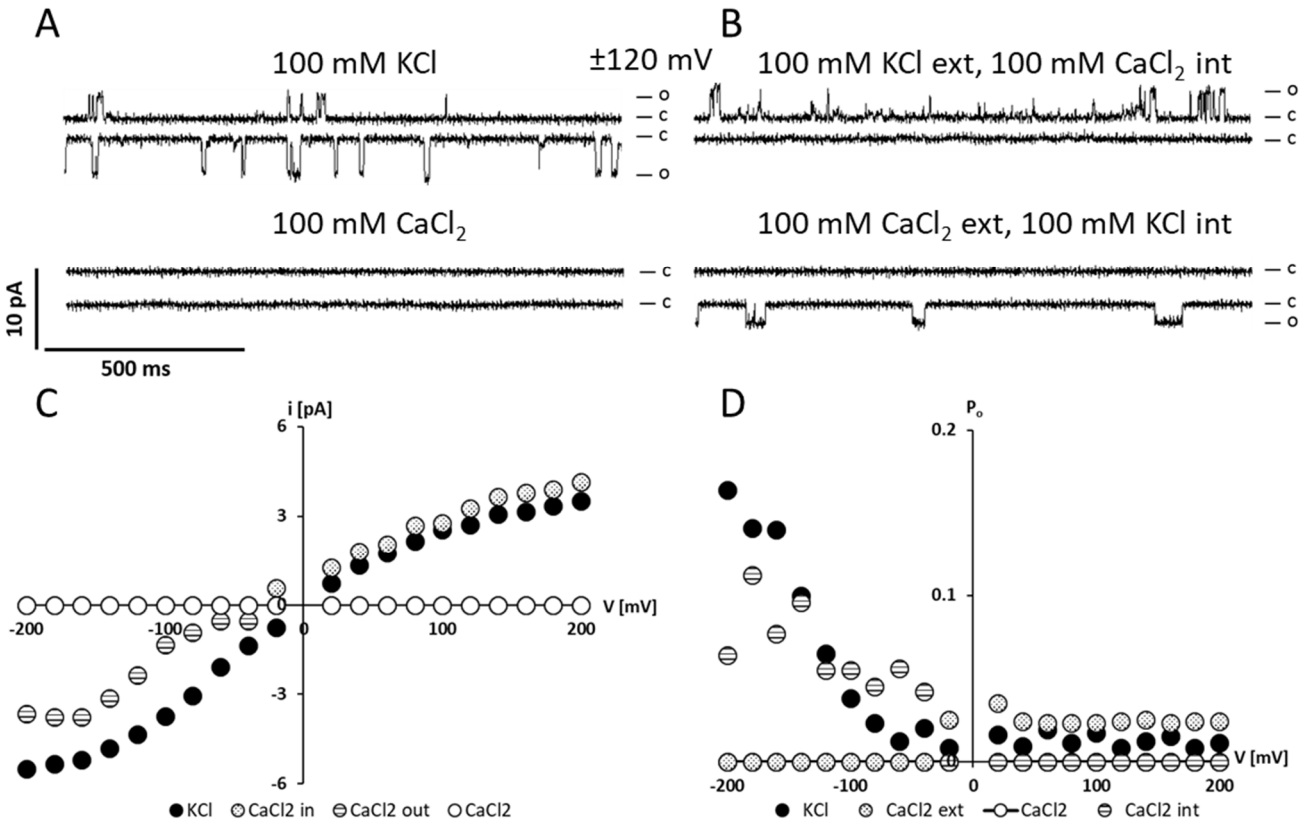

Fig. 47: Kmpv$_{12TOpt}$ does not conduct calcium ions

Representative single channel current traces of **(A)** Kmpv$_{12TOpt}$ at symmetric conditions with 100 mM KCl or 100 mM $CaCl_2$ or **(B)** at asymmetric conditions, with 100 mM KCl and 100 mM $CaCl_2$ at either the extracellular or the intracellular side at ±120 mV in DPhPC membranes. Closed (c) and open (o) levels are indicated next to the current traces. **(C)** Mean i/V curves for Kmpv$_{12TOpt}$ in KCl, and $CaCl_2$ under symmetric and asymmetric conditions. **(D)** Mean open probability for Kmpv$_{12TOpt}$ in KCl or $CaCl_2$ under symmetric and asymmetric conditions.

7.5. Light-dependent expression of Kcv_{NTS} does not affect its functional properties

After having established the unaltered functionality of the mitochondrial potassium channels under control of the CRY2 CIB1 system, the functionality of Kcv_{NTS}, which is sorted to the PM, was established in the CRY2 CIB1 system as well. To address this question, HEK293 cells were transfected with either the constitutive or the light-dependent Kcv_{NTS}, illuminated with 450 nm blue light and four hours later whole cell patch clamp experiments were performed.

Kcv_{NTS} has been extensively studied beforehand in both bilayer (Braun, 2014; Rauh, 2018) and patch clamp settings (Greiner, 2011; Kleuter, 2019). In his work, T. Greiner showed that Kcv_{NTS} exhibits two different current responses: one showing a slow inactivation at higher negative voltages and another one where this inactivation does not occur (Greiner, 2011). We therefore sought to establish these two gating modes in both the constitutive and the light-dependent Kcv_{NTS}.

Fig. 48 shows in the upper part representative current traces and the corresponding I/V curves for Kcv_{NTS} expressed constitutively. On the left-hand side, the channel shows and ohmic conductance devoid of the inactivation at higher negative voltages. The sensitivity to barium is slightly lower, compared to the phenotype showing the slow inactivation (Fig. 48, right-hand side). We managed to detect these two phenotypes for Kcv_{NTS} also if it was expressed under control of the CRY2 CIB1 system, representative current traces and I/V relations are shown in the lower part of Fig. 48.

Following page:

Fig. 48: Kcv_{NTS} retains its two distinct gating modes in the CRY2 CIB1 system

Current traces and I/V curves of Kcv_{NTS} expressed constitutively and under control of the CRY2 CIB1 system at voltages from +80 to -160 mV. **(A)** and **(B)** show the two characteristic current responses for Kcv_{NTS} measured in the presence of 100 mM K^+ (upper trace) and after the addition of 10 mM Ba^{2+} (lower trace). **(E)** and **(F)** show the current responses for CRY2 CIB1 Kcv_{NTS} measured in the presence of 100 mM K^+ (upper trace) and after the addition of 10 mM Ba^{2+} (lower trace). **(C)** and **(D)** show the I/V curves of the steady state currents of the traces for Kcv_{NTS} shown above with (white squares) and without Ba^{2+} (gray squares). **(G)** and **(H)** show the I/V curves of the steady state currents of the traces for CRY2 CIB1 Kcv_{NTS} shown above with (white squares) and without Ba^{2+} (gray squares).

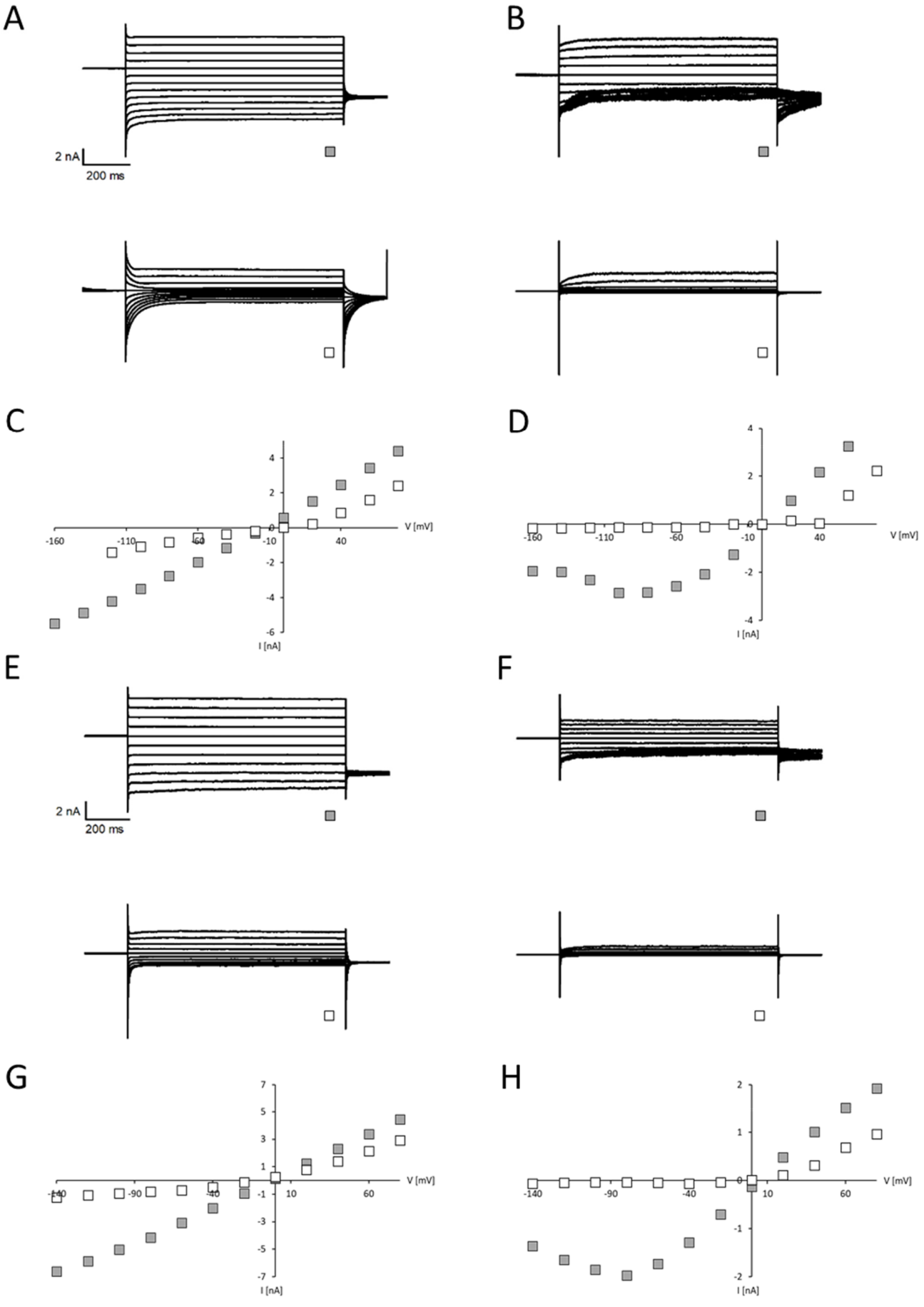
A
2 nA
200 ms
B
C
V [mV]
I [nA]
D
V [mV]
I [nA]
E
2 nA
200 ms
F
G
V [mV]
I [nA]
H
V [mV]
I [nA]

To establish a better overview of the properties of the two phenotypes of Kcv_{NTS}, the mean current at -100 mV and the blocking efficiency of barium at -120 mV were calculated (Fig. 49). Type I is the variant without and type II the variant with the slow inactivation. Here it becomes clearer still that light-dependent expression under the control of the CRY2 CIB1 system does not alter the functional properties of Kcv_{NTS}.

Type I shows a mean current of -5.2 nA for the constitutive and of -5.7±2 nA for Kcv_{NTS} expressed under control of the CRY2 CIB1 system. The mean current of type II was -1.7±1.5 nA for the constitutive and -1.3±1 nA for the channel if expressed under control of the CRY2 CIB1 system (Fig. 49 A). As the leak expression in the dark for Kcv_{NTS} under control of the CRY2 CIB1 system is well below the detection limit of a regular light-microscope, a high number of random cells were patched as dark state controls. The mean current of -0.051±0.059 nA is 100-fold smaller compared to the illuminated cells and matches the endogenous currents measured in untransfected HEK293 cells by D. Eckert of -0.059±0.067 nA (Eckert, 2018). As none of the dark state control cells showed any fluorescence under the widefield microscope during the patch clamp measurements and none of the 26 randomly selected cells showed a current above the level of endogenous HEK293 currents, it is reasonable to assume that the leak expression of Kcv_{NTS} at the plasma membrane in cells kept in the dark is negligible.

The efficiency of the barium block at -120 mV for type I is 66.4 % for the constitutive and 67.9±6 % for Kcv_{NTS} under control of the CRY2 CIB1 system. For type II the relative blocking efficiency is 81.3±14 % for the constitutive and 90.9±6 % for Kcv_{NTS} expressed under control of the CRY2 CIB1 system (Fig. 49 B).

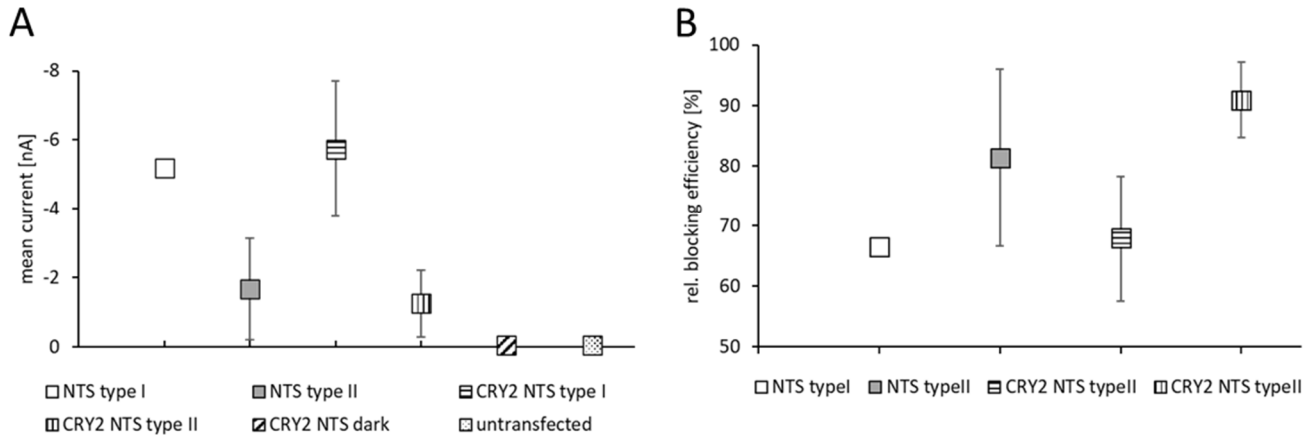

Fig. 49: Comparison of mean currents at -100 mV and relative blocking efficiency at -120 mV of the stationary currents with 10 mM Ba^{2+} for Kcv_{NTS} expressed constitutively and in the all-in-one CRY2 CIB1 system

(A) shows the mean currents [nA] at -100mV for Kcv_{NTS} type I (n=2), Kcv_{NTS} type II (n=6), CRY2 KcvNTS type I (n=3), CRY2 Kcv_{NTS} type II (n=9), CRY Kcv_{NTS} dark (n=26) and untransfected HEK293 cells (n=18) respectively, error bars represent standard deviation. **(B)** shows the relative blocking efficiency of 10 mM Ba^{2+} in % for Kcv_{NTS} type I (n=1), Kcv_{NTS} type II (n=4), CRY2 Kcv_{NTS} type I (n=4) and CRY2 Kcv_{NTS} type II (n=9) respectively. Error bars represent standard deviation.

Taken together, the results obtained from the patch-clamp measurements of Kcv_{NTS} clearly show that the channel remains functional and shows the same properties independent of the expression system used. This demonstrates the potential of the CRY2 CIB1 system as an optogenetic tool to induce long-term hyperpolarization of the PM with light. Additionally, the cells transfected with CRY2 CIB Kcv_{NTS} and kept in the dark did not show elevated currents compared to untransfected cells, which illustrates that the system does not induce leak currents if kept in darkness.

8. Conclusion and outlook

8.1. Both codon usage bias and linker length influence protein sorting efficiency

Adaptation of codon usage bias for heterologous gene expression has been shown to enhance protein levels (Kim et al., 1997; Inouye et al., 2015) and found numerous applications in producing protein and gene therapeutics (Alexaki et al., 2019; Joshi et al., 2019). However, it has been found that altering the codon usage bias does not only influence protein expression, but can also alter protein folding (Pechmann and Frydman, 2013; Thommen et al., 2017) and thereby its function (Zhou et al., 2013; Bali and Bebok, 2015).

This work demonstrates that altering the codon usage of the viral potassium channel Kesv, to optimize it for expression in mammalian cells augments sorting efficiency to the mitochondria. The same effect could also be observed for $Kmpv_{12T}$, another viral potassium channel which is sorted to the mitochondria when expressed heterologously in mammalian cells. This phenomenon of enhanced sorting to the mitochondria was observed consistently in five different mammalian cell lines, showing that this is a conserved mechanism in cells. The same is true for shortening of the protein linker between the channel and its GFP-tag. In particular, the impact of codon optimality on protein sorting has so far only been described for proteins which enter the secretory pathway and are sorted co-translationally in an SRP-dependent manner (Zalucki et al., 2009; Pechmann et al., 2014). The effect of codon usage on the sorting efficiency of Kesv, which is post-translationally sorted to the mitochondria (Balss et al., 2008), is most likely attributed to the increased translational velocity. This may hinder the interaction of the nascent protein with the SRP which in turn could promote interaction with post-translational sorting factors, like chaperones for example. Altogether, this could reduce mis-sorting of the Kesv channel protein to the ER (Kithil et al., 2020).

Another viral potassium channel, $Kcv_{PBCV\text{-}1}$, which is by default sorted to the plasma membrane upon heterologous expression in mammalian cells, was not sensitive to an increased in codon optimality for expression in mammalian cells. These findings are in line with observations showing that a slower translation velocity induced by non-optimal codons enhances SRP-binding and increases co-translational sorting efficiency (Pechmann et al., 2014; Buhr et al., 2016). As the speed of translation increases due to an exchange of rare for frequent codons (Novoa and Pouplana, 2012; Dana and Tuller, 2014), it was expected that optimizing $Kcv_{PBCV\text{-}1}$ would only increase its expression level but not its sorting efficiency.

8.2. Towards creating a light gated potassium channel located in the IMM

So far, there are only two optogenetic tools which allow light-inducible depolarization of the mitochondria to study mitochondrial function, both of which are based on channelrhodopsins (Tkatch et al., 2017; Ernst et al., 2019). Channelrhodopsins are non-selective cation channels mainly conducting sodium, but also potassium and calcium (Nagel et al., 2003). However, the physiological depolarization of mitochondria is carried by a variety of potassium channels in the inner mitochondrial membrane (Szewczyk et al., 2006; Szabo and Zoratti, 2014). A light-gated potassium channel in the inner mitochondrial membrane would therefore have the advantage in that it allows to study the effects of mitochondrial depolarization in a more physiological setting.

To design a mitochondrial light-gated potassium channel, the design of BLINK1 - a light-gated potassium channel which is expressed in the plasma membrane - was used as a template. BLINK1 is built from of a viral potassium channel which is coupled to the LOV-domain from *Avena sativa*. Upon illumination with blue light, the conformational change of the LOV-domain triggers channel opening (Cosentino et al., 2015). In the original design of BLINK1, a potassium channel which is targeted to the plasma membrane was used. An exchange of this channel for $Kesv_{Opt}$, a potassium channel which exhibits a robust sorting to the mitochondria, did not target the protein to the mitochondria. A systematic study of the single components of BLINK1 showed that none of the components was sorted to either the plasma membrane or the mitochondria on its own. N-terminal attachment of a COX8 mitochondrial targeting sequence to the BLINK-construct led to an observable mitochondrial sorting of the construct in 10% of the cells. Like in another study (Tkatch et al., 2017), a six fold repetition of the mitochondrial targeting sequence augmented targeting of MitoBLINK1 to the mitochondria in all cells observed. MitoBLINK1 awaits functional characterization e.g. by patch-clamp experiments on isolated mitochondria (Sorgato et al., 1987) and hopefully will prove to be a valuable contribution to the optogenetic toolkit.

8.3. Comparison of two light-induced gene expression systems: EL222 vs. CRY2 CIB1

A second set of experiments focused on the generation of potassium channel-based tools which allow for the manipulation of cells on a longer timescale. Two modular photoactuators were chosen to allow for light-inducible expression of potassium channels either at the plasma membrane or in the inner mitochondrial membrane.

The first one is based on the light-inducible dimerization of EL222, the LOV-domain of *Erythrobacter litoralis* (Spillantini and Goedert, 1998). Its dimerization causes binding of specific DNA sequences and can act as a transcriptional activator by bringing an activator domain within close proximity to a promotor sequence (Zoltowski et al., 2013; Motta-Mena et al., 2014).

The second system is based on the light-induced heterodimerization of cryptochrome 2 (CRY2) with its interacting partner CIB1 (Liu et al., 2008). Their interaction was in this case also applied to bring an activator domain in close proximity to the gene of interest, thereby initiating its transcription in a light-dependent manner (Pathak et al., 2017).
The experiments with the EL222 system for the light-induced expression of potassium channels showed that it requires very high doses of blue light applied over a prolonged time to evoke a measurable increase in channel expression levels. This is in agreement with data from other studies (Motta-Mena et al., 2014). However, even with those high light intensities, the expression levels remained in the present experiments on a low level. Additionally, the system was leaky in the sense that the potassium channels were already expressed in the dark. This finding differs from published data, which report a low leak expression in the dark and robust expression levels upon illumination (Jayaraman et al., 2016). However, most successful applications of the EL222 system for regulation of gene expression were reported in bacteria (Jayaraman et al., 2018; Zhao et al., 2018) and yeast (Benzinger and Khammash, 2018; Rullan et al., 2018; Perkins et al., 2020). Because of these multiple disadvantages, the EL222 system was not suitable for the light-dependent expression of potassium channels in mammalian cells.

In contrast to the EL222 system, the CRY2 CIB1 system showed almost no leak-expression in the dark, was fully activated with either very low light intensities or a short single light pulse. The resulting increase in protein levels upon activation were also much higher. After these encouraging observations, attempts were made to simplify the handling of the system in an all-in-one CRY2 CIB1 vector in which a potassium channel of choice can easily be inserted. This vector showed the same good characteristics of the initial three-vector design with the additional advantage of higher transfection rates. The modular design also allowed for the easy exchange of the potassium channels of interest in the construct. For experimental characterization, two mitochondrial and two PM sorted channels were cloned into the CRY2 CIB1 all-in-one cassette. All of the channels retained their desired sorting pattern with only minor differences in sorting efficiency.
To address the functionality of the two mitochondrial potassium channels, assays for their influence on mitochondrial membrane potential, mitochondrial calcium levels and induction of apoptosis were established. It became clear that $Kmpv_{12T}$, both in its wildtype and codon optimized version, depolarized the membrane potential and decreased the calcium levels of the mitochondria. These observations were independent of the expression system and seen in both constitutively and light-dependently expressing cells. Kesv did not induce these alterations in the mitochondria, which is in accordance with other experiments in which Kesv also failed to induce a depolarization of the mitochondria (Kithil, 2018). In other functional experiments, Kesv also did not show single-channel gating events in planar lipid bilayers. Taken together, these observations suggest that Kesv is non-functional; it can serve as a negative

control in the studies addressing effects of heterologous expression potassium channels in the mitochondria.

The findings for $Kmpv_{12T}$ are in accordance with multiple studies addressing the effects of potassium channels in the inner mitochondrial membrane. Potassium channel opening in the mitochondria has been shown to depolarize the mitochondria due to the influx of potassium ions (Garlid and Paucek, 2003; Szabo and Zoratti, 2014). Which in turn leads to the decrease in mitochondrial calcium levels, as the driving force for calcium import into the mitochondria is lower (Zorova et al., 2018). The depolarization of the mitochondria by both $Kmpv_{12T}$ and $Kmpv_{12TOpt}$ did not induce apoptosis. This finding is in accordance with studies showing that a mild uncoupling induced by potassium channels does not induce apoptosis, but has cytoprotective effects (Weisová et al., 2012). This cytoprotection plays an important role in minimizing the effects of ischemia by inducing preconditioning effects (Wang et al., 2011; Vishwakarma et al., 2019). This finding underlines the main advantage of a potassium channel-based optogenetic tool for studying mitochondrial function. In contrast to the construct described here, opsin-based tools, which are not selective for potassium, induce stronger unphysiological depolarization of the mitochondria, thereby inducing apoptosis (Tkatch et al., 2017; Ernst et al., 2019).

To establish the functionality of plasma membrane targeted potassium channels under control of the CRY2 CIB1 system, whole-cell patch clamp measurements were performed. Kcv_{NTS} exhibited the same whole-cell currents independent of a constitutive or light-dependent expression. This suggests that the combined system of light-induced expression of small viral potassium channels is suitable for inducing a long-lasting potassium channel conductance in mammalian cells.

8.4. Preliminary data in zebrafish illustrate the functionality of the CRY2 CIB1 system *in vivo*

After establishing the functionality of Kcv_{NTS} expressed under control of the CRY2 CIB1 system in mammalian cells, the question arose whether the system would also be a suitable tool for optogenetic studies *in vivo*. To address this question, S. Moleri and M. Beltrame at the Universita degli Studi di Milano injected the plasmid containing the full CRY2 CIB1 Kcv_{NTS} construct in *Danio rerio* embryos at one-cell stage. The embryos were either kept them in the dark or induced expression of the channel 24 hours post fertilization with a single 60 second blue light pulse. The embryos were imaged three or six hours post-induction. 44 % of the embryos which were induced with a single blue light pulse showed fluorescent spots, whereas none of the embryos that were kept in the dark showed any fluorescence (Fig. 50).

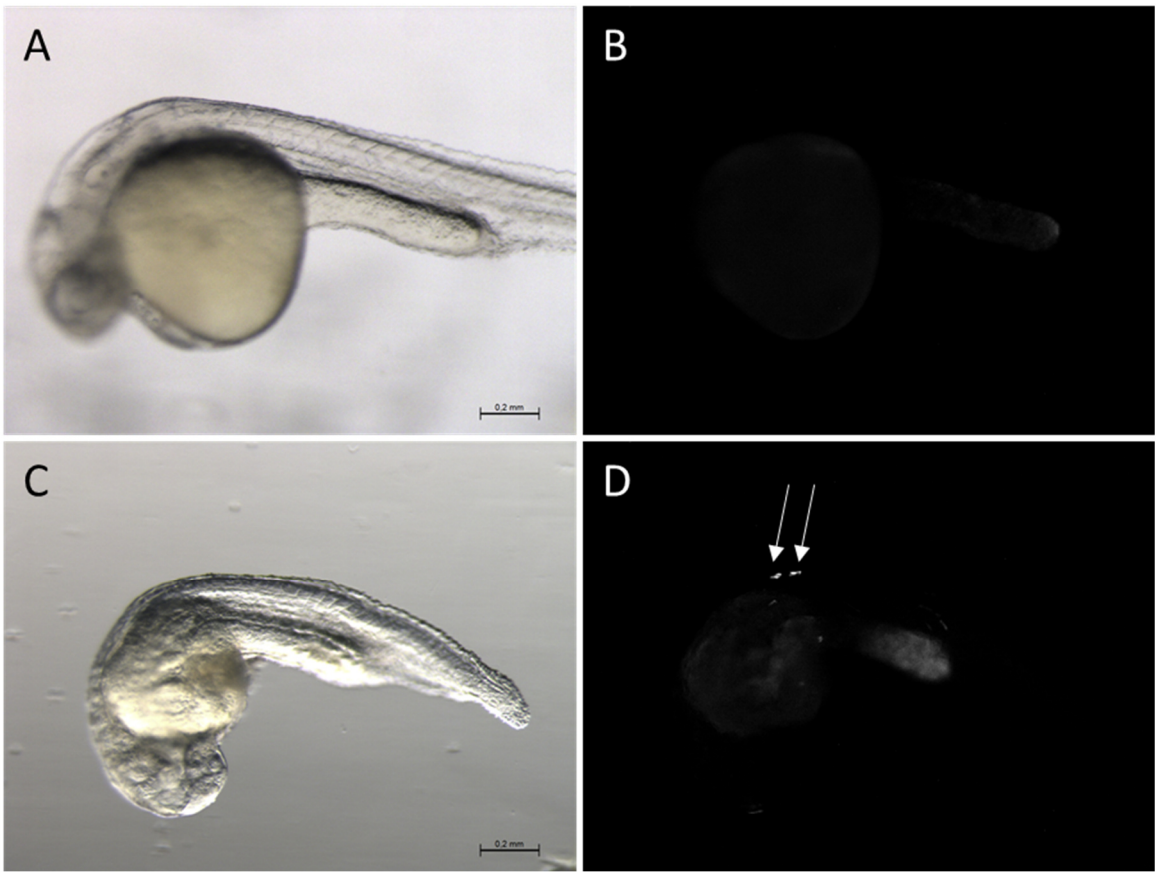

Fig. 50: Induction of CRY2 CIB1 Kcv_{NTS} with a single blue light pulse leads to expression of the channel in *Danio rerio* larvae

Confocal images of CRY2 CIB1 Kcv_{NTS} in *Danio rerio* larvae injected at one-cell stage. **(A & B)** Larvae were kept in the dark after injection: Panel A: Transmitted light, Panel B: Kcv_{NTS}::eGFP **(C & D)** Larvae were induced with a one minute light pulse 24 hours post fertilization and imaged 6 hours post-induction: Panel D: Transmitted light, Panel E: Kcv_{NTS}::eGFP. White arrows indicate fluorescent spots. Scale bars represent 200 µm. Images were kindly provided by S. Moleri and M. Beltrame

These preliminary data illustrate that the light-induced expression of Kcv_{NTS} is not only applicable in cultured mammalian cells, but also shows promising results in vivo in zebrafish larvae. To test the suitability of the construct for tissue-specific expression in zebrafish, the CMV promotor used in the initial construct was switched for a cardiomyocyte-specific (cardiac myosin light chain 2 – cmlc2) and a motoneuron-specific promotor (motoneuron and pancreas homeobox 1 - mnx1). These constructs currently undergo functional testing in Milano.

9. References

Agus, V., and Janovjak, H. (2017). Optogenetic methods in drug screening. Technologies and applications. Current opinion in biotechnology *48*, 8-14.

Ahmad, M., and Cashmore, A.R. (1993). HY4 gene of A. thaliana encodes a protein with characteristics of a blue-light photoreceptor. Nature *366*, 162-166.

Airan, R.D., Thompson, K.R., Fenno, L.E., Bernstein, H., and Deisseroth, K. (2009). Temporally precise in vivo control of intracellular signalling. Nature *458*, 1025-1029.

Alberio, L., Locarno, A., Saponaro, A., Romano, E., Bercier, V., Albadri, S., Simeoni, F., Moleri, S., Pelucchi, S., and Porro, A., et al. (2018). A light-gated potassium channel for sustained neuronal inhibition. Nature methods *15*, 969-976.

Alexaki, A., Hettiarachchi, G.K., Athey, J.C., Katneni, U.K., Simhadri, V., Hamasaki-Katagiri, N., Nanavaty, P., Lin, B., Takeda, K., and Freedberg, D., et al. (2019). Effects of codon optimization on coagulation factor IX translation and structure: Implications for protein and gene therapies. Scientific reports *9*, 15449.

Asakawa, K., Handa, H., and Kawakami, K. (2020). Optogenetic modulation of TDP-43 oligomerization accelerates ALS-related pathologies in the spinal motor neurons. Nature communications *11*, 1004.

Autret, A., and Martin, S.J. (2009). Emerging role for members of the Bcl-2 family in mitochondrial morphogenesis. Molecular cell *36*, 355-363.

Baaske, J., Gonschorek, P., Engesser, R., Dominguez-Monedero, A., Raute, K., Fischbach, P., Müller, K., Cachat, E., Schamel, W.W.A., and Minguet, S., et al. (2018). Dual-controlled optogenetic system for the rapid down-regulation of protein levels in mammalian cells. Scientific reports *8*, 15024.

Baaske, J., Mühlhäuser, W.W.D., Yousefi, O.S., Zanner, S., Radziwill, G., Hörner, M., Schamel, W.W.A., and Weber, W. (2019). Optogenetic control of integrin-matrix interaction. Communications biology *2*, 15.

Baden, T., Euler, T., and Berens, P. (2020). Understanding the retinal basis of vision across species. Nature reviews. Neuroscience *21*, 5-20.

Bahir, I., Fromer, M., Prat, Y., and Linial, M. (2009). Viral adaptation to host. A proteome-based analysis of codon usage and amino acid preferences. Molecular systems biology *5*, 311.

Bajar, B.T., Wang, E.S., Lam, A.J., Kim, B.B., Jacobs, C.L., Howe, E.S., Davidson, M.W., Lin, M.Z., and Chu, J. (2016). Improving brightness and photostability of green and red fluorescent proteins for live cell imaging and FRET reporting. Scientific reports *6*, 20889.

Bali, V., and Bebok, Z. (2015). Decoding mechanisms by which silent codon changes influence protein biogenesis and function. The international journal of biochemistry & cell biology *64*, 58-74.

Balss, J. (2007). Unterschiedliche zelluläre Sortierung zweier viraler K+-Kanäle: Die Bedeutung der zweiten Transmembrandomäne als Sortierungssignal. Dissertation (Darmstadt).

Balss, J., Papatheodorou, P., Mehmel, M., Baumeister, D., Hertel, B., Delaroque, N., Chatelain, F.C., Minor, D.L., JR, van Etten, J.L., and Rassow, J., et al. (2008). Transmembrane domain length of viral K+ channels is a signal for mitochondria targeting. Proceedings of the National Academy of Sciences of the United States of America *105*, 12313-12318.

Bamann, C., Kirsch, T., Nagel, G., and Bamberg, E. (2008). Spectral characteristics of the photocycle of channelrhodopsin-2 and its implication for channel function. Journal of molecular biology *375*, 686-694.

Banghart, M., Borges, K., Isacoff, E., Trauner, D., and Kramer, R.H. (2004). Light-activated ion channels for remote control of neuronal firing. Nature neuroscience *7*, 1381-1386.

Banghart, M.R., Mourot, A., Fortin, D.L., Yao, J.Z., Kramer, R.H., and Trauner, D. (2009). Photochromic blockers of voltage-gated potassium channels. Angewandte Chemie (International ed. in English) *48*, 9097-9101.

Banghart, M.R., Volgraf, M., and Trauner, D. (2006). Engineering light-gated ion channels. Biochemistry *45*, 15129-15141.

Barber, D.M., Schönberger, M., Burgstaller, J., Levitz, J., Weaver, C.D., Isacoff, E.Y., Baier, H., and Trauner, D. (2016). Optical control of neuronal activity using a light-operated GIRK channel opener (LOGO). Chemical science *7*, 2347-2352.

Barroso, G., Taylor, S., Morshedi, M., Manzur, F., Gaviño, F., and Oehninger, S. (2006). Mitochondrial membrane potential integrity and plasma membrane translocation of phosphatidylserine as early apoptotic markers. A comparison of two different sperm subpopulations. Fertility and sterility *85*, 149-154.

Bayburt, T. H., Carlson, J.W., and Sligar, S.G. (1998). Reconstitution and Imaging of a Membrane Protein in a Nanometer-Size Phospholipid Bilayer. Journal of Structural Biology *123*, 37-44.

Bednarczyk, P. (2009). Potassium channels in brain mitochondria. Acta Biochemica Polonica *56*, 385-392.

Bednarczyk, P., Wieckowski, M.R., Broszkiewicz, M., Skowronek, K., Siemen, D., and Szewczyk, A. (2013). Putative Structural and Functional Coupling of the Mitochondrial BKCa Channel to the Respiratory Chain. PloS one *8*, e68125.

Benedetti, L., Barentine, A.E.S., Messa, M., Wheeler, H., Bewersdorf, J., and Camilli, P. de (2018). Light-activated protein interaction with high spatial subcellular confinement. Proceedings of the National Academy of Sciences of the United States of America 115, e2238-e2245.

Benzinger, D., and Khammash, M. (2018). Pulsatile inputs achieve tunable attenuation of gene expression variability and graded multi-gene regulation. Nature communications *9*, 3521.

Bernard-Marissal, N., Chrast, R., and Schneider, B.L. (2018). Endoplasmic reticulum and mitochondria in diseases of motor and sensory neurons. A broken relationship? Cell death & disease *9*, 333.

Berndt, A., Schoenenberger, P., Mattis, J., Tye, K.M., Deisseroth, K., Hegemann, P., and Oertner, T.G. (2011). High-efficiency channelrhodopsins for fast neuronal stimulation at low light levels. Proceedings of the National Academy of Sciences of the United States of America *108*, 7595-7600.

Berry, B.J., Trewin, A.J., Milliken, A.S., Baldzizhar, A., Amitrano, A.M., Kim, M., and Wojtovich, A.P. (2020). Controlling the Mitochondrial Protonmotive Force with Light to Impact Cellular Stress Resistance. EMBO reports, e49113.

Beyer, H.M., Naumann, S., Weber, W., and Radziwill, G. (2015). Optogenetic control of signaling in mammalian cells. Biotechnology journal *10*, 273-283.

Bi, A., Cui, J., Ma, Y.-P., Olshevskaya, E., Pu, M., Dizhoor, A.M., and Pan, Z.-H. (2006). Ectopic expression of a microbial-type rhodopsin restores visual responses in mice with photoreceptor degeneration. Neuron *50*, 23-33.

Binder, J.L., Deretic, V., Weick, J.P., and Bhaskar, K. (2019). Optical induction of autophagy via Transcription factor EB (TFEB) reduces pathological tau in neurons. PLoS One 15, e0230026.

Biselli, T., Lange, S.S., Sablottny, L., Steffen, J., and Walther, A. (2019). Optogenetic and chemogenetic insights into the neurocircuitry of depression-like behaviour: A systematic review. The European journal of neuroscience 10, e14603.

Bitzenhofer, S.H., Ahlbeck, J., Wolff, A., Wiegert, J.S., Gee, C.E., Oertner, T.G., and Hanganu-Opatz, I.L. (2017). Layer-specific optogenetic activation of pyramidal neurons causes beta-gamma entrainment of neonatal networks. Nature communications *8*, 14563.

Bogomolni, R.A., and Spudich, J.L. (1982). Identification of a third rhodopsin-like pigment in phototactic Halobacterium halobium. Proceedings of the National Academy of Sciences of the United States of America *79*, 6250-6254.

Bolte, S., and Cordelieres, F.P. (2006). A guided tour into subcellular colocalization analysis in light microscopy. Journal of microscopy *224*, 213-232.

Bonora, M., Wieckowski, M.R., Sinclair, D.A., Kroemer, G., Pinton, P., and Galluzzi, L. (2018). Targeting mitochondria for cardiovascular disorders. Therapeutic potential and obstacles. Nature reviews. Cardiology 16, 33-55.

Boyden, E.S. (2011). A history of optogenetics: the development of tools for controlling brain circuits with light. F1000 Reports Biology *3*, 1-12.

Boyden, E.S., Zhang, F., Bamberg, E., Nagel, G., and Deisseroth, K. (2005). Millisecond-timescale, genetically targeted optical control of neural activity. Nature neuroscience *8*, 1263-1268.

Brady, N.R., Hamacher-Brady, A., and Gottlieb, R.A. (2006). Proapoptotic BCL-2 family members and mitochondrial dysfunction during ischemia/reperfusion injury, a study employing cardiac HL-1 cells and GFP biosensors. Biochimica et biophysica acta *1757*, 667-678.

Braun, C.J. (2014). Structure/function correlates and protein/lipid interaction of the viral potassium channel KcvNTS. Dissertation (Darmstadt).

Braun, C.J., Baer, T., Moroni, A., and Thiel, G. (2014). Pseudo painting/air bubble technique for planar lipid bilayers. Journal of Neuroscience Methods *233*, 13-17.

Brookes, P.S., Yoon, Y., Robotham, J.L., Anders, M.W., and Sheu, S.-S. (2004). Calcium, ATP, and ROS. A mitochondrial love-hate triangle. American journal of physiology. Cell physiology *287*, C817-33.

Buckley, A.M., Petersen, J., Roe, A.J., Douce, G.R., and Christie, J.M. (2015). LOV-based reporters for fluorescence imaging. Current opinion in chemical biology *27*, 39-45.

Bugaj, L.J., Choksi, A.T., Mesuda, C.K., Kane, R.S., and Schaffer, D.V. (2013). Optogenetic protein clustering and signaling activation in mammalian cells. Nature methods *10*, 249-252.

Buhr, F., Jha, S., Thommen, M., Mittelstaet, J., Kutz, F., Schwalbe, H., Rodnina, M.V., and Komar, A.A. (2016). Synonymous Codons Direct Cotranslational Folding toward Different Protein Conformations. Molecular cell *61*, 341-351.

Burgie, E.S., and Vierstra, R.D. (2014). Phytochromes: an atomic perspective on photoactivation and signaling. The Plant cell *26*, 4568-4583.

Busija, D.W., Gaspar, T., Domoki, F., Katakam, P.V., and Bari, F. (2008). Mitochondrial-mediated suppression of ROS production upon exposure of neurons to lethal stress. Mitochondrial targeted preconditioning. Advanced drug delivery reviews *60*, 1471-1477.

Busskamp, V., Picaud, S., Sahel, J.A., and Roska, B. (2012). Optogenetic therapy for retinitis pigmentosa. Gene therapy *19*, 169-175.

Campello, S., and Scorrano, L. (2010). Mitochondrial shape changes: orchestrating cell pathophysiology. EMBO reports *11*, 678-684.

Campello, Ricardo J. G. B., Moulavi, D., and Sander, J. (2013). Density-Based Clustering Based on Hierarchical Density Estimates. Advances in Knowledge Discovery and Data Mining. PAKDD 2013.

Chacinska, A., Koehler, C.M., Milenkovic, D., Lithgow, T., and Pfanner, N. (2009). Importing mitochondrial proteins. Machineries and mechanisms. Cell *138*, 628-644.

Chakrabarti, R., Ji, W.-K., Stan, R.V., Juan Sanz, J. de, Ryan, T.A., and Higgs, H.N. (2018). INF2-mediated actin polymerization at the ER stimulates mitochondrial calcium uptake, inner membrane constriction, and division. The Journal of cell biology *217*, 251-268.

Chakrabarty, S., Kabekkodu, S.P., Singh, R.P., Thangaraj, K., Singh, K.K., and Satyamoorthy, K. (2018). Mitochondria in health and disease. Mitochondrion *43*, 25-29.

Chaney, J.L., and Clark, P.L. (2015). Roles for Synonymous Codon Usage in Protein Biogenesis. Annual review of biophysics *44*, 143-166.

Chaney, J.L., Steele, A., Carmichael, R., Rodriguez, A., Specht, A.T., Ngo, K., Li, J., Emrich, S., and Clark, P.L. (2017). Widespread position-specific conservation of synonymous rare codons within coding sequences. PLoS computational biology *13*, e1005531.

Chapman, S., Faulkner, C., Kaiserli, E., Garcia-Mata, C., Savenkov, E.I., Roberts, A.G., Oparka, K.J., and Christie, J.M. (2008a). The photoreversible fluorescent protein iLOV outperforms GFP as a reporter of plant virus infection. Proceedings of the National Academy of Sciences of the United States of America *105*, 20038-20043.

Chapman, S., Faulkner, C., Kaiserli, E., Garcia-Mata, C., Savenkov, E.I., Roberts, A.G., Oparka, K.J., and Christie, J.M. (2008b). The photoreversible fluorescent protein iLOV outperforms GFP as a reporter of plant virus infection. PNAS *105*, 20038-20043.

Charpuis, C. von, Meckel, T., Moroni, A., and Thiel, G. (2015). The sorting of a small potassium channel in mammalian cells can be shifted between mitochondria and plasma membrane. Cell calcium *58*, 114-121.

Chaudhury, D., Walsh, J.J., Friedman, A.K., Juarez, B., Ku, S.M., Koo, J.W., Ferguson, D., Tsai, H.-C., Pomeranz, L., and Christoffel, D.J., et al. (2013). Rapid regulation of depression-related behaviours by control of midbrain dopamine neurons. Nature *493*, 532-536.

Che, D.L., Duan, L., Zhang, K., and Cui, B. (2015). The Dual Characteristics of Light-Induced Cryptochrome 2, Homo-oligomerization and Heterodimerization, for Optogenetic Manipulation in Mammalian Cells. ACS synthetic biology *4*, 1124-1135.

Checchetto, V., Azzolini, M., Peruzzo, R., Capitanio, P., and Leanza, L. (2018). Mitochondrial potassium channels in cell death. Biochemical and biophysical research communications *500*, 51-58.

Chen, D., Gibson, E.S., and Kennedy, M.J. (2013a). A light-triggered protein secretion system. The Journal of cell biology *201*, 631-640.

Chen, J., Cassar, S.C., Di Zhang, and Gopalakrishnan, M. (2005). A novel potassium channel encoded by Ectocarpus siliculosus virus. Biochemical and biophysical research communications *326*, 887-893.

Chen, X., Zaro, J.L., and Shen, W.-C. (2013b). Fusion protein linkers. Property, design and functionality. Advanced drug delivery reviews *65*, 1357-1369.

Cheng, Y., Gu, X.Q., Bednarczyk, P., Wiedemann, F.R., Haddad, G.G., and Siemen, D. (2008). Hypoxia Increases Activity of the BK-Channel in the Inner Mitochondrial Membrane and Reduces Activity of the Permeability Transition Pore. Cellular Physiology and Biochemistry, 127-136.

Christie, J.M., Gawthorne, J., Young, G., Fraser, N.J., and Roe, A.J. (2012a). LOV to BLUF. Flavoprotein contributions to the optogenetic toolkit. Molecular plant *5*, 533-544.

Christie, J.M., Hitomi, K., Arvai, A.S., Hartfield, K.A., Mettlen, M., Pratt, A.J., Tainer, J.A., and Getzoff, E.D. (2012b). Structural tuning of the fluorescent protein iLOV for improved photostability. The Journal of biological chemistry *287*, 22295-22304.

Christie, J.M., Salomon, M., Nozue, K., Wada, M., and Briggs, W.R. (1999). LOV (light, oxygen, or voltage) domains of the blue-light photoreceptor phototropin (nph1): Binding sites for the chromophore flavin mononucleotide. Proceedings of the National Academy of Sciences of the United States of America *96*, 8779-8783.

Chuong, A.S., Miri, M.L., Busskamp, V., Matthews, G.A.C., Acker, L.C., Sørensen, A.T., Young, A., Klapoetke, N.C., Henninger, M.A., and Kodandaramaiah, S.B., et al. (2014). Noninvasive optical inhibition with a red-shifted microbial rhodopsin. Nature neuroscience *17*, 1123-1129.

Clarke, T.F., and Clark, P.L. (2008). Rare codons cluster. PloS one *3*, e3412.

Cloix, C., Kaiserli, E., Heilmann, M., Baxter, K.J., Brown, B.A., O'Hara, A., Smith, B.O., Christie, J.M., and Jenkins, G.I. (2012). C-terminal region of the UV-B photoreceptor UVR8 initiates signaling through interaction with the COP1 protein. Proceedings of the National Academy of Sciences of the United States of America *109*, 16366-16370.

Cohen, S.N., Chang, A.C.Y., Boyer, H.W., and Helling, R.B. (1973). Construction of Biologically Functional Bacterial Plasmids In Vitro. PNAS *70*, 3240-3244.

Cosentino, C., Alberio, L., Gazzarrini, S., Aquila, M., Romano, E., Cermenati, S., Zuccolini, P., Petersen, J., Beltrame, M., and van Etten, J.L., et al. (2015). Optogenetics. Engineering of a light-gated potassium channel. Science (New York, N.Y.) *348*, 707-710.

Covington, H.E., Lobo, M.K., Maze, I., Vialou, V., Hyman, J.M., Zaman, S., LaPlant, Q., Mouzon, E., Ghose, S., and Tamminga, C.A., et al. (2010). Antidepressant effect of optogenetic stimulation of the medial prefrontal cortex. The Journal of neuroscience : the official journal of the Society for Neuroscience *30*, 16082-16090.

Crefcoeur, R.P., Yin, R., Ulm, R., and Halazonetis, T.D. (2013). Ultraviolet-B-mediated induction of protein-protein interactions in mammalian cells. Nature communications *4*, 1779.

Crick, F.H.C. (1979). Thinking about the brain. Scientific American *241*, 219-232.

Crick, F.H.C. (1999). The impact of molecular biology on neuroscience. Philosophical Transactions of the Royal Society Biological Sciences *354*, 2021-2025.

Crowley, L.C., Marfell, B.J., Scott, A.P., and Waterhouse, N.J. (2016). Quantitation of Apoptosis and Necrosis by Annexin V Binding, Propidium Iodide Uptake, and Flow Cytometry. Cold Spring Harbor protocols *2016*.

Csordás, G., Weaver, D., and Hajnóczky, G. (2018). Endoplasmic Reticulum-Mitochondrial Contactology. Structure and Signaling Functions. Trends in cell biology *28*, 523-540.

Cutler, T.A., Mills, B.M., Lubin, D.J., Chong, L.T., and Loh, S.N. (2009). Effect of interdomain linker length on an antagonistic folding-unfolding equilibrium between two protein domains. Journal of molecular biology *386*, 854-868.

D'Acunzo, P., Strappazzon, F., Caruana, I., Meneghetti, G., Di Rita, A., Simula, L., Weber, G., Del Bufalo, F., Dalla Valle, L., and Campello, S., et al. (2019). Reversible induction of mitophagy by an optogenetic bimodular system. Nature communications *10*, 1533.

Dana, A., and Tuller, T. (2014). The effect of tRNA levels on decoding times of mRNA codons. Nucleic acids research *42*, 9171-9181.

Davidson, S.M., Szabadkai, G., and Duchen, M.R. (2019). Fantastic beasts and how to find them-Molecular identification of the mitochondrial ATP-sensitive potassium channel. Cell calcium *84*, 102100.

Deisseroth, K. (2011). Optogenetics. Nature methods *8*, 26-29.

Demarsy, E., and Fankhauser, C. (2009). Higher plants use LOV to perceive blue light. Current Opinion in Plant Biology *12*, 69-74.

Devine, M.J., and Kittler, J.T. (2018). Mitochondria at the neuronal presynapse in health and disease. Nature reviews. Neuroscience *19*, 63-80.

Di Wu, Hu, Q., Yan, Z., Chen, W., Yan, C., Huang, X., Zhang, J., Yang, P., Deng, H., and Wang, J., et al. (2012). Structural basis of ultraviolet-B perception by UVR8. Nature *484*, 214-219.

Duan, J., Wainwright, M.S., Comeron, J.M., Saitou, N., Sanders, A.R., Gelernter, J., and Gejman, P.V. (2003). Synonymous mutations in the human dopamine receptor D2 (DRD2) affect mRNA stability and synthesis of the receptor. Human molecular genetics *12*, 205-216.

Duan, L., Hope, J., Ong, Q., Lou, H.-Y., Kim, N., McCarthy, C., Acero, V., Lin, M.Z., and Cui, B. (2017). Understanding CRY2 interactions for optical control of intracellular signaling. Nature communications *8*, 547.

Eckert, D. (2018). Analyse von zwei strukturell ähnlichen aber funktionell unterschiedlichen viralen K+-Kanälen: Strukturelle Ursache der inhärenten Einwärtsgleichrichtung. Dissertation (Darmstadt).

Edelstein, A., Amodaj, N., Hoover, K., Vale, R., and Stuurman, N. (2010). Computer control of microscopes using μManager. Current protocols in molecular biology *14*, 1-17.

Edelstein, A.D., Tsuchida, M.A., Amodaj, N., Pinkard, H., Vale, R.D., and Stuurman, N. (2014). Advanced methods of microscope control using μManager software. Journal of biological methods *1*, 1-10.

Eltzschig, H.K., and Eckle, T. (2011). Ischemia and reperfusion--from mechanism to translation. Nature medicine *17*, 1391-1401.

Endo, M., and Ozawa, T. (2017). Strategies for development of optogenetic systems and their applications. Journal of Photochemistry and Photobiology C: Photochemistry Reviews *30*, 10-23.

Engel, A.J. (2014). Untersuchungen am viralen K+ - Kanal Kesv: Die Bedeutung der zweiten Transmembrandomäne als Sortierungssignal. Studies of the viral potassium channel Kesv: The role of the second transmembrane domain in protein sorting. Bachelor Thesis (Darmstadt).

Engel, A.J. (2016). Duale Sortierung von Membranproteinen: Der Einfluss der zweiten Transmembrandomäne und der Codon Usage auf die Sortierung des viralen Kaliumkanals Kesv. Dual sorting of membrane proteins: Influence of the second transmembrane domain and codon usage on sorting of the viral potassium channel Kesv. Master Thesis (Darmstadt).

Ernst, P., Xu, N., Qu, J., Chen, H., Goldberg, M.S., Darley-Usmar, V., Zhang, J.J., O'Rourke, B., Liu, X., and Zhou, L. (2019). Precisely Control Mitochondria with Light to Manipulate Cell Fate Decision. Biophysical Journal 117, 631-645.

Etzl, S., Lindner, R., Nelson, M.D., and Winkler, A. (2018). Structure-guided design and functional characterization of an artificial red light-regulated guanylate/adenylate cyclase for optogenetic applications. The Journal of biological chemistry *293*, 9078-9089.

Fåhraeus, R., Marin, M., and Olivares-Illana, V. (2016). Whisper mutations. Cryptic messages within the genetic code. Oncogene *35*, 3753-3759.

Fath, S., Bauer, A.P., Liss, M., Spriestersbach, A., Maertens, B., Hahn, P., Ludwig, C., Schafer, F., Graf, M., and Wagner, R. (2011). Multiparameter RNA and codon optimization. A standardized tool to assess and enhance autologous mammalian gene expression. PloS one *6*, e17596.

Feldbauer, K., Zimmermann, D., Pintschovius, V., Spitz, J., Bamann, C., and Bamberg, E. (2009). Channelrhodopsin-2 is a leaky proton pump. PNAS *106*, 12317-12322.

Fenno, L., Yizhar, O., and Deisseroth, K. (2011). The development and application of optogenetics. Annual review of neuroscience *34*, 389-412.

Fieni, F., Parkar, A., Misgeld, T., Kerschensteiner, M., Lichtman, J.W., Pasinelli, P., and Trotti, D. (2010). Voltage-dependent inwardly rectifying potassium conductance in the outer membrane of neuronal mitochondria. The Journal of biological chemistry *285*, 27411-27417.

Fish, K.N. (2009). Total internal reflection fluorescence (TIRF) microscopy. Current protocols in cytometry *Chapter 12*, Unit12.18.

Fomicheva, A., Zhou, C., Sun, Q.-Q., and Gomelsky, M. (2019). Engineering Adenylate Cyclase Activated by Near-Infrared Window Light for Mammalian Optogenetic Applications. ACS synthetic biology *8*, 1314-1324.

Fortin, D.L., Banghart, M.R., Dunn, T.W., Borges, K., Wagenaar, D.A., Gaudry, Q., Karakossian, M.H., Otis, T.S., Kristan, W.B., and Trauner, D., et al. (2008). Photochemical control of endogenous ion channels and cellular excitability. Nature methods *5*, 331-338.

Fraikin, G.Y., Strakhovskaya, M.G., Belenikina, N.S., and Rubin, A.B. (2015). Bacterial photosensory proteins: Regulatory functions and optogenetic applications. Microbiology *84*, 461-472.

Frank, S., Gaume, B., Bergmann-Leitner, E.S., Leitner, W., Robert, E.G., Catez, F., Smith, C.L., and Youle, R.J. (2001). The Role of Dynamin-Related Protein 1, a Mediator of Mitochondrial Fission, in Apoptosis. Developmental cell *1*, 515-525.

Frey, T.G., and Mannella, C.A. (2000). The internal structure of mitochondria. Trends in biochemical sciences *25*, 319-324.

Friedman, J.R., Lackner, L.L., West, M., DiBenedetto, J.R., Nunnari, J., and Voeltz, G.K. (2011). ER Tubules Mark Sites of Mitochondrial Division. Science *334*, 358-362.

Galluzzi, L., Zamzami, N., La Motte Rouge, T. de, Lemaire, C., Brenner, C., and Kroemer, G. (2007). Methods for the assessment of mitochondrial membrane permeabilization in apoptosis. Apoptosis : an international journal on programmed cell death *12*, 803-813.

Garlid, K.D., and Paucek, P. (2003). Mitochondrial potassium transport. The K+ cycle. Biochimica et Biophysica Acta - Bioenergetics *1606*, 23-41.

Gartner, J.J., Parker, S.C.J., Prickett, T.D., Dutton-Regester, K., Stitzel, M.L., Lin, J.C., Davis, S., Simhadri, V.L., Jha, S., and Katagiri, N., et al. (2013). Whole-genome sequencing identifies a recurrent functional synonymous mutation in melanoma. Proceedings of the National Academy of Sciences of the United States of America *110*, 13481-13486.

Gasser, C., Taiber, S., Yeh, C.-M., Wittig, C.H., Hegemann, P., Ryu, S., Wunder, F., and Möglich, A. (2014). Engineering of a red-light-activated human cAMP/cGMP-specific phosphodiesterase. Proceedings of the National Academy of Sciences of the United States of America *111*, 8803-8808.

Gibson, D.G., Young, L., Chuang, R.-Y., Venter, J.C., Hutchison, C.A., and Smith, H.O. (2009). Enzymatic assembly of DNA molecules up to several hundred kilobases. Nature methods *6*, 343-345.

Giorgi, C., Danese, A., Missiroli, S., Patergnani, S., and Pinton, P. (2018a). Calcium Dynamics as a Machine for Decoding Signals. Trends in cell biology *28*, 258-273.

Giorgi, C., Marchi, S., and Pinton, P. (2018b). The machineries, regulation and cellular functions of mitochondrial calcium. Nature reviews. Molecular cell biology 19, 713-730.

Glick, D., Barth, S., and Macleod, K.F. (2010). Autophagy: cellular and molecular mechanisms. The Journal of pathology *221*, 3-12.

Godley, B.F., Shamsi, F.A., Liang, F.-Q., Jarrett, S.G., Davies, S., and Boulton, M. (2005). Blue light induces mitochondrial DNA damage and free radical production in epithelial cells. The Journal of biological chemistry *280*, 21061-21066.

Gómez-Suaga, P., Bravo-San Pedro, J.M., González-Polo, R.A., Fuentes, J.M., and Niso-Santano, M. (2018). ER-mitochondria signaling in Parkinson's disease. Cell death & disease *9*, 337.

Gottlieb, E., Armour, S.M., Harris, M.H., and Thompson, C.B. (2003). Mitochondrial membrane potential regulates matrix configuration and cytochrome c release during apoptosis. Cell death and differentiation *10*, 709-717.

Gourinchas, G., Etzl, S., and Winkler, A. (2019). Bacteriophytochromes - from informative model systems of phytochrome function to powerful tools in cell biology. Current opinion in structural biology *57*, 72-83.

Govorunova, E.G., Sineshchekov, O.A., Janz, R., Liu, X., and Spudich, J.L. (2015). Natural light-gated anion channels: A family of microbial rhodopsins for advanced optogenetics. Science *349*, 647-650.

Greiner, T. (2011). Characterization of novel potassium transport proteins from Chlorella viruses. Dissertation (Darmstadt).

Griesche, N., Sanchez, G., Hermans, C., and Idevall-Hagren, O. (2019). Cortical mitochondria regulate insulin secretion by local Ca2+ buffering in rodent beta cells. Journal of cell science *132*.

Guidarelli, A., Fiorani, M., Cerioni, L., and Cantoni, O. (2019). Calcium signals between the ryanodine receptor- and mitochondria critically regulate the effects of arsenite on mitochondrial superoxide formation and on the ensuing survival vs apoptotic signaling. Redox biology *20*, 285-295.

Guntas, G., Hallett, R.A., Zimmerman, S.P., Williams, T., Yumerefendi, H., Bear, J.E., and Kuhlman, B. (2015). Engineering an improved light-induced dimer (iLID) for controlling the localization and activity of signaling proteins. Proceedings of the National Academy of Sciences of the United States of America *112*, 112-117.

Guthmann, T. (2013). The outer transmembrane domain of the Kesv channel determines its intracellular localization. A molecular and microscopic analysis of protein sorting. Dissertation (Darmstadt).

Hahsler, M., Piekenbrock, M., and Doran, D. (2019). dbscan : Fast Density-Based Clustering with R. J. Stat. Soft. *91*.

Hajnóczky, G., Csordás, G., Das, S., Garcia-Perez, C., Saotome, M., Sinha Roy, S., and Yi, M. (2006). Mitochondrial calcium signalling and cell death. Approaches for assessing the role of mitochondrial Ca2+ uptake in apoptosis. Cell calcium *40*, 553-560.

Hanson, G., and Coller, J. (2018). Codon optimality, bias and usage in translation and mRNA decay. Nature reviews. Molecular cell biology *19*, 20-30.

Hartong, D.T., Berson, E.L., and Dryja, T.P. (2006). Retinitis pigmentosa. The Lancet *368*, 1795-1809.

Häusser, M. (2014). Optogenetics: the age of light. Nature methods *11*, 1012-1014.

Heckman, K.L., and Pease, L.R. (2007). Gene splicing and mutagenesis by PCR-driven overlap extension. Nature protocols *2*, 924-932.

Hehl, S., Golard, A., and Hille, B. (1996). Involvement of mitochondria in intracellular calcium sequestration by rat gonadotropes. Cell calcium *20*, 515-524.

Henry, C.M., Hollville, E., and Martin, S.J. (2013). Measuring apoptosis by microscopy and flow cytometry. Methods *61*, 90-97.

Hertel, B. (2005). Struktur-Funktions-Beziehung in dem minimalen viralen K+-Kanal Kcv: Funktionelle Rolle des N-Terminus bei der Regulation von Kanalaktivität. Dissertation (Darmstadt).

Hille, B. (1978). Ionic channels in excitable membranes. Current problems and biophysical approaches. Biophysical Journal *22*, 283-294.

Ho, S.N., Hunt, H.D., Horton, R.M., Pullen, J.K., and Pease, L.R. (1989). Site-directed mutagenesis by overlap extension using the polymerase chain reaction. Gene *77*, 51-59.

Hörner, M., Chatelle, C., Mühlhäuser, W.W.D., Stocker, D.R., Coats, M., Weber, W., and Radziwill, G. (2018). Optogenetic control of focal adhesion kinase signaling. Cellular signalling *42*, 176-183.

Horton, R.M., Hunt, H.D., Ho, S.N., Pullen, J.K., and Pease, L.R. (1989). Engineering hybrid genes without the use of restriction enzymes: gene splicing by overlap extension. Gene 77, 61-68.

Horvath, S.E., and Daum, G. (2013). Lipids of mitochondria. Progress in lipid research *52*, 590-614.

Hoth, M., Fanger, C.M., and Lewis, R.S. (1997). Mitochondrial Regulation of Store-operated Calcium Signaling in T Lymphocytes. The Journal of cell biology *137*, 633-648.

Houtkooper, R.H., and Vaz, F.M. (2008). Cardiolipin, the heart of mitochondrial metabolism. Cellular and molecular life sciences *65*, 2493-2506.

Idevall-Hagren, O., Dickson, E.J., Hille, B., Toomre, D.K., and Camilli, P. de (2012). Optogenetic control of phosphoinositide metabolism. Proceedings of the National Academy of Sciences of the United States of America *109*, E2316-23.

Inoue, H., Nojima, H., and Okayama, H. (1990). High efficiency transformation of Escherichia coli with plasmids. Gene *96*, 23-28.

Inouye, S., Sahara-Miura, Y., Sato, J.-i., and Suzuki, T. (2015). Codon optimization of genes for efficient protein expression in mammalian cells by selection of only preferred human codons. Protein expression and purification *109*, 47-54.

Jacobson, G.N., and Clark, P.L. (2016). Quality over quantity. Optimizing co-translational protein folding with non-'optimal' synonymous codons. Current opinion in structural biology *38*, 102-110.

Javahery, R., Khachi, A., Lo, K., Zenzie-Gregory, B., and Smale, S.T. (1994). DNA Sequence Requirements for Transcriptional Initiator Activity in Mammalian Cells. Molecular and Cellular Biology, 116-127.

Jayaraman, P., Devarajan, K., Chua, T.K., Zhang, H., Gunawan, E., and Poh, C.L. (2016). Blue light-mediated transcriptional activation and repression of gene expression in bacteria. Nucleic acids research *44*, 6994-7005.

Jayaraman, P., Yeoh, J.W., Zhang, J., and Poh, C.L. (2018). Programming the Dynamic Control of Bacterial Gene Expression with a Chimeric Ligand- and Light-Based Promoter System. ACS synthetic biology *7*, 2627-2639.

Joshi, S., Mangaonkar, K., and Krishnan, A. (2019). Expression Enhancement of Trastuzumab in CHO Cells Using Codon Optimization and Promoter Selection for Mammalian Expression Vector. IJPSDR *11*.

Kaberniuk, A.A., Shemetov, A.A., and Verkhusha, V.V. (2016). A bacterial phytochrome-based optogenetic system controllable with near-infrared light. Nature methods *13*, 591-597.

Kaemmerer, W.F. (2017). Optogenetics for Neurological Disorders: What Is the Path to the Clinic? In Optogenetics. From neuronal function to mapping and disease biology, K. Appasani, ed. (Cambridge: Cambridge University Press), pp. 169–180.

Kalish, D.I., Cohen, C.M., Jacobson, B.S., and Branton, D. (1978). Membrane Isolation on Polylysine-Coated Glass Beads. Asymmetry of Bound Membrane. Biochemica et Biophysica Acta *506*, 97-110.

Kamar, S., Howlett, M.H.C., Klooster, J., Graaff, W.d., Csikós, T., Rabelink, M.J.W.E., Hoeben, R.C., and Kamermans, M. (2020). Degenerated Cones in Cultured Human Retinas Can Successfully Be Optogenetically Reactivated. International journal of molecular sciences *21*.

Kang, J.-Y., Kawaguchi, D., Coin, I., Xiang, Z., O'Leary, D.D.M., Slesinger, P.A., and Wang, L. (2013). In vivo expression of a light-activatable potassium channel using unnatural amino acids. Neuron *80*, 358-370.

Karbowski, M., and Youle, R.J. (2003). Dynamics of mitochondrial morphology in healthy cells and during apoptosis. Cell death and differentiation *10*, 870-880.

Kasahara, M., Swartz, T.E., Olney, M.A., Onodera, A., Mochizuki, N., Fukuzawa, H., Asamizu, E., Tabata, S., Kanegae, H., and Takano, M., et al. (2002). Photochemical properties of the flavin mononucleotide-binding domains of the phototropins from Arabidopsis, rice, and Chlamydomonas reinhardtii. Plant physiology *129*, 762-773.

Kennedy, M.J., Hughes, R.M., Peteya, L.A., Schwartz, J.W., Ehlers, M.D., and Tucker, C.L. (2010). Rapid blue-light-mediated induction of protein interactions in living cells. Nature methods *7*, 973-975.

Kiernan, M.C., Vucic, S., Cheah, B.C., Turner, M.R., Eisen, A., Hardiman, O., Burrell, J.R., and Zoing, M.C. (2011). Amyotrophic lateral sclerosis. The Lancet *377*, 942-955.

Kim, C.H., Oh, Y., and Lee, T.H. (1997). Codon optimization for high-level expression of human erythropoietin (EPO) in mammalian cells. Gene *199*, 293-301.

Kim, N.Y., Lee, S., Yu, J., Kim, N., Won, S.S., Park, H., and Heo, W.D. (2020). Optogenetic control of mRNA localization and translation in live cells. Nature cell biology 22, 341-352.

Kithil, M., Engel, A.J., Langhans, M., Rauh, O., Cartolano, M., van Etten, J.L., Moroni, A., and Thiel, G. (2020). Codon bias determines sorting of ion channel protein. bioRxiv, 10.1101/2020.03.17.994780.

Kithil, M.E. (2018). Die Sortierung von Membranproteinen: Der Einfluss der codon usage auf die Sortierung von Modell-Kaliumkanälen. Dissertation (Darmstadt).

Klapoetke, N.C., Murata, Y., Kim, S.S., Pulver, S.R., Birdsey-Benson, A., Cho, Y.K., Morimoto, T.K., Chuong, A.S., Carpenter, E.J., and Tian, Z., et al. (2014a). Independent optical excitation of distinct neural populations. Nature methods *11*, 338-346.

Klapoetke, N.C., Murata, Y., Kim, S.S., Pulver, S.R., Birdsey-Benson, A., Cho, Y.K., Morimoto, T.K., Chuong, A.S., Carpenter, E.J., and Tian, Z., et al. (2014b). Independent optical excitation of distinct neural populations. Nature methods *11*, 338-346.

Klapper, S.D., Swiersy, A., Bamberg, E., and Busskamp, V. (2016). Biophysical Properties of Optogenetic Tools and Their Application for Vision Restoration Approaches. Frontiers in systems neuroscience *10*, 74.

Kleuter, M. (2019). Gating evaluation and light inducible regulation of the viral potassium channel KcvNTS. Master Thesis (Darmstadt).

Kliebenstein, D.J., Lim, J.E., Landry, L.G., and Last, R.L. (2002). Arabidopsis UVR8 regulates ultraviolet-B signal transduction and tolerance and contains sequence similarity to human regulator of chromatin condensation 1. Plant physiology *130*, 234-243.

Konermann, S., Brigham, M.D., Trevino, A.E., Hsu, P.D., Heidenreich, M., Le Cong, Platt, R.J., Scott, D.A., Church, G.M., and Zhang, F. (2013). Optical control of mammalian endogenous transcription and epigenetic states. Nature *500*, 472-476.

Krabbendam, I.E., Honrath, B., Culmsee, C., and Dolga, A.M. (2018). Mitochondrial Ca2+-activated K+ channels and their role in cell life and death pathways. Cell calcium *69*, 101-111.

Krömmelbein, A. (2020). Verfeinerung präklinischer Studien durch Einzelmolekülmikroskopie am Beispiel der FAK. Dissertation (Darmstadt).

Kruman, I.I., and Mattson, M.P. (1999). Pivotal Role of Mitochondrial Calcium Uptake in Neural Cell Apoptosis and Necrosis. Journal of Neurochemistry *72*, 529-540.

Kupcho, K., Shultz, J., Hurst, R., Hartnett, J., Zhou, W., Machleidt, T., Grailer, J., Worzella, T., Riss, T., and Lazar, D., et al. (2019). A real-time, bioluminescent annexin V assay for the assessment of apoptosis. Apoptosis : an international journal on programmed cell death *24*, 184-197.

Kuse, Y., Ogawa, K., Tsuruma, K., Shimazawa, M., and Hara, H. (2014). Damage of photoreceptor-derived cells in culture induced by light emitting diode-derived blue light. Scientific reports *4*, 5223.

Kushibiki, T., and Ishihara, M. (2018). Application of Optogenetics in Gene Therapy. Current gene therapy *18*, 40-44.

Kushibiki, T., Okawa, S., Hirasawa, T., and Ishihara, M. (2015). Optogenetic control of insulin secretion by pancreatic β-cells in vitro and in vivo. Gene therapy *22*, 553-559.

Lagali, P.S., Balya, D., Awatramani, G.B., Münch, T.A., Kim, D.S., Busskamp, V., Cepko, C.L., and Roska, B. (2008). Light-activated channels targeted to ON bipolar cells restore visual function in retinal degeneration. Nature neuroscience *11*, 667-675.

Lamolle, G., Marin, M., and Alvarez-Valin, F. (2006). Silent mutations in the gene encoding the p53 protein are preferentially located in conserved amino acid positions and splicing enhancers. Mutation research *600*, 102-112.

Lanyi, J.K., and MacDonald, R.E. (1976). Existence of Electrogenic Hydrogen Ion/Sodium Ion Antiport in Halobacterium halobium Cell Envelope Vesicles. Biochemistry *15*, 4608-4614.

Laskowski, M., Augustynek, B., Kulawiak, B., Koprowski, P., Bednarczyk, P., Jarmuszkiewicz, W., and Szewczyk, A. (2016). What do we not know about mitochondrial potassium channels? Biochimica et biophysica acta *1857*, 1247-1257.

Lazrak, A., Fu, L., Bali, V., Bartoszewski, R., Rab, A., Havasi, V., Keiles, S., Kappes, J., Kumar, R., and Lefkowitz, E., et al. (2013). The silent codon change I507-ATC-ATT contributes to the severity of the ΔF508 CFTR channel dysfunction. FASEB journal : official publication of the Federation of American Societies for Experimental Biology *27*, 4630-4645.

Leanza, L., Romio, M., Becker, K.A., Azzolini, M., Trentin, L., Managò, A., Venturini, E., Zaccagnino, A., Mattarei, A., and Carraretto, L., et al. (2017). Direct Pharmacological Targeting of a Mitochondrial Ion Channel Selectively Kills Tumor Cells In Vivo. Cancer cell *31*, 516-531

Legris, M., Ince, Y.Ç., and Fankhauser, C. (2019). Molecular mechanisms underlying phytochrome-controlled morphogenesis in plants. Nature communications *10*, 5219.

Lerich, A., Langhans, M., Sturm, S., and Robinson, D.G. (2011). Is the 6 kDa tobacco etch viral protein a bona fide ERES marker? Journal of experimental botany *62*, 5013-5023.

Levskaya, A., Weiner, O.D., Lim, W.A., and Voigt, C.A. (2009). Spatiotemporal control of cell signalling using a light-switchable protein interaction. Nature *461*, 997-1001.

Lewis, S.C., Uchiyama, L.F., and Nunnari, J. (2016). ER-mitochondria contacts couple mtDNA synthesis with mitochondrial division in human cells. Science (New York, N.Y.) *353*, 5549.

Li, J., Li, G., Wang, H., and Wang Deng, X. (2011). Phytochrome signaling mechanisms. The Arabidopsis book *9*, e0148.

Li, Z., Okamoto, K.-I., Hayashi, Y., and Sheng, M. (2004). The importance of dendritic mitochondria in the morphogenesis and plasticity of spines and synapses. Cell *119*, 873-887.

Lima, S.Q., and Miesenböck, G. (2005). Remote control of behavior through genetically targeted photostimulation of neurons. Cell *121*, 141-152.

Lin, J.Y., Knutsen, P.M., Muller, A., Kleinfeld, D., and Tsien, R.Y. (2013). ReaChR: a red-shifted variant of channelrhodopsin enables deep transcranial optogenetic excitation. Nature neuroscience *16*, 1499-1508.

Liu, B., Liu, H., Zhong, D., and Lin, C. (2010). Searching for a photocycle of the cryptochrome photoreceptors. Current Opinion in Plant Biology *13*, 578-586.

Liu, H., Liu, B., Zhao, C., Pepper, M., and Lin, C. (2011). The action mechanisms of plant cryptochromes. Trends in plant science *16*, 684-691.

Liu, H., Wang, Q., Liu, Y., Zhao, X., Imaizumi, T., Somers, D.E., Tobin, E.M., and Lin, C. (2013). Arabidopsis CRY2 and ZTL mediate blue-light regulation of the transcription factor CIB1 by distinct mechanisms. Proceedings of the National Academy of Sciences of the United States of America *110*, 17582-17587.

Liu, H., Yu, X., Li, K., Klejnot, J., Yang, H., Lisiero, D., and Lin, C. (2008). Photoexcited CRY2 Interacts with CIB1 to Regulate Transcription and Floral Initiation in Arabidopsis. Science (New York, N.Y.) *322*, 1535-1539.

Liu, Q., and Tucker, C.L. (2017). Engineering genetically-encoded tools for optogenetic control of protein activity. Current opinion in chemical biology *40*, 17-23.

Lo, C.-L., Choudhury, S.R., Irudayaraj, J., and Zhou, F.C. (2017). Epigenetic Editing of Ascl1 Gene in Neural Stem Cells by Optogenetics. Scientific reports *7*, 42047.

Lo, E.H., Dalkara, T., and Moskowitz, M.A. (2003). Mechanisms, challenges and opportunities in stroke. Nature reviews. Neuroscience *4*, 399-415.

Lungu, O.I., Hallett, R.A., Choi, E.J., Aiken, M.J., Hahn, K.M., and Kuhlman, B. (2012). Designing photoswitchable peptides using the AsLOV2 domain. Chemistry & biology *19*, 507-517.

Luo, Y.H.-L., and da Cruz, L. (2016). The Argus(®) II Retinal Prosthesis System. Progress in retinal and eye research *50*, 89-107.

Ma, G., He, L., Liu, S., Xie, J., Huang, Z., Jing, J., Lee, Y.-T., Wang, R., Luo, H., and Han, W., et al. (2020). Optogenetic engineering to probe the molecular choreography of STIM1-mediated cell signaling. Nature communications *11*, 1039.

Macé, E., Caplette, R., Marre, O., Sengupta, A., Chaffiol, A., Barbe, P., Desrosiers, M., Bamberg, E., Sahel, J.-A., and Picaud, S., et al. (2015). Targeting channelrhodopsin-2 to ON-bipolar cells with vitreally administered AAV Restores ON and OFF visual responses in blind mice. Molecular therapy : the journal of the American Society of Gene Therapy *23*, 7-16.

MacKinnon, R. (2003). Potassium channels. FEBS Letters *555*, 62-65.

Malinska, D., Mirandola, S.R., and Kunz, W.S. (2010). Mitochondrial potassium channels and reactive oxygen species. FEBS Letters *584*, 2043-2048.

Mann, J.R., Gleixner, A.M., Mauna, J.C., Gomes, E., DeChellis-Marks, M.R., Needham, P.G., Copley, K.E., Hurtle, B., Portz, B., and Pyles, N.J., et al. (2019). RNA Binding Antagonizes Neurotoxic Phase Transitions of TDP-43. Neuron *102*, 321-338.e8.

Marc, R.E., Jones, B.W., Watt, C.B., and Strettoi, E. (2003). Neural remodeling in retinal degeneration. Progress in retinal and eye research *22*, 607-655.

Marchi, S., Patergnani, S., and Pinton, P. (2014). The endoplasmic reticulum-mitochondria connection. One touch, multiple functions. Biochimica et biophysica acta *1837*, 461-469.

McDonald, D., Vodicka, M.A., Lucero, G., Svitkina, T.M., Borisy, G.G., Emerman, M., and Hope, T.J. (2002). Visualization of the intracellular behavior of HIV in living cells. The Journal of cell biology *159*, 441-452.

Mitra, S.K., Hanson, D.A., and Schlaepfer, D.D. (2005). Focal adhesion kinase: in command and control of cell motility. Nature reviews. Molecular cell biology *6*, 56-68.

Miyazono, Y., Hirashima, S., Ishihara, N., Kusukawa, J., Nakamura, K.-I., and Ohta, K. (2018). Uncoupled mitochondria quickly shorten along their long axis to form indented spheroids, instead of rings, in a fission-independent manner. Scientific reports *8*, 350.

Montal, M., and Mueller, P. (1972). Formation of Bimolecular Membranes from Lipid Monolayers and a Study of Their Electrical Properties. Proceedings of the National Academy of Sciences of the United States of America *69*, 3561-3566.

Motta-Mena, L.B., Reade, A., Mallory, M.J., Glantz, S., Weiner, O.D., Lynch, K.W., and Gardner, K.H. (2014). An optogenetic gene expression system with rapid activation and deactivation kinetics. Nature chemical biology *10*, 196-202.

Mueller, S., Papamichail, D., Coleman, J.R., Skiena, S., and Wimmer, E. (2006). Reduction of the rate of poliovirus protein synthesis through large-scale codon deoptimization causes attenuation of viral virulence by lowering specific infectivity. Journal of virology *80*, 9687-9696.

Mühlhäuser, W.W.D., Fischer, A., Weber, W., and Radziwill, G. (2017). Optogenetics - Bringing light into the darkness of mammalian signal transduction. Biochimica et biophysica acta *1864*, 280-292.

Muir, J., Lopez, J., and Bagot, R.C. (2019). Wiring the depressed brain: optogenetic and chemogenetic circuit interrogation in animal models of depression. Neuropsychopharmacology : official publication of the American College of Neuropsychopharmacology *44*, 1013-1026.

Muller, K., Engesser, R., Metzger, S., Schulz, S., Kampf, M.M., Busacker, M., Steinberg, T., Tomakidi, P., Ehrbar, M., and Nagy, F., et al. (2013). A red/far-red light-responsive bi-stable toggle switch to control gene expression in mammalian cells. Nucleic acids research *41*, e77.

Muller, K., Naumann, S., Weber, W., and Zurbriggen, M.D. (2015). Optogenetics for gene expression in mammalian cells. Biological chemistry *396*, 145-152.

Müller, K., Engesser, R., Schulz, S., Steinberg, T., Tomakidi, P., Weber, C.C., Ulm, R., Timmer, J., Zurbriggen, M.D., and Weber, W. (2013). Multi-chromatic control of mammalian gene expression and signaling. Nucleic acids research *41*, e124.

Müller, K., Engesser, R., Timmer, J., Zurbriggen, M.D., and Weber, W. (2014). Orthogonal optogenetic triple-gene control in Mammalian cells. ACS synthetic biology *3*, 796-801.

Murray, E.E., Lotzer, J., and Eberle, M. (1989). Codon usage in plant genes. Nucleic acids research *17*, 477-498.

Nagatani, A. (2010). Phytochrome: structural basis for its functions. Current Opinion in Plant Biology *13*, 565-570.

Nagel, G., Brauner, M., Liewald, J.F., Adeishvili, N., Bamberg, E., and Gottschalk, A. (2005). Light activation of channelrhodopsin-2 in excitable cells of Caenorhabditis elegans triggers rapid behavioral responses. Current biology *15*, 2279-2284.

Nagel, G., Ollig, D., Fuhrmann, M., Kateriya, S., Musti, A.M., Bamberg, E., and Hegemann, P. (2002). Channelrhodopsin-1: A Light-Gated Proton Channel in Green Algae. Science *296*, 2395-2398.

Nagel, G., Szellas, T., Huhn, W., Kateriya, S., Adeishvili, N., Berthold, P., Ollig, D., Hegemann, P., and Bamberg, E. (2003). Channelrhodopsin-2, a directly light-gated cation-selective membrane channel. PNAS *100*, 13940-13945.

Ngugi, A.K., Kariuki, S.M., Bottomley, C., Kleinschmidt, I., Sander, J.W., and Newton, C.R. (2011). Incidence of epilepsy. A systematic review and meta-analysis. Neurology *77*, 1005-1012.

Nguyen, T., Chin, W.-C., and Verdugo, P. (1998). Role of Ca2+/K+ ion exchange in intracellular storage and release of Ca2+. Nature *395*, 908-912.

Novoa, E.M., and Pouplana, L.R. de (2012). Speeding with control. Codon usage, tRNAs, and ribosomes. Trends in genetics : TIG *28*, 574-581.

Nunnari, J., and Suomalainen, A. (2012). Mitochondria. In sickness and in health. Cell *148*, 1145-1159.

O'Neill, P.R., and Gautam, N. (2014). Subcellular optogenetic inhibition of G proteins generates signaling gradients and cell migration. Molecular biology of the cell *25*, 2305-2314.

Oesterhelt, D., and Stoeckenius, W. (1971). Rhodopsin-like Protein from the Purple Membrane of Halobacterium halobium. Nature *233*, 149-152.

Ong, S.-B., and Hausenloy, D.J. (2010). Mitochondrial morphology and cardiovascular disease. Cardiovascular research *88*, 16-29.

O'Rourke, B. (2007). Mitochondrial ion channels. Annual review of physiology *69*, 19-49.

Ovesný, M., Křížek, P., Borkovec, J., Svindrych, Z., and Hagen, G.M. (2014). ThunderSTORM. A comprehensive ImageJ plug-in for PALM and STORM data analysis and super-resolution imaging. Bioinformatics (Oxford, England) *30*, 2389-2390.

Paech, S. (2019). Analysis of the linkage of GRB2 clustering with the phosphorylation ratio of FAK (Y397) in focal adhesion sites. Master Thesis (Darmstadt).

Palmer, C.S., Osellame, L.D., Stojanovski, D., and Ryan, M.T. (2011). The regulation of mitochondrial morphology: intricate mechanisms and dynamic machinery. Cellular signalling *23*, 1534-1545.

Pan, Z.-H., Ganjawala, T.H., Lu, Q., Ivanova, E., and Zhang, Z. (2014). ChR2 mutants at L132 and T159 with improved operational light sensitivity for vision restoration. PloS one *9*, e98924.

Paoletti, P., Ellis-Davies, G.C.R., and Mourot, A. (2019). Optical control of neuronal ion channels and receptors. Nature reviews. Neuroscience *20*, 514-532.

Papanatsiou, M., Petersen, J., Henderson, L., Wang, Y., Christie, J.M., and Blatt, M.R. (2019). Optogenetic manipulation of stomatal kinetics improves carbon assimilation, water use, and growth. Science (New York, N.Y.) *363*, 1456-1459.

Paredes, R.M., Etzler, J.C., Watts, L.T., Zheng, W., and Lechleiter, J.D. (2008). Chemical calcium indicators. Methods (San Diego, Calif.) *46*, 143-151.

Park, H., Kim, N.Y., Lee, S., Kim, N., Kim, J., and Heo, W.D. (2017). Optogenetic protein clustering through fluorescent protein tagging and extension of CRY2. Nature communications *8*, 30.

Pathak, G.P., Spiltoir, J.I., Hoglund, C., Polstein, L.R., Heine-Koskinen, S., Gersbach, C.A., Rossi, J., and Tucker, C.L. (2017). Bidirectional approaches for optogenetic regulation of gene expression in mammalian cells using Arabidopsis cryptochrome 2. Nucleic acids research 45, e167.

Paz, J.T., Davidson, T.J., Frechette, E.S., Delord, B., Parada, I., Peng, K., Deisseroth, K., and Huguenard, J.R. (2013). Closed-loop optogenetic control of thalamus as a tool for interrupting seizures after cortical injury. Nature neuroscience *16*, 64-70.

Pechmann, S., Chartron, J.W., and Frydman, J. (2014). Local slowdown of translation by nonoptimal codons promotes nascent-chain recognition by SRP in vivo. Nature structural & molecular biology *21*, 1100-1105.

Pechmann, S., and Frydman, J. (2013). Evolutionary conservation of codon optimality reveals hidden signatures of cotranslational folding. Nature structural & molecular biology *20*, 237-243.

Perkins, M.L., Benzinger, D., Arcak, M., and Khammash, M. (2020). Cell-in-the-loop pattern formation with optogenetically emulated cell-to-cell signaling. Nature communications *11*, 1355.

Perlak, F.J., Fuchs, R.L., Dean, D.A., McPherson, S.L., and Fischhoff, D.A. (1991). Modification of the coding sequence enhances plant expression of insect control protein genes. Proceedings of the National Academy of Sciences of the United States of America *88*, 3324-3328.

Pham, V.N., Kathare, P.K., and Huq, E. (2018). Phytochromes and Phytochrome Interacting Factors. Plant physiology *176*, 1025-1038.

Piatkevich, K.D., Subach, F.V., and Verkhusha, V.V. (2013). Engineering of bacterial phytochromes for near-infrared imaging, sensing, and light-control in mammals. Chemical Society reviews *42*, 3441-3452.

Piwonska, M., Szewczyk, A., Schröder, U.H., Reymann, K.G., and Bednarczyk, P. (2016). Effectors of large-conductance calcium-activated potassium channel modulate glutamate excitotoxicity in organotypic hippocampal slice cultures. Acta Neurobiologiae Experimentalis *76*, 20-31.

Pizzo, L., Iriarte, A., Alvarez-Valin, F., and Marín, M. (2015). Conservation of CFTR codon frequency through primates suggests synonymous mutations could have a functional effect. Mutation research *775*, 19-25.

Plugge, B., Gazzarrini, S., Nelson, M., Cerana, R., van Etten, J.L., Derst, C., DiFrancesco, D., Moroni, A., and Thiel, G. (2000). A Potassium Channel Protein Encoded by Chlorella Virus PBCV-1. Science *287*, 1641-1644.

Polesskaya, O., Baranova, A., Bui, S., Kondratev, N., Kananykhina, E., Nazarenko, O., Shapiro, T., Nardia, F.B., Kornienko, V., and Chandhoke, V., et al. (2018). Optogenetic regulation of transcription. BMC Neurosci *19*, 5547.

Polstein, L.R., and Gersbach, C.A. (2015). A light-inducible CRISPR-Cas9 system for control of endogenous gene activation. Nature chemical biology *11*, 198-200.

Prakriya, M. (2009). The molecular physiology of CRAC channels. Immunological reviews *231*, 88-98.

Presnyak, V., Alhusaini, N., Chen, Y.-H., Martin, S., Morris, N., Kline, N., Olson, S., Weinberg, D., Baker, K.E., and Graveley, B.R., et al. (2015). Codon optimality is a major determinant of mRNA stability. Cell *160*, 1111-1124.

Prosdocimi, E., Checchetto, V., and Leanza, L. (2019). Targeting the Mitochondrial Potassium Channel Kv1.3 to Kill Cancer Cells: Drugs, Strategies, and New Perspectives. SLAS Discovery, 1-11.

Prudent, J., and McBride, H.M. (2017). The mitochondria-endoplasmic reticulum contact sites. A signalling platform for cell death. Current opinion in cell biology *47*, 52-63.

Pudasaini, A., El-Arab, K.K., and Zoltowski, B.D. (2015). LOV-based optogenetic devices. Light-driven modules to impart photoregulated control of cellular signaling. Frontiers in molecular biosciences *2*, 18.

Rademacher, A., Erdel, F., Trojanowski, J., Schumacher, S., and Rippe, K. (2017). Real-time observation of light-controlled transcription in living cells. Journal of cell science *130*, 4213-4224.

Rauh, O. (2018). Molecular explanations for gating in simple model K+ channels. Dissertation (Darmstadt).

Rauh, O., Urban, M., Henkes, L.M., Winterstein, T., Greiner, T., van Etten, J.L., Moroni, A., Kast, S.M., Thiel, G., and Schroeder, I. (2017). Identification of Intrahelical Bifurcated H-Bonds as a New Type of Gate in K(+) Channels. Journal of the American Chemical Society *139*, 7494-7503.

Reynwar, B.J., Illya, G., Harmandaris, V.A., Müller, M.M., Kremer, K., and Deserno, M. (2007). Aggregation and vesiculation of membrane proteins by curvature-mediated interactions. Nature *447*, 461-464.

Rimon, G., Bazenet, C.E., Philpott, K.L., and Rubin, L.L. (1997). Increased surface phosphatidylserine is an early marker of neuronal apoptosis. Journal of Neuroscience Research *48*, 563-570.

Ritchie, T.K., Grinkova, Y.V., Bayburt, T.H., Denisov, I.G., Zolnerciks, J.K., Atkins, W.M., and Sligar, S.G. (2009). Reconstitution of Membrane Proteins in Phospholipid Bilayer Nanodiscs. In Liposomes. Part F, N. Düzgüneş, ed. (San Diego, CA: Elsevier Academic Press), pp. 211–231.

Rockwell, N.C., and Lagarias, J.C. (2010). A brief history of phytochromes. Chemphyschem : a European journal of chemical physics and physical chemistry *11*, 1172-1180.

Rullan, M., Benzinger, D., Schmidt, G.W., Milias-Argeitis, A., and Khammash, M. (2018). An Optogenetic Platform for Real-Time, Single-Cell Interrogation of Stochastic Transcriptional Regulation. Molecular cell *70*, 745-756.e6.

Ryu, M.-H., Kang, I.-H., Nelson, M.D., Jensen, T.M., Lyuksyutova, A.I., Siltberg-Liberles, J., Raizen, D.M., and Gomelsky, M. (2014). Engineering adenylate cyclases regulated by near-infrared window light. Proceedings of the National Academy of Sciences of the United States of America *111*, 10167-10172.

Safiulina, D., Veksler, V., Zharkovsky, A., and Kaasik, A. (2006). Loss of mitochondrial membrane potential is associated with increase in mitochondrial volume. Physiological role in neurones. Journal of cellular physiology *206*, 347-353.

Salomon, M., Christie, J.M., Knieb, E., Lempert, U., and Briggs, W.R. (2000). Photochemical and Mutational Analysis of the FMN-Binding Domains of the Plant Blue Light Receptor, Phototropin. Biochemistry, 9401-9410.

Sandoz, G., Levitz, J., Kramer, R.H., and Isacoff, E.Y. (2012). Optical control of endogenous proteins with a photoswitchable conditional subunit reveals a role for TREK1 in GABA(B) signaling. Neuron *74*, 1005-1014.

Santel, A., and Fuller, M.T. (2000). Human homologs of Drosophila Fzo-GTPase. Journal of cell science *114*, 867-874.

Sarris, M., Olekhnovitch, R., and Bousso, P. (2016). Manipulating leukocyte interactions in vivo through optogenetic chemokine release. Blood *127*, e35-41.

Schaepfer, D.D., Hauck, C.R., and Sieg, D.J. (1999). Signaling through focal adhesion kinase. Progress in biophysics and molecular biology *71*, 435-478.

Schindelin, J., Arganda-Carreras, I., Frise, E., Kaynig, V., Longair, M., Pietzsch, T., Preibisch, S., Rueden, C., Saalfeld, S., and Schmid, B., et al. (2012). Fiji: an open-source platform for biological-image analysis. Nature methods *9*, 676-682.

Schmidt, D., Tillberg, P.W., Chen, F., and Boyden, E.S. (2014). A fully genetically encoded protein architecture for optical control of peptide ligand concentration. Nature communications *5*, 3019.

Sengupta, A., Chaffiol, A., Macé, E., Caplette, R., Desrosiers, M., Lampič, M., Forster, V., Marre, O., Lin, J.Y., and Sahel, J.-A., et al. (2016). Red-shifted channelrhodopsin stimulation restores light responses in blind mice, macaque retina, and human retina. EMBO molecular medicine *8*, 1248-1264.

Serrano-Albarrás, A., Estadella, I., Cirera-Rocosa, S., Navarro-Pérez, M., and Felipe, A. (2018). Kv1.3. A multifunctional channel with many pathological implications. Expert opinion on therapeutic targets *22*, 101-105.

Sharp, P.M., and Li, W.-H. (1987). The codon adaptation index - a measure of directional synonymous codon usage bias, and its potential applications. Nucleic acids research *15*, 1281–1295.

Shashkova, S., and Leake, M.C. (2017). Single-molecule fluorescence microscopy review. Shedding new light on old problems. Bioscience reports *37*, BSR20170031.

Shcherbakova, D.M., Shemetov, A.A., Kaberniuk, A.A., and Verkhusha, V.V. (2015). Natural photoreceptors as a source of fluorescent proteins, biosensors, and optogenetic tools. Annual review of biochemistry *84*, 519-550.

Shewmake, T.A., Solis, F.J., Gillies, R.J., and Caplan, M.R. (2008). Effects of linker length and flexibility on multivalent targeting. Biomacromolecules *9*, 3057-3064.

Shi, F., Kawano, F., Park, S.-H.E., Komazaki, S., Hirabayashi, Y., Polleux, F., and Yazawa, M. (2018). Optogenetic Control of Endoplasmic Reticulum-Mitochondria Tethering. ACS synthetic biology *7*, 2-9.

Shivanandan, A., Unnikrishnan, J., and Radenovic, A. (2016). On characterizing protein spatial clusters with correlation approaches. Scientific reports *6*, 31164.

Sinnen, B.L., Bowen, A.B., Forte, J.S., Hiester, B.G., Crosby, K.C., Gibson, E.S., Dell'Acqua, M.L., and Kennedy, M.J. (2017). Optogenetic Control of Synaptic Composition and Function. Neuron *93*, 646-660.e5.

Siotto, F. (2017). Mining and analysis of new viral potassium channel proteins. A structure and function study of new viral potassium channels from marine picoplankton and chlorella viruses. Dissertation (Darmstadt).

Sjöstrand, F.S. (1963). A comparison of plasma membrane, cytomembranes, and mitochondrial membrane elements with respect to ultrastructural features. Journal of Ultrastructure Research *9*, 561-580.

Somers, D.E., Devlin, P.F., and Kay, S.A. (1998). Phytochromes and Cryptochromes in the Entrainment of the Arabidopsis Circadian Clock. Science *282*, 1488-1490.

Song, S.-H., Freddolino, P.L., Nash, A.I., Carroll, E.C., Schulten, K., Gardner, K.H., and Larsen, D.S. (2011). Modulating LOV domain photodynamics with a residue alteration outside the chromophore binding site. Biochemistry *50*, 2411-2423.

Sorgato, M.C., Keller, B.U., and Stühmer, W. (1987). Patch-clamping of the inner mitochondrial membrane reveals a voltage-dependent ion channel. Nature *330*, 498-500.

Spillantini, M.G., and Goedert, M. (1998). Tau protein pathology in neurodegenerative diseases. Trends in neurosciences *21*, 428-433.

Spinelli, J.B., and Haigis, M.C. (2018). The multifaceted contributions of mitochondria to cellular metabolism. Nature cell biology *20*, 745-754.

Stingl, K., Bartz-Schmidt, K.U., Besch, D., Chee, C.K., Cottriall, C.L., Gekeler, F., Groppe, M., Jackson, T.L., MacLaren, R.E., and Koitschev, A., et al. (2015). Subretinal Visual Implant Alpha IMS--Clinical trial interim report. Vision research *111*, 149-160.

Strickland, D., Lin, Y., Wagner, E., Hope, C.M., Zayner, J., Antoniou, C., Sosnick, T.R., Weiss, E.L., and Glotzer, M. (2012). TULIPs: tunable, light-controlled interacting protein tags for cell biology. Nature methods *9*, 379-384.

Strickland, D., Moffat, K., and Sosnick, T.R. (2008). Light-activated DNA binding in a designed allosteric protein. PNAS *105*, 10709-10714.

Strickland, D., Yao, X., Gawlak, G., Rosen, M.K., Gardner, K.H., and Sosnick, T.R. (2010). Rationally improving LOV domain-based photoswitches. Nature methods *7*, 623-626.

Su, X., Zhang, L., Kang, H., Zhang, B., Bao, G., and Wang, J. (2019). Mechanical, nanomorphological and biological reconstruction of early-stage apoptosis in HeLa cells induced by cytochalasin B. Oncology reports *41*, 928-938.

Supek, F., Miñana, B., Valcárcel, J., Gabaldón, T., and Lehner, B. (2014). Synonymous mutations frequently act as driver mutations in human cancers. Cell *156*, 1324-1335.

Suzuki, R., Hotta, K., and Oka, K. (2018). Transitional correlation between inner-membrane potential and ATP levels of neuronal mitochondria. Scientific reports *8*, 2993.

Szabadkai, G., Simoni, A.M., Chami, M., Wieckowski, M.R., Youle, R.J., and Rizzuto, R. (2004). Drp-1-dependent division of the mitochondrial network blocks intraorganellar Ca2+ waves and protects against Ca2+-mediated apoptosis. Molecular cell *16*, 59-68.

Szabo, I., and Zoratti, M. (2014). Mitochondrial channels. Ion fluxes and more. Physiological reviews *94*, 519-608.

Szabò, I., Bock, J., Grassme, H., Soddemann, M., Wilker, B., Lang, F., Zoratti, M., and Gulbins, E. (2008). Mitochondrial potassium channel Kv1.3 mediates Bax-induced apoptosis in lymphocytes. PNAS *105*, 14861-14866.

Szendroedi, J., Phielix, E., and Roden, M. (2011). The role of mitochondria in insulin resistance and type 2 diabetes mellitus. Nature reviews. Endocrinology *8*, 92-103.

Szewczyk, A., Jarmuszkiewicz, W., and Kunz, W.S. (2009). Mitochondrial potassium channels. IUBMB life *61*, 134-143.

Szewczyk, A., Kajma, A., Malinska, D., Wrzosek, A., Bednarczyk, P., Zabłocka, B., and Dołowy, K. (2010). Pharmacology of mitochondrial potassium channels. Dark side of the field. FEBS Letters *584*, 2063-2069.

Szewczyk, A., Skalska, J., Głab, M., Kulawiak, B., Malińska, D., Koszela-Piotrowska, I., and Kunz, W.S. (2006). Mitochondrial potassium channels: from pharmacology to function. Biochimica et biophysica acta *1757*, 715-720.

Tait, S.W.G., and Green, D.R. (2010). Mitochondria and cell death. Outer membrane permeabilization and beyond. Nature reviews. Molecular cell biology *11*, 621-632.

Takenouchi, O., Yoshimura, H., and Ozawa, T. (2018). Unique Roles of β-Arrestin in GPCR Trafficking Revealed by Photoinducible Dimerizers. Scientific reports *8*, 677.

Taslimi, A., Vrana, J.D., Chen, D., Borinskaya, S., Mayer, B.J., Kennedy, M.J., and Tucker, C.L. (2014). An optimized optogenetic clustering tool for probing protein interaction and function. Nature communications *5*, 4925.

Taslimi, A., Zoltowski, B., Miranda, J.G., Pathak, G.P., Hughes, R.M., and Tucker, C.L. (2016). Optimized second-generation CRY2-CIB dimerizers and photoactivatable Cre recombinase. Nature chemical biology *12*, 425-430.

Testai, L., Martelli, A., Marino, A., D'Antongiovanni, V., Ciregia, F., Giusti, L., Lucacchini, A., Chericoni, S., Breschi, M.C., and Calderone, V. (2013). The activation of mitochondrial BK potassium channels contributes to the protective effects of naringenin against myocardial ischemia/reperfusion injury. Biochemical pharmacology *85*, 1634-1643.

Thommen, M., Holtkamp, W., and Rodnina, M.V. (2017). Co-translational protein folding. Progress and methods. Current opinion in structural biology *42*, 83-89.

Thorn, K. (2017). Genetically encoded fluorescent tags. Molecular biology of the cell *28*, 848-857.

Thyagarajan, S., van Wyk, M., Lehmann, K., Löwel, S., Feng, G., and Wässle, H. (2010). Visual function in mice with photoreceptor degeneration and transgenic expression of channelrhodopsin 2 in ganglion cells. The Journal of neuroscience : the official journal of the Society for Neuroscience *30*, 8745-8758.

Tilbrook, K., Arongaus, A.B., Binkert, M., Heijde, M., Yin, R., and Ulm, R. (2013). The UVR8 UV-B Photoreceptor: Perception, Signaling and Response. The Arabidopsis book *11*, e0164.

Tindle, R.W. (2002). Immune evasion in human papillomavirus-associated cervical cancer. Nature Reviews Cancer 2, 59-65.

Tkatch, T., Greotti, E., Baranauskas, G., Pendin, D., Roy, S., Nita, L.I., Wettmarshausen, J., Prigge, M., Yizhar, O., and Shirihai, O.S., et al. (2017). Optogenetic control of mitochondrial metabolism and Ca(2+) signaling by mitochondria-targeted opsins. Proceedings of the National Academy of Sciences of the United States of America 114, 5167-5176.

Tomita, H., Sugano, E., Isago, H., Hiroi, T., Wang, Z., Ohta, E., and Tamai, M. (2010). Channelrhodopsin-2 gene transduced into retinal ganglion cells restores functional vision in genetically blind rats. Experimental eye research *90*, 429-436.

Tonnesen, J., Sorensen, A.T., Deisseroth, K., Lundberg, C., and Kokaia, M. (2009). Optogenetic control of epileptiform activity. PNAS *106*, 12162-12167.

Tønnesen, J., Ledri, M., and Kokaia, M. (2017). Toward an Optogenetic Therapy for Epilepsy. In Optogenetics. From neuronal function to mapping and disease biology, K. Appasani, ed. (Cambridge: Cambridge University Press), pp. 292–307.

Toshiyuki Yamamoto (1963). On the Thickness of the Unit Membrane. The Journal of cell biology, 413-421.

Trimmer, P.A., Swerdlow, R.H., Parks, J.K., Keeney, P., Bennett, J.P., Miller, S.W., Davis, R.E., and Parker, W.D. (2000). Abnormal mitochondrial morphology in sporadic Parkinson's and Alzheimer's disease cybrid cell lines. Experimental neurology *162*, 37-50.

Trudeau, K., Molina, A.J.A., Guo, W., and Roy, S. (2010). High glucose disrupts mitochondrial morphology in retinal endothelial cells: implications for diabetic retinopathy. The American journal of pathology *177*, 447-455.

Trumpower, B.L., and Katki, A. (1975). Effect of Bathophenanthroline and Carbonylcyanide-m-Chlorophenyl Hydrazone on Cytochrome C Reductase Activity of resolved Succinate Cytochrome C Reductase Complex. Biochemical and biophysical research communications *62*, 282-288.

Ullrich, S., Gueta, R., and Nagel, G. (2013). Degradation of channelopsin-2 in the absence of retinal and degradation resistance in certain mutants. Biological chemistry *394*, 271-280.

van Bergeijk, P., Adrian, M., Hoogenraad, C.C., and Kapitein, L.C. (2015). Optogenetic control of organelle transport and positioning. Nature *518*, 111-114.

Vermes, I., Haanen, C., Steffens-Nakken, H., and Reutelingsperger, C. (1995). A novel assay for apoptosis Flow cytometric detection of phosphatidylserine early apoptotic cells using fluorescein labelled Annexin V. Journal of Immunological Methods 184, 39-51.

Verstreken, P., Ly, C.V., Venken, K.J.T., Koh, T.-W., Zhou, Y., and Bellen, H.J. (2005). Synaptic mitochondria are critical for mobilization of reserve pool vesicles at Drosophila neuromuscular junctions. Neuron *47*, 365-378.

Vishwakarma, V.K., Upadhyay, P.K., Chaurasiya, H.S., Srivasatav, R.K., Ansari, T.M., and Srivastava, V. (2019). Mechanistic Pathways of ATP Sensitive Potassium Channels Referring to Cardio-Protective Effects and Cellular Functions. Drug research *69*, 365-373.

Wang, L., Zhu, Q.-L., Wang, G.-Z., Deng, T.-Z., Chen, R., Liu, M.-H., and Wang, S.-W. (2011). The protective roles of mitochondrial ATP-sensitive potassium channels during hypoxia-ischemia-reperfusion in brain. Neuroscience letters *491*, 63-67.

Wang, X., Song, K., Li, Y., Tang, L., and Deng, X. (2019). Single-Molecule Imaging and Computational Microscopy Approaches Clarify the Mechanism of the Dimerization and Membrane Interactions of Green Fluorescent Protein. International journal of molecular sciences *20*, 1410.

Wasilewski, M., and Scorrano, L. (2009). The changing shape of mitochondrial apoptosis. Trends in endocrinology and metabolism: TEM *20*, 287-294.

Watanabe, M., Katsura, K.-i., Ohsawa, I., Mizukoshi, G., Takahashi, K., Asoh, S., Ohta, S., and Katayama, Y. (2008). Involvement of mitoKATP channel in protective mechanisms of cerebral ischemic tolerance. Brain research *1238*, 199-207.

Weisová, P., Anilkumar, U., Ryan, C., Concannon, C.G., Prehn, J.H.M., and Ward, M.W. (2012). 'Mild mitochondrial uncoupling' induced protection against neuronal excitotoxicity requires AMPK activity. Biochimica et biophysica acta *1817*, 744-753.

Werth, J.L., and Thayer, S.I. (1994). Mitochondrial Buffer Physiological Calcium Loads in Cultured Rat Dorsal Root Ganglion Neurons. The Journal of neuroscience : the official journal of the Society for Neuroscience *14*, 348-356.

Wiegert, J.S., Gee, C.E., and Oertner, T.G. (2017). Stimulating Neurons with Heterologously Expressed Light-Gated Ion Channels. Cold Spring Harbor protocols *2017*, pdb.top089714.

Wietek, J., Beltramo, R., Scanziani, M., Hegemann, P., Oertner, T.G., and Wiegert, J.S. (2015). An improved chloride-conducting channelrhodopsin for light-induced inhibition of neuronal activity in vivo. Scientific reports *5*, 14807.

Wietek, J., Wiegert, J.S., Adeishvili, N., Schneider, F., Watanabe, H., Tsunoda, S.P., Vogt, A., Elstner, M., Oertner, T.G., and Hegemann, P. (2014). Conversion of channelrhodopsin into a light-gated chloride channel. Science (New York, N.Y.) *344*, 409-412.

Winterstein, L.-M. (2019). Einflüsse verschiedener Membranen auf die viralen Kaliumkanäle KcvNTS, KcvS und Kmpv12T. Dissertation (Darmstadt).

Winterstein, L.-M., Kukovetz, K., Rauh, O., Turman, D.L., Braun, C., Moroni, A., Schroeder, I., and Thiel, G. (2018a). Reconstitution and functional characterization of ion channels from nanodiscs in lipid bilayers. The Journal of general physiology *150*, 637-646.

Winterstein, L.-M., Kukovetz, K., Rauh, O., Turman, D.L., Braun, C., Moroni, A., Schroeder, I., and Thiel, G. (2018b). Reconstitution and functional characterization of ion channels from nanodiscs in lipid bilayers. The Journal of general physiology *150*, 637-646.

Wojtovich, A.P., Sherman, T.A., Nadtochiy, S.M., Urciuoli, W.R., Brookes, P.S., and Nehrke, K. (2011). SLO-2 is cytoprotective and contributes to mitochondrial potassium transport. PloS one *6*, e28287.

Wolter, K.G., Hsu, Y.-T., Smith, C.L., Nechushtan, A., Xi, X.-G., and Youle, R.J. (1997). Movement of Bax from the Cytosol to Mitochondria during Apoptosis. The Journal of cell biology *139*, 1281-1292.

Wu, Y., Chen, M., and Jiang, J. (2019). Mitochondrial dysfunction in neurodegenerative diseases and drug targets via apoptotic signaling. Mitochondrion *49*, 35-45.

Wu, Y.I., Frey, D., Lungu, O.I., Jaehrig, A., Schlichting, I., Kuhlman, B., and Hahn, K.M. (2009). A genetically encoded photoactivatable Rac controls the motility of living cells. Nature *461*, 104-108.

Wykes, R.C., Heeroma, J.H., Mantoan, L., Zheng, K., MacDonald, D.C., Deisseroth, K., Hashemi, K.S., Walker, M.C., Schorge, S., and Kullmann, D.M. (2012). Optogenetic and potassium channel gene therapy in a rodent model of focal neocortical epilepsy. Science translational medicine *4*, 161ra152.

Xu, Y., Di Nan, Fan, J., Bogan, J.S., and Toomre, D. (2016). Optogenetic activation reveals distinct roles of PIP3 and Akt in adipocyte insulin action. Journal of cell science *129*, 2085-2095.

Yamada, M., Nagasaki, S.C., Ozawa, T., and Imayoshi, I. (2020). Light-mediated control of Gene expression in mammalian cells. Neuroscience research 152, 66-77.

Yen, S.-T., Trimmer, K.A., Aboul, N., Mullen, R.D., Culver, J.C., Dickinson, M.E., Behringer, R.R., and Eisenhoffer, G.T. (2019). CreLite: An Optogenetically Controlled Cre/loxP System Using Red Light bioRxiv 49, 823971.

Yokoyama, S., Nakagawa, I., Ogawa, Y., Morisaki, Y., Motoyama, Y., Park, Y.S., Saito, Y., and Nakase, H. (2019). Ischemic postconditioning prevents surge of presynaptic glutamate release by activating mitochondrial ATP-dependent potassium channels in the mouse hippocampus. PloS one *14*, e0215104.

Yoon, Y., Krueger, E.W., Oswald, B.J., and McNiven, M.A. (2003). The mitochondrial protein hFis1 regulates mitochondrial fission in mammalian cells through an interaction with the dynamin-like protein DLP1. Molecular and Cellular Biology *23*, 5409-5420.

Youle, R.J., and Narendra, D.P. (2011). Mechanisms of mitophagy. Nature reviews. Molecular cell biology *12*, 9-14.

Yu, C.-H., Dang, Y., Zhou, Z., Wu, C., Zhao, F., Sachs, M.S., and Liu, Y. (2015). Codon Usage Influences the Local Rate of Translation Elongation to Regulate Co-translational Protein Folding. Molecular cell *59*, 744-754.

Yu, T., Robotham, J.L., and Yoon, Y. (2006). Increased production of reactive oxygen species in hyperglycemic conditions requires dynamic change of mitochondrial morphology. PNAS *103*, 2653-2658.

Yu, X., Liu, H., Klejnot, J., and Lin, C. (2010). The Cryptochrome Blue Light Receptors. The Arabidopsis book *8*, e0135.

Yurkov, V., Stackebrandt, E., Holmes, A., Fuerst, J.A., Hugenholtz, P., Golecki, J., Gad'on, N., Gorlenko, V.M., Kompantseva, E.I., and Drews, G. (1994). Phylogenetic Positions of Novel Aerobic, Bacteriochlorophyll a-Containing Bacteria and Description of Roseococcus thiosulfatophilus gen. nov., sp. nov., Erythromicrobium amosum gen. nov., sp. nov., and Erythrobacter litoralis sp. nov. International journal of systematic bacteriology *44*, 427-434.

Yüz, S.G., Ricken, J., and Wegner, S.V. (2018). Independent Control over Multiple Cell Types in Space and Time Using Orthogonal Blue and Red Light Switchable Cell Interactions. Adv. Sci. *84*, 1800446.

Zalucki, Y.M., Beacham, I.R., and Jennings, M.P. (2009). Biased codon usage in signal peptides. A role in protein export. Trends in microbiology *17*, 146-150.

Zhang, D.X., Chen, Y.-F., Campbell, W.B., Zou, A.-P., Gross, G.J., and Li, P.-L. (2001). Characteristics and Superoxide-Induced Activation of Reconstituted Myocardial Mitochondrial ATP-Sensitive Potassium Channels. Circulation Research *89*, 1177-1183.

Zhang, F., Wang, L.-P., Brauner, M., Liewald, J.F., Kay, K., Watzke, N., Wood, P.G., Bamberg, E., Nagel, G., and Gottschalk, A., et al. (2007). Multimodal fast optical interrogation of neural circuitry. Nature *446*, 633-639.

Zhang, H., and Cohen, A.E. (2017). Optogenetic Approaches to Drug Discovery in Neuroscience and Beyond. Trends in biotechnology *35*, 625-639.

Zhang, M., Lin, X., Zhang, J., Su, L., Ma, M., Ea, V.L., Liu, X., Wang, L., Chang, J., and Li, X., et al. (2019). Blue light-triggered optogenetic system for treating uveal melanoma. Oncogene 39, 2118-2124.

Zhang, Y., Ivanova, E., Bi, A., and Pan, Z.-H. (2009). Ectopic expression of multiple microbial rhodopsins restores ON and OFF light responses in retinas with photoreceptor degeneration. The Journal of neuroscience : the official journal of the Society for Neuroscience *29*, 9186-9196.

Zhang, Y.-P., and Oertner, T.G. (2007). Optical induction of synaptic plasticity using a light-sensitive channel. Nature methods *4*, 139-141.

Zhao, E.M., Zhang, Y., Mehl, J., Park, H., Lalwani, M.A., Toettcher, J.E., and Avalos, J.L. (2018). Optogenetic regulation of engineered cellular metabolism for microbial chemical production. Nature *555*, 683-687.

Zhou, M., Guo, J., Cha, J., Chae, M., Chen, S., Barral, J.M., Sachs, M.S., and Liu, Y. (2013). Non-optimal codon usage affects expression, structure and function of clock protein FRQ. Nature *495*, 111-115.

Zimmerman, S.P., Hallett, R.A., Bourke, A.M., Bear, J.E., Kennedy, M.J., and Kuhlman, B. (2016). Tuning the Binding Affinities and Reversion Kinetics of a Light Inducible Dimer Allows Control of Transmembrane Protein Localization. Biochemistry *55*, 5264-5271.

Zoeteweij, J.P., van de Water, B., de Bont, Hans J. G. M., Mulder, G.J., and Nagelkerke, J.F. (1993). Calcium-induced Cytotoxicity in Hepatocytes after Exposure to Extracellular ATP Is Dependent on Inorganic Phosphate - Effects on mitochondrial calcium. The Journal of biological chemistry *268*, 3384-3388.

Zoltowski, B.D., Motta-Mena, L.B., and Gardner, K.H. (2013). Blue light-induced dimerization of a bacterial LOV-HTH DNA-binding protein. Biochemistry *52*, 6653-6661.

Zorova, L.D., Popkov, V.A., Plotnikov, E.Y., Silachev, D.N., Pevzner, I.B., Jankauskas, S.S., Babenko, V.A., Zorov, S.D., Balakireva, A.V., and Juhaszova, M., et al. (2018). Mitochondrial membrane potential. Analytical biochemistry *552*, 50-59.

Züchner, S., Mersiyanova, I.V., Muglia, M., Bissar-Tadmouri, N., Rochelle, J., Dadali, E.L., Zappia, M., Nelis, E., Patitucci, A., and Senderek, J., et al. (2004). Mutations in the mitochondrial GTPase mitofusin 2 cause Charcot-Marie-Tooth neuropathy type 2A. Nature genetics *36*, 449-451.

10. Appendix

10.1. Nucleotide and amino acid sequences of the viral potassium channels used in this work

$Kesv_{Wt}$

ATGTCCCGGCGACTGTTTGCGACTTGCGGCATCGCTATCGCGCTCAGGGGACTGGTGGTGAGCGGGGGCGTAAAAG
AGATTGTATCGTTCAGGCCACTGATTGATACTTCGCTCGTCGGCGGAATATTGTCTAATCTGATTTTGCTCGTCGTTT
TCGCTGAACTTTATTGGCAGCTGGACCAAGGGGATGATCACACACACTTCGGCTTCTCGTCCGCGATCGACGCTTAC
TACTTCAGTGCGGTCACGTCTTCCTCTGTCGGATACGGCGATTTGTTGCCGAAAACTCCGAAGGCAAAATTGCTTAC
CATCGCACACATTTTGGCCATGTTCTTCGTGATGCTCCCCGTTGTCGCGAAGGCTCTCGAGAAG

MSRRLFATCGIAIALRGLVVSGGVKEIVSFRPLIDTSLVGGILSNLILLVVFAELYWQLDQGDDHTHFGFSSAIDAYYFSAVT
SSSVGYGDLLPKTPKAKLLTIAHILAMFFVMLPVVAKALEK

$Kesv_{Opt}$

ATGAGCAGACGGCTGTTCGCCACCTGTGGAATCGCCATTGCCCTGCGGGGCCTGGTGGTGTCTGGCGGCGTGAAAG
AAATCGTGTCCTTCCGGCCCCTGATCGACACCAGCCTCGTGGGAGGCATCCTGAGCAACCTGATCCTGCTGGTGGTG
TTCGCCGAGCTGTACTGGCAGCTGGACCAGGGCGACGACCACACCCACTTCGGCTTCAGCAGCGCCATCGACGCCT
ACTACTTCAGCGCCGTGACCAGCAGCAGCGTGGGCTACGGCGACCTGCTGCCCAAGACCCCCAAGGCCAAGCTGCT
GACAATCGCCCACATCCTGGCCATGTTCTTCGTGATGCTGCCCGTGGTGGCCAAGGCCCTGGAAAAGG

MSRRLFATCGIAIALRGLVVSGGVKEIVSFRPLIDTSLVGGILSNLILLVVFAELYWQLDQGDDHTHFGFSSAIDAYYFSAVT
SSSVGYGDLLPKTPKAKLLTIAHILAMFFVMLPVVAKALEK

$Kesv_{NbOpt}$

ATGAGCAGAAGGCTTTTCGCTACCTGCGGTATTGCTATTGCTCTGAGGGGTCTTGTTGTGAGCGGTGGTGTGAAAGA
GATCGTTTCTTTCAGGCCTCTGATCGACACCTCTCTGGTTGGTGGTATTCTGAGCAACCTTATCCTGCTGGTTGTGTT
CGCTGAGCTTTACTGGCAACTGGATCAGGGTGATGACCACACTCACTTCGGTTTCAGCTCTGCTATCGACGCCTACT
ACTTCTCTGCTGTGACCTCCTCTTCTGTTGGTTACGGTGATCTGCTGCCTAAGACTCCTAAGGCTAAGCTGCTTACTA
TCGCTCACATCCTGGCTATGTTCTTCGTGATGCTTCCTGTGGTGGCTAAGGCTCTTGAAAAG

MSRRLFATCGIAIALRGLVVSGGVKEIVSFRPLIDTSLVGGILSNLILLVVFAELYWQLDQGDDHTHFGFSSAIDAYYFSAVT
SSSVGYGDLLPKTPKAKLLTIAHILAMFFVMLPVVAKALEK

$Kmpv_{12T}$

ATGAGAAACCTAATTATAATTTCCACACTGTTTGGAATCATATATAGTTCGTTAGAACCAGGGCATTTCCAGTTTAAG
AGTGTGTTAGATCCATTTTATTTTTCTTTTACGACTATGTCTTCTGTGGGTTACGGCGATATTACACCAAAAACAAAT
CTTGCAAAGGTTCTGGTCATGTGTCAACAGTCGTTACTTTTTAACGAACTTATGCAGGTGGCTAAAATGATTAAATAT

MRNLIIISTLFGIIYSSLEPGHFQFKSVLDPFYFSFTTMSSVGYGDITPKTNLAKVLVMCQQSLLFNELMQVAKMIKY

Kmpv$_{12TOpt}$

ATGCGGAACCTGATCATCATCAGCACCCTGTTCGGCATCATCTACAGCAGCCTGGAACCTGGCCACTTCCAGTTCAA
GAGCGTGCTGGACCCCTTCTACTTCAGCTTCACCACCATGAGCAGCGTCGGCTACGGCGACATCACCCCTAAGACCA
ATCTGGCCAAGGTGCTGGTCATGTGCCAGCAGAGCCTGCTGTTCAACGAGCTGATGCAGGTCGCCAAGATGATCAA
GTAC

MRNLIIISTLFGIIYSSLEPGHFQFKSVLDPFYFSFTTMSSVGYGDITPKTNLAKVLVMCQQSLLFNELMQVAKMIKY

Kcv$_{NTS}$

ATGTTGCTGCTTATCATACATCTCAGCATTTTGGTAATTTTCACTGCCATCTACAAGATGCTGCCCGGCGGCATGTTC
TCAAACACAGACCCGACTTGGGTCGATTGCCTGTACTTTTCGGCATCAACGCACACCACAGTGGGGTACGGGGACCT
CACGCCAAAATCACCCGTGGCAAAACTCACGGCAACGGCACACATGCTGATCGTATTCGCGATCGTCATTTCTGGCT
TCACGTTCCCGTGG

MLLLIIHLSILVIFTAIYKMLPGGMFSNTDPTWVDCLYFSASTHTTVGYGDLTPKSPVAKLTATAHMLIVFAIVISGFTFPW

Kcv$_{PBCV-1Wt}$

ATGTTAGTGTTTAGTAAATTTCTAACGCGAACTGAACCATTCATGATACATCTCTTTATTCTCGCAATGTTCGTGATG
ATCTATAAATTCTTCCCGGGAGGGTTCGAAAATAACTTCTCTGTTGCAAACCCGGACAAAAAGGCATCATGGATAGA
TTGTATATACTTCGGAGTAACGACACACTCTACTGTCGGATTCGGAGATATACTGCCAAAGACGACCGGCGCAAAGC
TTTGTACGATAGCACATATAGTAACAGTGTTCTTCATCGTTCTAACTTTA

MLVFSKFLTRTEPFMIHLFILAMFVMIYKFFPGGFENNFSVANPDKKASWIDCIYFGVTTHSTVGFGDILPKTTGAKLCTIA
HIVTVFFIVLTL

Kcv$_{PBCV-1Opt}$

ATGCTGGTGTTCAGCAAGTTCCTGACCCGGACCGAGCCCTTCATGATCCACCTGTTCATCCTGGCCATGTTCGTGAT
GATCTACAAGTTCTTCCCAGGCGGCTTCGAGAACAACTTCAGCGTGGCCAACCCCGACAAGAAGGCCAGCTGGATCG
ACTGCATCTACTTCGGCGTGACCACCCACAGCACCGTGGGCTTCGGCGACATCCTGCCTAAGACCACCGGCGCCAAG
CTGTGCACAATCGCCCACATCGTGACCGTGTTCTTCATCGTGCTGACCCTG

MLVFSKFLTRTEPFMIHLFILAMFVMIYKFFPGGFENNFSVANPDKKASWIDCIYFGVTTHSTVGFGDILPKTTGAKLCTIA
HIVTVFFIVLTL

10.2. Plasmid maps of key constructs

MitoBLINK1

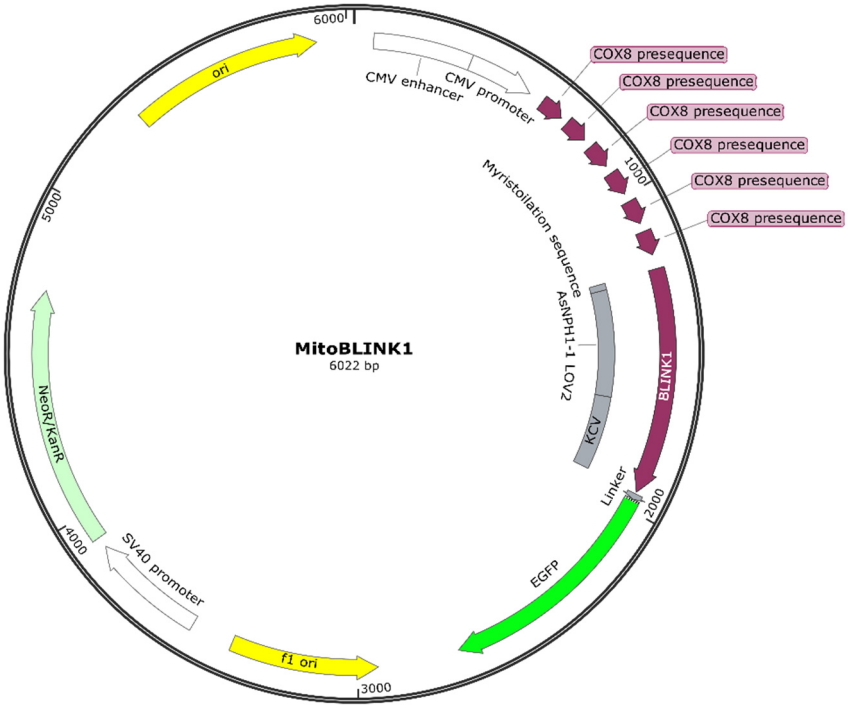

All-in-one CRY2 CIB1 Kmpv$_{12TOpt}$

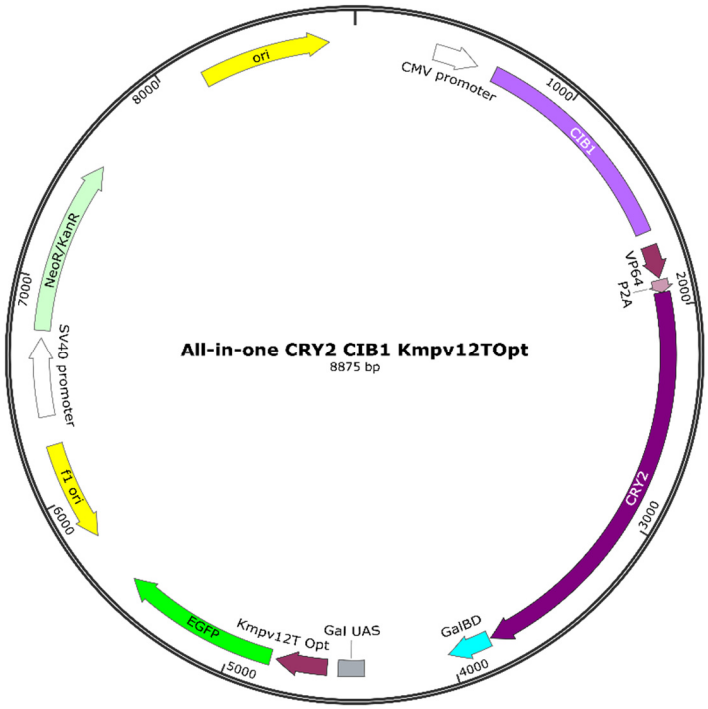

10.3. Primer sequences

Linker length (SL and LL) in peGFP-N2

KesvWt SL (peGFP-N2 linearized with HindIII and BamHI)

KesvWtSL BamHI HRPVAT rev	CATGGTGGCGACCGGCCGGTGGATCCCCTTCTCGAGAGCCTTCGCGACAACG
KesvWtSL HindIII fw	GGACTCAGATCTCGAGCTCAAGCTTATGTCCCGGCGACTGTTTGCGACTTG

KesvOpt LL (peGFP-N2 linearized with BglII and EcoRI)

KesvOptLL BglII fw	CGCTAGCGCTACCGGACTCAGATCTATGAGCAGACGGCTGTTCGCCACCTG
KesvOptLL EcoRI 18AS rev	CGCGGTACCGTCGACTGCAGAATTCCTTTTCCAGGGCCTTGGCCACCACG

Kmpv12TLL in peGFP-N2

Kmpv12T LL Insert fw	GCGCTACCGGACTCAGATCTCGAGATGAGAAACCTAATTATAATTTCCAC
Kmpv12T LL Insert rev	GCGGTACCGTCGACTGCAGAATTCATATTTAATCATTTTAGCCACCTGCATAAG
Kmpv12T LL Vector fw	CTTATGCAGGTGGCTAAAATGATTAAATATGAATTCTGCAGTCGACGGTACCGC
Kmpv12T LL Vector rev	GTGGAAATTATAATTAGGTTTCTCATCTCGAGATCTGAGTCCGGTAGCGC

LOV constructs and MitoBLINK1 (in peGFP-N2)

LOV in peGFP-N2

SacI_atg_atLOV_fw	cGAGCTCatgATCGAGAAGAACTTCG
KpnI_atLOV_rev	ccGGTACCgAACGTGGTCGCTGC

MyLOV in peGFP-N2

BglII_My_fw	GGAAGATCTATGGGCTGTACCGTGT
KpnI_atLOV_rev	ccGGTACCgAACGTGGTCGCTGC

MTS_LOV in peGFP-N2

BglII_MTS_fw	ggaAGATCTATGTCCGTCCTGACG
SacI MTS rev	CGAGCTCGGTGGCGACCGGTGGATCCC

MyLOV KesvOpt in peGFP-N2 and MTS-LOV KesvOpt in peGFP-N2

fw KesvOpt Linker eGFP	GCCAAGGCCCTGGAAAAGCACCGGCCGGTCGCCACC
rev KesvOpt Linker eGFP	GGTGGCGACCGGCCGGTGCTTTTCCAGGGCCTTGGC

MitoBLINK1 in peGFP-N2

Gibson Vector mitoBLINK1 rev	GAGCTCGGTGGCGACCGGTGTC
Gibson Insert mitoBLINK1 fw	CACCGGTCGCCACCGAGCTCATGGGATGTACAGTCTCTGC
Gibson Insert mitoBLINK1 rev	GCGACCGGCCGGTGGGATCCTAAAGTTAGAACGATGAAGA
Gibson Vector mitoBLINK1 fw	GGATCCCACCGGCCGGTCGCC

EL222 constructs (in pcDNA3.1)

KesvOpt in pcDNA3.1

5xC120 KesvOpt eGFP fw	ccgGAATTCATGAGCAGACGG
5xC120 KesvOpt eGFP rev	taaaGCGGCCGCTTACTTGTACAG

KcvOpt in pcDNA3.1

BcuI KcvOpt fw	GACTAGTATGCTGGTGTTCAGCAAG
NotI eGFP rev	tttaGCGGCCGCTTTACTTGTACAGC

BLINK1 in pcDNA3.1

EcoRI Blink fw	cggaattcATGGGATGTACAGTCTCTGC
KpnI Blink rev	gccggtaccTTATAAAGTTAGAACGATGAAGAACACTG
KpnI Linker eGFP fw	cggggtaccCACCGGCCGGTCGC
NotI pEGFP rev	TTAGCGGCCGCTTTACTTGTACAGCT

CRY2 CIB1 constructs (in pGL2 or peGFP-N2)

KesvOpt in pGL2

33020 EcoRI KesvOpt fw	gtactgttggtaaaGAATTCATGAGCAGACGGCTGTTCGC
33020 EcoRI KesvOpt rev_2	GCGAACAGCCGTCTGCTCATGAATTCtttaccaacagtaccggaatgccaag
eGFP NotI 33020 fw_2	TGTACAAGTAAAGCGGCCGCaatgtaactgtattcagcgatgacgaaattc
eGFP NotI 33020 rev	gttacattGCGGCCGCTTTACTTGTACAGCTCGTCCATGC

All-in-one KesvOpt in peGFP-N2

KpnI GalBS fw A	CGGggtaccgagctcttacgcgtgctagc
eGFP NotI rev B	gttacattGCGGCCGCTTTACTTGTACAGCTCGTCCATGC
peGFP CIB fw C	gctcaagcttcgaattctgcagtcgacggtacatgaatggagctataggaggtgacctttg

VP64 P2A rev D

AGGTCCAGGGTTCTCCTCCACGTCTCCAGCCTGCTTCAGCAGGCTGAAGTTAGTAGCTCCGCTTCCTAACATATCGA GATCGAAATCGTCCAGAG

P2A CRY2 fw E

GGAAGCGGAGCTACTAACTTCAGCCTGCTGAAGCAGGCTGGAGACGTGGAGGAGAACCCTGGACCTatgaagatggaca aaaagactatagtttgg

GalBD GalBS rev F

CGCGTAAGAGCTCGGAGATCtcgagctagcacgcgtaagagctcgTTATCTAGATCCGGTGGATCCCCTAG

All-in-one Kmpv12T in peGFP-N2

Gibson Cry CIB P2A fw	CACCGGCCGGTCGCCACCATG
Gibson CryCIB P2A rev	GAATTCtttaccaacagtaccggaatgc

All-in-one Kmpv12TOpt in peGFP-N2

Cry Cib P2A Kmpv12TOpt fw	ATGCAGGTCGCCAAGATGATCAAGTACGGGATCCACCGGCCGGTCGCCACCATG
Cry Cib P2A Kmpv12TOpt rev	GGTGCTGATGATGATCAGGTTCCGCATGAATTCtttaccaacagtaccggaatg
Gibson Cry CIB P2A fw	CACCGGCCGGTCGCCACCATG
Gibson CryCIB P2A rev	GAATTCtttaccaacagtaccggaatgc

All-in-one KcvPBCV-1Opt in peGFP-N2

Gibson KcvOpt CryCIBP2A fw	gtactgttggtaaaGAATTCATGCTGGTGTTCAGCAAG
Gibson KcvOpt CryCIBP2A rev	CATGGTGGCGACCGGCCGGTGGAATTCCAGGGTCAGCACG
Gibson Cry CIB P2A fw	CACCGGCCGGTCGCCACCATG
Gibson CryCIB P2A rev	GAATTCtttaccaacagtaccggaatgc

All-in-one KcvNTS in peGFP-N2

Gibson KcvNTS CryCIBP2A fw	ggtactgttggtaaaGAATTCATGTTGCTGCTTATCATACATC
Gibson KcvNTS CryCIBP2A rev	CATGGTGGCGACCGGCCGGTGCCACGGGAACGTGAAGCCAG
Gibson Cry CIB P2A fw	CACCGGCCGGTCGCCACCATG
Gibson CryCIB P2A rev	GAATTCtttaccaacagtaccggaatgc

All-in-one KcvNTS mClover3 in peGFP-N2

Gibson Cry Cib P2A mClover fw	CCGTGGCACCGGCCGGTCGCCACCatggtgagcaagggcgaggagctg
Gibson Cry Cib P2A mClover rev	gattatgatctagagtcgcggccGCTtcacttgtacagctcgtccatgcc
Gibson Cry Cib P2A fw	AGCggccgcgactctagatcataatc
Gibson Cry Cib P2A NTS rev	GGTGGCGACCGGCCGGTGCCACGG

All-in-one mCherry KcvNTS eGFP (All-in-one KcvNTS in peGFP-N2 linearized with MluI)

Gibson P2A mCherry fw

GGGGATCCACCGGATCTAGAGCTACTAACTTCAGCCTGCTGAAGCAGGCTGGAGACGTGGAGGAGAACCCTGGACC TATGGTGAGCAAGGGCGAGGAGG

Gibson mCherry rev	GCTCGGAGATCtcgagctagcCTAGCCGCCACACTTGTACAGC

All-in-one CRY1-488EEDD KesvOpt

Cry2 1-488 EEDD fw	gctaaagctatttcaagaaccgaggaggacgacgGCGGCCGCATGAAGCTACTGTCTTC
Cry2 1-488 EEDD rev	GACAGTAGCTTCATGCGGCCGCcgtcgtcctcctcggttcttgaaatagctttagc

<u>CRY2 CIB1 Zebrafish (in pMnx1)</u>

All-in-one CRY2 CIB1 KcvNTS in pMnx1 (pMnx1 linearized with BamHI and Eco1051)

CIB1 ZF fw	aggaagcttgatatcgaattcctgGCTGAGCcagcccggggcatgaatggagctataggaggtgacctttgctcaatt
eGFP ZF rev	tatcatgtctggatcatcatcggatatcgagaccacttacgcggccGCTTTACTTGTACAGCTCGTCCATGC

All-in-one CRY2 CIB1 KcvNTS in pMnx1 BH promotor (All-in-one CRY2 CIB1 KcvNTS in pMnx1 linearized with KpnI and Bpu1102I)

BH prom fw	atacgactcactatagggcgaattgggtacTGGTCTGGGCTCCTGGGT
BH prom rev	cctatagctccattcatgccccgggctgGCTCTCTCATTCACGTCCCCCT

Kesv in N. benthamiana

Kesv in pCambia1300mRuby3 (pCambia linearized with SalI)

Gibson KesvWt fw ggtacccggggatcctctagaATGTCCCGGCGACTGTTTGCG

Gibson KesvWt rev CACCATCTTTGCCGCCGCCTCCTTCTCGAGAGCCTTCGCGAC

KesvN.b.Opt in pCambia1300mRuby3 (pCambia linearized with SacI and SalI)

SacI KesvNb pCambia fw ggaAGATCTGAGCTcATGAGCAGAAGGC

SalI KesvNb pCambia rev GAATTCGTCGACCTTTTCAAGAGCCTTAGC

In vitro expression for Bilayer Kmpv12TOpt

Kmpv12TOpt in pET24dellac (pET24dellac linearized with NdeI and SalI)

Kmpv12T pET24 fw

CTAGAAATAATTTTGTTTAACTTTAAGAAGGAGATATACAATGCGGAACCTGATCATCATCAG

Kmpv12T pET24 rev

GTGGTGGTGGTGCTCGAGTTAACAGCATGGACCACAGCAGCTAGTACTTGATCATCTTGGCGACCTGC

10.4. List of linkers used in this work

Listed here are all linkers used in this work to attach the eGFP-tag to the constructs and, in the right column, the dominant sorting pattern for each of the constructs.

Constitutive constructs (peGFP-N2)					**Localization**
$Kesv_{LL}$	EFC	SRRYRGP	GI	HRPVAT	mitochondria/ER
$Kesv_{SL}$			GI	HRPVAT	mitochondria
$Kesv_{OptLL}$	EFC	SRRYRGP	GI	HRPVAT	mitochondria
$Kesv_{OptSL}$			GI	HRPVAT	mitochondria
$Kmpv_{12TML}$		SRRYRGP	GI	HRPVAT	mitochondria
$Kmpv_{12TLL}$	EFC	SRRYRGP	GI	HRPVAT	not sorted
$Kmpv_{12TOpt}$	EFC	SRRYRGP	GI	HRPVAT	mitochondria
$Kcv_{PBCV\text{-}1}$	EFC	SRRYRGP	GI	HRPVAT	ER
$Kcv_{PBCV\text{-}1Opt}$	EFC	SRRYRGP	GI	HRPVAT	ER
Kcv_{NTS}	EFC	SRRYRGP	GI	HRPVAT	ER
pCambia (expression in N. benthamiana)					
Kesv				DEAAK	ER
$Kesv_{NbOpt}$				EAAK	cytosol
LOV constructs					
LOV		RYRGP	GI	HRPVAT	not sorted
MyLOV		RYRGP	GI	HRPVAT	not sorted
MTSLOV		RYRGP	GI	HRPVAT	not sorted
MyLOV $Kesv_{Opt}$				HRPVAT	ER
MTSLOV $Kesv_{Opt}$				HRPVAT	ER
6xMTSLOV $Kesv_{Opt}$			GS	HRPVAT	mitochondria
MitoBLINK1			GS	HRPVAT	mitochondria
EL222 constructs					
EL222 $Kesv_{Opt}$			GI	HRPVAT	mitochondria
EL222 $Kcv_{PBCV\text{-}1Opt}$	EFC	SRRYRGP	GI	HRPVAT	mitochondria
EL222 BLINK1			GI	HRPVAT	ER

All-in-one CRY2 CIB1 constructs

$Kesv_{Opt}$		GI	HRPVAT	mitochondria
$Kmpv_{12T}$	GRR	GI	HRPVAT	not sorted
$Kmpv_{12TOpt}$		GI	HRPVAT	mitochondria
Kcv_{NTS}			HRPVAT	ER
$Kcv_{PBCV\text{-}1Opt}$		TLEF	HRPVAT	not sorted
Kcv_{NTS} mClover			HRPVAT	ER
mCherry Kcv_{NTS}			HRPVAT	ER
CRY2 1-488EEDD $Kesv_{Opt}$		GI	HRPVAT	mitochondria
pMnx1 (expression in zebrafish)				
CRY2 CIB1 Kcv_{NTS} pMnx1			HRPVAT	?
CRY2 CIB1 Kcv_{NTS} BH prom.			HRPVAT	?

10.5. List of cleavage sites for the SL, ML and LL

Name of enzyme	Number of cleavages	Positions of cleavage sites
Arg-C proteinase	4	7 8 10 16
Asp-N endopeptidase + N-terminal Glu	1	2
CNBr	1	21
Chymotrypsin-high specificity (C-term to [FYW], not before P)	3	2 4 9
Chymotrypsin-low specificity (C-term to [FYWML], not before P)	5	2 4 9 15 21
Clostripain	4	7 8 10 16
Glutamyl endopeptidase	1	3
LysC	1	1
NTCB (2-nitro-5-thiocyanobenzoic acid)	1	4
Pepsin (pH1.3)	1	4
Pepsin (pH>2)	3	1 2 4
Proline-endopeptidase	1	17
Proteinase K	9	2 3 4 9 14 18 19 20 22
Staphylococcal peptidase I	1	3
Thermolysin	5	13 17 18 20 21
Trypsin	4	1 7 8 10

Cleavage sites determined with: https://web.expasy.org/cgi-bin/peptide_cutter/peptidecutter.pl

10.6. Mitochondrial membrane potential – Changes in maximum intensity

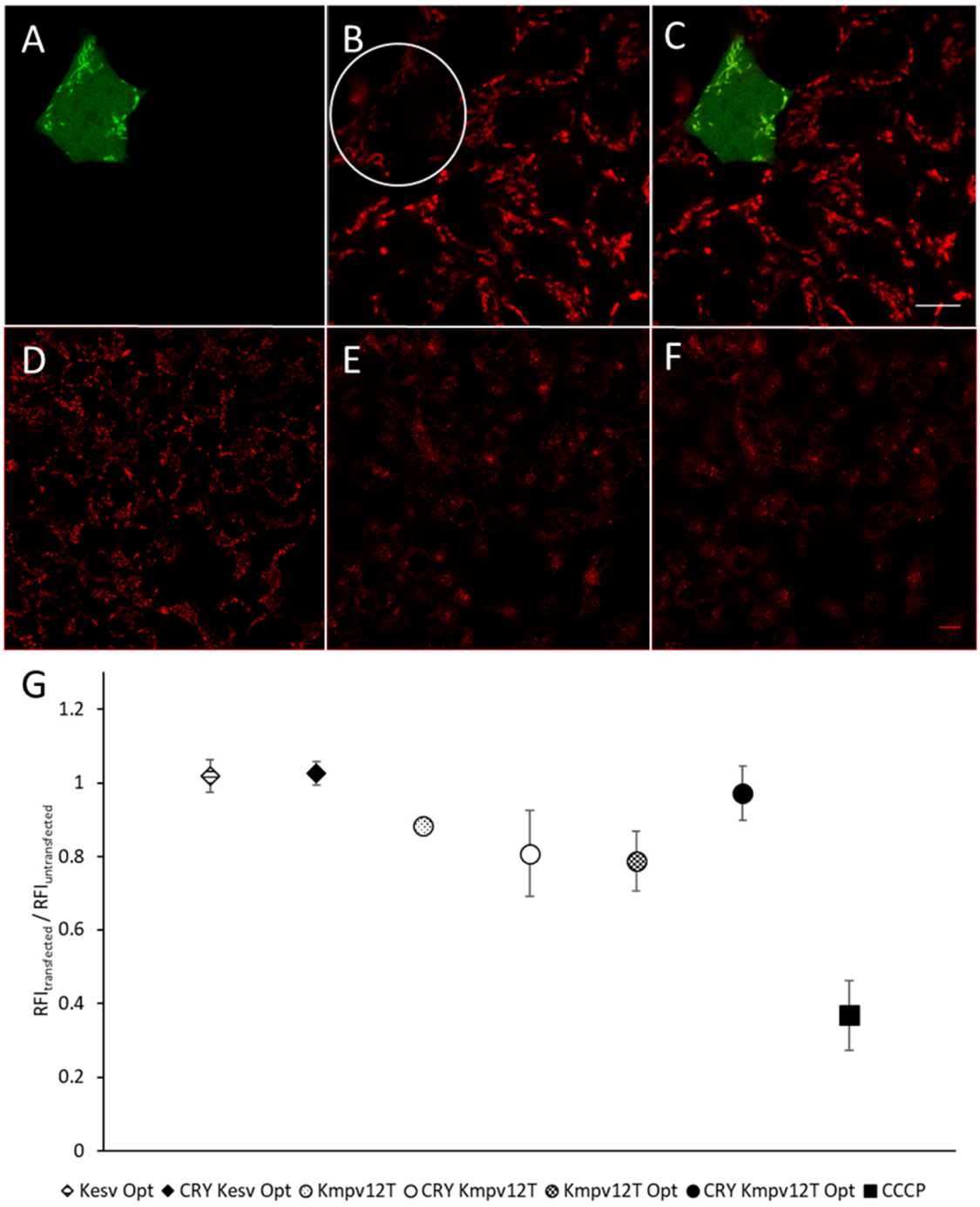

Fig. 51: The maximum intensity does not reflect the changes in mitochondrial membrane potential induced by $Kmpv_{12T}$ and $Kmpv_{12TOpt}$ expressed both constitutively and light-dependently but underlines the effects of CCCP

(A-C): Confocal image of $Kmpv_{12TOpt}$::eGFP, Panel A: $Kmpv_{12TOpt}$::eGFP, Panel B: MitoTracker CMXRos, transfected cell is indicated by a white circle, Panel C: Merged Image of A and B. Scale bar represents 10 µm.**(D-E)** Cells stained with MitoTracker CMXRos 5, 10 and 15 minutes after CCCP treatment. **(G)** Ratio of mean RFI of MitoTracker CMXRos transfected / untransfected cells for $Kesv_{Opt}$ (N=3, n_{transf}=90, $n_{untransf}$=273), CRY $Kesv_{Opt}$ (N=3, n_{transf}=56, $n_{untransf}$=162), $Kmpv_{12T}$ (N=3, n_{transf}=54, $n_{untransf}$=200), CRY $Kmpv_{12T}$ (N=3, n_{transf}=41, $n_{untransf}$=165), $Kmpv_{12TOpt}$ (N=3, n_{transf}=59, $n_{untransf}$=205), CRY $Kmpv_{12TOpt}$ (N=3, n_{transf}=34, $n_{untransf}$=178) and untransfected cells treated with CCCP (N=4, n=1088).

10.7. List of abbreviations

AA	amino acid
ACR	anion channelrhodopsin
AsLOV	light oxygen voltage domain of *Avena sativa*
AtLOV	light oxygen voltage domain of *Arabidopsis thaliana*
ATP	adenosine triphosphate
BR	bacteriorhodopsin
C	closed state
CAI	codon adaptation index
CCCP	Carbonyl Cyanide M-Chloro Phenyl Hydrazone
CCE	CRY C-terminal extension
ChloC	chloride conducting channelrhodopsin
CHO	Chinese hamster ovary cell line
ChR	channelrhodopsin
CIB	cryptochrome interacting partner
CLSM	confocal laser scanning microscopy
COP1	constitutive photomorphogenic 1
Cos7	*Cercopithecus aethiops* (African green monkey) kidney cell line
COX8	cytochrome c oxidase, subunit 8
CRAC	calcium release-activated channel
CRY	cryptochrome
DNA	deoxyribonucleic acid
DPhPC	1,2-diphytanoyl-sn-glycero-3-phosphocholine
E. coli	*Escherichia coli*
EL222	LOV domain of *Erythrobacter litoralis*
ER	endoplasmic reticulum
ERES	ER exit sites
EsV-1	*Ectocarpus siliculosus* virus 1
Ext	extracellular
FAD	flavin adenine dinucleotide
FAK	focal adhesion kinase
FMN	flavin mononucleotide
fw	forward
GFP	green fluorescent protein
HaCaT	human aneuploid keratinocyte cell line

HEK293	human embryonic kidney cell line 293
HR	halorhodopsin
i	single channel current
I	macroscopic current
iLID	improved light-induced dimer
IMM	inner mitochondrial membrane
Int	intracellular
Jaws	cruxhaolrhodopsin from *Halobacterium salinarum*
Kcv	K+ channel chlorella virus
Kir	inward rectifying potassium channel
LOV	light oxygen voltage
MC	mander's coefficient
mitoBK$_{Ca}$	mitochondrial large conductance calcium regulated potassium channel
mitoIK$_{Ca}$	mitochondrial intermediate conductance calcium regulated potassium channel
mitoSK$_{Ca}$	mitochondrial small conductance calcium regulated potassium channel
mitoK$_{ATP}$	mitochondrial ATP-regulated potassium channel
mitoK$_{V}$	mitochondrial voltage-gated potassium channel
mitoTASK-3	mitochondrial twin-pore domain potassium channel
MMP	mitochondrial membrane potential
mPTP	mitochondrial permeability transition pore
MTS	mitochondrial targeting sequence
n	number of samples
N	number of experiments
N. benthamiana	*Nicotiana benthamiana*
NpHR	*Natromonas pharaonis* Halorhodopsin
o	open state
OMM	outer mitochondrial membrane
opt	optimized
P_o	open probability
PBCV-1	*Paramecium bursaria* chlorella virus 1
PBS	phosphate buffered saline
PCC	pearson's correlation coefficient
PCR	polymerase chain reaction
pH	potential of hydrogen
PHR	photolyase homology region

Phy	phytochrome
PM	plasma membrane
rev	reverse
ROI	region of interest
ROS	reactive oxygen species
RsLOV	light oxygen voltage domain of *Rhodobacter sphaeroides*
TIRF	total internal reflection fluorescence (microscopy)
TULIP	tunable light-controlled interacting protein tags
UV	ultraviolet
UVR8	UV-B resistance locus 8
V	voltage
VVD	LOV domain of *Neurospora crassa*
Wt	wildtype
YtvA	LOV domain of *Bacillus subtilis*

10.8. List of figures

10.9. Own work

- For the studies on cell type specificity (chapter 3.3) and influence of linker length (chapter 3.2), data obtained by M. Kithil (PhD student) during her PhD research were reevaluated for $Kesv_{Opt\text{-}SL}$ and $Kesv_{LL}$ and combined with my own data.

- The construct $Kmpv_{12T\,LL}$ (chapter 3.2) was cloned during the practical course by S. Mach and D. Scheub (Master students) under my supervision

- The planar lipid bilayer measurements of $Kmpv_{12T}$ (chapter 7.3) were provided by L. Winterstein (Post Doc) as well as the calcium measurements of $Kmpv_{12TOpt}$ (chapter 7.4). The measurements of $Kmpv_{12TOpt}$ with potassium chloride (chapter 7.3) were done with the help of L. Winterstein as well.

- Injection of Danio rerio larvae with CRY2 CIB1 Kcv_{NTS} and subsequent imaging was done in the Moroni lab at the Universita degli Studi di Milano by Silivia Moleri and Monica Beltrame.

10.10. Declaration – Ehrenwörtliche Erklärung

Ich erkläre hiermit ehrenwörtlich, dass ich die vorliegende Arbeit entsprechend den Regeln guter wissenschaftlicher Praxis selbstständig und ohne unzulässige Hilfe Dritter angefertigt habe.

Sämtliche aus fremden Quellen direkt oder indirekt übernommenen Gedanken sowie sämtliche von Anderen direkt oder indirekt übernommenen Daten, Techniken und Materialien sind als solche kenntlich gemacht. Die Arbeit wurde bisher bei keiner anderen Hochschule zu Prüfungszwecken eingereicht.

Darmstadt, den ……

10.11. Curriculum vitae

Personal information

Name	Engel
Surname	Anja Jeannine
Date of Birth	08/31/1986
Place of Birth	Darmstadt, Germany
Nationality	German

Education and working experience

07/2016 to 06/2020

Doctoral candidate at Technische Universität Darmstadt in the Membrane Biophysics Group of Prof. Dr. Gerhard Thiel

10/2014 to 06/2016

Master of Science Technische Biologie at Technische Universität Darmstadt

Elective courses: Biophysics, Neurobiology, Radioation biology and Plant biotechnology

Specialization: Membrane biophysics, confocal microscopy and electrophysiology

Master Thesis: Duale Sortierung von Membranproteinen: Der Einfluss der zweiten Transmembrandomäne und der Codon Usage auf die Sortierung des viralen Kaliumkanals Kesv (Dual sorting of membrane proteins: Influence of the second transmembrane domain and codon usage on sorting of the viral potassium channel Kesv)

10/2011 to 09/2014

Bachelor of Science Biologie at Technische Universität Darmstadt

Bachelor thesis: Untersuchungen am viralen K^+ - Kanal Kesv: Die Bedeutung der zweiten Transmembrandomäne als Sortierungssignal (Studies of the viral potassium channel Kesv: The role of the second transmembrane domain in protein sorting)

Since 10/2009

Gesundheits- und Krankenpflegerin at Klinikum Darmstadt

Employed at the clinic for neurology and neuro-intensive medicine

10/2006 to 09/2009

Training as Gesundheits- und Krankenpflegerin at Klinikum Darmstadt

2006

General University Entrance Qualification at Justus von Liebig Gymnasium Darmstadt

10.12. Acknowledgements – Danksagung

Zuallererst möchte ich mich bei **Prof. Gerhard Thiel** für die Vergabe eines herausfordernden und spannenden Themas bedanken. Er gab mir stets die nötige Unterstützung, aber auch die nötigen Freiheiten um an meiner Arbeit zu wachsen und eigene Ideen zu entwickeln.

Ein ganz besonderer Dank geht auch an meine persönliche Patch-Clamp-Heldin **Dr. Brigitte Hertel**, die mich seit meiner Bachelorarbeit durch das Studium begleitet und stets ein offenes Ohr für alle Sorgen und Nöte hatte. Als meine stete Retterin in der Not kann ich dir nur sagen – danke für deine guten Ratschläge und aufmunternden Worte – und jede Menge Spaß!

An meine Reisegefährtin für die erste Tour über den großen Teich und – viel gefährlicher – ins wilde Saarland, **Marina Kithil**, geht ebenfalls ein herzliches Dankeschön. Die Codon Usage hat uns zusammengebracht und jetzt möchte ich dich keinesfalls mehr missen! New Orleans bleibt unvergessen und erst recht unsere gemeinsamen Statistik-Sessions am CLSM.

Ganz herzlich bedanken möchte ich mich auch bei meinem Diskussionspartner bei allen größeren und kleineren Problemchen, **Dr. Markus Langhans**. Nicht nur als mein Klonierungs-Lexikon und persönlicher CLSM-Notdienst, sondern auch bei vielen anderen Fragen stand er mir mit Rat und Tat zur Seite. Auch dem Rest der **AG Meckel - Robert Lehn, Steffen Paech** und **Alexander Krömmelbein** - bin ich für die Hilfe vor allem zum Thema Bildanalyse, TIRF und natürlich Clusteranalyse sehr dankbar.

Für viele, viele glückliche HEK-Zellen, auch bei Sonder- und Großbestellungen, möchte ich mich herzlich bei **Mirja Manthey** bedanken. Viele Abbildungen und Versuche in dieser Arbeit wären nicht so schön geworden, hättest du dich nicht so liebevoll um die Zellkultur gekümmert.

Vielen Dank auch an meine Kollegen im mittlerweile „grünen“ Büro, **Kerri Kukovetz** und **Sebastian Höler**. Dank Kerri weiß ich jetzt was sich in einer Glossy Box befindet, wie man Strumpfhosen umgestaltet, und wen man immer um eine Pesto-Spende bitten kann… Danke auch für das geduldige beantworten aller Fragen zum Thema Bilayer und fürs ganz genau nachmessen bei Postern und Präsentationen.

Danke auch an meine Kollegen aus dem Kinderzimmer: An **Dominique Tandl** für viel Spaß und eine tolle Zeit in Hamburg, Baltimore und natürlich New York! Natürlich auch für tolle Tipps zum Thema „Wie töte ich meine Zellen am schnellsten?“ und „Wie ist das eigentlich mit Calcium?“. An **Laura Winterstein** für die Hilfe bei allem rund um Bilayer und als gute Co-Fahrerin über alle Pässe und durch

alle engen Gässchen am Gardasee. Und natürlich auch an alle anderen jetzigen und ehemaligen Doktoranden der **AG Thiel**, die alle zu unvergesslichen 3,5 Jahren beigetragen haben.

Ganz herzlich bedanken möchte ich mich auch bei allen meinen **Freunden** und meiner **Familie** für die tolle Unterstützung in dieser doch stressigen Zeit. Danke an alle, die mich immer wieder aufgemuntert und auf andere Gedanken gebracht haben.